Quasiparticle Self-Consistent GW-Approximation for Molecules

Calculation of Single-Particle Excitation Energies for Molecules

Zur Erlangung des akademischen Grades eines
Doktors der Naturwissenschaften
(Dr.Rer.Nat)

von der Fakultät für Physik
des Karlsruher Instituts für Technologie (KIT)

genehmigte
DISSERTATION

von

Dipl.-Phys. Ferdinand Kaplan

Datum der mündlichen Prüfung:	11. Dezember 2015
Referent:	Prof. Dr. Ferdinand Evers
Korreferent:	Prof. Dr. Alexander Shnirman

Acknowledgements

Many people have contributed to this thesis. All of them supported me as much as they could. Here, I like to carry on the tradition and especially thank:

- first of all my supervisor Prof. Ferdinand Evers who offered me to do a PhD on a very exciting and interesting topic. Furthermore, I like to thank him for his extensive support and all the help he offered. Many thanks for critical questions as well as great ideas which made, if any, the progress in this work possible
- Michiel van Setten, who has been open for questions and discussion anytime. His support and knowledge have been essential in the realization of this work. His throughout positive attitude made the enlightening discussions always fun as well
- Prof. Shnirman for accepting as Co-Referee
- Florian Weigend, who help me especially with specific issues with the TURBOMOLE package and introduced me into the structure of the code
- especially Pablo Schad, Tim Ludwig and Philip Wollfarth but also Ulf Briskot, Nikolaos Kainaris and Patrik Hlobil for proof reading the thesis
- all the colleagues from the CCMT group at the INT for the fun, entertaining and scientific- and life-enriching time
- all the people at the TKM for the nice atmosphere, fun coffee breaks and exciting discussions

Furthermore, I like to thank my parents who supported me all the time of my Diploma and my PhD. Last but not least, I am very grateful for my friends and my girlfriend for the wonderful time in Karlsruhe.

Contents

Chapter 1

1 Introduction

The calculation of the electronic properties of the hydrogen atom is discussed in almost all basic quantum-mechanics textbooks. But, as soon as one asks for the electronic structure of larger atoms or complex molecules a throughout challenging task is faced. An (exact) analytic solution for a system of many interacting electrons is not achievable. Therefore, the many-body nature of the problem is usually tackled with the help of numerical methods and the massive use of computers, at least when quantitative information is required.

The calculation of the electronic structure of molecules is native in the field of quantum chemistry, and computational surface and nano-sciences. Numerical models examine many intermediate steps in chemical reaction processes. The ground state of individual atoms and molecules, the excited states, binding geometries and charge transfers of adsorbed species, and even magnetic properties are well investigated. Computational studies are performed nowadays in practically all branches of nano-sciences, always with the aim of a comprehensive understanding of the (electronic) structure of molecular matter.

1.1 Electronic Structure Theory in the Nanosciences

Computational electronic structure methods can be used to predict the possibility of so far entirely unknown molecules or to explore reaction mechanisms that are not readily studied by experimental means. Moreover, the interplay of experimental spectroscopy measurements and theoretical studies allows for an interpretation of previously not accessible intermediate steps of complex reaction pathways (e.g. Matthiesen et al., 2009). For example, the improvement of catalytic processes relies strongly on an comprehensive understanding of the electronic structure of the reactants. In order to illustrate the possible impact such improvements could have, it is mentioned that catalysis has become a 900 Billion Dollar per year industry; currently 90% of all commercially produced chemical products rely on catalysis in some form.

Furthermore, knowledge about the electronic structure of molecules may also become relevant for the development of future electronic devices like computers, smartphones and tablets. As is well known, the driving force behind the breakthroughs in information

technology is the miniaturization of electronic building blocks, i.e. transistors and diodes. It has already been shown that a silicon based transistor of the size of only 5 nm is realizable (Lee et al., 2006). At present, a major problem are leakage currents due to more narrow insulating layers. Another problem relates to the higher current densities that drive strong heating on very small length scales. Even if some or all of the difficulties can be dealt with: at some point the silicon based top down technology will inevitably reach a technological limit close to the atomic scale.

Motivated by these and other problems such as availability and cost of rare-earth material components, research fields have been established which are looking for alternatives to the common top-down technologies. *Molecular Electronics* is one of them. Indeed, certain primitive functions have been demonstrated some time ago, e.g. a transistor made of a single organic molecule (Kubatkin et al., 2003), or a single-molecule diode (Elbing et al., 2005). But admittedly, even ten years later realistic applications of single-molecule devices in information technologies are still out of sight. Nevertheless, the field continues to attract researchers of many communities. The reason is that the basic problems that are to be overcome before molecules go into device technology are fundamental and ubiquitous, particularly charge transfer and charge excitation. These processes occur at molecular interfaces and in general in (nano-scale) hetero-structures.

A reliable description of charge transfer and excitation processes is crucial for the understanding and development of catalysis, electro-chemistry, organic electronics and photovoltaics – in short, it is essential in all branches of nanotechnology where an atomistic or molecular quantum system contacts with some kind of a reservoir. A basis for an understanding of these processes is always laid-out by computational electronic structure theory calculations. Particularly important observables to be brought about in theoretical studies relate to electronic excitations and energy-level alignments. An example is provided by the leading Ionization Potential (IP), i.e. the minimum energy needed to remove one electron from the system and bring it up to the vacuum level (with zero kinetic energy).

1.2 Overview over Electronic Structure Theory Methods

Due to the need for accurate and fast theoretical studies, an impressive variety of numerical tools and methods have been developed. Presumably, the most popular approach is the Density Functional Theory (DFT) in its different flavors. It allows for computationally affordable theoretical studies of molecules, nano-scale and even bigger systems. Formally, it has a scaling of $\mathcal{O}(N^3)$, where N denotes the number of basis states that represents real-space on a digital machine (Kresse and Furthmüller, 1996, Martin, 2005)[1].

Canonical DFT is a ground-state theory and therefore is not directly suitable for excitation processes. This would be the domain of an extension, the *time dependent* DFT (TDDFT), which has been devised by Runge and Gross (1984). Unfortunately, TDDFT

[1] Adopting further approximation techniques mostly justified for metallic systems, one can achieve nearly linear scaling in some situations (Fonseca Guerra et al., 1998).

relies on propagation kernels that are known only in crude (adiabatic) approximations. Their use for or dc-transport does not appear to offer additional accuracy.

Also the practical implementation of (ground state) DFT employs ad hoc approximations, e.g., the neglect of correlation physics such as the Coulomb blockade (missing "derivative-discontinuity"). A closely related defect is the "self-interaction error" implying that common DFT variants that rely on local or semilocal approximations cannot accurately describe the hydrogen atom. As a result, artifacts in the description of charge transfer processes occur even on the ground state level. They enter, e.g., the description of molecule-metal interfaces so that the charge distribution and the energy level alignment can be affected significantly. Furthermore, the most common variants of DFT, the Local Density Approximation (LDA) (Kohn and Sham, 1965) and the Generalized Gradient Approximation (GGA)(Becke, 1988, Langreth and Mehl, 1983, Perdew et al., 1993) are both neglecting image charges and van der Waals forces. In practice, different approximations are employed and the computational results often vary significantly between them. Because it is not always obvious which approximation works best for a given system, there is a sizable systematic uncertainty associated with quantitative predictions.

An alternative to DFT are *wavefunction based methods* such as "configuration interaction". In contrast to DFT, which aims at optimizing the ground-state density, these methods aim at an optimal approximation of the many-body wave function of the ground state. In the class of wavefunction based methods the Hartree-Fock (HF) approach takes into account an exact description of the exchange processes. Being an orbital dependent non-local theory, problems due to local approximations, like the self-interaction error, are not present in HF. A disadvantage of HF is the neglect of correlation effects. In particular, the neglect of screening leads to large quantitative errors in systems with delocalized electrons (polarizable matter).

More accurate than HF are Coupled-Cluster(CC) approaches. CC extends HF by an expansion of the many-body wavefunction including many more Slater determinants. The accuracy is determined by a cutoff parameter that, roughly speaking, corresponds to the number of particle-hole excitations that is kept in the expansion: S = singlett, D = doublett, T = triplett etc. (Szabo and Ostlund, 1996). A whole family of approaches unfolds; the so called CCSD(T), is prevalent. CCSD(T) is known to be highly accurate in the determination of ground state properties of small systems (Cramer, 2004). Similar to DFT it lacks the description of excitation processes. In contrast to DFT it is computationally quite demanding, formally it has a scaling of $\mathcal{O}(N^7)$ (Cramer, 2004, Raghavachari et al., 1989). Thus, this approach is limited to systems not exceeding 30-50 electrons, typically.

Summarizing, the existing approaches for the calculation of electronic properties of molecules and nano-scale systems are either computationally fast but somewhat inaccurate (DFT) or highly accurate but computationally extremely demanding (wavefunction based methods). In addition, the standard methods focus on ground states, mostly, and moreover lack the description of electronic excitations. That is why there is need for a computational approach for the calculation of electronic properties of molecules and nano-scale systems which fulfills the following criteria:

(a) *Capability of the direct description of charge excitation processes*

(b) *Independence of adjustable parameters, hence true 'ab initio'*

(c) *Suitable for medium size molecules and nano scale systems*

The major aim to be achieved in this thesis is the development and implementation of an approach which matches all these specifications.

Here it is proposed to exploit the many-body perturbation theory (MBPT) (Abrikosov et al., 1975, Fetter and Walecka, 2003) as natural framework for an *ab initio*, i.e. parameter-free, description of photo-ionization processes and charged excitations (Hedin and Lundqvist, 1971) of molecules matter. The central object in MBPT is the electronic Green's Function G. The poles of G describe the single particle excitation energies and lifetimes. Hence, Green's Function based methods match requirement (a). The exact Green's Function G can be computed, in principle, from a self consistent set of equations, the *Hedin equations* (Hedin, 1965, 1999). This set of equations is a representation of G in terms of a power series of the screened Coulomb interaction W. Unfortunately, the Hedin equations contain functional derivatives that are difficult to evaluate. They make such an exact description of the molecule practically unachievable. However, already Hedin proposed a numerically tractable approximation (Hedin, 1965), the GW-approximation. The resulting, again self-consistent, set of equations is called GW*-equations*. Due to the self-consistent formulation there is usually no dependence on initializing conditions and other external assumptions, hence GW matches requirement (b) very well.

The diagrammatic form of GW is similar to HF but with a Coulomb interaction that is dynamically screened, remedying the most serious deficiency of HF. The GW approximation is (qualitatively) correct for certain limiting cases (Hedin, 1995). Thus, its applicability is widely suited for a large class of materials, metals or insulators. In atoms, screening is relatively weak and GW approaches HF; in metals screening is known to be very important and can be well described by GW. Finally, for semiconductors it can be shown that GW corrects the HF gaps, to more realistic values.

Different GW implementations were successfully applied for band structure calculations (e.g. Rinke et al., 2005, 2008) and for molecules (e.g. Blase and Attaccalite, 2011, Rostgaard et al., 2010). While DFT systimatically underastimates band gaps by up to 5 eV (Hedin, 1999, Sham and Schlueter, 1985, van Leeuwen and Baerends, 1994), GW predicts for a large range of semiconductors the fundamental band gap correctly up to a few tenth of eV (Baroni et al., 1985, Godby et al., 1987, Hedin, 1999).

Aryasetiawan and Gunnarsson (1998) survey the variety of approaches to GW and its applications. All implementations have in common that GW is still demanding due to its computational complexity of $\mathcal{O}(N^5)$. Therefore, a current emphasis in electronic structure research is to further reduce the GW-cost by inventing further approximate approaches to investigate large and complex systems.

Hybertsen and Louie (1986) put the numerical application of GW forward giving up self-consistency. They suggested to stop the GW-loop after only one iteration, starting from an DFT based initial guess. This computationally affordable approach is know as

G_0W_0. The status of this approximation is still under debate, i.e. not fully clear. For instance, Holm and von Barth (1998) found that G_0W_0 agrees better with experiments for nearly free-electron metals then GW. Also first applications to small molecules gave good agreement with experimental data for the first Ionization Potential (Van Setten et al., 2013).

In spite of the success of G_0W_0, the procedure has inherent deficits compared to GW. Two are mentioned. Due to its lack of self-consistency the results of G_0W_0 are closely tied to the quality of the starting point (Bruneval, 2012, Fuchs et al., 2007, Marom et al., 2012). Furthermore, G_0W_0 is not a conserving approximation in the sense of Baym and Kadanoff (1961). This implies, that G_0W_0 violates a number of Ward identities.

Van Schilfgaarde et al. (2006) suggested another approximation to GW for the application to extended systems, the *quasiparticle self-consistent GW* (qsGW). Applied to solids, qsGW is more accurate than G_0W_0 (Kotani et al., 2007). Concerning the computational efficiency, the qsGW allows for a description of the self-consistency cycle in which energy integration can be performed analytically. In contrast, full GW requires a numerical solutions of all energy integrals, in the known formulations. Therefore, the qsGW is supposed to be computationally notably less demanding and to be a promising contender to full-fill requirement (c).

Up to now, implementations of the qsGW-method existed only for solids, respectively plane wave codes which employed a periodic formulation. A formulation (and numerical implementation) working for molecules was not available. Motivated by this observation, the development and implementation of the qsGW-method for molecules using a localized basis set is the primary aim of this thesis. The ultimate goal is the accurate and computationally fast calculation of the electronic structure of medium size molecules and nano-structures.

This task is solved taking advantage of the already existing implementation of the G_0W_0 in the quantum chemical package TURBOMOLE. The qsGW implementation is tested for the calculation of the electronic structure over a wide range of different molecules. Transition metals as well as organic molecules with more then one hundred electrons are treated in less then three days on standard workstation computers. Results of qsGW are in very good agreement with the highly accurate CCSD(T) for the calculation of first ionization energies. The mean absolute deviation over the test set is 0.2 eV. Furthermore, qsGW shows equally good accuracy for the calculation of electronic energy-level alignments, which are not accessible with CCSD(T) nor with DFT or HF. Also, in the calculation of dipole moments qsGW has a remarkably higher accuracy then the popular HF and DFT approaches. The computational complexity is reduced by one order in practice.

In addition, further reductions of the computational demands have been developed as well. They rely on approximations which are developed and extensively tested. These approaches reduce the computational complexity while yielding reliable and comparable accurate electronic level- alignments like qsGW.

All in all, qsGW measures up to the expectations and is the method that throughout satisfies requirements (a), (b) and (c).

1.3 Structure of the Thesis

The dissertation is structured as follows: Chap. 2 introduces the GW-method and the different established approximations and approaches towards its implementations. The formulation of the qsGW-approach for molecules as well as convergence and performance tests are presented in Chap. 3. The chapter closes with a study which compares the results of the qsGW method to established methods like CCSD(T) and DFT as well as experiments for the prediction of ionization energies and dipole moments of molecules. In Chap. 5, two G_0W_0 based approximations on qsGW are suggested and tested. These approaches treat dominant contributions introduced from qsGW isolated. One approach takes into account updates in the spatial shape of the orbitals, the other applies the quasiparticle shifts of the poles of the Green's Function in the construction of the G_0W_0 self-energy. Based on these findings Chap. 6 suggests and benchmarks an alternative (approximate) approach to the self-consistent qsGW. It does not take into account any updates in the spatial shape of the orbitals but introduces a throughout self-consistent treatment of the poles of the Green's Function. Thus, the quasiparticle shift is taken into account in the calculation of the screened interaction W as well. In Chap. 7, the thesis is closed with summarizing remarks and an outlook.

Chapter 2

2 GW: An Electronic Structure Theory Method for Weakly Correlated Systems

The aim of this thesis is the computational implementation of the quasiparticle self-consistent GW (qsGW) formalism for molecules. The formalism is introduced in the chapter step by step.

First, the major benefits of a Green's function based approach in comparison to established quantum chemical approaches are pointed out. Afterward, technical aspects of the Green's function technique are introduced. Employing this technique, the Hedin equations, which are the underlying set of equations of the GW formalism, are presented. In the following section the GW-approximation is introduced. It gives a self-consistent set of equations which is computationally tractable, in contrast to the full Hedin equations. Partially self-consistent GW-based schemes are also frequently employed. They are given in the following section. The quasiparticle (QP-)approximation is applied on GW in the last section of the chapter. Finally, the major differences of the full self-consistent GW (scGW) formalism and the quasiparticle self-consistent GW (qsGW) formalism are beeing discussed.

The GW method, which is presented here, is well documented in various review articles and partially also in text books. The compact introduction at hand, which is leaned on the class by Schindlmayr and Friedrich (2006) and a review by Held et al. (2011). It is a round-up which sums up the necessary techniques and leads directly to the approach realized within the present work.

2.1 Motivation

In the context of electronic-structure calculations, techniques employing an effective-single particle picture are widely used. Approaches like the Hartree-Fock (HF) approximation or the Density Functional Theory (DFT) are by design ground state methods.

Figure 2.1: The diagrammatic representation of the interacting Green's function $G(12)$. It describes the probability for a particle which has been created at space and time coordinate 2 to be picked up at 1.

In contrast, Green's function techniques allow for a formal treatment of excitations in many-particle systems. Within this framework L.Hedin derived a set of equations which yield in principle an exact description of single-particle excitations and many other observables described by single-particle operators like the ground-state density and the total energy. Solving Hedin's equations is computationally very demanding however. It is expected that solving them exactly won't be applicable even in the not-so-near future for real systems. Therefore one approximation within this set of equations is applied, which in the end gives a simpler set of equations, the GW equations. A numerical implementation which solves the GW-equations for molecular systems is the major achievement of this thesis.

2.2 Green's function Formalism

The central object of the GW-approach is the Green's function G. It is a matrix that depends on two spatial, two spin and two time coordinates. Hence, an element of the matrix reads $G\left((\mathbf{r}_1, \xi_1, t_1), (\mathbf{r}_2, \xi_2, t_2)\right)$. First, with the purpose to simplify the notation, the common convention of combined coordinates is introduced here:

$$i = (\mathbf{r}_i, \xi_i, t_i) \tag{2.1}$$

The matrix element $G(12)$ is defined such that $\mathrm{i}\hbar G(12)$ gives the probability amplitude for the propagation of a particle or hole that is created at space and time coordinate $(\mathbf{r}_2, \xi_2, t_2)$ to be picked up at the point $(\mathbf{r}_1, \xi_1, t_1)$. This object can be represented by a straight line with an arrow going from 2 to 1 within the diagrammatic technique as shown in Fig. 2.1. The reader might note the reverse order in (1) and (2).

The case of the propagation of an additional electron in a many-electron system described by an Hamiltonian $\hat{H}$ is considered first. The process brings the system from the N-electron ground state $\left|\Psi_0^N(t_2)\right\rangle$ to a final state $\left|\Psi_f^N(t_1)\right\rangle$ by the successive action of operators on the initial state,

$$\left|\Psi_f^N(t_1)\right\rangle = \hat{\psi}(\mathbf{r_1})\hat{U}(t_1, t_2)\hat{\psi}^+(\mathbf{r}_2)\left|\Psi_0^N(t_2)\right\rangle \quad . \tag{2.2}$$

First an electron is added to the system with the electron creation operator $\psi^+(\mathbf{r}')$. Then the evolution operator

$$\hat{U}(t_1, t_2) = \exp(-\frac{\mathrm{i}}{\hbar}\hat{H}(t_1 - t_2)) \tag{2.3}$$

propagates the $N+1$ particle state in time. The application of the electron annihilation operator $\hat{\psi}(\mathbf{r})$ removes an electron again from the system. The probability amplitude to

find an electron at (2) if it is added at (1) is given by the overlap of the initial state with the final state, the Green's function of an electron e^- becomes

$$G^{\mathrm{e}}(12) = -\frac{\mathrm{i}}{\hbar}\left\langle \Psi_0^N(t_1)\right| \hat{\psi}(\mathbf{r_1})\hat{U}(t_1,t_2)\hat{\psi}^+(\mathbf{r}_2)\left|\Psi_0^N(t_2)\right\rangle \Theta(t_1-t_2) \tag{2.4}$$

$$= -\frac{\mathrm{i}}{\hbar}\left\langle \Psi_{0,\mathrm{H}}^N\right| \hat{\psi}_{\mathrm{H}}(\mathbf{r_1},\mathbf{t_1})\hat{\psi}_{\mathrm{H}}^+(\mathbf{r}_2,t_2)\left|\Psi_{0,\mathrm{H}}^N\right\rangle \Theta(t_1-t_2)\ , \tag{2.5}$$

with the Heaviside step function

$$\Theta(t_1-t_2) = \begin{cases} 1 \text{ if } t_1 > t_2\ , \\ 0 \text{ if } t_1 < t_2\ . \end{cases} \tag{2.6}$$

Furthermore, in Eq. (2.5) the representation was changed from the Schrödinger to the Heisenberg picture via

$$|\Psi_H\rangle = \hat{U}(0,t)\,|\Psi_S(t)\rangle \text{ and } \hat{A}_H(t) = \hat{U}(0,t)\hat{A}_S\hat{U}(t,0)\ . \tag{2.7}$$

The definition for the electron Green's function Eq. (2.5) leads directly to the Green's function for the propagation of a hole from (2) to (1). It reads

$$G^{\mathrm{h}}(12) = -\frac{\mathrm{i}}{\hbar}\left\langle \Psi_0^N\right| \hat{\psi}^+(\mathbf{r_1},\mathbf{t_1})\hat{\psi}(\mathbf{r}_2,t_2)\left|\Psi_0^N\right\rangle \Theta(t_1-t_2)\ . \tag{2.8}$$

The combination of the electron- and the hole Green's function gives the time-ordered Green's function

$$G(12) = G^{\mathrm{e}}(12) - G^{\mathrm{h}}(21) \tag{2.9}$$

$$= -\frac{\mathrm{i}}{\hbar}\left\langle \Psi_0^N\right| \hat{T}\left[\hat{\psi}(1)\hat{\psi}^+(2)\right]\left|\Psi_0^N\right\rangle \tag{2.10}$$

with the time-ordering operator $\hat{T}$, which arranges a series of field operators in order of descending time arguments from left to right with a factor (-1) for each pair of permutation. Hence, depending on the time order in Eq. (2.10) the propagation of an electron $(t_1 > t_2)$ or a hole $(t_1 < t_2)$ is described.

To proceed the time-ordered Green's function $G(\mathbf{r_1},\mathbf{r_2},\tau)$ of a stationary system with $\tau = t_1 - t_2$ is considered. Furthermore a projection operator $\sum_i \left|\Psi_i^{N\pm1}\right\rangle\left\langle\Psi_i^{N\pm1}\right|$ onto the complete set of state vectors $\{\Psi_i^{N\pm1}\}$ of the $(N\pm1)$-particle system is inserted into the time-ordered Green's function Eq. (2.10). Then the Green's function is transformed to the Schrödinger picture and the definitions

$$\psi_i^{N-1}(\mathbf{r}) = \left\langle \Psi_i^{N-1}\right| \hat{\psi}(\mathbf{r})\left|\Psi_0^N\right\rangle \text{ and } \psi_i^{N+1}(\mathbf{r}) = \left\langle \Psi_0^N\right| \hat{\psi}(\mathbf{r})\left|\Psi_i^{N+1}\right\rangle \tag{2.11}$$

are used in combination with the (single-particle) excitation energies

$$\varepsilon_i^{N-1} = E_0^N - E_i^{N-1} \text{ and } \varepsilon_i^{N+1} = E_i^{N+1} - E_0^N\ . \tag{2.12}$$

This leads us to the following representation of the Green's function;

$$\begin{aligned} G(\mathbf{r}_1, \mathbf{r}_2; \tau) = &- \frac{\mathrm{i}}{\hbar} \sum_i \Psi_i^{N+1}(\mathbf{r}) \bar{\Psi}_i^{N+1}(\mathbf{r}') e^{-\mathrm{i}\varepsilon_i^{N+1}\tau/\hbar} \theta(\tau) \\ &+ \frac{\mathrm{i}}{\hbar} \sum_i \Psi_i^{N-1}(\mathbf{r}) \bar{\Psi}_i^{N-1}(\mathbf{r}') e^{-\mathrm{i}\varepsilon_i^{N-1}\tau/\hbar} \theta(-\tau) \ . \end{aligned} \tag{2.13}$$

The sums are over all states of the $(N-1)$ respectively the $(N+1)$ particle system. The bar in $\bar{\Psi}_i$ denotes the complex conjugate. Furthermore, the superscript † denotes the conjugate transpose.

This implies that the Green's function contains the complete (single-particle) excitation spectrum of the $(N \pm 1)$-particle system.

Now, employing the Fourier transformation of the Heaviside step function

$$\theta(\omega) = \frac{1}{2\pi} \int_{-\infty}^{\infty} \mathrm{d}\tau \ \theta(\tau) e^{\mathrm{i}\omega\tau - \eta|\tau|} = \frac{\mathrm{i}}{2\pi(\omega + \mathrm{i}\eta)} \tag{2.14}$$

and dropping the $(N \pm 1)$ superscripts leads via Fourier transformation to the energy representation of the Green's function Eq. (2.13), the Lehmann representation:

$$G(\mathbf{r}_1, \mathbf{r}_2; \omega) = \sum_i \frac{\Psi_i(\mathbf{r}_1) \bar{\Psi}_i(\mathbf{r}_2)}{\hbar\omega - \varepsilon_i + \mathrm{i}\eta \mathrm{sgn}(z_i - \mu)} \ , \tag{2.15}$$

with the chemical potential μ. The Green's function has poles at $z_n = \varepsilon_n + \mathrm{i}\gamma_n$, the single-particle excitation energies ε_i and their (single particle) lifetimes $\gamma_n = 2\pi/\tau_n$ of the interacting many-body system. These energies and lifetimes refer to the excitation of the $(N \pm 1)$ particle system; they are measured in direct and indirect photo-electron spectroscopy experiments. In the case of a closed non-interacting (or mean-field) system, the poles are infinitely close to the real axis $z_n = \varepsilon_n - \mathrm{i}\eta \mathrm{sgn}(\varepsilon_n - \mu)$ and $\Psi_i(\mathbf{r})$ are simply occupied and unoccupied single-particle wave functions.

The electron density $n(\mathbf{r})$ can be deduced from the Green's function as follows,

$$n(\mathbf{r}) = -\frac{1}{\pi} Im \left[\int_{-\infty}^{\mu} G(\mathbf{r}, \mathbf{r}, \omega) \ \mathrm{d}\omega \right] \ . \tag{2.16}$$

2.3 Hedin equations

The previous section introduced the powerful tool of the Green's function. From a given Green's function one can directly obtain estimates for single-particle excitation energies. Furthermore it allows the direct calculation of ground state properties like the ground state density from it.

This chapter will sketch a derivation of a set of equations which define the Green's function for a many-body system of interacting electrons in an external potential.

2.3.1 Derivation of the Hedin equations

In order to to describe a general, fully interacting, many electron system the many-body Hamiltonian (cf. Eq. (A.1)) is recalled. In terms of field operators it reads

$$\hat{H} = \int \mathrm{d}\mathbf{r}\hat{\psi}^{+}(\mathbf{r})\hat{h}(\mathbf{r})\hat{\psi}(\mathbf{r}) + \frac{1}{2}\int\int \mathrm{d}\mathbf{r}\ \mathrm{d}\mathbf{r}'\hat{\psi}^{+}(\mathbf{r})\hat{\psi}^{+}(\mathbf{r}')v(\mathbf{r},\mathbf{r}')\hat{\psi}(\mathbf{r}')\hat{\psi}(\mathbf{r}) \tag{2.17}$$

with the Coulomb interaction $v(\mathbf{r},\mathbf{r}')$ and the one particle operator,

$$\hat{h}(\mathbf{r}) = -\frac{\hbar^2}{2m}\nabla_i^2 + \hat{V}_{\mathrm{ext}}(\mathbf{r}) \ . \tag{2.18}$$

which accounts for the kinetic energy contribution, $-\frac{\hbar^2}{2m}\nabla_i^2$, and the (external) potential of the ions , $\hat{V}_{\mathrm{ext}}$. Implicitly, the Born-Oppenheimer approximation is applied already. Hence, the Ions are assumed to be stationary.

From the Coulomb integral in the right hand side of Eq. (2.17) a contribution which is still describable in a non-interacting single-particle picture can be separated, the Hartree term. It accounts for the (local) mean-field contributions $\hat{V}_{\mathrm{H}}$. The Hartree-Hamiltonian reads

$$\hat{\mathcal{H}}_{\mathrm{H}} = \hat{h}(\mathbf{r}) + \hat{V}_{\mathrm{H}}(\mathbf{r}) \ . \tag{2.19}$$

From this Hamiltonian the Hartree Green's function can be constructed via,

$$G_{\mathrm{H}}^{-1}(z) = z - \hat{\mathcal{H}}_{\mathrm{H}} \ . \tag{2.20}$$

With the aim to derive a (time-dependent) solution of the many-body system, the equation of motion of the annihilation operators is recalled,

$$\mathrm{i}\hbar\frac{\mathrm{d}}{\mathrm{d}t}\hat{\psi}(\mathbf{r},t) = \left[\hat{\psi}(\mathbf{r},t),\hat{H}\right] \ . \tag{2.21}$$

Employing the equation of motion Eq. (2.21), its complex-conjugate, and the two-particle Green's function

$$G(1234) = -\frac{1}{\hbar^2}\left\langle\Psi_0^N\right|\hat{T}\left[\hat{\psi}(1)\hat{\psi}(2)\hat{\psi}^{+}(3)\hat{\psi}^{+}(4)\right]\left|\Psi_0^N\right\rangle \tag{2.22}$$

leads to a formulation of the equation of motion of the single-particle Green's function $G(12)$

$$\mathrm{i}\hbar\frac{\mathrm{d}}{\mathrm{d}t_1}G(12) = \delta(12) + \hat{h}(1)G(12) - \mathrm{i}\hbar\int v(1^{+}3)G(1323^{+})\mathrm{d}3 \ , \tag{2.23}$$

for the system described by the Hamiltonian $\hat{H}$, see Eq. (2.17). The superscript $^{+}$ indicates that an additional infinitesimal time was added to ensure correct time ordering.

At this point the functional-derivative method is employed by introducing an external potential, which is again set to zero in the end. This lengthy derivation is skipped at this

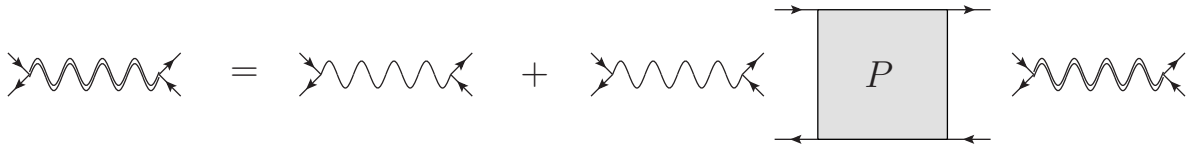

Figure 2.2: The Screened Interaction W, represented by a double wiggled line, is derived within a self-consistend defintion from the bare Cuolomb interaction v, represented by a single wiggled line and corrections due to screening processes wich are described by the Polarization function P.

place. For a full derivation it is referred, to the helpful elaborations in (Held et al., 2011). The derivation gives the screened interaction

$$W(12) = v(12) + \int d(34)v(13)P(34)W(42) \tag{2.24}$$

with the Polarization function

$$P(12) = -\mathrm{i}\int d(34)G(13)\Gamma(324)G(41^+) \ . \tag{2.25}$$

The screened interaction $W(12)$ describes the effective potential at (1) due to an electron present at (2) including all the polarizations due to all electrons: the Coulomb potential of the electron at (2) repels other electrons in its neighborhood and thus gives rise to the formation of a correlation hole with an effective positive charge. This effective charge in turn screens the bare Coulomb interaction of the electron at (2). Analogously, an effective negative charge forms around a hole which in turn screens the Coulomb potential of the hole. Therefore, the screened interaction W is considerably weaker than the Coulomb interaction. This in turn has the major advantage that a perturbative expansion for the screened interaction W should converge considerably faster than the expansion within the bare Coulomb interaction v. The diagrammatic representation of the perturbative expansion is shown in Fig. 2.2. The feasibility of the expansion into the screened interaction has been already emphasized in earlier work (Phillips, 1961). The concept of the screened interaction was first introduced by Hubbard (1957, 1958a,b).

The formation of the polarization cloud can be understood in terms of the presence of all possible multiscattering events between electrons and holes. These events within such an interacting many-particle system are described by the the vertex function $\Gamma(324)$. It is defined by the Bethe-Salpeter Equation

$$\Gamma(123) = \delta(1-2)\delta(2-3) + \int d(4567)\frac{\delta\hat{\Sigma}(12)}{\delta G(45)}G(46)G(75)\Gamma(673) \ . \tag{2.26}$$

Here, the new object $\hat{\Sigma}(12)$ is the non-Hermitian self-energy operator. It takes account for all many-body exchange and correlation effects beyond the so called Hartree contributions

Eq. (2.19). It is given by the convolution of the Green's function G, the screened interaction W and the vertex function Γ,

$$\hat{\Sigma}(12) = \mathrm{i} \int d(34) G(13^+) W(14) \Gamma(324) \ . \tag{2.27}$$

With the self-energy operator $\hat{\Sigma}$ one is able to connect the Green's function G_{H} of the non-interaction mean-field system (described by Eq. (A.4)) with the Green's function of the full interacting many-body system G via the Dyson Equation;

$$G(12) = G_{\mathrm{H}}(12) + \int d(34) G_{\mathrm{H}}(13) \hat{\Sigma}(34) G(42) \ . \tag{2.28}$$

The diagrammatic representation of the Dyson Equation is shown in Fig. 2.3.

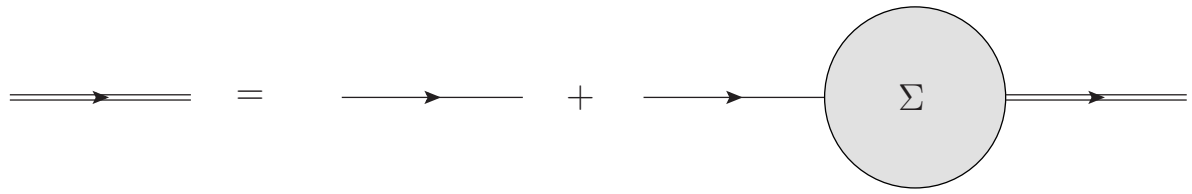

Figure 2.3: The Dyson Equation connects the interacting Green's function G, depicted by the double line, the non-interaction Green's function G_{H}, depicted by the single line and the self-energy $\hat{\Sigma}$.

2.3.2 Hedin's Self-Consistency Cycle

With the Dyson equation Eq. (2.28), the definition for the self-energy $\hat{\Sigma}$, Eq. (2.27), the screened-interaction W and the vertex function Γ one finds a closed set of equations which constitute a self-consistency problem

$$G(12) = G_{\mathrm{H}}(12) + \int d(34) G_{\mathrm{H}}(13) \hat{\Sigma}(34) G(42) \tag{2.29}$$

$$\hat{\Sigma}(12) = \mathrm{i} \int d(34) G(13^+) W(14) \Gamma(324) \tag{2.30}$$

$$W(12) = v(12) + \int d(34) v(13) P(34) W(42) \tag{2.31}$$

$$P(12) = -\mathrm{i} \int d(34) G(13) \Gamma(324) G(41^+) \tag{2.32}$$

$$\Gamma(123) = \delta(1-2)\delta(2-3) + \int d(4567) \frac{\delta \hat{\Sigma}(12)}{\delta G(45)} G(46) G(75) \Gamma(673) \ . \tag{2.33}$$

This set of equations is named 'Hedin equations'. A full self-consistent solution for the Green's function governs all many body effects in a given system, and hence can be considered to be the exact solution for such a problem.

2.4 GW Approximation to Hedin's Equations

The equations Eq. (2.29) to Eq. (2.33) denote the exact Green's function G for an interacting many-body system. However, it is not practical for actual calculations. The right hand side of the Bethe Selpeter Equation Eq. (2.33) with the functional derivative of the the self-energy $\hat{\Sigma}$ introduces a complexity which computationally is not tractable for real systems. Therefore approximations to find a computationally affordable and physically still meaningful approximation to the Hedin equations needs to be found.

2.4.1 Random-Phase Approximation and GW equations

The GW formalism neglects all higher vertex corrections which are given by the integral right hand side of the Bethe Salpeter Equation Eq. (2.33). Hence, the vertex function reduces to,

$$\Gamma(123) \approx \delta(1-2)\delta(2-3) \ . \tag{2.34}$$

This approximation is often called Random Phase Approximation (RPA). It corresponds to allowing only for a subset of scattering processes in the many-electron system. Here, it needs to be pointed out that the RPA in the original formulation employed for the calculation of the polarization, Eq. (2.32), a Hartree-Fock (HF) based Green's function. (For an introduction to the HF-formalism see Sec. A.1.) Within computational quantum chemistry it became popular to employ instead of the HF a Green's function based on the Khon-Sham states and energies from Density Functional Theory (DFT).

An overview over the different approaches and the implications of the RPA for computational chemistry and materials science is given in the review of Ren et al. (2012).

Applying the RPA Eq. (2.34) to the Hedin equations, Eq. (2.29) to Eq. (2.33), leads directly to the self-consistent set of equations which neglect higher order vertex corrections:

$$G(12) = G_{\mathrm{H}}(12) + \int d(34) G_{\mathrm{H}}(13)\hat{\Sigma}(34)G(42) \tag{2.35}$$

$$\hat{\Sigma}(12) = \mathrm{i}G(12^{+})W(12^{+}) \tag{2.36}$$

$$W(12) = v(12) + \int d(34) v(13)P(34)W(42) \tag{2.37}$$

$$P(12) = -\mathrm{i}G(12)G(21^{+}) \tag{2.38}$$

The expression for the self-energy Eq. (2.36) is name-giving for the GW-Approximation. The diagrammatic representation is shown in Fig. 2.4. The diagrammatic representation of the screened interaction W within the GW-approximation, Eq. (2.37), is shown in Fig. 2.5.

Within the RPA all bubble diagrams are picked up to take into account all lowest order scattering processes. In contrast to the original formulation of RPA, the reference system within GW is constantly readjusted in a self-consistent manner. In the diagrams this is depicted by the double lines within the bubble diagrams in Fig. 2.5. The self-consistent update of the Green's function is introduced via the the Dyson Equation, Eq. (2.29).

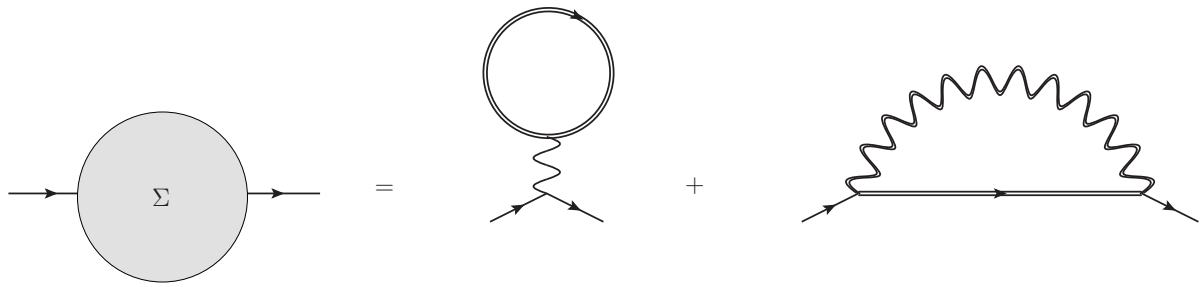

Figure 2.4: The Self-Energy is given by the term G times W within the GW-approximation. It turns out to be a Hartree term plus a Fock-like term which is however determined with the screened Coulomb interaction W (double wiggled line) instead of the bare Coulomb interaction V (single wiggled line).

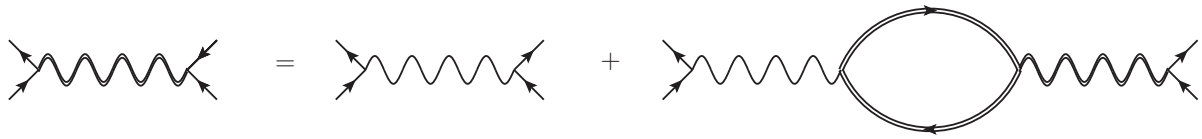

Figure 2.5: The Screened Interaction W depicted by a double wiggled line is calculated from the bare Coulom interation v, depicted by single wiggled lines and corrections from screening processes. In the GW-Approximation the screening is given by the RPA. Hence, a geometric series of single bubbles connected to the screened interaction generates the solution.

2.4.2 GW Self-Consistency Cycle

A solution of the GW-equations, (2.35) to (2.38), can be constructed by inversion of the Dyson equation (2.35) and (2.37). But, typically, they are solved in an iterative fashion. The resulting iterative cycle is visualized in Fig. 2.6. Technically the cycle needs to be initialized from a first guess Green's function G_0. The Dyson Equation suggests intuitively to start the iterative collection of all bubble diagrams from the mean-field Green's function G_{H}.

In this work only weakly interaction systems are considered. Hence, the self-consistent solution is adiabatically connected to the non-interacting Green's function and far away from multiple solutions. Therefore, it is expected that the iterative flow from the non-interacting Green's function to the interacting one will be stable and find one single fixed point solution. Hence, starting from an improved guess for the initial Green's function the resulting self-consistent solution is identical. For example if a Green's Function from a DFT calculation is used as the starting point, the iteration cycle is going to construct automatically the correct sequence of diagrams for the self-energy to find in the end the identical self-consistent solution as from any other reference system.

Since the formalism converges into the same fixed point solution it is beneficial to start the calculation from a suitable first guess for the Green's function G_0. Using this G_0 the polarization P is calculated via, Eq. (2.38). Employing P the screened interaction W can be computed via Eq. (2.37) where on the right hand side instead of W the reference interaction of the previous iteration, for the first iteration the bare Coulomb interaction, is employed. With the updated W and the reference Green's function G_0 the self-energy is calculated via Eq. (2.36). This self-energy is then plugged into the Dyson Equation. There, on the right side of Eq. (2.35) not the full Green's function is employed, but the Green's function from the previous iteration, respectively the Green's function of the reference system for the first iteration.

2.5 Partially Self-Consistent Flavors of GW

The ultimate goal of a GW calculation is to find a Green's function G which solves the GW-equations Eq. (2.4.1) self-consistently. Such a solution has important advantages. Most notably, as previously mentioned, the self-consistent solution for G may be assumed to be independent of the initial guess, at least if the effective interactions are sufficiently weak. Such calculations have been done already for molecules using the GW implementation within the FHI-Aims package (Caruso et al., 2013) and show especially that they yield solutions independent of the chosen reference Green's function.

2.5.1 GW with Fixed Screening

Typically the fully self-consistent solutions are still computationally expensive and therefore not always affordable. Hence, for large scale applications one hopes that self-consistency is

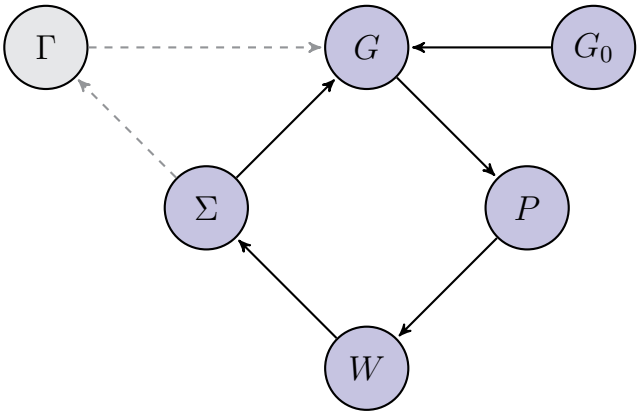

Figure 2.6: Schematic representation of the fully self-consistent GW cycle versus the exact *Hedin equations*. The arrows denote the flow of subsequent calculations in the iterative cycle. The exact Hedin equations include the full vertex functions Γ. In contrast, within GW the vertex is approximated by it's zeroth order term in an expansion of W, $\Gamma(123) \approx \delta(1-2)\delta(2-3)$. This approximation leads to a selfconsistet cycle, depicted by equations Eq. (2.35) to Eq. (2.38), to compute the interacting Green's function G. Typically this procedure is initialized by an Green's function G_0 obtained from a parent DFT or HF calculation.

not required to obtain a useful result so that a simplified and cheaper version of GW may be applied. In such cases partial self-consistency schemes are a tempting alternative.

The most time consuming part within GW is the (iterative) calculation of the polarization P. Therefore, one approach is to keep the screening (and hence the screened interaction W) fixed as given by the reference system. The self-energy $\hat{\Sigma}$ in this approximation reads

$$\hat{\Sigma}_{GW_0}(12) = \mathrm{i}G(12^+)W_0(12^+) \ . \tag{2.39}$$

Here, the self-consistency is achieved only at the level of the Green's function. The later then still has an inherent dependence on the initializing Green's function G_0.

2.5.2 Single-Shot G_0W_0

An even simpler approach is to abandon self-consistency completely and terminate the self-consistency cycle after one iteration (G_0W_0). A common procedure is to initialize this one-shot approach with an DFT based Green's function:

Employing the energies ϵ_n and the orbitals ϕ_n, which solve the Kohn-Sham equations of DFT, an initial Green's function $G^{(0)}$ can be constructed,

$$G_0(\mathbf{r}, \mathbf{r}', z) = \sum_{n=1}^{N} \frac{\phi_n(\mathbf{r})\bar{\phi}_n(\mathbf{r}')}{z - \epsilon_n + \mathrm{i}\eta\,\mathrm{sgn}(\epsilon_n - \mu)} \ , \tag{2.40}$$

which will function as a DFT-reference system.

The self-energy in G_0W_0 reads

$$\hat{\Sigma}_{G_0W_0}(12) = \mathrm{i}G_0(12^+)W_0(12^+) \ . \tag{2.41}$$

Again, a representation in energy space is employed by performing a Fourier transformation

$$\hat{\Sigma}_{G_0W_0}(\mathbf{r},\mathbf{r}',z) = \frac{\mathrm{i}}{2\pi}\int \mathrm{d}E' \ G_0(\mathbf{r},\mathbf{r}',z-E')W_0(\mathbf{r},\mathbf{r}',E')e^{(-\mathrm{i}\delta E')} \ . \tag{2.42}$$

From this self-energy, the external potential $\hat{V}_{\mathrm{ext}}$ from the Ions, and the Hartree potential $\hat{V}_{\mathrm{H}}[G_0]$ an energy-dependent non-interacting effective potential $V_{GW}(z)$ is constructed as follows:

$$V_{GW}(z) = V_{\mathrm{ext}} + V_{\mathrm{H}}[G_0] + \Sigma(z) \ . \tag{2.43}$$

The potential $\hat{V}_{\mathrm{H}}[G_0]$ is (still) calculated from the electron density of G_0, respectively the underlying (effective) non-interacting system. With the potential $V_{GW}(z)$ the G_0W_0 approach can be understood as a prescript which generates an energy dependent perturbative correction $\Delta V(z)$ to the exchange-correlation potential $\hat{V}_{\mathrm{xc}}$ from DFT given by

$$\Delta V(z) = \Sigma(z) - \hat{V}_{\mathrm{xc}} \ . \tag{2.44}$$

Employing this result, the one-body G_0W_0 Green's function $G_{G_0W_0}$ is given as

$$G^{-1}_{G_0W_0}(z) = E - H_{G_0W_0}(z) \tag{2.45}$$

with

$$H_{G_0W_0}(z) = -\frac{\nabla^2}{2m} + V_{GW}(z) \tag{2.46}$$

$$= -\frac{\nabla^2}{2m} + V_{\mathrm{H}} + V_{\mathrm{ext}} + \Sigma(z) \tag{2.47}$$

$$= -\frac{\nabla^2}{2m} + V_{\mathrm{H}} + V_{\mathrm{ext}} + \hat{V}_{\mathrm{xc}} + \Delta V(z) \ . \tag{2.48}$$

The pole positions of $G_{G_0W_0}$ respectively the QP-energies $\varepsilon_{n'}$ are found as solutions of the QP-equation (Hedin and Lundqvist, 1971),

$$\left(H_{G_0W_0}(\varepsilon_{n'}) - \varepsilon_{n'}\right)|\psi_n\rangle = 0 \ , \tag{2.49}$$

with the QP-orbitals $|\psi_n\rangle$.

In a simpler flavor of G_0W_0, one approximates the QP-orbitals with Kohn-Sham sates $\psi_n \approx \phi_n$. In this spirit, all off-diagonal elements in the QP-equation Eq. (2.49) are neglected and the QP-energies are calculated from

$$\varepsilon_{n'} \approx \langle\phi_n| - \frac{\nabla^2}{2m} + V_{\mathrm{ext}} + V_{\mathrm{H}} + \hat{V}_{\mathrm{xc}} + \Delta V(\varepsilon_{n'})\,|\phi_n\rangle \tag{2.50}$$

$$= \langle\phi_n| - \frac{\nabla^2}{2m} + V_{\mathrm{ext}} + V_{\mathrm{H}} + \hat{V}_{\mathrm{xc}}\,|\phi_n\rangle + \langle\phi_n|\,\Sigma(\varepsilon_{n'}) - \hat{V}_{\mathrm{xc}}\,|\phi_n\rangle \tag{2.51}$$

$$= \epsilon_n + \langle\phi_n|\,\Sigma(\varepsilon_{n'}) - \hat{V}_{\mathrm{xc}}\,|\phi_n\rangle \tag{2.52}$$

with the Kohn-Sham energies ϵ_n and the perturbative G_0W_0 correction from (2.44) which is given for each single energy by the matrix element $\langle\phi_n|\,\Sigma(\varepsilon_{n'}) - \hat{V}_{\text{xc}}\,|\phi_n\rangle$.

This one-shot approach does give access to perturbative corrections of the parent (effective) single-particle estimates for excitation energies. As was shown in recent studies, these corrections can be very significant reducing the discrepancy between DFT-based estimates and the experimental results by one order of magnitude. (Baumeier et al., 2012, Blase et al., 2011, Del Puerto et al., 2006, Ke, 2011, Lopez Del Puerto et al., 2008, Rostgaard et al., 2010, Sharifzadeh et al., 2012, Van Setten et al., 2013).

In spite of this success, the G_0W_0 approach is not the ultimate solution. Due to its pertubative nature the results are inherently dependent on the choice of the functional in the initializing DFT calculation. Hence, the predictive power of this approach is limited. For tuned inital guesses reliable results can be obtained from G_0W_0. Vice versa, for a bad initial guess will G_0W_0 not give reliable results. The effects of this dependence are benchmarked in Sec. 3.2.3.1.

2.6 Quasiparticle Self-Consistent *GW*

To overcome the starting point dependence and and also to calculate corrections to the DFT-based initial density, an adequate approximate scheme is quasiparticle self-consistent *GW* (qs*GW*). It does not aim at a fully self-consistent solution of the *GW*-equations but rather aims to find the (effective) single-particle Green's function closest to the full solution (in some sense).

The qs*GW* formalism is best understood in the context of G_0W_0. It is a prescription to determine the optimum effective single-particle system

$$H_{\text{eff}} = -\frac{\nabla^2}{2m} + V_{\text{H}} + V_{\text{ext}} + \tilde{\Sigma} \tag{2.53}$$

with a (effective) non-local potential $\tilde{\Sigma}$ such that the G_0W_0 perturbative correction is minimal if the Hamiltonian H_{eff} is considered as the reference rather than the KS-Hamiltonian of DFT. Based on a self-consistent perturbation theory the effective potential $\tilde{\Sigma}$ is constructed such that the time evolution determined by H_{eff} is as close as possible to that determined by $H_{G_0W_0}(z)$ in Eq. (2.47) within the random phase approximation (RPA). This optimization is typically solved in a description employing a self-consistency cycle which is visualized in Fig. 2.7.

A crucial step within the qs*GW* cycle is the approximation of the energy-dependent system $H_{G_0W_0}(z)$ by an energy independent (effective) system given by H_{eff} and especially $\tilde{\Sigma}$, respectively. There exists various approaches to construct such an optimum H_{eff} (Faleev et al., 2004, Sakuma et al., 2009, Van Schilfgaarde et al., 2006), the one which was used within this thesis is presented in more detail in Sec. 3.1.5.

To gain a physical understanding of the qs*GW* formalism, first Landau's QP-picture is recalled. The poles of the Green's function are fundamental one-particle like excitations which are denoted as quasiparticles, at least close to the Fermi energy. Within a finite time

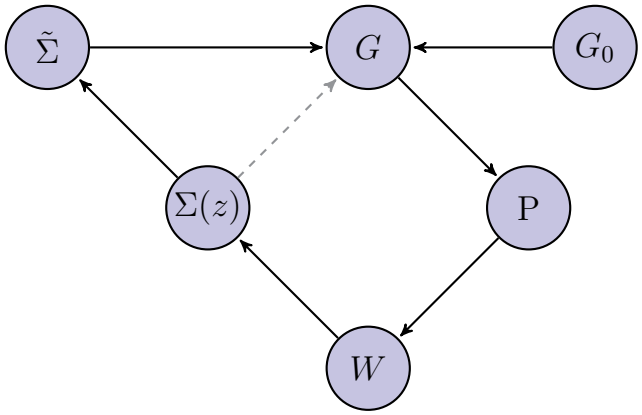

Figure 2.7: Schematic representation of the qsGW cycle. The calculated self-energy $\Sigma(z)$ at the G_0W_0 level is used to define a new effective (energy-independent) non-local potential $\tilde{\Sigma}$. Employing the solutions of the system employing the new (effective) potential $\tilde{\Sigma}$ a single particle Green's function is contructed which serves as the new starting point for the next G_0W_0 like iteration. The procedure is repeated until a stable $\tilde{\Sigma}$ respectivly a stable single-particle Green's function G is found. This method is based on a heuristic mapping from $\Sigma(z) \rightarrow \tilde{\Sigma}$.

scale t smaller then the QP-lifetimes τ_n ($t << \tau_n$) these holes/electrons live within a certain state in the molecule till the many body system relaxes. These particles can be thought of as of electrons/holes which carry a screening cloud with them. For the sake of distinction the quasiparticles carrying a screening cloud are referred to as *dressed* quasiparticles. In contrast, within qsGW one deals with another one-particle picture, the one described by H_{eff}. The solutions of H_{eff} are referred to as *bare* quasiparticles. These *bare* quasiparticles do not carry any screening cloud anymore.

The *bare* quasiparticles evolve into the dressed quasiparticles if one switches on interaction adiabatically in H_{eff}. The dressed quasiparticles again consist of a central bare quasiparticle and an induced polarization cloud consisting of other bare quasiparticles. Hence, H_{eff} represents a virtual reference system just for theoretical convenience which generates bare quasiparticles. Still, there is an ambiguity how to determine H_{eff}. Following the ideas of Van Schilfgaarde et al. (2006), as introduced in the beginning of this section, the qsGW determines H_{eff} in a self-consistent manner to find bare quasiparticles from H_{eff} which reproduce the dressed quasiparticles as best as possible.

Transferring these ideas to the Green's function language, it is convenient to split the Green's function up into two parts. A quasiparticle part G^{QP} which is weighted with a renormalization factor Z and an incoherent part $\bar{G}$.

$$G = ZG^{\text{QP}} + \bar{G} \tag{2.54}$$

The quasiparticle part G^{QP} takes account for the single particle excitations and hence exhibits a strongly energy dependent, respectively state dependent structure. This part is in addition weighted with the renormalization factor Z. The incoherent part $\bar{G}$ takes

account for the intermediate states which resemble in the many-body nature of the present problem.

The Green's function constructed from the solutions from H_{eff} takes into account only the quasiparticle part G^{QP} in the self-consistent procedure. Therefore one uses the name quasiparticle self-consistent GW (qsGW), in contrast to fully self-consistent GW (scGW). Besides neglecting $\bar{G}$ in qsGW, furthermore it is assumed that $Z = 1$, i.e. the quasiparticle is not renormalized.

2.6.1 Discussion

Neglecting the incoherent part $\bar{G}$ and assuming $Z = 1$ seems to be a rather rough approximation at the first sight. In general, the Z-factor is less than one for interacting many-body systems, which stands in contrast to the qsGW approximation. But, there is a clear argument in favor of the qsGW approximation. It follows the discussion of Kotani et al. (2007).

On the one hand, consider the exact dynamical screened Coulomb interaction denoted by W^{ex} and the exact proper polarization function P^{ex} as they are defined in the full Hedin equations. On the other hand, consider both objects in RPA W^{RPA} and P^{RPA}. The latter are the objects used within GW.

For the remainder of this section symbolic notation is used to enhance readability. The exact self-energy Σ is calculated from

$$\Sigma = G^{\text{ex}} W^{\text{ex}} \Gamma \ . \tag{2.55}$$

Within this calculation the vertex part Γ as well as the Green's function G^{ex} contribute with factors of Z. Hence, a consistent, well balanced treatment of the Z factor within G and Γ is desirable.

The integration $GW\Gamma$ is dominated by the long-range, static part of W, with $q \to 0$ and $\omega \to 0$. One finds for the insulator case,

$$\Gamma \to 1 - \frac{\delta \Sigma}{\delta \omega} = Z^{-1} \ . \tag{2.56}$$

It turns out that if Z is not equal to one, it makes a major contribution to the vertex corrections Γ, at least for the insulator case. But, for the calculation of Σ one finds a factor of Z from ZG^{QP} and the inverse factor Z^{-1} from Γ which cancel. In total there are three cases,

$$\text{exact}: \quad \Sigma = G^{\text{QP}} W^{\text{ex}} + \bar{G} W^{\text{ex}} Z^{-1} \ , \tag{2.57}$$

$$\text{qs}GW: \quad \Sigma = G^{\text{QP}} W^{\text{RPA}} \ , \tag{2.58}$$

$$\text{sc}GW: \quad \Sigma = Z G^{\text{QP}} W^{\text{RPA}} + \bar{G} W^{\text{RPA}} \ . \tag{2.59}$$

The incoherent contribution $\bar{G}$ can be assumed to be rather structureless and and energy independent. Therefore is $\bar{G}$ expected to cause a simple shift in the chemical potential.

Hence, one finds that the approximation $\Sigma \approx G^{\mathrm{QP}} W^{\mathrm{RPA}}$ reproduces characteristic features of the exact solution. But, it is still in question which Z does W^{RPA} collect in comparison to W^{ex}.

For the screened Coulomb interaction $W = v(1 - vP)^{-1}$ the Polarization P is rewritten employing the two particle Green's Fucntions G_2, as follows

$$P(14) = \bar{P}(11;44) \tag{2.60}$$
$$= G_2 + G_2 I \bar{P} \ . \tag{2.61}$$

Here, I represents the two-particle irreducible kernel which introduces all the steps from the ladder diagrams. If one considers a pertubative expansion which begins from a non-interaction Green's function, all renormalization contributions can only be introduced via the pair excitations of the intermediate states of $\bar{P}$. Therefore the derivative of $\bar{P}$ with respect to the number of the intermediate states of $\bar{P}$ is considered. Following Kotani et al. (2007) it is

$$\Delta P(14) = \Gamma(122) \Delta G_2(22'; 33') \Gamma(4\,3'3) \ . \tag{2.62}$$

The two particle Green's function contributes with a weight of Z^2 because it contains $ZG^{\mathrm{QP}} \times ZG^{\mathrm{QP}}$. This combines with the two Z^{-1} contributions from the Γ contributions, following Eq. (2.56), again to a cancellation of the Z factors. Thus, if one starts from a non-interacting Green's function the Polarization function won't introduce any renormalization factor $Z < 1$. This is the commonly called Z-factor cancellation mechanism which has been shown by Bechstedt et al. (1997) also in practice.

Hence, it is shown that the consideration of only the quasiparticle part G^{QP} with $Z = 1$ within qsGW introduces a consistent treatment of the Z-factor. In contrast does the full scGW assumes on the one hand $Z \neq 1$ for the Green's function but on the other hand ignores the Z-factor contributions from the vertex corrections Γ. In addition, did these considerations show that one is consistent with the exact treatment if one assumes $Z = 1$.

Chapter 3

3 New Formulation: Quasiparticle Self-Consistent GW for Molecular Matter

The previous chapter discussed the diagrammatic derivation of GW and approximate approaches to solve the GW-equations.

On the basis of the spectral-representation of the Green's function an iteratively connected expression is developed, which is related to the quasiparticle (QP-)equation. In the iterative approach, the most challenging task is the calculation of matrix elements of the self-energy. The approach to solve for such matrix elements is described in detail. To reduce the computational effort, several tricks are introduced.

3.1 Quasiparticle Self-Consistent GW Formalism in a Basis of Local Orbitals

The previous chapter introduced the concept of the qsGW in a general framework. In this section, the approach is adopted for localized basis sets suitable for the application to molecules.

3.1.1 Spectral Representation of the Green's function

The (quasi-spectral) Lehmann representation of the Green's function G is recalled, with QP-orbitals $\{\psi_{r,n}(\mathbf{r}, z), \psi_{l,n}(\mathbf{r}', z)\}$ and QP-energies $\{\varepsilon_n(z)\}$

$$G(\mathbf{r}, \mathbf{r}', z) = \sum_n \frac{\psi_{r,n}(\mathbf{r}, z)\psi_{l,n}^{(i)\,\dagger}(\mathbf{r}', z)}{z - \varepsilon_n(z) + i\eta \mathrm{sgn}(\varepsilon_n(z) - \eta)} \quad . \tag{3.1}$$

The indices r and l denote right and left eigenvectors. The energies $\{\varepsilon_n(z)\}$ follow the pole-condition

$$z - \varepsilon_n(z) = 0 \quad , \tag{3.2}$$

The superscript † denotes the conjugate transpose. The running index (i) accounts for the iterative nature of the GW formalism.

3.1.2 Iterative Flow of the Green's function

To employ an iterative scheme a prescription $G^{(i-1)}(\mathbf{r},\mathbf{r}',z) \rightarrow G^{(i)}(\mathbf{r},\mathbf{r}',z)$ is needed. The tactic is to iteratively connect the QP-orbitals $\{\psi_{r,n}(\mathbf{r},z),\psi_{l,n}(\mathbf{r},z)\}$ of single iterations (i) of the GW-scheme via matrices $\mathfrak{A}_{n\underline{n}},\tilde{\mathfrak{A}}_{n\underline{n}}$ as follows

$$\psi^{(i)}_{r,n}(\mathbf{r},z) = \sum_{\underline{n}} \mathfrak{A}^{(i)}_{n\underline{n}}(z)\psi^{(i-1)}_{\underline{n}}(\mathbf{r},z) \ , \tag{3.3}$$

$$\psi^{(i)}_{l,n}(\mathbf{r},z) = \sum_{\underline{n}} \tilde{\mathfrak{A}}^{(i)}_{n\underline{n}}(z)\bar{\psi}^{(i-1)}_{\underline{n}}(\mathbf{r},z) \ , \tag{3.4}$$

where the bar in $\bar{\psi}$ denotes the transpose. Employing the representation Eq. (3.1) a solution of the Dyson equation Eq. (2.28) is constructed . In the region where the imaginary part of the self-energy is small, following the spirit of Fermi-liquid theory, the QP-orbitals and the QP-energies satisfy the QP-equations,

$$\left(\varepsilon_n(z) - \hat{\mathcal{H}}_{\mathrm{H}} - \hat{\Sigma}(\mathbf{r},\mathbf{r}',z)\right)\psi_{r,n}(\mathbf{r}',z) = 0 \ , \tag{3.5}$$

$$\psi_{l,n}(\mathbf{r},z)\left(\varepsilon_n(z) - \hat{\mathcal{H}}_{\mathrm{H}} - \hat{\Sigma}(\mathbf{r},\mathbf{r}',z)\right) = 0 \ . \tag{3.6}$$

To improve the readability, in these two equations the integration of the inner spatial indices is implicated. Furthermore, the running index of the GW iterations will be omitted for the following derivations and recalled in the end.

The formulation of a numerical scheme to solve these equations is possible, but the computational effort to find a solution is high mainly due to in total four reasons: First, the computation of such a solution needs the introduction of a basis that is capable of the description of the energy dependence of the orbitals; the dimensionality of the problem is increased. Second, the closing of the full GW scheme requires a numerical integration over the energy if one takes account for the energy-dependence of the orbitals. Third, the energy-dependent self-energy is non-Hermitian. Hence, a separate treatment of left and right eigenvectors is necessary. Last, each pole requires the separate the solution of the QP-equation. Therefore, each GW iteration would generate a full set of new poles. Therefore, the number of poles would increase exponentially with the number of iterations. Furthermore, each pole itself in turn requires a separate diagonalization of the QP-equation, which causes intractable computational effort.

In a central step, qsGW introduces an approximation to overcome the effort due to the energy dependence of the self-energy. Within qsGW, the non-local, energy-dependent self-energy $\hat{\Sigma}(\mathbf{r},\mathbf{r}',z)$ is mapped on an effective, non-local, energy independent, and Hermitian potential $\tilde{\Sigma}(\mathbf{r},\mathbf{r}')$,

$$\hat{\Sigma}(\mathbf{r},\mathbf{r}',z) \rightarrow \tilde{\Sigma}(\mathbf{r},\mathbf{r}') \ . \tag{3.7}$$

Using this approximation, the operator in Eq. (3.5) and Eq. (3.6) becomes energy independent and Hermitian. Therefore, the separation between the left and right QP-orbitals is omitted,

$$\psi_{r,n}(\mathbf{r}, z) \to \psi_n(\mathbf{r}) \ , \tag{3.8}$$

$$\psi_{l,n}(\mathbf{r}, z) \to \overline{\psi}_n^{\,(i+1)}(\mathbf{r}) \ . \tag{3.9}$$

Hence, instead of two transformation matrices from Eq. (3.3) and Eq. (3.4) only one single transformation matrix $\mathfrak{A}_{n\underline{n}}$ is needed to describe the iterative connection between the orbitals of the *GW* iterations (i) and $(i-1)$

$$\psi_n^{(i)}(\mathbf{r}) = \sum_{\underline{n}} \mathfrak{A}_{n\underline{n}}^{(i)} \psi_{\underline{n}}^{(i-1)}(\mathbf{r}) \ . \tag{3.10}$$

Employing the energy independent potential $\tilde{\Sigma}(\mathbf{r}, \mathbf{r}')$, Eq. (3.7) and the prescription Eq. (3.10) lets the QP-equations Eq. (3.5) and Eq. (3.6) coincide. The problem is written in the following way, again suppressing the running index of the *GW* iterations,

$$\hat{\mathcal{H}}_{\mathrm{H}} \sum_{\underline{n}} \mathfrak{A}_{n'\underline{n}} \, \psi_{\underline{n}}(\mathbf{r}) + \int \mathrm{d}\mathbf{r}' \tilde{\Sigma}(\mathbf{r}, \mathbf{r}') \sum_{\underline{n}} \mathfrak{A}_{n'\underline{n}} \, \psi_{\underline{n}}(\mathbf{r}') = \varepsilon_{n'} \sum_{\underline{n}} \mathfrak{A}_{n'\underline{n}} \, \psi_{\underline{n}}(\mathbf{r}) \ . \tag{3.11}$$

In this effective single-particle description the orbitals $\{\psi_n(\mathbf{r})\}$ are orthonormal by construction. Multiplication with $\overline{\psi}_n(\mathbf{r})$ from the left and full integration $\int \mathrm{d}\mathbf{r}$ leads from Eq. (3.11) to

$$\sum_{\underline{n}} \mathfrak{A}_{n'\underline{n}} \int \mathrm{d}\mathbf{r} \, \overline{\psi}_n(\mathbf{r}) \hat{\mathcal{H}}_{\mathrm{H}} \psi_{\underline{n}}(\mathbf{r}) + \sum_{\underline{n}} \mathfrak{A}_{n'\underline{n}} \int \mathrm{d}\mathbf{r} \int \mathrm{d}\mathbf{r}' \, \overline{\psi}_n(\mathbf{r}) \tilde{\Sigma}(\mathbf{r}, \mathbf{r}') \, \psi_{\underline{n}}(\mathbf{r}')$$
$$= \varepsilon_{n'} \sum_{\underline{n}} \mathfrak{A}_{n'\underline{n}} \int \mathrm{d}\mathbf{r} \, \overline{\psi}_n(\mathbf{r}) \psi_{\underline{n}}(\mathbf{r}) \ . \tag{3.12}$$

Introducing the bracket notation $\psi_n(\mathbf{r}) = \langle \mathbf{r} | n \rangle$ simplifies Eq. (3.12) to

$$\sum_{\underline{n}} \mathfrak{A}_{n'\underline{n}} \, \langle n | \, \hat{\mathcal{H}}_{\mathrm{H}} \, | \underline{n} \rangle + \sum_{\underline{n}} \mathfrak{A}_{n'\underline{n}} \langle n | \, \tilde{\Sigma} \, | \underline{n} \rangle = \varepsilon_{n'} \sum_{\underline{n}} \mathfrak{A}_{n'\underline{n}} \, \langle n | \underline{n} \rangle \ . \tag{3.13}$$

Taking advantage of the orthonormality of the QP-orbitals implies,

$$\sum_{\underline{n}} \mathfrak{A}_{n'\underline{n}} \, \langle n | \, \hat{\mathcal{H}}_{\mathrm{H}} \, | \underline{n} \rangle + \sum_{\underline{n}} \mathfrak{A}_{n'\underline{n}} \langle n | \, \tilde{\Sigma} \, | \underline{n} \rangle = \varepsilon_{n'} \sum_{\underline{n}} \mathfrak{A}_{n'\underline{n}} \, \delta_{n,\underline{n}} \tag{3.14}$$

$$\sum_{\underline{n}} \mathfrak{A}_{n'\underline{n}} \, \langle n | \, \hat{\mathcal{H}}_{\mathrm{H}} + \tilde{\Sigma} \, | \underline{n} \rangle = \varepsilon_{n'} \mathfrak{A}_{n'n} \ . \tag{3.15}$$

In the last equation, the problem takes the typical form of a linear matrix equation for each single n'. Hence, under the assumption that the matrix elements $\langle n | \, \hat{\mathcal{H}}_{\mathrm{H}} \, | \underline{n} \rangle$ and $\langle n | \, \tilde{\Sigma} \, | \underline{n} \rangle$ are known, the qs*GW* cycle can be closed as follows:

(0) guess initial parent $G^{(0)}$ (from DFT or HF)

(1) calculate all matrix elements $\left\langle n^{(i)}\right| \hat{\mathcal{H}}_{\mathrm{H}} \left|\underline{n}^{(i)}\right\rangle$ and $\left\langle n^{(i)}\right| \tilde{\Sigma^{(i)}} \left|\underline{n}^{(i)}\right\rangle$

(2) calculate $\varepsilon_{n'}^{(i+1)}$ and $\mathfrak{A}_{n'\underline{n}}^{(i+1)}$ by diagonalizing Eq. (3.15)

(3) calculate $\left|n^{(i+1)}\right\rangle$ respectively $\psi_n^{(i+1)}(\mathbf{r})$ from Eq. (3.10) using $\mathfrak{A}_{n'\underline{n}}^{(i+1)}$

(4) construct updated, non-interacting Green's function $G^{(i+1)}$

$$G^{(i+1)}(\mathbf{r},\mathbf{r}',E) = \sum_n \frac{\psi_n^{(i+1)}(\mathbf{r})\overline{\psi}_n^{(i+1)}(\mathbf{r}')}{E-\varepsilon_n^{(i+1)}+\mathrm{i}\eta\mathrm{sgn}(\varepsilon_n^{(i+1)}-\eta)} \ . \tag{3.16}$$

(5) return to step (1) replacing $G^{(i)}$ and $\left|n^{(i)}\right\rangle$ with its updates $G^{(i+1)}$ and $\left|n^{(i+1)}\right\rangle$

This procedure is iterated until the Green's function $G^{(i+1)}$ from $G^{(i)}$ meet the convergence criteria introduced in Sec. 3.2.2.

Further details are discussed in separate sections. In Sec. 3.1.3 step **(0)** is discussed. See Sec. 3.1.4 for details on step **(1)**.

3.1.3 Initialization from a Free Particle Green's function

In this section the initialization of the iterative cycle (step **(0)**) is discussed in more detail.

Up to now the Green's function is expressed with respect to an initial set of orbitals $\psi_n^{(0)}(\mathbf{r})$ and an initial set of pole positions $\varepsilon_n^{(0)}$. The obvious choice for the initial Green's function is the Hartree Green's function G_{H}. This corresponds to the non-interaction reference in the original derivation of the GW scheme. G_{H} can be constructed from the eigenstates $\phi_n(\mathbf{r})$ and the eigenvalues ϵ_n of the Hartree-Hamiltonian $\hat{\mathcal{H}}_{\mathrm{H}}$, see Eq. (A.5). As already discussed in Sec. 2.5.2, alternative starting points are also possible and in fact might exhibit a faster convergence behavior. Indeed, DFT or HF, tend to be closer to the fixed point solution compared to G_{H} (e.g. Hybertsen and Louie, 1986, Rostgaard et al., 2010). Hence, in this work an initial reference Green's function,

$$G^{(0)}(\mathbf{r},\mathbf{r}',E) = \sum_n \frac{\psi_n^{(0)}(\mathbf{r})\psi_n^{(0)*}(\mathbf{r}')}{E-\varepsilon_n^{(0)}+\mathrm{i}\eta\mathrm{sgn}(\epsilon_n-\eta)} \ , \tag{3.17}$$

is constructed using eigenstates $\psi_n^{(0)}(\mathbf{r})$ and eigenvalues $\varepsilon_n^{(0)}$ from a DFT or HF-type calculation. In Sec. 3.2.3.1, an analysis is performed to find the optimum starting point.

3.1.4 Calculation of the Matrix Elements of the Self-Energy

In this section step **(1)** in the iterative procedure is discussed. The task is to calculate the matrix elements $\langle n|\,\hat{\mathcal{H}}_{\mathrm{H}}\,|\underline{n}\rangle$ and $\langle n|\,\tilde{\Sigma}\,|\underline{n}\rangle$. Hartree type matrix elements are provided

by most standard quantum chemistry methods, whether it is DFT, HF, or the advanced wave function based methods. Hence, the calculation is done by employing already existing routines in TURBOMOLE (Ahlrichs et al., 1989)[1]. The self-energy contributions are dealt with in the same way as a previous G_0W_0 implementation within TURBOMOLE (Van Setten et al., 2013). A small extension is necessary though, since the previous implementation has been done only for diagonal matrix elements, while qsGW requires off-diagonal contributions $\langle n|\,\tilde{\Sigma}\,|\underline{n}\rangle$ for general (QP-)orbitals $\psi_{n/\underline{n}}(\mathbf{r})$. The method for the calculation of the matrix elements $\langle n|\,\Sigma(z)\,|\underline{n}\rangle$ including the full energy dependence is outlined in this chapter. The subsequent approximation, neglecting the energy dependence, is performed in Sec. 3.1.5.

To find a solution for the screened interaction W via the Polarization function P as it is depicted in Eq. (2.37), an inversion is required. This becomes obvious if one recalls the dielectric function ϵ,

$$\epsilon(12) = \delta(12) - \int \mathrm{d}(3) v(13) P(32) \ , \tag{3.18}$$

with the bare Coulomb interaction v, and cast the expression Eq. (2.37) into the more convenient form

$$W(12) = \int \mathrm{d}(3) \epsilon^{-1}(13) v(32) \ . \tag{3.19}$$

As before, the coordinate 1, 2,... represent four coordinates of a particle: space and time $(1) = (\mathbf{r}_1, t_1)$. The spin index is suppressed. The inverse ϵ^{-1} is implicitly implemented in the standard TURBOMOLE package since it features the determination of optical excitation spectra. The full density response χ calculated in TURBOMOLE is related to the inverse of the dielectric function ϵ by

$$\epsilon^{-1}(12) = \delta(12) + \int \mathrm{d}(3) v(13) \chi(32) \ . \tag{3.20}$$

Hence, the screened interaction W is related to the full dielectric response χ via

$$W(12) = v(12) + \int \mathrm{d}(34) v(13) \chi(34) v(42) \ , \tag{3.21}$$

which translates into the frequency domain as,

$$W(\omega) = v + v \cdot \chi(\omega) \cdot v \ . \tag{3.22}$$

Here, the spatial indices are suppressed by the application of a matrix notation where $A \cdot B$ stands for $\int \mathrm{d}\mathbf{r}'' A(\mathbf{r}, \mathbf{r}'') B(\mathbf{r}'', \mathbf{r}')$ and AB for $A(\mathbf{r}, \mathbf{r}') B(\mathbf{r}, \mathbf{r}')$.

The full response function $\chi(\omega)$ is specified in the spectral representation in terms of its residues in the complex plane and the transition densities ρ_m. It reads, with $z = \omega + \mathrm{i}2\eta$,

$$\chi(\mathbf{r}, \mathbf{r}', \omega) = \sum_m \rho_m(\mathbf{r}) \rho_m \mathbf{r}') \left(\frac{1}{z - \Omega_m} - \frac{1}{z^* + \Omega_m} \right) \ . \tag{3.23}$$

[1] Although the calculation of Hartree matrix elements is a well established task, they can be difficult to extract because they do not usually appear isolated (in the code) from other terms unwanted here.

The singularities Ω_m are the charge neutral excitation energies. The index m runs over all single particle-hole excitations. The number equals the product of the number of occupied states times the number of unoccupied states, respectively. For the calculation of $\chi(\omega)$, the relation to the Polarization function P is recalled,

$$\chi(\omega) = P(\omega) + P(\omega) \cdot v \cdot \chi(\omega) \ . \tag{3.24}$$

The inversion leads to the relation

$$\chi^{-1}(\omega) = P^{-1}(\omega) - v \ . \tag{3.25}$$

Here, the rather easily calculated inverse $P^{-1}(\omega)$ and the inverse $\chi^{-1}(\omega)$ enter. The inversion of $P(\omega)$ is done employing, a spectral representation in the space of the QP-orbitals $\psi_n(\mathbf{r})$

$$P(\mathbf{r},\mathbf{r}',\omega) = \sum_i \sum_a \psi_a^*(\mathbf{r})\psi_n(\mathbf{r})\psi_i^*(\mathbf{r}')\psi_a(\mathbf{r}')\left[\frac{1}{z-(\varepsilon_a-\varepsilon_i)} - \frac{1}{z^*+(\varepsilon_a-\varepsilon_i)}\right] \ . \tag{3.26}$$

Here, the lower index i sums over all occupied states and the index a over all unoccupied states.

The inversion of $\chi(\omega)$ is performed efficiently within TURBOMOLE as introduced in the following. The poles Ω_m are directly obtained from analyzing the inverse of the spectrum of χ. Namely, the poles $z = \Omega_m$ of $\chi(\omega)$ correspond to zero eigenvalues of χ^{-1}. Hence, the pole positions are calculated by the computation of the combination of z and $\xi^{(m)}$ such that $\chi^{-1}(z)\xi^{(m)} = 0$ has a solution, explicitly

$$(P^{-1}(\Omega_m) - v)\xi^{(m)} = 0 \ . \tag{3.27}$$

With $\xi^{(m)}$ one finds, in the end, expansion coefficients to express the transition densities $\rho_m(\mathbf{r})$ in terms of $\psi_n(\mathbf{r})$. The full derivation can be found in (Van Setten et al., 2013).

For the subsequent derivation of the final expression of the self-energy, it is taken advantage of Eq. (3.21). This expression allows to split up the self-energy into an energy independent, Hermitian exchange $\hat{\Sigma}_\mathrm{x}$ and an energy-dependent correlation $\hat{\Sigma}_\mathrm{c}(E)$ part

$$\hat{\Sigma}(E) = \hat{\Sigma}_\mathrm{x} + \hat{\Sigma}_\mathrm{c}(E) \ , \tag{3.28}$$

$$\hat{\Sigma}_\mathrm{x} = \frac{\mathrm{i}}{2\pi}\int \mathrm{d}\omega \ e^{-\mathrm{i}\omega 0^+} G(E-\omega)v \ , \tag{3.29}$$

$$\hat{\Sigma}_\mathrm{c}(E) = \frac{\mathrm{i}}{2\pi}\int \mathrm{d}\omega \ e^{-\mathrm{i}\omega 0^+} G(E-\omega)v\cdot\chi(\omega)\cdot v \ . \tag{3.30}$$

The correlation part of the self-energy, Eq. (3.30) is rewritten employing the spectral representation of the Green's function. It reads, non-interacting QP-states,

$$A(\mathbf{r},\mathbf{r}',E) = \sum_n \psi_n(\mathbf{r})\bar{\psi}_n(\mathbf{r})\delta(E-\varepsilon_n) \ . \tag{3.31}$$

Hence, the Green's function in (quasi-spectral) Lehmann representation Eq. (3.1) can be written as follows,

$$G(E) = \int_{-\infty}^{\infty} \mathrm{d}E \frac{A(E')}{E - E' + \mathrm{i}\eta \mathrm{sgn}(E' - \mu)} \quad . \tag{3.32}$$

Combining the previous expression for $\hat{\Sigma}_\mathrm{x}$ in Eq. (3.29), the spectral function Eq. (3.31) and the quasi-spectral representation of the Green's function, Eq. (3.32), allows to write an expression for the matrix element of the exchange part of the self-energy $\hat{\Sigma}_\mathrm{x}$ in the QP-orbital space:

$$\langle n| \Sigma_\mathrm{x} |n'\rangle = \langle n| - \int_{-\infty}^{\mu} \mathrm{d}E' A(E' - \mu) \cdot v \, |n'\rangle \tag{3.33}$$

$$= \sum_{\underline{n}} \left\langle \psi_n(\mathbf{r}) \psi_{\underline{n}}(\mathbf{r}') \right| - \int_{-\infty}^{\mu} \mathrm{d}E' \delta(E' - \varepsilon_{\underline{n}}) \cdot v(\mathbf{r}, \mathbf{r}') \left| \psi_{n'}(\mathbf{r}') \psi_{\underline{n}}(\mathbf{r}) \right\rangle \tag{3.34}$$

$$= \sum_{\underline{n}}^{\mathrm{occ}} (n\underline{n}|\underline{n}n') = \sum_i (ni|in') \tag{3.35}$$

with the common notation of so called Coulomb-exchange integrals

$$(pq|rs) = \int \mathrm{d}\mathbf{r} \int \mathrm{d}\mathbf{r}' p(\mathbf{r}) q(\mathbf{r}) v(\mathbf{r}, \mathbf{r}') r(\mathbf{r}') s(\mathbf{r}') \quad . \tag{3.36}$$

The numerical integration associated with the calculation of Coulomb-exchange integrals, Eq. (3.36), is the computationally most demanding step in the presented routine. Fortunately, there exist optimized routines for the evaluation of such integrals. Furthermore, there exist well-tested and efficient approximations to speed up the calculation of such integrals. Eichkorn et al. (1995) and Weigend (2006) implemented into TURBOMOLE an approximation which employs a density fitting, also called "resolution of the identity" (RI). The central step in this approach is to approximate products of basis functions by a series of so-called auxiliary basis functions. For all calculations presented in this thesis the RI approximation will always be applied.

The right hand side term in Eq. (3.35) is identical to the exact exchange (Fock) contribution from the HF formalism. Therefore, the neglect of the correlation self-energy Eq. (3.30) in the qsGW formalism leads to the HF solution.

So far, the calculation of the exchange contribution Σ_x was discussed. Now, the correlation part of the self-energy $\hat{\Sigma}_\mathrm{c}(E)$ is considered. Plugging the spectral function Eq. (3.31) and the Lehmann representation of the Green's function Eq. (3.32) into the expression for $\hat{\Sigma}_\mathrm{c}(E)$ and performing the energy integration gives

$$\langle n| \Sigma_\mathrm{c}(E) |n'\rangle = \sum_m \sum_{\underline{n}} \frac{(n\underline{n}|\rho_m)(\rho_m|n'\underline{n})}{E - \varepsilon_{\underline{n}} - Z_m \mathrm{sgn}(\varepsilon_{\underline{n}} - \mu)} \quad , \tag{3.37}$$

with $Z_m = \Omega_m - 3\mathrm{i}\eta$.

As mentioned before, the transition densities ρ_m are expressed in terms of QP-states. Hence, the objects $(n\underline{n}|\rho_m)$, which appear in the nominator of Eq. (3.37), take the form of

coulomb exchange integrals, Eq. (3.36), too. Therefore, it is possible to take advantage of established routines and approximations for the calculation of the correlation part of the self-energy Σ_c.

Due to the mapping on a Hermitian problem, only the real part of the self-energy Eq. (3.37) is needed within qsGW. Taking this into account, the sum over all poles $\varepsilon_{\underline{n}}$ is split up into the sum over the poles above the real axis, labeled with the index a, and the sum of the poles below the real axis, labeled with the index i,

$$\langle n|\,\Sigma_\mathrm{c}(E)\,|n'\rangle = \sum_m \left[\sum_{\underline{n}} \frac{(\underline{n}n|\rho_m)(\rho_m|n'\underline{n})}{E-\varepsilon_n - Z_m \mathrm{sgn}(\varepsilon_{\underline{n}}-\mu)}\right] \tag{3.38}$$

$$= \sum_m \left[\sum_i^{\mathrm{occ}} \frac{(in|\rho_m)(\rho_m|n'i)}{E-\varepsilon_i+(\Omega_m-3\mathfrak{i}\eta)} + \sum_a^{\mathrm{unocc}} \frac{(an|\rho_m)(\rho_m|n'a)}{E-\varepsilon_a-(\Omega_m-3\mathfrak{i}\eta)}\right] . \tag{3.39}$$

Within qsGW only the real part of Σ_c is taken into account. It reads, after the expansion with the complex conjugate of the denominator, employing the minimal shift $3\eta \to \bar{\eta}$,

$$\begin{aligned}\mathrm{Re}\left(\langle n|\,\Sigma_\mathrm{c}(E)\,|n'\rangle\right) = \sum_m \Bigg[&\sum_i^{\mathrm{occ}} (in|\rho_m)(\rho_m|n'i) \times \frac{E-\varepsilon_i+\Omega_m}{(E-\varepsilon_i+\Omega_m)^2+\bar{\eta}} \\ &+ \sum_a^{\mathrm{unocc}} (an|\rho_m)(\rho_m|n'a) \times \frac{E-\varepsilon_a-\Omega_m}{(E-\varepsilon_a-\Omega_m)^2+\bar{\eta}}\Bigg] .\end{aligned} \tag{3.40}$$

In the actual numerical calculation of the correlation part of the self-energy Σ_c the shift $\bar{\eta}$ is chosen so small that all (orbital-)energies are converged within 1 meV. Typically $\eta = 1\,\mathrm{meV}$ satisfies this condition.

Each GW iteration step requires the reevaluation of several objects. First, the Hartree Contribution $\left\langle n^{(i)}\right|\hat{\mathcal{H}}_\mathrm{H}\left|n'^{(i)}\right\rangle$ originating from the updated orbitals is recalculated, with the running index (i) of the GW iteration. Second, all Coulomb-exchange integrals, Eq. (3.36), which give the exchange part of the self-energy via

$$\left\langle n^{(i)}\right|\Sigma_\mathrm{x}^{(i)}\left|n'^{(i)}\right\rangle = \sum_i (ni|in')^{(i)} \ . \tag{3.41}$$

Third, the recalculation of all single particle-hole excitation densities ρ_m and energies Ω_m is essential. Then follows the construction of the correlation part of the self-energy,

$$\begin{aligned}\mathrm{Re}\left(\left\langle n^{(i)}\right|\Sigma_\mathrm{c}^{(i)}(E)\left|n'^{(i)}\right\rangle\right) = \sum_m \Bigg[&\sum_i^{\mathrm{occ}} (in|\rho_m)^{(i)}(\rho_m|n'i)^{(i)} \times \frac{E-\varepsilon_i^{(i)}+\Omega_m^{(i)}}{(E-\varepsilon_i^{(i)}+\Omega_m^{(i)})^2+\bar{\eta}} \\ &+ \sum_a^{\mathrm{unocc}} (an|\rho_m)^{(i)}(\rho_m|n'a)^{(i)} \times \frac{E-\varepsilon_a^{(i)}-\Omega_m^{(i)}}{(E-\varepsilon_a^{(i)}-\Omega_m^{(i)})^2+\bar{\eta}}\Bigg] ,\end{aligned} \tag{3.42}$$

again with iteration index (i) on all updated objects. In a last step the QP-equation, (3.15), is diagonalized employing the (approximated) self-energy $\tilde{\Sigma}^{(i)}$.

3.1.5 Quasi-Static Approximation of the Self-Energy

The crucial step in qsGW in comparison to the fully scGW is the approximation of the self-energy at a (energy-independent) non-local potential. The chosen approach is

$$\langle n|\,\tilde{\Sigma}\,|\underline{n}\rangle = \frac{1}{2}\Big(\,\langle n|\,\hat{\Sigma}(\varepsilon_{n'})\,|\underline{n}\rangle\,\delta_{nn'} + \langle n|\,\hat{\Sigma}(\varepsilon_{n'})\,|\underline{n}\rangle\,\delta_{n\underline{n}}\Big)\ . \tag{3.43}$$

In literature one finds different approaches for such approximate self-energies (Faleev et al., 2004, Sakuma et al., 2009, Van Schilfgaarde et al., 2006). However, so far they have been used in the context of extended, periodic systems. This work deals with finite systems and in this respect the application is new.

One argument for the approach from Eq. (3.7) is as follows: To find a suitable approximation, a norm M, which measures the deviations of the effective system $\hat{\mathcal{H}}_{\text{eff}}$, Eq. (2.53) to the real energy-dependent system $H(z)$,

$$\Delta V(z) = H(z) - \hat{\mathcal{H}}_{\text{eff}} \tag{3.44}$$

is needed. Van Schilfgaarde et al. (2006) suggest

$$M[\tilde{\Sigma}] = \mathrm{Tr}\Big[\Delta V\delta(z-\hat{\mathcal{H}}_{\text{eff}})\{\Delta V\}^{\dagger}\Big] + \mathrm{Tr}\Big[\{\Delta V\}^{\dagger}\delta(z-\hat{\mathcal{H}}_{\text{eff}})\Delta V\Big] \tag{3.45}$$

as such a norm, where the trace Tr is taken over spatial and energy indices. Due to the energy-dependence of $\Delta V(z)$, exact minimization of M is not achievable. Nevertheless, an approximate solution can be found.

If one considers only the first part of the norm M, Eq. (3.45), and ignores for the moment the restriction that $\tilde{\Sigma}$ needs to be Hermitian the trivial minimum is $M[\tilde{\Sigma}] = 0$ with $\tilde{\Sigma} = \sum_{ij}|\Psi_i\rangle\,\Sigma(\varepsilon_j)\,\langle\Psi_j|$ where $\{\Psi_i, \varepsilon_i\}$ are eigenfunctions and eigenvalues of $\hat{\mathcal{H}}_{\text{eff}}$. The minimum of M taking only the second part into account is similiar, with $\Sigma(\varepsilon_i) \to \Sigma(\varepsilon_j)$. Therefore, one finds a Hermitian minimum solution by taking the average, which gives Eq. (3.43). In this sense, the approximation from Eq. (3.43) minimizes the deviation of the effective energy-independent system and the energy-dependent system, Eq. (3.44).

3.1.6 Consistency Check of the Quasi-Static Approximation

The static self-energy of the qsGW formalism, Eq. (3.43), allows for another interpretation of the self-consistency cycle. Within qsGW an effective single particle picture is employed where the final fixed point solution for the static self-energy can be understood as an effective, non-local, energy-independent potential.

To test whether this approximation is valid some results are fetched ahead. The reference results are obtained from a technique suggested in Sec. 5.2.1.2, the so-called 2nd-order framework. It accounts for the full energy dependence of the self-energy in a self-consistent solution of the QP-equation. Furthermore, this approach gives results nearly identical to the full-diagonalizing solution of the QP-equation.

The application of the 2nd-order framework, Sec. 5.2.1.2, on the fixed point solution of the qsGW-cycle is a method to compare results obtained from approximate quasi-static self-energies to results employing to the full, energy-dependent self-energy. In this way the stability of the qsGW solution in relation to the solution of the QP-equation with full energy dependence is tested. A comparison to the full GW result would require further iterations within the GW cycle.

Fig. 3.1 shows the first Ionization Potential (IP) energies obtained from qsGW and results where the 2nd-order framework was applied on top of qsGW results. Within the Green's function formalism the first IP is given by the energy of the highest occupied molecular orbital (HOMO). It is the minimum energy needed to remove one electron from the molecule and lift it to the vacuum energy level. The (first) IP is a standard observable for testing electronic structure methods for several reasons, which are discussed in Sec. 4.2.1. All in all, it is a good first measure for the accuracy of a method and typically yields as a first benchmark for the accuracy of electronic structure calculations. Results show that the application of the 2nd-order framework gives results nearly identical to qsGW. The maximum difference between the energy-dependent solution and the results employing the quasi-static self-energy is below 10 meV. Results for higher IPs are exemplary shown for the molecule Naphthalene in Fig. 3.2. There, the maximum distance between the poles of the combined approach and the qsGW approach is below 10 meV, too.

Overall, the agreement between both results is very good. This indicates, first, that especially the self-energy is diagonal in the converged qsGW system. Second, it indicates that the static approximation, Eq. (3.43), for the self energy is a very good and reliable choice.

3.2 Technical Details

In this section essential numerical parameters are specified. First, the realization of the QP-orbitals in a local basis set is introduced in Sec. 3.2.1, including a study which shows the dependence of qsGW results on the choice of the basis. Second, the chosen convergence criteria which prompts the exit of the iterative qsGW cycle are presented in Sec. 3.2.2.

3.2.1 Convergence with the Basis Set

The field of application of the presented qsGW implementation are molecules and nano-size structures. That do not usually exhibit a high degree of symmetry. Hence, a formulation in terms of a local basis is appropriate.

To implement the basis functions, it is taken advantage of the TURBOMOLE package which comes with different groups of basis functions, i.e. basis sets. All basis functions contained in TURBOMOLE are of the contracted Gaussian type, which is introduced in Sec. 3.2.1.1.

In general, the implementation of qsGW of this thesis can work with any basis set that is implemented in the TURBOMOLE package. For the benchmarks and results presented

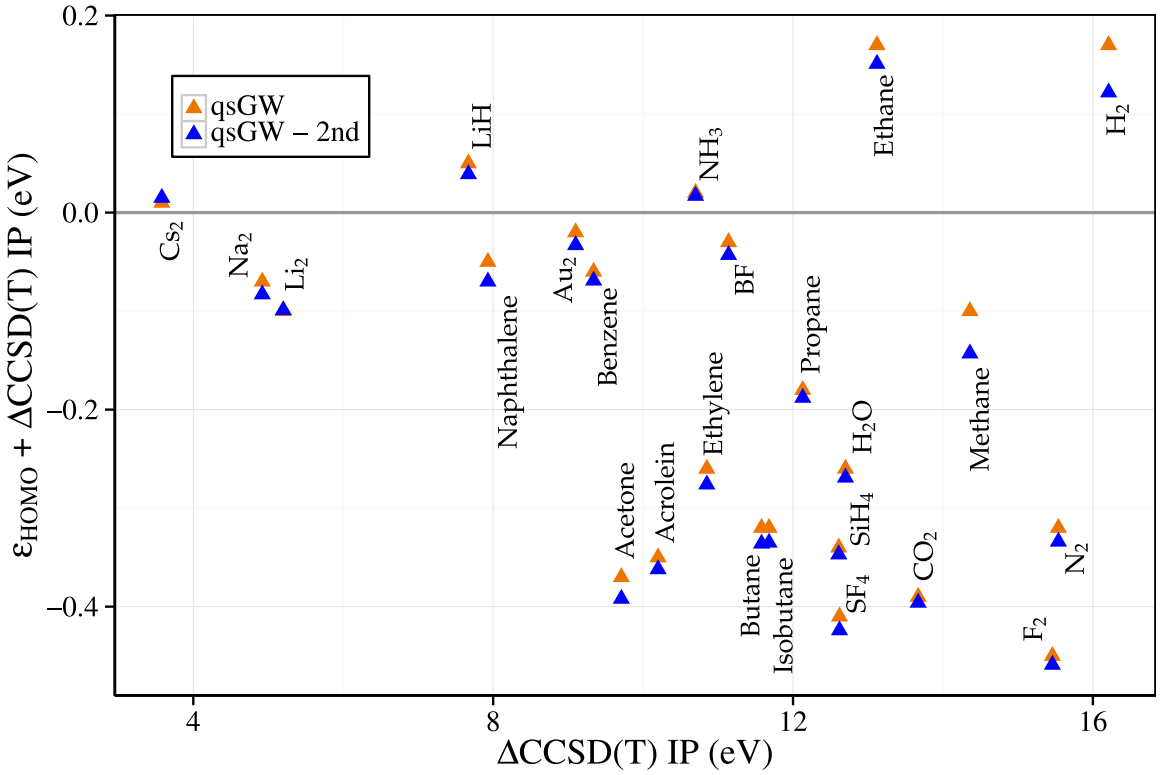

Figure 3.1: The deviation of theoretical IPs obtained from qs*GW* and from the 2nd-order extension plotted over the ΔCCSD(T) reference IPs (Krause et al., 2015). The plain qs*GW* results employ the quasi-static approximation. In contrast, the qs*GW*-2nd results take into account the self-consistent solution of the QP-equation employing the energy-dependent self-energy. The difference of the qs*GW* results and qs*GW*-2nd results is a measure for the error made due to the quasi-static approximation.

in this thesis basis sets of the def2-SV type are employed. While the phrase def2 simply refers to the fact that this set is of the second revision, the label SV refers to split-valence. In Sec. 3.2.1.2 the construction of basis sets of the SV type is introduced.

3.2.1.1 Contracted Gaussion Type Orbitals

The orbitals in TURBOMOLE are realized by a representation in terms of so-called contracted Gaussian type orbitals (CGTO). Hence, each single orbital is made up of a linear combination of orbitals

$$f^{\mathrm{GTO}}(\alpha, \mathbf{r}) = (2\alpha/\pi)^{(3/4)} \exp(-\alpha \mathbf{r}^2) \tag{3.46}$$

multiplied by a spherical harmonic $Y_{lm}(\hat{r})$. Each orbital takes the general CGTO form

$$\chi_\alpha(\mathbf{r}) = \Big(c_1 f^{\mathrm{GTO}}(\alpha_1, \mathbf{r}) + c_2 f^{\mathrm{GTO}}(\alpha_2, \mathbf{r}) c_3 f^{\mathrm{GTO}}(\alpha_3, \mathbf{r}) + ...\Big) Y_{lm}(\hat{r}) \ . \tag{3.47}$$

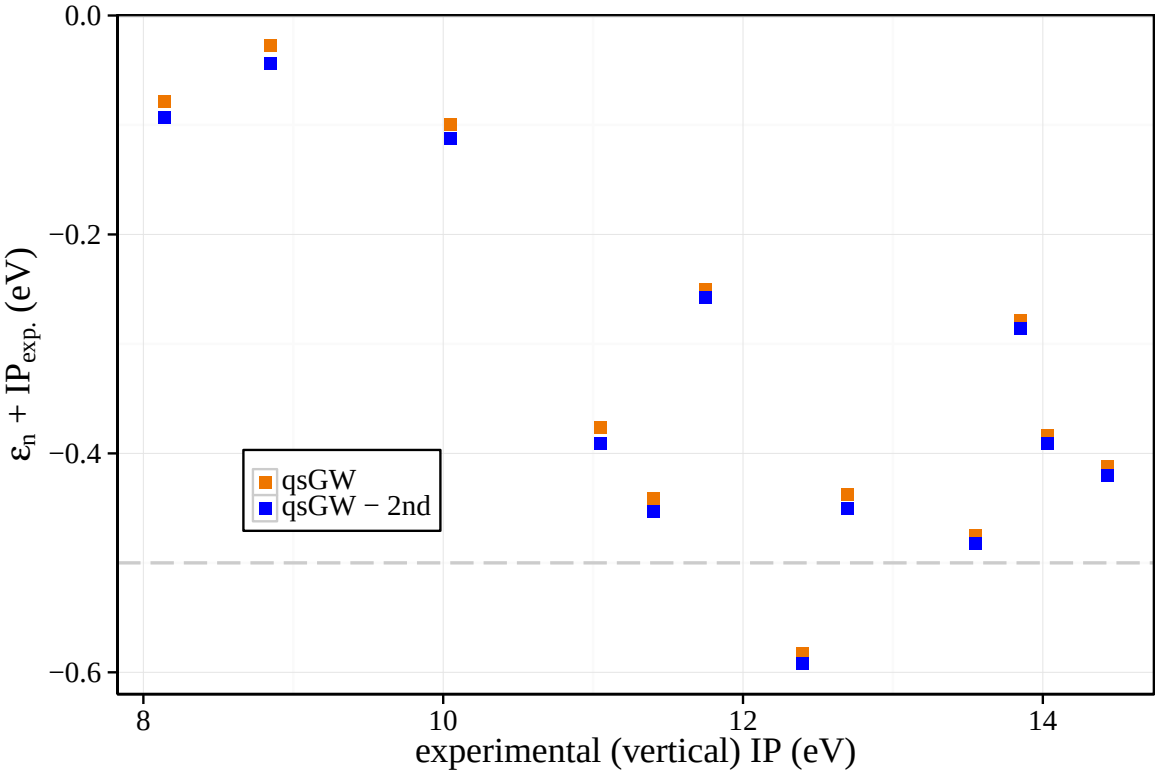

Figure 3.2: The deviation of the calculated QP-energies calculated via qs*GW* and the extension qs*GW*-2nd from the experimental higher vertical IPs of the molecule Naphthalene. Similar to results from Fig. 3.1 is the distance of the qs*GW* QP-energies to the qs*GW*-2nd QP-energies a measure for the error made due to the quasi-static approximation.

The principal reason for the use of such Gaussian basis functions is the *Gaussian Product Theorem*, which guarantees that the product of two GTOs centered on two different atoms is a finite sum of Gaussians centered at a point along the axis connecting them. In this manner, four-center integrals are reduced to finite sums of two-center integrals, and in a subsequent step to finite sums of one-center integrals.

3.2.1.2 Split-Valence (SV) Basis Sets

For the numerical calculations presented in this thesis basis sets of the split-valence (SV) type are considered. The SV basis sets assign the electrons into *core* and *valence* type. For each *core* electron one single CGTO is considered. For the *valence* electrons one, three, or even more CGTO orbitals are considered leading to single-ζ (SV), triple-ζ (TZV), and so on, basis sets. To account for polarization effects basis functions with a larger angular momentum are added to the set. The extended basis sets including larger angular momenta are labeled with an additional P: SVP, TZVP, TZVPP, and so on.

The QP-orbitals $\psi_n(\mathbf{r})$ are expressed in terms of the CGTO $\chi_\nu(\mathbf{r})$ via the transformation matrix $c_{\nu n}$ by

$$\psi_n(\mathbf{r}) = \sum_\nu \chi_\nu(\mathbf{r}) \ {}^{(i)}c_{\nu n} \ , \tag{3.48}$$

where the sum is over all basis functions $\chi_\nu(\mathbf{r})$. Therefore, for each n there is a closed block of ν coefficients.

3.2.1.3 Basis Set Dependence

Within a numerical implementation one is limited to the use of a finite number of basis functions. Since one is usually interested in the continuous limit, i.e. the limit of infinite number of basis functions, a cut off criteria for the number of basis functions needs to be introduced. On the one hand, the number of basis functions can be converged up to a number where the results does not change under the addition of further basis functions. Such a basis set is called the converged Basis set (CBS). On the other hand, the addition of further basis functions increases the computational cost. The theoretical scaling of the computational effort with the number of basis functions N of the qsGW formalism is $\mathcal{O}(N^5)$. For example a calculation with twice as many basis functions would need roughly 32 times as long[2]. Therefore, it is essential to find a basis set which offers a good trade-off between accuracy and computational cost.

The observable which is chosen as the target reference within the optimization of the basis set is (again) the (first) Ionization Potential (IP). It yields a good indicator for the accuracy of the overall calculation. The study of the basis set dependence of the qsGW IPs begins with a comparison for small molecules, H_2O, N_2 and CH_4. The results, obtained using the def2-SVP, TZVP, TZVPP and QZVP basis set, are shown in Fig. 3.3. The calculated (first) IPs are plotted against the inverse of the size of the basis set. Hence the ordinate offset of the linear fit gives an estimate for the extrapolated CBS result.

In a similar manner as shown in Fig. 3.3, a full study of the test set of molecules, which is introduced in Sec. 4.1.1, has been performed. The results are shown in Fig. 3.4. In this study the CBS limit is calculated for each molecule over the complete set. Fig. 3.4 shows that the SVP basis set has maximum error larger than 0.8 eV. Furthermore, the largest deviations are found in systems with strong polar covalent bonds (H_2O, LiH, CO_2, NH_3). Van Setten et al. (2013) observed this already for G_0W_0. The reason for the deviation in both approaches is that the SVP basis set is not able to describe the bonding very accurately. Hence, for these molecules the SVP results are excluded from the linear fit to obtain the CBS limit.

Overall, the TZVP basis has a maximum deviation of roughly 0.4 eV. Adding another set of polarization functions, namely the TZVPP basis set, for most molecules the deviation drops below 0.3 eV. The conclusion of these results is that the TZVPP basis offers a good trade-off between computational cost and accuracy and will be used therefore for all calculations and further benchmarks presented in this thesis.

[2]The actual scaling of the qsGW formalism is identified in Sec. 5.5.

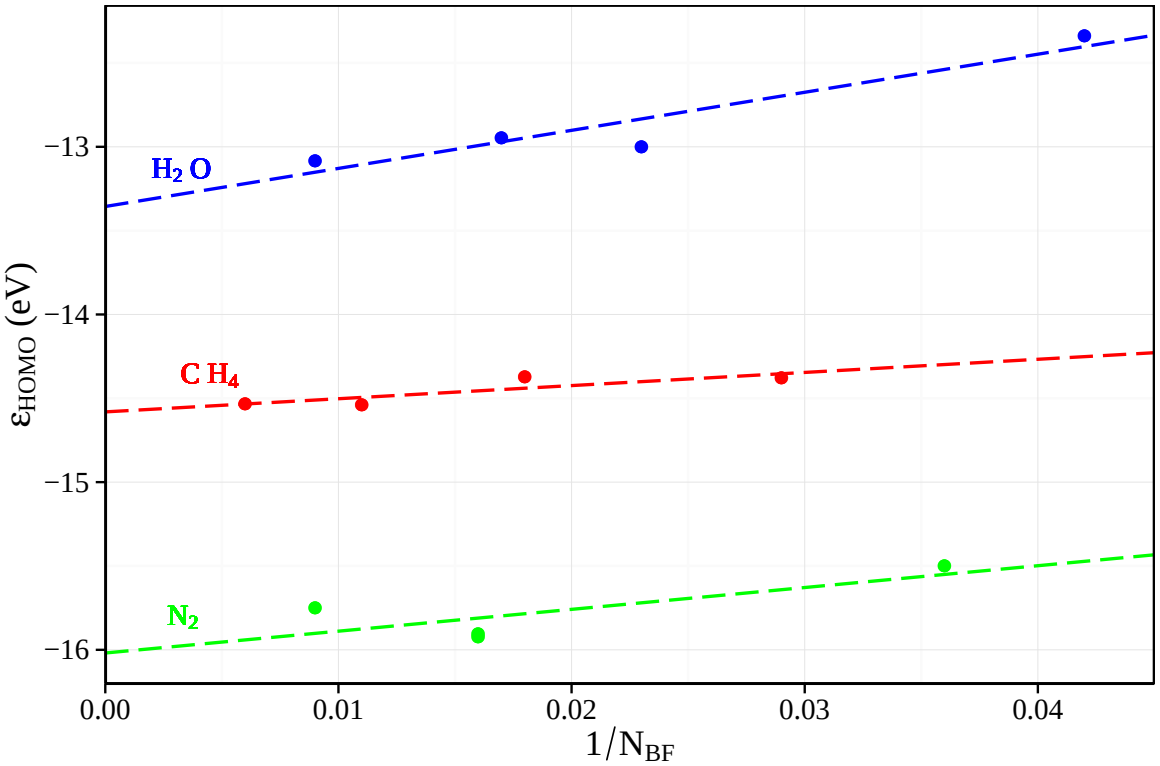

Figure 3.3: Convergence test of the calculated qs*GW* HOMO energy with respect to the basis set (using the def2-SVP, TZVP, TZVPP, QZVP basis sets) with increasing number of basis functions N_{BF} from right to left of nitrogen (N_2), water (H_2) and methane (CH_4). A linear fit through the HOMO energies for each seperate molecule is indicated. The intersection of this fit with the the ordinate gives an estimate for the converged basis set limit (CBS). The data scatters as there are different kind of orbitals added (s, p, d,... type) which don't show a strict linear impact on the accuracy.

3.2.2 Abort Criteria of the Iterative Formalism

The qs*GW* cycle iteratively updates the full Green's function. Hence, a measure which checks for the full difference between two Green's functions is needed. Within the present implementation a check for the norm of the differences of the Green's functions as the

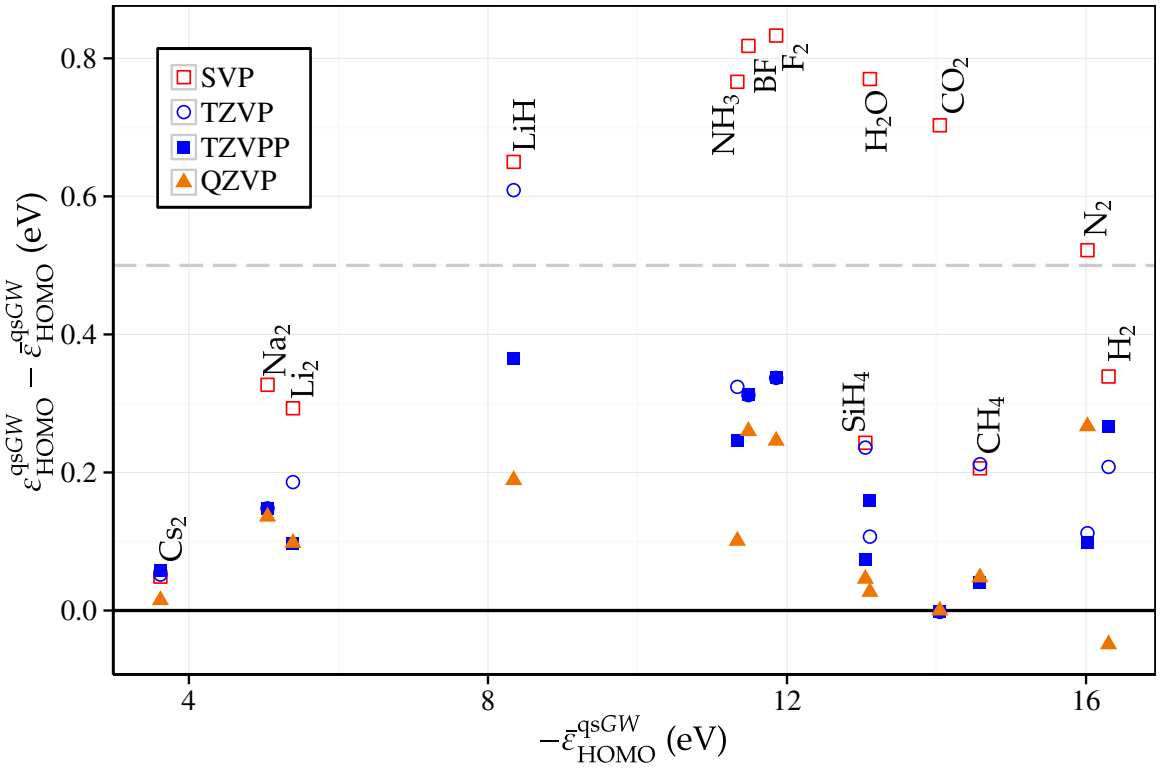

Figure 3.4: Convergence test of the qsGW ionization potential with respect to the basis set (using the def2-SVP, TZVP,TZVPP,QZVP basis sets) of a set of molecules with the CBS ($\bar{\varepsilon}^{qsGW}_{HOMO}$), from a linear interpolation over the inverse of the number of basis functions, see Fig. 3.3 for explanation, as the reference. The difference of the calculated energy using one specific basis to the CBS is an estimate for the error made due to the incompleteness of the basis set.

convergence criteria is implemented, as suggested by Caruso et al. (2013):

$$\Delta = \frac{1}{N^2_{\text{Orbitals}}} \left[\sum_{n,\underline{n}} |G_{n\underline{n}}(E=0) - G^{(i-1)}_{n\underline{n}}(E=0)|^2 \right]^{\frac{1}{2}} \tag{3.49}$$

$$= \frac{1}{N^2_{\text{Orbitals}}} \left[\sum_{n} |G_{nn}(E=0) - G^{(i-1)}_{nn}(E=0)|^2 \right]^{\frac{1}{2}} \tag{3.50}$$

$$\tag{3.51}$$

Where $G_{n\underline{n}}$ denotes the Green's function in the basis of QP-states. The difference Δ tests for the convergence of all pole positions of the Green's functions. Nevertheless, prime interest are the energies of the frontier orbitals and the next lower poles. Therefore, convergence is typically achieved at $\Delta << 10^{-7}$ which corresponds to HOMO energies converged within 10^{-4} eV.

If one only aims for the calculation of one single orbital energy, i.e. the HOMO energy, the code allows to set a convergence critera for the single orbital energy ε_n as well;

$$\Delta_n = \varepsilon_n - \varepsilon_n^{(i-1)} \ , \tag{3.52}$$

and stop the iterative flow at any cutoff, i.e. $\Delta_n < 10^{-4}\,\mathrm{eV}$.

For all results within this thesis it was assure that all shown QP-energies were separately converged within 1 meV.

3.2.3 Improvements to Reduce the Number of Iterations

A study aiming to find an optimized starting point and therefore reducing the total number of iterations needed in the GW-cycle has been done which is presented in Sec. 3.2.3.1. Within the context of Sec. 3.2.3.1 the starting point dependence of G_0W_0 is discussed in further detail as well. Furthermore a mixing procedure is introduced as a tool to adjust the step width between the GW iterations. An optimised choice for this parameter reduces the needed number of iterations as well by typically a factor of 4. The discussion can be found in Sec. 3.2.3.2.

3.2.3.1 Choosing the Optimum Initial Green's function

The self-consistent solution of qsGW is independent from the starting point. Whether an initialization with G_0 based on a Hartree, HF or a DFT calculation is employed, all will eventually flow to the same fixed point solution within qsGW.

How to find an optimum initial DFT based Green's function has been investigated by C.Rodenenbeck within her Bachelor Thesis (Rodenbeck, 2014), supervised by the author of this thesis. The principal concept was to systematically vary the DFT functional along a linear connection of PBE-DFT exchange and exact Fock exchange. Specifically, use has been made of a PBE based hybrid functional which is called in the following PBEλ. Within PBEλ exact Fock Exchange Σ_x is systematically mixed into the exchange-correlation contribution E_xc via

$$E_\mathrm{xc}(\lambda) = E_\mathrm{c} + (1-\lambda)E_\mathrm{x} + \lambda\Sigma_\mathrm{x} \ . \tag{3.53}$$

The amount of exact exchange is controlled via the mixing parameter λ which was varied from 0 to 1. The choice of $\lambda = 0.25$ gives the popular functional PBE0. Furthermore, the choice of $\lambda = 1$ gives HF with the addition of a correlation contribution to the HF-exchange functional due to the untouched correlation contribution E_c in PBEλ. The motivation for such kind of hybrid functional is, primarily, that the exact exchange cancels the major source of errors in local approximations in the functional, the so called self-interaction error.

The systematic variation of λ leads to various different estimate for the Ionization Potential (IP), exemplary shown in Fig. 3.5 for the molecule Benzene.

The study shows that the DFT estimate for the IP can vary by several eV based on the choice in the functional. In contrast, already on the G_0W_0-level the dependency of the

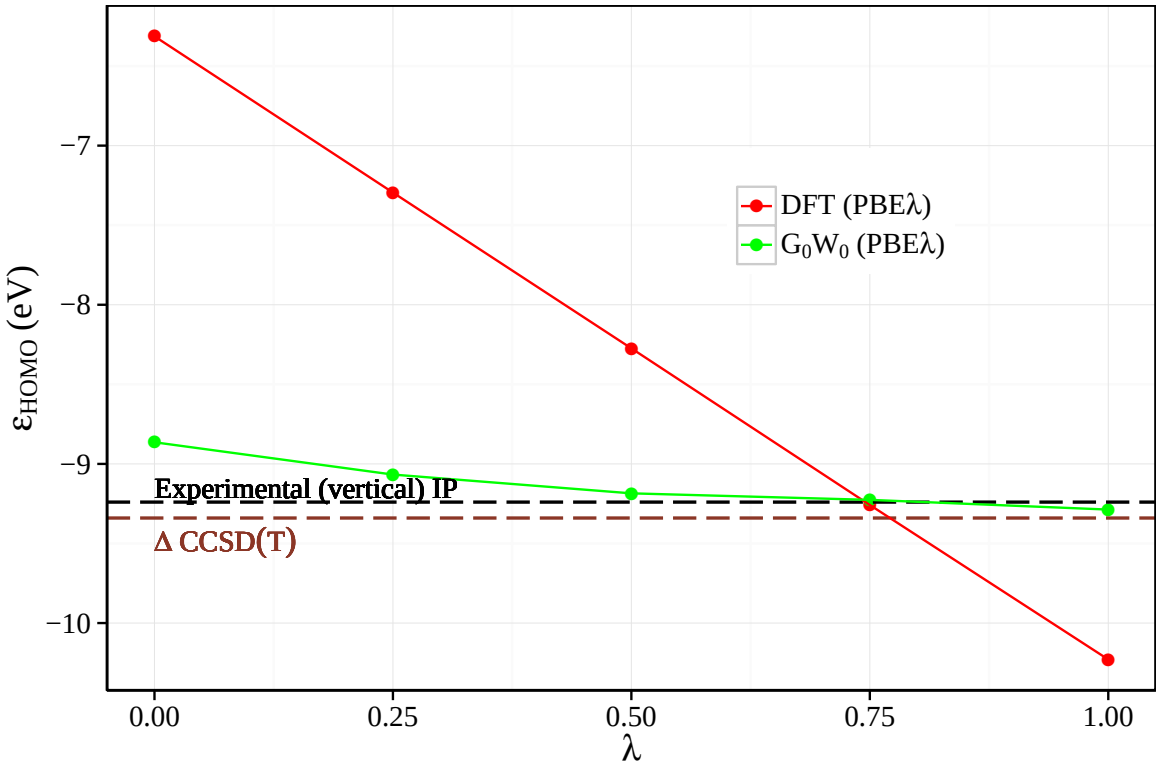

Figure 3.5: HOMO energies, which are interpretated as estimates for the first IP, plotted overthe amount of exact exchange in the functional PBEλ for the molecule Benzene. G_0W_0 performed on top of such DFT(PBEλ) calculations shows still a dependence on λ. The difference Δ_λ of the maximum HOMO energies, typically at $\lambda = 0$, to the minimum HOMO energy, typically at $\lambda = 1$, is used as a measure for the dependence of the method on the coice of the functional. A study of the starting point dependence of G_0W_0 in comparison to DFT(PBEλ) over the full basis set is reported in Fig. 3.6. The first IP from a ΔCCSD(T) calculation as well as the experimental (vertical) IP is shown as reference for the accuracy of the DFT and G_0W_0 calculations. Best agreemt of DFT (PBEλ), G_0W_0(PBEλ and experiment is obtained with the choice $\lambda = 0.75$.

HOMO on the reference functional is decreased by an order of magnitude. This is confirmed in Fig. 3.6. It shows that the λ- dependence in G_0W_0 is suppressed in comparison to the dependence in DFT over the full test set. Nevertheless, the calculated IPs in G_0W_0 still vary by up to 2 eV depending on the choice of the functional. This dependence will be resolved within the qsGW approach.

The optimum choice for the mixing λ is the one which generates a G_0 which is closest to the fixed point solution. This is the G_0 which is minimally changed within the G_0W_0 process. Approximately, this is the one for which the DFT(PBEλ) IP estimate is closest

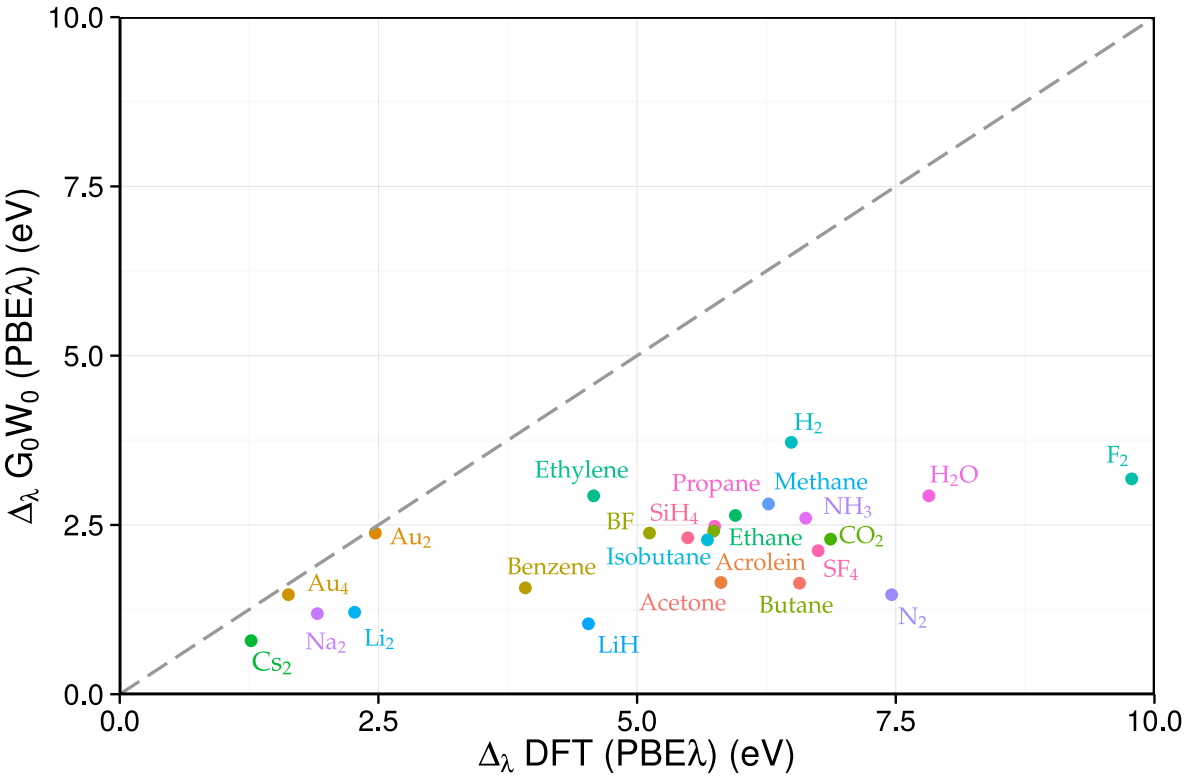

Figure 3.6: The spread Δ_λ, see Fig. 3.5, resulting from G_0W_0 calculations with different parent DFT(PBEλ) calculations plotted over the Δ_λ from the parent DFT(PBEλ) calculation: Formally: $\Delta_\lambda \mathrm{DFT} = \epsilon^{\mathrm{DFT}}_{\mathrm{HOMO}}\_\lambda = 1 - \epsilon^{\mathrm{DFT}}_{\mathrm{HOMO}}|_{\lambda=0}$ and $\Delta_\lambda G_0W_0 = \varepsilon^{G_0W_0}_{\mathrm{HOMO}}|_{\lambda=1} - \varepsilon^{G_0W_0}_{\mathrm{HOMO}}|_{\lambda=0}$. The dashed line is the diagonal. Hence, the spread Δ_λ, and the functional dependence of the results, in DFT(PBEλ) is larger then in G_0W_0 for all cases where the data points are below the dashed line.

to the one from the following G_0W_0 calculation. Rodenbeck (2014) showed for a larger set molecules that, in this sense the best choice is $\lambda \approx 0.75$, see Tab. 3.1[3].

An extension of this study has been performed in this work. It shows that the choice $\lambda \approx 0.75$ typically gives best agreement with experiment as well, see Tab. 3.2. This behaviour can be seen in the example Benzene shown in Fig. 3.5, too. In contrast does the comparison to the ΔCCSD(T) IP estimates, see Tab. 3.3, show best agreement on average at $\lambda \approx 0.5$.

Summarizing, the choice of a hybrid PBE functional with 0.75 exact exchange is a good choice for G_0W_0 based calculations of estimates for the experimental IPs. This does not hold

[3]Due to a small error in the original G_0W_0 code the data C.Rodenbeck reported in her thesis needed to be reproduced in this work. Nevertheless, the changes from the fix were negligible small. Therefore, her findings are still valid.

in the comparison to the ΔCCSD(T) IPs. Nevertheless, $\lambda = 0.75$ is a promising choice for the generation of optimized DFT based initial Green's functions G_0 for the qsGW method. Already at G_0W_0 level the update on the Green's function was minimal. Hence, choosing $\lambda = 0.75$ is supposed to minimize the needed number of iterations till full convergence. Typically, for $\lambda = 0.75$ the number of iterations till convergence was reduced by a factor of 4 compared to the choice $\lambda = 0$.

	PBE00	PBE25	PBE50	PBE75	PBE100
ME	3.51	2.48	1.32	0.14	-1.11
MAE	3.51	2.48	1.32	0.30	1.11
Variance	1.28	0.57	0.17	0.12	0.49
MaxAE	5.58	4.02	2.57	1.05	3.02
MinAE	1.10	0.84	0.52	0.03	0.20

Table 3.1: Evaluation over the full test set of the difference between the G_0W_0 HOMO energies to the parent DFT(PBEλ) HOMO energies. λ has been varied in steps of 0.25 from 0 to 1. The λ which minimizes the difference between the G_0W_0 HOMO and the DFT HOMO is a guess for the choice of the functional to construct the optimum DFT based initial G_0. Reportet are the mean error (ME), the mean absulute error (MAE), the maximum absolute error (MaxAE) and the minimum absolute error (MinAE) as well as the variance (σ^2) over the data obtained on a test set of 29 molecules. The test set is introduced in Sec. 4.1.1.

	@PBE00	@PBE25	@PBE50	@PBE75	@PBE100
ME	0.44	0.15	-0.01	-0.15	-0.22
MAE	0.52	0.36	0.31	0.40	0.49
σ^2	0.23	0.17	0.20	0.30	0.37
MaxAE	1.41	1.16	1.30	1.50	1.64
MinAE	0.01	0.01	0.01	0.01	0.01

Table 3.2: Evaluation over the full test set of the difference between the G_0W_0 HOMO energies to the experimental (vertical) IP.

3.2.3.2 Linear Mixing in the Quasiparticle Equation

As it turns out, the numerical formalism, introduced in Sec. 3.1.2, does not always converge nicely into a fixed point solution. It happens that the step width from one qsGW iteration to the next one is too large. In such cases the system oscillates around the fixed point. This occurs for example for the case of BF.

To overcome this problem, a linear mixing scheme is introduced. It mixes into the updated Green's function a contribution of the previous one to decrease the step width

	@PBE00	@PBE25	@PBE50	@PBE75	@PBE100
ME	0.54	0.26	0.09	-0.05	-0.12
MAE	0.59	0.27	0.13	0.21	0.29
σ^2	0.15	0.03	0.02	0.10	0.14
MaxAE	1.44	0.61	0.42	1.17	1.25
MinAE	0.14	0.05	0.00	0.00	0.01

Table 3.3: Evaluation over the full test set of the difference between the G_0W_0 HOMO energies to the ΔCCSD(T) IP estimates.

between two iterations. Strictly speaking not the equation,

$$\left(\varepsilon_n - \hat{\mathcal{H}}_{\mathrm{HF}}(n) - \hat{\Sigma}_{\mathrm{c}}[G]\right) \cdot \psi_n = 0 \ , \tag{3.54}$$

is solved anymore, but

$$\left[\tilde{\varepsilon}_n - \left(\alpha(\hat{\mathcal{H}}_{\mathrm{HF}}[G] + \hat{\Sigma}_{\mathrm{c}}[G]) - (1-\alpha)\varepsilon_n\right)\right] \cdot \tilde{\psi}_n = 0 \ , \tag{3.55}$$

with the solutions $\tilde{\varepsilon}$ and $\tilde{\psi}$. The iteration is proceeded identical to the formalism without this mixing, but with the alternative solutions used to construct the updated Green's function.

The mixing parameter α allows to optimize the step width in a way to reduce the needed number of iterations as well. Hence, an optimum combination of an initial Green's function G_0 which is closest to the fixed point solution and a mixing α which reduces the step with to improve the convergence is to be found.

Fig. 3.7, Fig. 3.8, and Fig. 3.9 show the convergence behavior of the HOMO energy of the molecule Benzene. Different combinations of the starting point varied via the amount of exact exchange in the PBEλ functional in dependence of λ and the linear mixing parameter α were tested. Over the full test set of molecules, the result of the Benzene study, the combination of $\lambda = 0.7$ and $\alpha = 0.3$, proved as convenient good choice to reduce the needed number of iterations and to guarantee convergence.

Within qsGW the final fixed point solution is always independent on the initial choice for the Green's function in contrast to the G_0W_0 based results. Whether the parent calculation employed a LDA, PBE or Hybrid functional, it did not effect the fixed point solution, see i.e. Fig. 3.7.

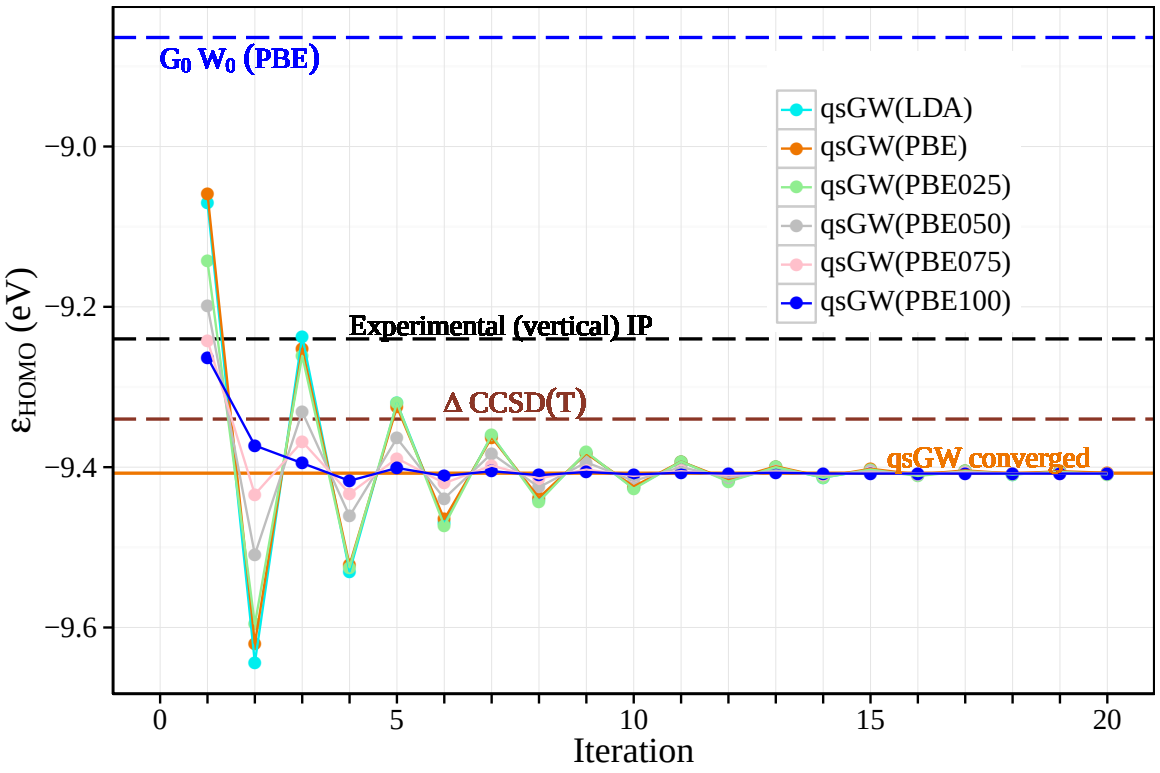

Figure 3.7: The convergence of the HOMO energy for Benzene with the qsGW iteration. In this example the self-consistency cycle was initialized with a KS-DFT Green's function calculated employing LDA, PBE and PBE hybrid XC-functionals with an exact exchange contribution of 25% (PBE0), 50%, 75%, and 100%. For comparison also the G_0W_0, the experimental, and Δ CCSD(T)(Krause et al., 2015) results are shown. Independent of the choice of the functional in the initial DFT(PBEλ) run, the self-consistent qsGW converges into the identical fixed point solution. The linear mixing parameter here is chosen $\alpha = 0.0$. See Fig. 3.8 and Fig. 3.9 for the convergence behaviour with different mixing and starting points combinations.

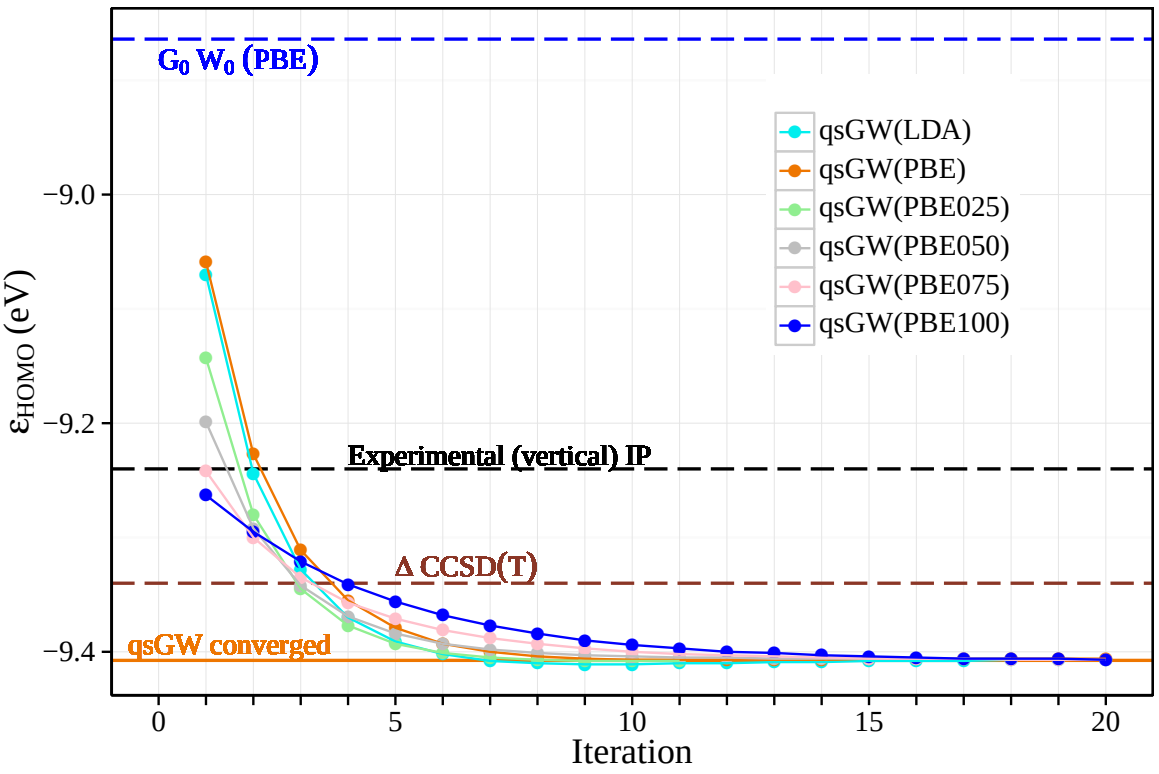

Figure 3.8: Continuation of the Benzene study from Fig. 3.7, here with mixing of $\alpha = 0.7$. The reduced step width between the iterations supresses the osszillations and enforces a smooth convergence. The cost is the need for a rather high number of iterations irrespective of the chosen parent DFT(PBEλ) system.

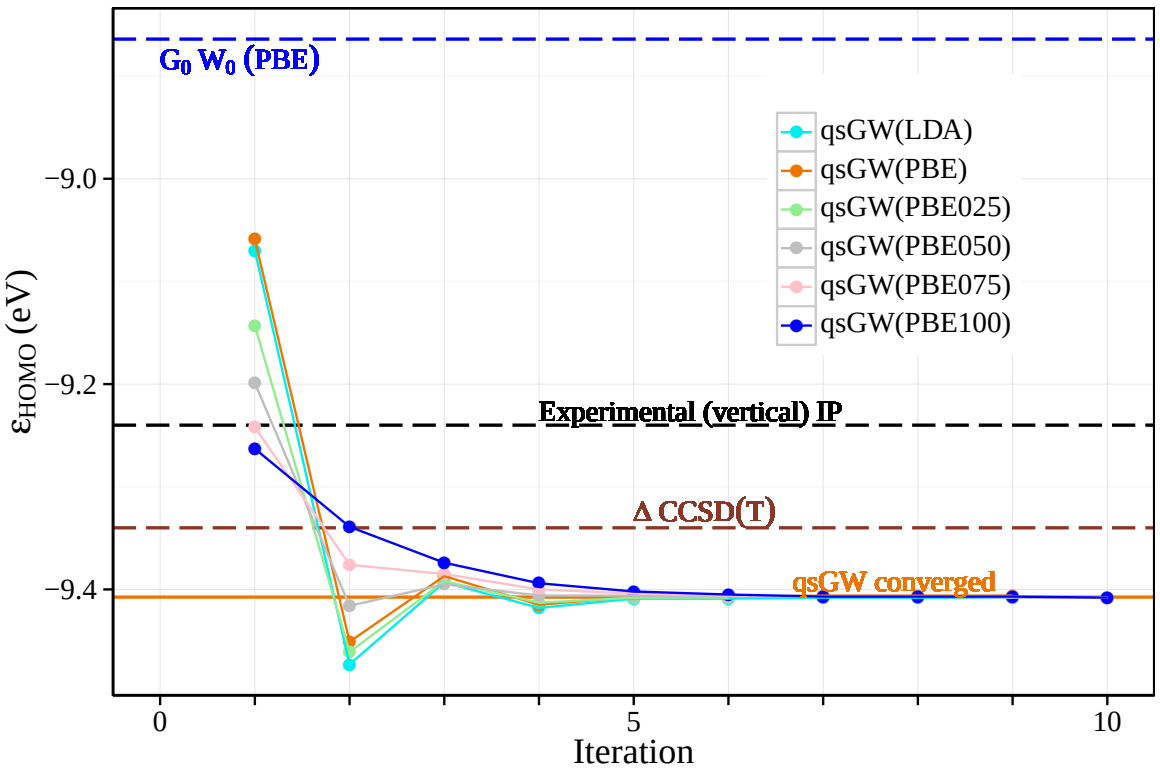

Figure 3.9: Continuation of the Benzene study from Fig. 3.7, here with mixing of $\alpha = 0.3$. With this mixing the oszillations are supressed in comparison to the convergence with $\alpha = 0.0$ In combination with an optimized starting point (here $\lambda = 0.7$) the number of iterations is reduced by a factor of $2-3$ till convergence in qsGW.

Chapter 4

4 Application of Quasiparticle Self-Consistent GW

To test the new implementation, calculations are performed with qsGW, G_0W_0, Density Functional Theory (DFT) and Hartree-Fock (HF). The results compared with reference results obtained from the CCSD(T) method and with experimental results.

In Sec. 4.1 the test set of molecules is introduced and numerical parameters are specified. Results for the first Ionization Potential (IP) are presented and discussed in Sec. 4.2.1, higher IPs are shown in Sec. 4.2.2. The calculation of ground state electron density and dipole moments are presented and discussed in Sec. 4.2.3.

The test of the accuracy of the method operates on a set of 29 molecules, GW29. We find that quasiparticle self-consistent GW (qsGW) is nearly as accurate as the reference ΔCCSD(T) for the calculation of first Ionization Potentials (IP) of molecules while the computational effort is remarkably smaller. ΔCCSD(T) has a formal computational scaling N^7 with the number of basis functions N. In contrast, the measured scaling of qsGW is N^3 as test in Sec. 5.5 show. Furthermore, we observe that qsGW agrees significantly better with experiment in the calculation of higher IPs compared to G_0W_0. Similarly, qsGW improves agreement with experiment in comparison to HF, DFT and over scGW for the prediction of dipole moments of small dimer molecules.

4.1 Setup of the Comparison to Established Quantum-Chemistry Methods

4.1.1 Test Set of Molecules

The test set GW29 consists of 25 molecules from the GW27 test set which was used in the benchmark of the G_0W_0 implementation within TURBOMOLE (Van Setten et al., 2013). This set is extended by four medium size organic molecules which have been proposed as candidates for electronic devices (Caruso et al., 2013).

The set GW29 entails from small molecules (e.g. H_2), up to medium size molecules (e.g. Naphthalene). Different categories, like organic molecules (Benzene) and transition metals (Au_4) are considered. Thus, molecules where a good description of localized charges is essential are considered (e.g. Li_2). But, molecules of sizes where a good description of the screening of the coulomb interaction is crucial are considered as well (e.g. Au_4). In addition, systems with different bonding properties are considered, for example H_2O is included as an example of strongly polar bond.

4.1.1.1 Structural Data

The molecular structure of the ions was chosen such that it is closest to the experiment. Therefore, most of the required structural data for the test set of molecules, with high accuracy, is supplied by the TURBOMOLE distribution. Furthermore, in this way it is assured that qsGW calculations as well as DFT, HF and ΔCCSD(T) operate on the same molecular structure. This is otherwise an unwanted source of differences in the results. Structure optimizations are performed for some dimers and the four additional molecules not contained in the TURBOMOLE distribution. The optimization used identical parameters as for the ones from the database. In this way the accuracy for these structures is on the same order as for the supplied system. The comparison of the calculated dipole moments is done on further dimer molecules. Here, the scGW calculations employed actual experimental distances in the molecular structure. Therefore, for the comparison to these results, in the calculations performed here, the experimental distance is employed as well. This way differences due to structural discrepancies are ruled out in this comparison.

4.1.2 Reference Methods and Data

A major criterion for the selection of molecules is that reference data is available. In order to demonstrate the accuracy of the qsGW method, one compares to results of computationally much more expensive, high-precision reference calculations, -if such are available.

4.1.2.1 CCSD(T)

Except for H_2, there are no *exact* results available. At present the most accurate reference is provided, the coupled-cluster method in the ΔCCSD(T) approximation, which is briefly introduced in the appendix in Sec. A.3. Such calculations provide purely electronic vertical IPs (McKechnie et al., 2015). ΔCCSD(T) data for the GW27 have been given by Krause et al. (2015). Data for the four additional organic molecules was provided by Dr. M. Harding (INT). Such accurate calculation are computationally demanding. In the present test set, the molecules are still tractable but the rather high scaling of (N^7) makes the treatment of larger molecules an extensive task. For example, the overall time needed for the Benzene molecule is in ΔCCSD(T) about 4 hours, while G_0W_0 takes 40 minutes. qsGW

is converged after roughly 4 hours as well[1]. Due to the better scaling of qsGW will perform increasingly better for larger molecules. Additionally, ΔCCSD(T) gives only access to the first IP, while qsGW gives estimates for higher IPs in the same calculation as well.

The ΔCCSD(T) reference results were obtained using the same structural data and the exact same basis set as used for the qsGW calculations as well as for all other shown results.

4.1.2.2 Experiment

In addition to ΔCCSD(T), experiments can sometimes be a relevant reference. For the whole GW27 set and for the four additional organic molecules experimental data for the first Ionization Potential is available. In general, the comparison to experimental results has to be taken with great care. A systematic distinction between vertical and adiabatic ionisation energies is difficult in the available data. Furthermore, vibrational effects are always present in the experiment but are ignored in the computations.

The higher IPs are not accessible in the CCSD(T) scheme. But, at least for a smaller set of molecules, experimental data is available that serves us as a reference for the calculations of higher IPs.

The accuracy of ground state densities from qsGW is tested as well by comparing the dipole moments resulting from qsGW densities with experimentally measured data (DataBase and Benchmark, 2015).

4.2 Comparison to Established Quantum Chemistry Methods

4.2.1 First Ionization Energies

IPs are standard observables for testing electronic structure methods, because (i) they are an important indicator to understand charge transfer processes, (ii) experimental reference data is available and (iii) one has access to results using more accurate theories (at least for small size molecules). The first IP measures the (negative) energy of the highest occupied molecular orbital (HOMO).

The deviation of the HOMO energies calculated with DFT (employing the PBE functional), HF, G_0W_0 and qsGW from the ΔCCSD(T) reference data is shown in Fig. 4.1. Deviations from the experimental data are shown in Fig. 4.2. In both figures also HF and DFT provide a quantitative measure for the improvement that is achieved using different GW approaches with respect to frequently applied procedures. The actual numbers which enter the plot are reported in Tab. 4.1.

[1]For this comparison all calculations have been done using the same computational resources. Furthermore, similar numerical parameters have been chosen. A full study for the comparison of the computational cost would need such a setup for a larger test set. The results here give a good estimate, while a full study is byond the scope of this work.

molecule	ΔCCSD(T)	Exp.	DFT	HF	G_0W_0	qsGW
H_2	16.21	15.42	10.25	15.96	15.57	16.04
Li_2	5.20	5.11	3.21	4.89	4.95	5.30
Na_2	4.92	4.89	3.13	4.50	4.78	4.99
Cs_2	3.58	3.70	2.30	3.10	3.40	3.57
F_2	15.46	15.70	8.97	17.68	14.55	15.91
N_2	15.54	15.58	10.20	16.54	14.69	15.86
BF	11.14	11.00	6.80	11.07	10.43	11.17
LiH	7.93	7.90	4.36	8.18	6.52	7.98
CO_2	13.67	13.78	9.02	14.79	12.96	14.06
H_2O	12.61	12.62	7.02	13.85	11.87	12.95
NH_3	10.85	10.85	6.02	11.69	10.24	11.11
SiH_4	12.70	12.82	8.47	13.15	12.11	12.96
SF_4	12.62	12.30	8.09	13.81	11.88	13.03
Au_2	9.10	9.50	6.32	7.90	9.84	9.12
Au_4	7.67	8.60	5.63	6.41	7.45	7.62
Methane	14.36	14.35	9.44	14.83	13.79	14.46
Ethane	13.12	12.00	8.13	13.23	12.22	12.95
Propane	12.13	11.51	7.67	12.59	11.54	12.31
Butane	11.58	11.09	7.58	12.43	11.39	11.90
Isobutane	11.68	11.13	7.60	12.46	11.26	12.00
Ethylene	10.70	10.68	6.78	10.33	10.24	10.68
Acetone	9.71	9.70	5.59	11.20	8.84	10.08
Acrolein	10.20	10.11	5.96	10.72	9.23	10.55
Benzene	9.34	9.24	6.31	9.17	8.87	9.40
Naphthalene	8.04	8.09	5.50	7.94	7.68	8.22
Thiophene	8.96	8.85	5.83	8.87	8.48	9.02
Benzothiazole	8.70	8.75	5.98	8.73	8.24	8.83
1,2,5-thiadiazole	11.15	10.11	6.93	10.03	9.65	10.18
Tetrathiofulvalene	6.42	6.72	3.87	6.64	5.98	6.56

Table 4.1: HOMO energies calculated from qsGW and G_0W_0 (initialized from DFT employing the PBE functional), Hartree-Fock (HF) and DFT employing the PBE functional, as well as experimental (vertical) Ionization Potentials and estimates from ΔCCSD(T)(Krause et al., 2015) . All numbers are in units of eV.

4.2.1.1 DFT

Janak's theorem guaranties, that in exact DFT, the HOMO energy level coincides with the negative first IP(Perdew and Levy, 1997, 1983, Perdew et al., 1982). That is no true argument for the higher IPs. Hence, deviations of the DFT-estimates at the first IP from the exact result are due to approximations in the exchange-correlation (xc-)functionals, e.g.

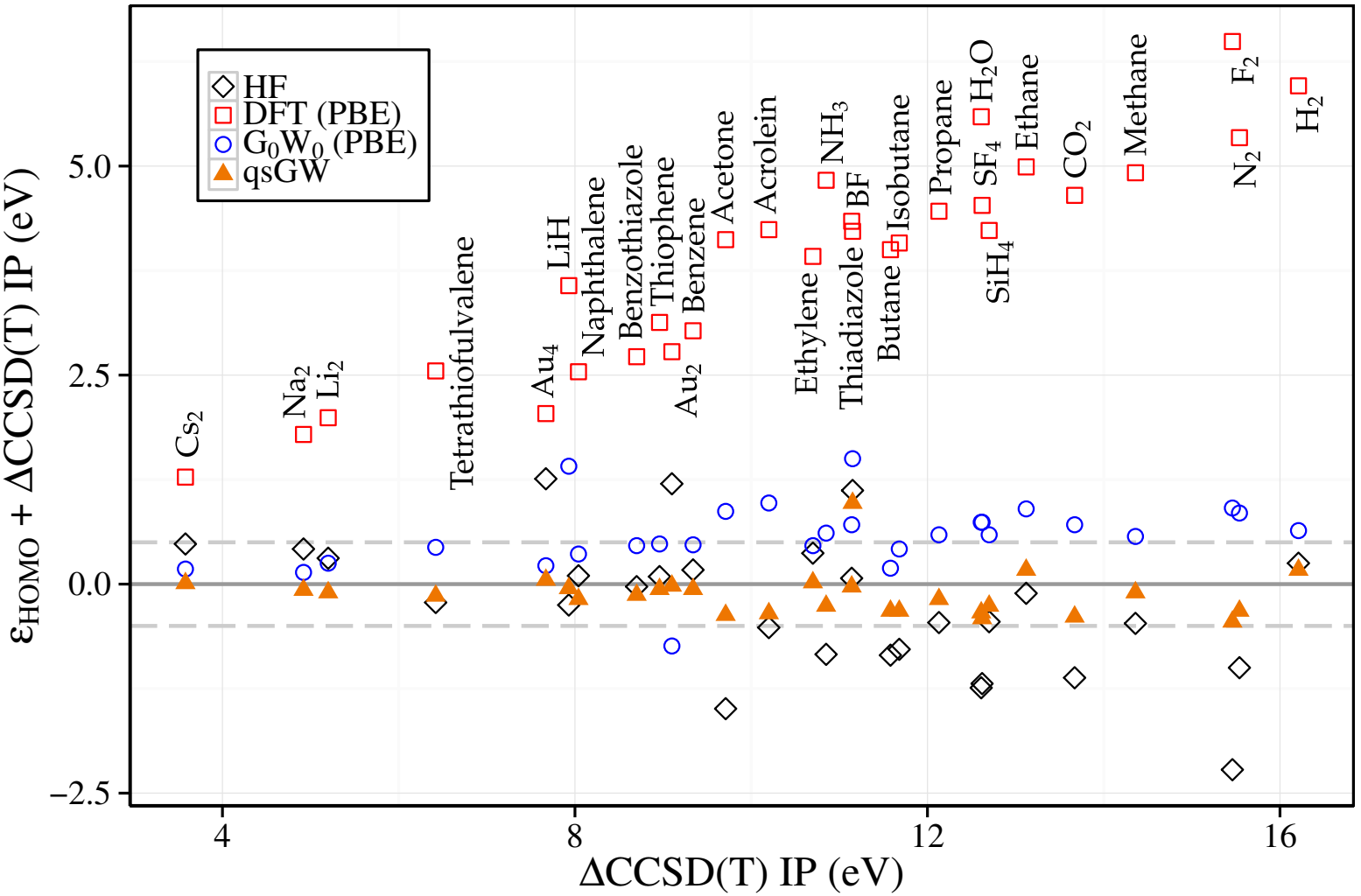

Figure 4.1: The deviation of the theoretical IP, calculated from the reference ΔCCSD(T) IP, to the HOMO energy from considered approaches (vertical axis) over the ΔCCSD(T) reference. Results are obtained from a Hartree-Fock (HF) calculation, a Density Functional Theory (DFT) calculation employing the PBE functional, single-shot G_0W_0 employing a DFT(PBE) parent and results obtained from qsGW. The light grey dashed lines indicate diviations of 0.5 eV to the ΔCCSD(T) result.

LDA or GGA. In contrast, the DFT-based estimates at higher IPs would not reproduce the exact result, even if the xc-functional would be exact.

The DFT-results show the typical undershooting in the calculated IPs. This is a well-know artifact of local approximations in LDA and GGA-type exchange-correlation functionals (e.g. PBE which is used here), the so called self-interaction error. Due to local approximations each charge inevitably interacts with itself. The effect decreases the binding energy at the HOMO level and delocalizes the associated charge density. The error is most pronounced for systems with localized charge densities, i.e. small molecules and transition metals. On a quantitative level we extract from Fig. 4.1 that DFT estimates fall systematically roughly 37% above the reference ΔCCSD(T) result. The overall mean absolute error (MAE) is 3.87 eV and systematic errors are included in a variance of $\sigma^2 = 1.63\,\mathrm{eV}^2$, see Tab. 4.2.

4.2.1.2 Hartree-Fock

According to Koopman's theorem also HF yields direct access to the IP via the HOMO energy. As opposed to LDA or GGA based DFT, HF treats exchange exactly, so in contrast to the DFT results, there is no self-interaction error. Correlation effects are neglected completely, however. The outcome in Fig. 4.1 is that IPs exceed DFT estimates considerably. Comparing HF data with DFT results gives further insight: HF-band approximation errors due to the neglect of correlation effects are typically much smaller than the self-interaction error in DFT (as long as one deals with small molecules); they differ by roughly one order of magnitude. Since the correlation contribution tends to weaken bonding. IPs from HF show an overestimation of the reference IPs. This effect is strongly pronounced for Benzene, for example, see Fig. 4.1. For most other molecules the deviation is relatively small, as confirmed by the MAE of 0.66 eV (see Tab. 4.2). This is, primarily, due to the test set focusing on small molecules where the correlation contributions play a minor role. But, in the data the weaknesses of HF can be observed as well. System with small gaps exhibit a large deviation from the ΔCCSD(T) data, 1.60 eV and 2.19 eV for the transition metal molecules, Au_2 and Au_4. The trend in the data -larger errors with in increasing binding energies, reflects in the variance of $\sigma^2 = 0.64\,\mathrm{eV}^2$, see Tab. 4.2.

4.2.1.3 G_0W_0

Employing G_0W_0 can correct DFT band estimates by reintroducing exact exchange. In this way the self-interaction of KS-particles is removed. Therefore, the G_0W_0 IP estimates increase from DFT(PBE) results towards HF-estimates. In addition to exact exchange, G_0W_0 considers correlation directly as well. This can be observed in the results in the sense that HF typically marks an upper bound for the IPs obtained from G_0W_0. The calculated IPs from G_0W_0 are usually a few hundred meV too small compared to ΔCCSD(T) IPs. The overall MAE of 0.62 eV is comparable HF, with a mean error (ME) that has a different sign as compared to HF. A remarkable feature of G_0W_0 is the absence of a systematic trend in the error, i.e. , the error does not increase with IP energy. Accordingly, the variance is

rather small, $\sigma^2 = 0.17\,\mathrm{eV}^2$, see Tab. 4.2.

4.2.1.4 Quasiparticle Self-Consistent *GW*

Up to now the canonical hierarchy of methods has been reported. Here, we investigate how qsWG performs.

The benchmark, Fig. 4.1, shows that self-consistency typically introduces a shift to higher IPs compared to G_0W_0, shifting data closer to the HF results. This effect is readily observed for the molecules LiH and Methane in Fig. 4.1.

Compared to the reference ΔCCSD(T) first IPs obtained from qsGW are slightly too large. Nevertheless, the self-consistent qsGW improves the agreement significantly, compared to the G_0W_0 results, decreasing the MAE down to 0.22 eV. Overall the maximum error in the test set is 0.97 eV, the molecule 1,2,5-Thiadizole (cf. Tab. 4.1). There is no systematic trend in the deviations. Over the full test set the error is reliably low, which reflects in a variance of only $\sigma^2 = 0.07\,\mathrm{eV}^2$.

4.2.1.5 Summary of Comparison to ΔCCSD(T)

Before proceeding to the comparison to experimental results we present a short summary.

For the considered set of molecules, G_0W_0 as well as qsGW strongly improve agreement with the reference ΔCCSD(T) compared to the underlying parent DFT calculation, see Fig. 4.1. HF and G_0W_0 are found to show comparable overall accuracy. The major advantage of G_0W_0 was the reduced trend, see table Tab. 4.2. Using the qsGW the trend is removed and the MAE improves down to 0.22 eV with a variance of only $0.07eV^2$. The accuracy is similar for all types of molecules, be it organic or transition metal molecules.

	DFT	HF	G_0W_0	qsGW
ME	3.87	-0.26	0.57	-0.12
MAE	3.87	0.66	0.62	0.22
σ^2	1.63	0.64	0.17	0.07
MaxAE	6.49	2.22	1.49	0.97
MinAE	1.28	0.04	0.14	0.01

Table 4.2: Evaluation over the data shown in Fig. 4.1. Evaluated is the deviation from DFT (emplying a PBE functional), Hartree-Fock (HF), G_0W_0 (initialized from a DFT (PBE) system) and from qsGW to the ΔCCSD(T) reference first IPs. Considered are the mean errer (ME), the mean absolute error (MAE), the maximum absolut error (MaxAE) and the minimum absolute error (MinAE) as well as the variance (σ^2).

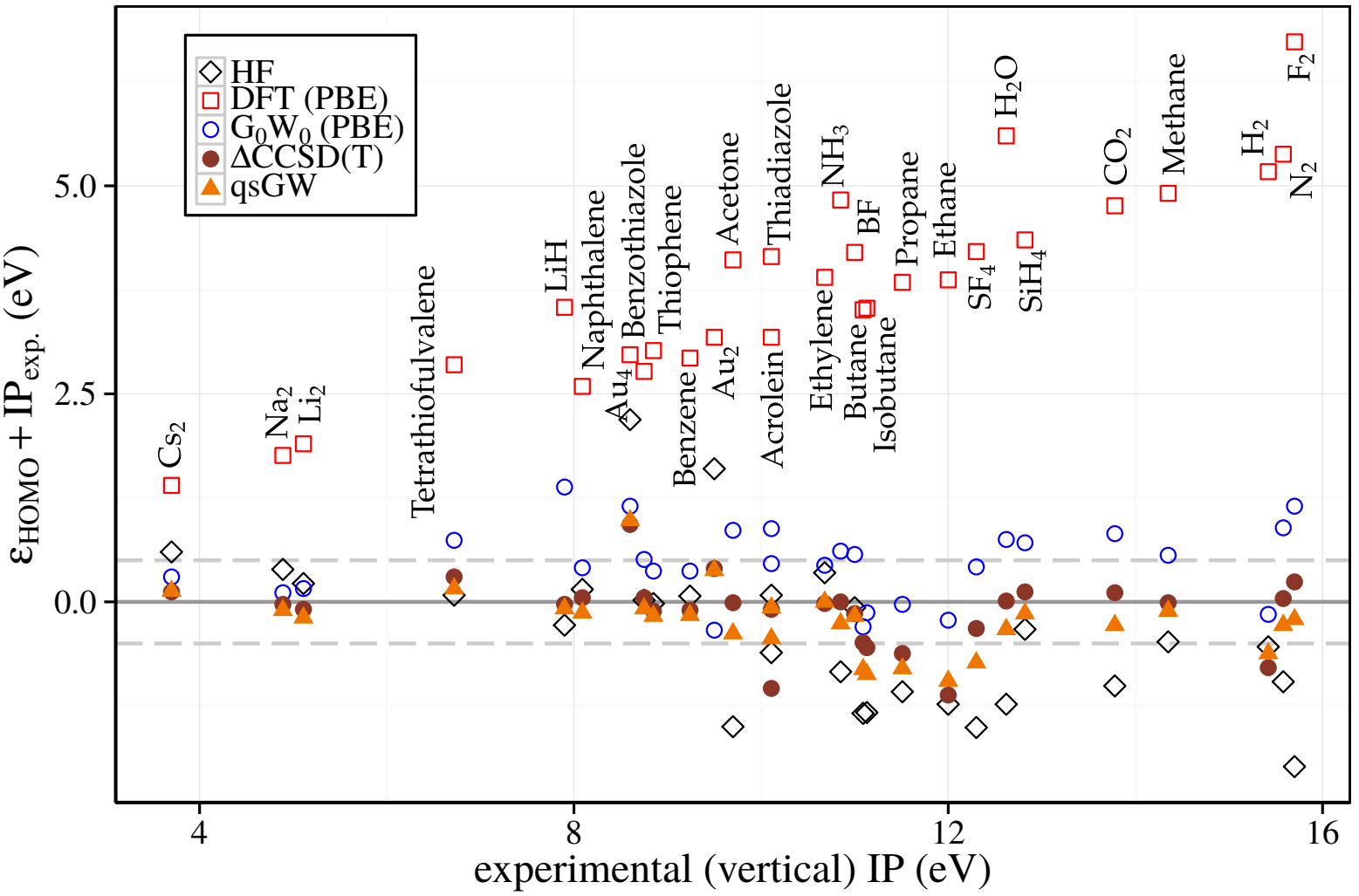

Figure 4.2: The deviation of the theoretical HOMO energy to the experimental vertical Ionization Energy (vertical axis) over the experimental value. Results were obtained from Hartree-Fock (HF), DFT employing the PBE functional, G_0W_0 initialized from DFT(PBE) parent calculations, from Coupled Cluster in the ΔCCSD(T) approximation, and obtained from qsGW. The dashed line indicates a difference of 0.5 eV to the experimental result.

4.2.1.6 Comparison to Experiment

In the following section, we will also consider higher IPs. Since ΔCCSD(T) data for these are not available as a reference, we need to rely on an experimental comparison. In order to illustrate to what extend does experiment can serve as a reference for validation, we here show the deviation of qsGW to the experimental IPs in Fig. 4.2 as well. The resulting statistical measures are reported in Tab. 4.3. Since the ΔCCSD(T) approach reproduces experimental results very well, the predictive quality of methods with respect to experimental data is similar to the one with respect to the ΔCCSD(T) data.

Remarkably, qsGW has a comparably low MAE of 0.35 eV similar to ΔCCSD(T), with a MAE of 0.27 eV, although it is computationally much less demanding (see the study regarding the computational scaling in Sec. 5.5).

	ΔCCSD(T)	DFT	HF	G_0W_0	qsGW
ME	-0.11	3.76	-0.36	0.46	-0.23
MAE	0.27	3.76	0.76	0.54	0.35
σ^2	0.17	1.39	0.83	0.19	0.15
MaxAE	1.12	6.73	2.19	1.38	0.98
MinAE	0.00	1.40	0.02	0.03	0.00

Table 4.3: Data similar to Tab. 4.2, here evaluated for Fig. 4.2.

4.2.2 Higher Ionization Energies

In this section, the accuracy of qsGW for the calculation of higher IPs is discussed on the example of simple molecules, Nitrogen (N_2), water (H_2O), and Benzene (C_6H_6). Here, our interest is in removal energies (higher IPs) of electrons in inner shells. Electrons that are more strongly bound than the HOMO-energy.As we already mentioned, such observables are not accessible via the coupled-cluster approaches as used for the reference data in the previous section, Sec. 4.2.1. Therefore, the reference in the discussion here is experimental data. In Green's function based theories the higher IPs are given by the pole-positions corresponding to bound states (real part at pole positions).

The difference of calculated single particle excitation energies to experimental (vertical) higher Ionization Potentials for Benzene are shown in Fig. 4.3, the results for H_2O and N_2 in Fig. 4.4. Results for further molecules are given in the appendix in Fig. C.1.

4.2.2.1 DFT

In exact DFT, only the energy of the highest occupied Kohn-Sham orbital has a precise meaning. Nevertheless, it s a common practice in electronic structure theory to assign also to all other Kohn-Sham energies a meaning and treat them as estimates for excitation energies and band gaps. This ad-hoc procedure can be very useful, e.g., for the calculation

of band-structure of simple metals. However, as is also known it can fail, spectacularly, e.g. , when predicting optical gaps of semiconductors.

We include DFT-data for higher IPs in Fig. 4.3 and Fig. 4.4 for illustration. As can be see, spectra from the DFT calculations differ from the experiment by up to 5 eV for all molecules. Furthermore, the systematic energy dependence in the error, found in the calculations of the first IPs, is also present for higher IPs. The error increases with energy.

4.2.2.2 HF and G_0W_0

HF calculations show an error increasing with higher IPs, see Fig. 4.3. The first IPs are a few meV close to the qsGW IPs at least for small, non-metallic systems. This is true for the G_0W_0 order as well. The agreement with experiment is improved in G_0W_0 compared to the parent DFT(PBE) calculations as well as in comparison to HF over the whole spectrum. Nevertheless, errors increase with the energy of the IP as well as in G_0W_0 order.

4.2.2.3 Quasiparticle Self-Consistent GW

The systemic increasing of errors with energy seen in HF and G_0W_0 is not observed in the qsGW data in Fig. 4.3. Over the whole spectrum the method gives IPs which are at maximum 0.6 eV off the experiment free of any systematic trend. This supports an impression that qsGW is a reliable and efficient tool to calculate estimates for IPs.

4.2.3 Electron Density

A self-consistent solution of the GW equations introduces corrections to the spatial shape of QP-orbitals.

Hence, one observes corrections to the ground state charge density as compared to the starting guess, e.a., a DFT parent calculation. In contrast, corrections to the density are not accessible with G_0W_0 due to the lack of self-consistency.

4.2.3.1 Benzene

The change of the density from parent DFT(PBE) and DFT(PBE0) calculations compared to the qsGW density for Benzene is shown in Fig. 4.5. Each method reproduces in the are shown a homogeneously distributed density with a six-fold symmetry. Small differences show with increasing exchange contribution; they exhibit a stronger localized density around the C-H bonds. From PBE to PBE0 the density is dragged away from outer regions around the benzene ring closer towards the single C-H pairs. Furthermore, charge is dragged away from the bonding region between the carbon atoms towards the C-H pairs. The effect of stronger localization is slightly stronger pronounced in the qsGW density.

The effect of stronger localization of the charge is primarily due to the reduction of the self-interaction that goes together with an exact-exchange treatment. Therefore, consecutive stronger localization in comparison to the plain PBE calculation is observed from PBE0 to qsGW.

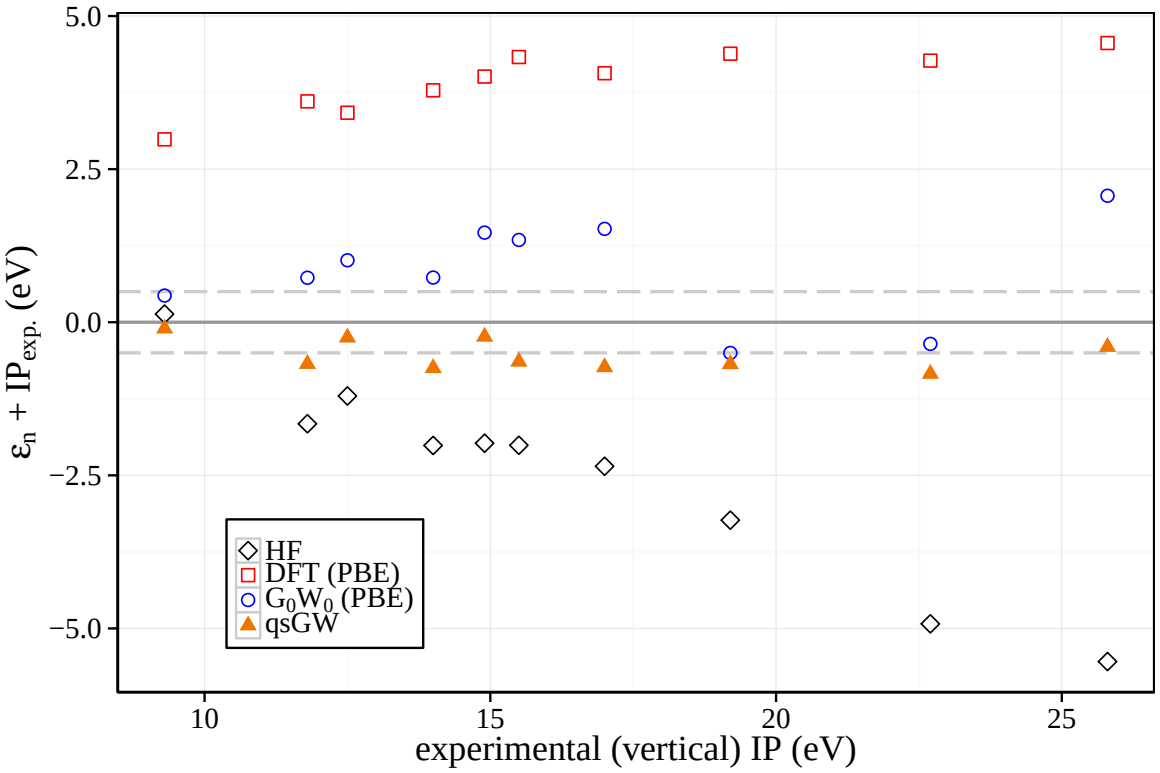

Figure 4.3: The deviation of the calculated QP-energies from G_0W_0 and qsGW, respectively the orbital eigenenergies from HF and DFT employing a PBE functional to the experimental (higher) IPs over the experimental IPs for the molecule Benzene. The G_0W_0 was initialized from a DFT calcualtion employing the PBE functional.

The scale of the difference in densities is typically two orders of magnitude smaller as the total density of the separate approaches. In areas of maximum differences it is at maximum still one order of magnitude smaller. Hence, the correction on the density introduced within qsGW is small; a self-consistent solution for the spatial shape of the QP-orbitals of Green's Function is not essential for a consistent description of the (electron) density.

4.2.3.2 Hydrogen Fluoride

To investigate the relative change from PBE and HF to qsGW also in a polar molecule, the electron density of the HF dimer is analyzed. Fig. 4.6 shows the difference between the calculated density from a DFT(PBE) calculation and the density from a qsGW calculation normalized to the (initial) DFT density. Similar to the results for the Benzene molecule, also here the qsGW shows a stronger localized density, here around the Fluoride atom. Furthermore, Fig. 4.6 shows that a portion of the charge of the non-bonding side of the hydrogen atom is dragged away, towards an outer circle around the Flouride atom in the

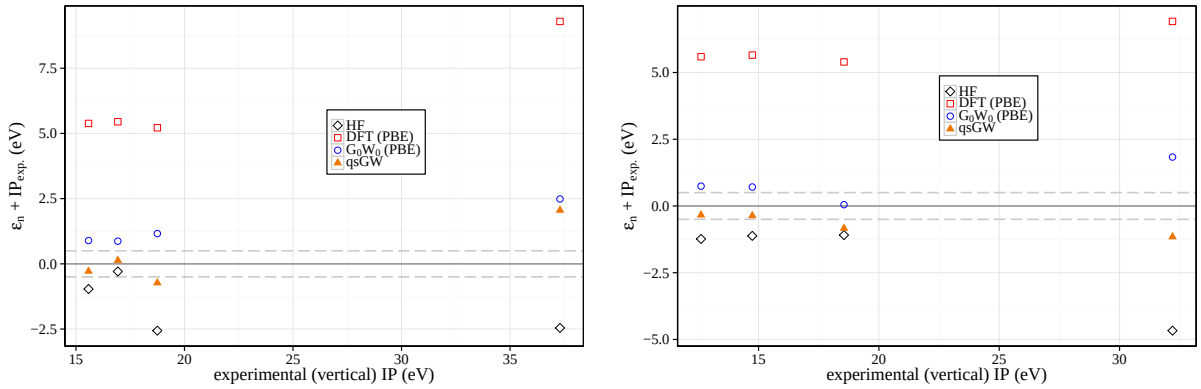

Figure 4.4: The deviation of the calculated QP-energies from G_0W_0 and qsGW, respectively the orbital eigenenergies from HF and DFT employing the PBE functional to the experimental (higher) IPs over the experimental IPs for the molecules N_2(left) and H_2O (right). The G_0W_0 was initialized from a DFT calcualtion employing the PBE functional.

qsGW result.

Fig. 4.7 shows the difference between the density calculated from HF and from qsGW normalized to the HF density. The comparison to the HF density gives qualitatively similar results as obtained with scGW by Caruso et al. (2013). The behavior is contrary to the previous analysis with respect to the DFT(PBE) density. In qsGW more charge resides within the bonding region between the hydrogen and the flouride atom. While HF tend to strongly localized charge densities due to the lack of correlation, qsGW does considered correlation between the electrons and thus smears the charge density out.

4.2.4 Dipole Moments

A good quantity to test the quality of the calculated ground state density is the dipole moment of the system. A comparison with experimental results is shown in Tab. 4.4. Different density distributions from different methods give, as a consequence, different estimates for dipole moments.

The HF results typically overestimate the dipole moment of dimers. In contrast DFT (PBE) calculations typically underestimate the dipole moment and show a MAE of 0.18 Debye. qsGW shows good agreement with an overall MAE of only 0.03 Debye. This error is in the same order of magnitude as for calculations using scGW.

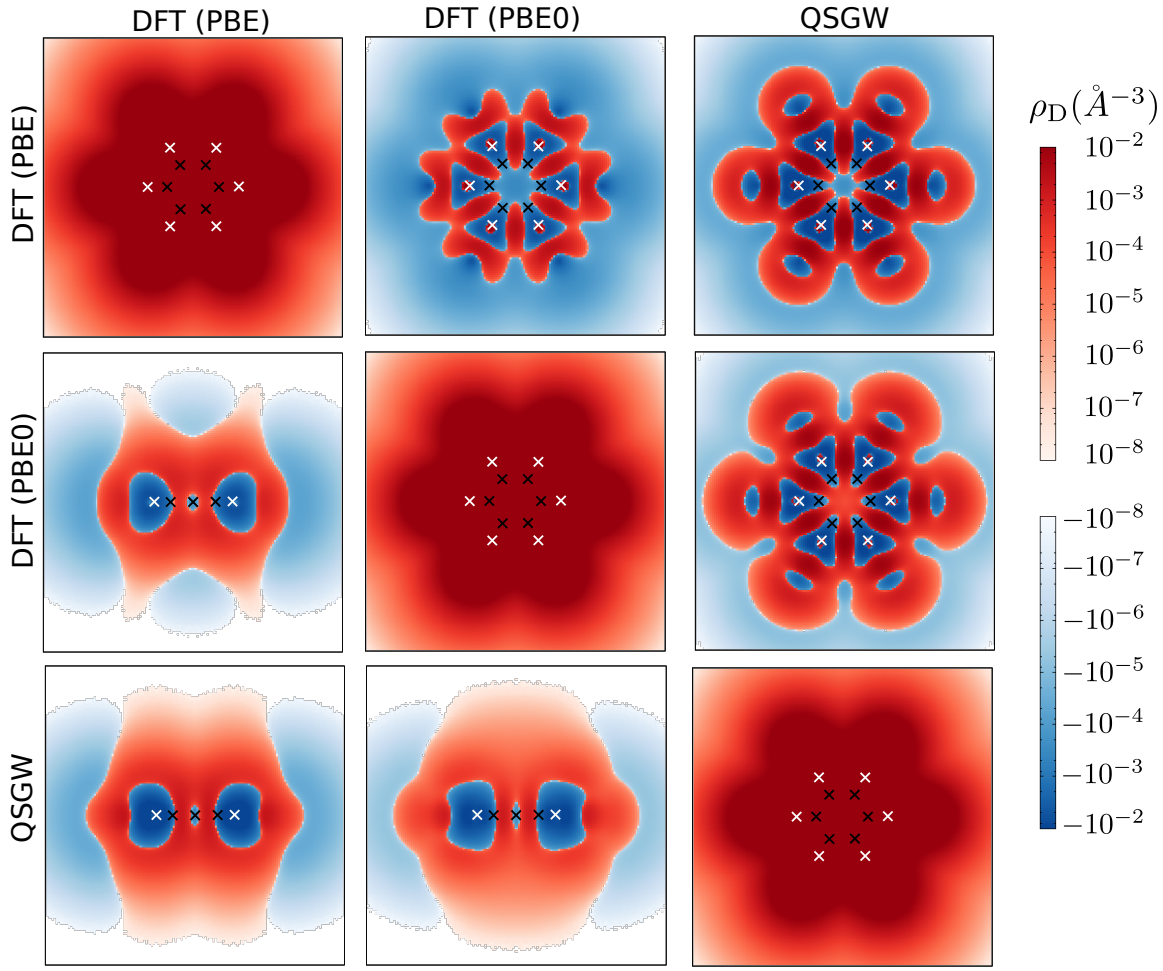

Figure 4.5: Charge density of benzene. Diagonal: density as obtained from PBE, PBE0 qsGW. A x-y plane cut at $z = 0.1$ Å through the total density of the single seperate methods are shown. On the offidagonals the differences between the-densities are shown. The x-y plane cuts, again at $z = 0.1$ Å, of the density differences of the DFT(PBE) - DFT(PBE0), DFT(PBE) - qsGW and DFT(PBE0) - qsGW density are shown in the upper right triangle. The y-z plane cuts, at $x = 0.1$ Å, through the same density differences are shown in the lower left triangle. The black crosses denote the positions of the carbon atoms, the white crosses the positions of the hydrogen atoms.

4.3 Comparison of Quasiparticle Self-Consistent GW to Full GW

Previous tests of higher IPs using qsGW are extended for five organic molecules which are candidates for optical devices. For these molecules, data obtained using the fully self-

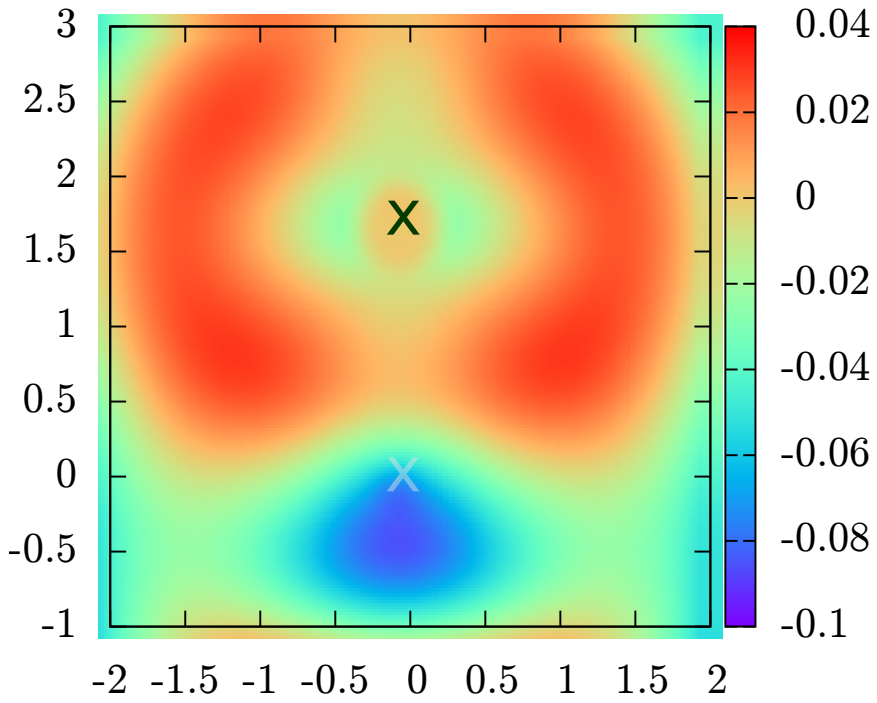

Figure 4.6: Difference between the calculated density for the system Hydrogen Fluoride between the DFT(PBE) density and the qsGW density normalized on the (initial) DFT density. The postition of the Floride atom is is denotes as a green cross, the position from the Hydrogen atom as a grey cross.

	LiH	HF	LiF	CO	MAE
Exp.	5.88	1.82	6.28	0.11	-
PBE	5.60	1.80	5.99	0.24	0.18
HF	6.03	1.95	6.50	0.26	0.16
scGW	5.90	1.85	6.48	0.07	0.07
qsGW	5.83	1.84	6.29	0.07	0.03

Table 4.4: Comparison between experimental and theoretical dipole moments from DFT (PBE), HF, fully scGW (FHI-AIMs) and qsGW. For all calculations the experimental equilibrium bond length was considered.

consistent GW approach (scGW)[2] from the FHI-Aims Package is available (Caruso et al., 2013). These five molecules serve as a benchmark to investigate effects of the different treatment of the incoherent part of the Green's Function and the Z-factor.

In this comparison one needs to be aware that the atomic structure is identical, but due

[2]The introduction of a special label for the full GW might seem contradictory and unnecessary at first sight, plain GW should be sufficient. The reason is that in the GW-community the plain label GW is often (misleadingly) used as the label for one-shot G_0W_0 calculations. To prevent any wrong interpretations the unique label scGW is introduced here.

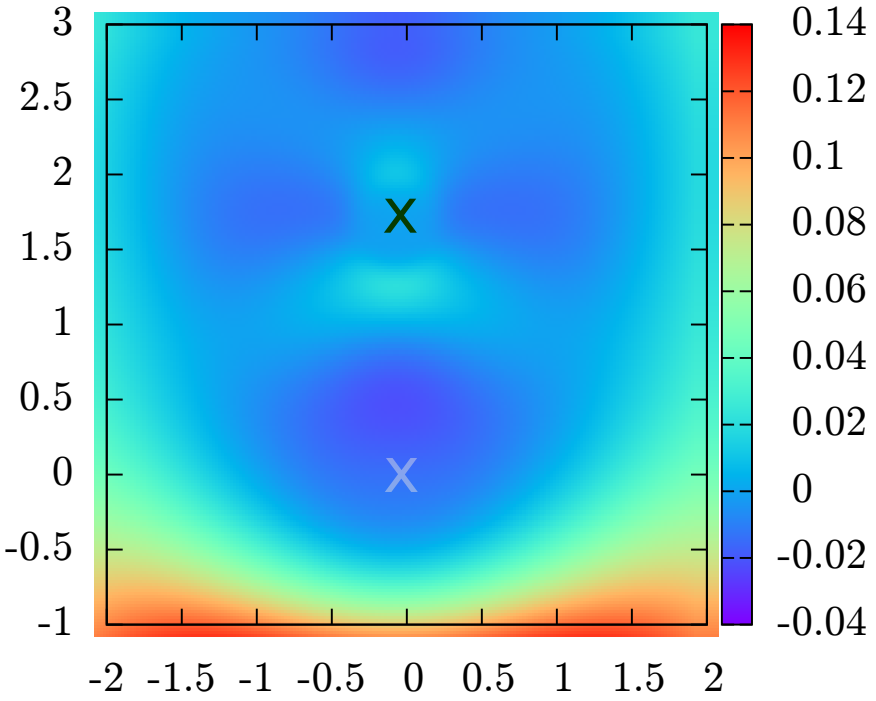

Figure 4.7: Difference between the calculated denstiy for the system Hydrogen Fluoride between the HF density and the qsGW density normalized on the (initial) HF density. The position of the Floride atom is denoted as a green cross, the position from the Hydrogen atom as a grey cross.

to technical reasons there are (minor) differences in numerical specifications. The basis set used in scGW is of comparable size, but nevertheless different, from the Gaussian Type dft2-TZVPP basis set. There is no implementation of the scGW available supporting the Gaussian-Type basis set as used in TURBOMOLE and, on the other hand, there is no implementation of the qsGW using a basis set identical to the numerical basis from the FHI-Aims package.

In Fig. 4.8 differences of the higher IPs using G_0W_0, qsGW, scGW from experimental (vertical) IPs are shown for Naphthalene; comparison of four molecules is found in the appendix (Fig. C.1). DFT, HF and G_0W_0 serve again as a reference to illustrate the improvement from scGW and qsGW.

G_0W_0 and qsGW show a relative error in the calculated higher IPs as observed before for systems N_2, H_2O and Benzene. Calculated IPs from scGW give comparable agreement with experiment as qsGW. Remarkable is that qsGW typically shows an overestimation of IPs compared to experiment. In contrast, the scGW approach typically underestimates IPs. Furthermore, there is a rigid shift of about 0.6 eV for all energy levels from qsGW to scGW for most of the molecules that were considered.

The major difference between scGW and qsGW can be understood by recalling the split of the Green's Function into the QP-part and the incoherent part $G = ZG^{\mathrm{QP}} + \bar{G}$, see Sec. 2.6. In qs$GW$ Z is equal to one and the incoherent part $\bar{G}$ is neglected. In contrast,

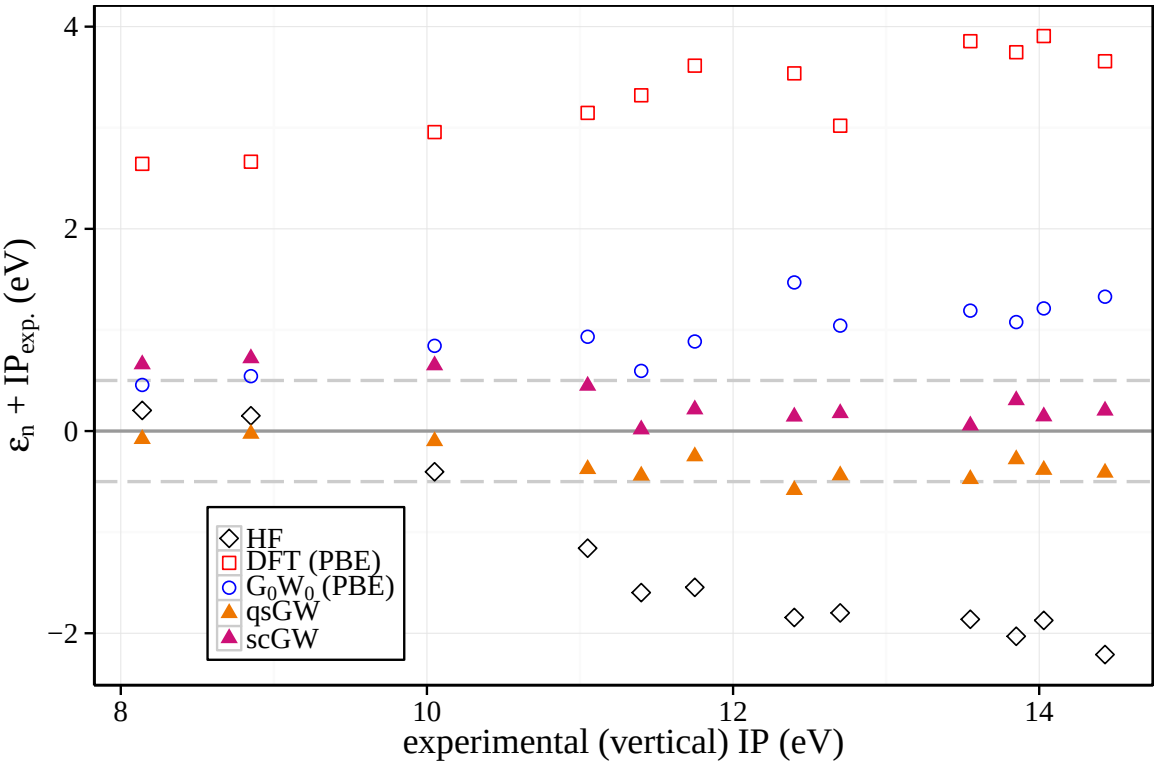

Figure 4.8: The deviation of the calculated QP-energies from G_0W_0, from qsGW, and the orbital eigenenergies from HF and DFT employing the PBE functional, respectivly, to the experimental higher IPs for the molecule Naphthalene. In addition results obtained from a scGW calculation from the FHI-Aims software package are shown (Caruso et al., 2013).

scGW takes both parts into account. Since $\bar{G}$ is relatively structureless in energy, its contribution $\bar{\Sigma} = \imath\bar{G}W$ could explain the rigid shift of qsGW-data against scGW-data seen in Fig. 4.8.

4.4 Summary

The quasiparticle self-consistent GW (qsGW) method for molecules has been implemented within the program package TURBOMOLE. The code takes advantage of existing routines especially for the construction of the response function χ, achieving high computational efficiency. qsGW scales formally with number of basis functions N with $\sim N^5$ which can be tuned down to $\sim N^4$ in practice. On the one hand, this is computationally more demanding than Density Functional Theory (DFT), which has a formal scaling of $\sim N^3$. On the other hand, qsGW is computationally less demanding then the highly accurate ΔCCSD(T) which has a formal scaling of $\sim N^7$. Therefore, larger and more complex molecules and even small

nano-structures are computationally accessible using the qsGW method. In comparison to DFT and the perturbative approach, G_0W_0, qsGW shows no dependence on the functional at all. Hence, it is truly *ab initio*.

The comparison of qsGW estimates to results obtained from popular methods like DFT, Hartree-Fock (HF) and CCSD(T) supports the impression that qsGW is a very promising tool for the theoretical investigation of electronic properties of molecules.

The first benchmark in Sec. 4.2.1 investigated the accuracy of qsGW for the prediction of first Ionization Potentials (IP). Here, the first IP served as a good first measure for the overall quality of the method. The mean absolute error (MAE) to the ΔCCSD(T) estimates improved from 0.66 eV in G_0W_0 (employing a DFT(PBE) parent system) down to 0.22 eV in qsGW, over the full test set. The MEA to the experimental (vertical) IPs showed that qsGW is nearly as accurate as ΔCCSD(T). The MEA to the experiment is in qsGW 0.35 eV and in ΔCCSD(T) 0.27 eV. The maximum error found in the test set is even smaller for qsGW then for ΔCCSD(T), see Tab. 4.3.

The benchmark of the calculation of the higher IPs, see Sec. 4.2.2, gives a further measure for the overall accuracy of the calculated Green's Function and hence for further observables. The higher IPs are the pole positions of the Green's Function. These quantities are are not accessible with CCSD(T). Even with DFT and HF higher IPs are not accessible, although it is popular to interpret lower eigenvalues as such. In comparison to the experiment DFT, HF and even G_0W_0 showed an increasing error with increasing IPs. This is not the case for estimates from qsGW. Overall qsGW shows very good agreement with experimental higher IPs over full spectra.

The comparison to estimates of higher IPs from the full self-consistent GW (scGW), which takes into account the incoherent contributions in the Green's Function and the QP-renormalization factor Z, shows that the full spectrum is shifted by a nearly constant contribution of roughly 0.6 eV for several molecules (see Sec. 4.3). This indicates that the incoherent contribution takes a rather structureless, energy independent form.

Last of all it is shown in Sec. 4.2.4 that the estimates for the ground state density from qsGW give Dipole Moments which are in better agreement with experiment than the estimates from DFT(PBE), HF and scGW. The MAE of the estimates from qsGW is only0.03 Debye over the considered set of molecules, see Tab. 4.4.

Concluding, it is shown that qsGW is an computationally efficient tool which is capable of the treatment of at least medium size molecules. It gives estimates for several primer observables in very good agreement with computationally more demanding methods and with experiment. Hence, qsGW is an efficient and accurate method to construct the Green's Function for a given molecular system which, in turn, allows access to further observables.

Chapter 5

5 Approximate Strategies for Solving the G_0W_0 Quasiparticle Equation

The quasiparticle self-consistent GW (qsGW) method is a promising tool for the investigation of electronic properties of molecules. Nevertheless, qsGW is computationally demanding. Therefore, the aim of this chapter is to develop an approximation to qsGW which is computationally more efficient but still capable to produce results of comparable accuracy.

The qsGW formalism introduces corrections on the (initial) KS-Green's Function on two levels. First, the quasiparticle (QP-)orbitals are updated. Second, qsGW introduces shifts in the poles of the Green's Function. In this chapter two approaches are developed which investigate the effect of both corrections separately, on the level of G_0W_0. The first one introduces corrections based on off-diagonal elements of the QP-equation. Hence, it takes into account shifts of the QP-energies due to corrections on the spatial shape of the orbitals. The second approach keeps the orbitals fixed, and takes into account QP-corrections in the construction of the self-energy.

Test calculations are performed for first and higher ionization potentials (IP) employing three different functionals in the parent DFT calculation. Both suggested approaches show a strong dependence on the choice of the functional. The results are compared to results obtained from qsGW. This comparison suggests that the major correction that is introduced in qsGW is due to the update of the QP-energies in the Green's Function. Whereas the update of the orbital does not influence the results in a significant way. Furthermore, the approach which considers QP-shifts in the construction of the self-energy incorporates the major beneficial features on the IP spectra introduced from qsGW.

Finally, a combined approach of both methods is suggested. A benchmark shows that it agrees even better with experiment and CCSD(T) than the qsGW approach. But, its results still strongly depend on the choice of the functional in the parent calculation.

5.1 Motivation

This section chapter introduces two distinct (approximate) treatments of the full QP-equation and of self-energy matrix elements. The resulting approaches are close relatives to G_0W_0.

The first approach, Sec. 5.2, includes off-diagonal elements of the QP-equation to account for corrections on the spatial shape of the (QP-)orbitals due to GW-corrections. To make such a treatment applicable a perturbative approach is applied and tested against the exact diagonalization, Sec. 5.4.1.2. In contrast to expectations based on qsGW corrections on the electron density, Sec. 4.2.3, rather insignificant corrections of the pole positions are found. Including the off-diagonal terms shifts the IP (usually towards less binding) at maximum only by 10meV. Which is much less then the overall correction from traditional diagonal-only G_0W_0 on the parent DFT IP estimates. The data presented in the previous chapter in Tab. 4.1 shows that this correction can reach more then 5 eV .

The second approach, Sec. 5.3, ignores all off-diagonal contributions. Whereas, it takes into account the self-consistent solution of the QP-equation. Thus, the pole positions of the Green's Function are updated for the construction of the self-energy. The benchmark shows that the approach with self-consistent poles in the construction of the self-energy introduces major corrections on the final pole positions, towards the qsGW results.

5.2 Corrections from Off-Diagonal Elements

A central step in G_0W_0 is the solution of the QP-equation. It yields the poles of the (approximate) many-body Green's Function, that define the QP-energies. A common simplification in this procedure, introduced in Sec. 2.5.2, is to neglect all off-diagonal elements of the self-energy matrix entering the QP-equation. In this section the error of this approximation is investigated quantitatively for a typical set of molecules.

5.2.1 Formalism and Implementation

In the G_0W_0 approach only one GW iteration is performed. The scheme typically starts from an improved guess, based upon an effective single-particle theory. Hence, the initial Green's Function G_0 is constructed from the initial orbitals $\psi_n^{(0)}(\mathbf{r})$ and energies $\varepsilon_n^{(0)}$ as shown in Eq. (3.17). There is no energy dependence in the QP-orbitals, $\psi_n(\mathbf{r}, z) \to \psi_n(\mathbf{r})$. Therefore the QP-equations Eq. (3.5) and Eq. (3.6) coincide in G_0W_0 and take the form,

$$\sum_{\underline{n}} \mathfrak{A}^{(1)}_{n'\underline{n}}(z)\Bigg[\int \mathrm{d}\mathbf{r}' \int \mathrm{d}\mathbf{r}\; \psi_n^{(0)}(\mathbf{r})\Big(\hat{\mathcal{H}}_{\mathrm{H}}(n^0)\delta(\mathbf{r}-\mathbf{r}')+ \\ + \hat{\Sigma}(\mathbf{r},\mathbf{r}',z)\Big)\psi_{\underline{n}}^{(0)}(\mathbf{r}')\Bigg] = \varepsilon^{(1)}_{n'}(z)\mathfrak{A}^{(1)}_{n'n}(z) \quad . \quad (5.1)$$

To improve readability, the upper index for the numbering of the iteration is omitted in the remainder of this chapter ($\mathfrak{A}^{(1)}_{n'\underline{n}}(z) \rightarrow \mathfrak{A}_{n'\underline{n}}(z)$). In addition the Braket notation is introduced to shorten the notation. The orbitals with index n, n' and $\underline{n}$ always refer to Kohn-Sham states. Furthermore, the QP-equation Eq. (5.1) can be rewritten as

$$\sum_{\underline{n}=1}^{N} \mathfrak{A}_{n'\underline{n}} \langle n|\Sigma(\varepsilon_{n'}) - V_{\mathrm{xc}}|\underline{n}\rangle = (\varepsilon_{n'} - \epsilon_n)\ \mathfrak{A}_{n'n} \ , \tag{5.2}$$

with the Kohn-Sham energies ϵ_n and the contribution of the exchange-correlation potential $\langle n|\, V_{\mathrm{xc}}\, |\underline{n}\rangle$. To establish a notation closer to the actual implementation, the matrix

$$\mathcal{M}_{n\underline{n}}(\varepsilon_{n'}) = \langle n|\Sigma(\varepsilon_{n'}) - V_{\mathrm{xc}}|\underline{n}\rangle \tag{5.3}$$

is introduced. The formal structure of the QP-equation Eq. (5.2) then reads:

$$\sum_{\underline{n}} \mathfrak{A}_{n'\underline{n}}(z) \mathcal{M}_{n\underline{n}}(z) = (\varepsilon_{n'}(z) - \epsilon_n)\, \mathfrak{A}_{n'n}(z) \ , \tag{5.4}$$

with the pole condition

$$0 = \varepsilon_{n'}(z) - z \ . \tag{5.5}$$

The matrices $\mathcal{M}(z)$ are the G_0W_0-'perturbative corrections' on top of the eigenvalues ϵ_n towards the QP-energies $\varepsilon_{n'}$.

For the following derivations the matrix family $\mathcal{M}(z)$ is assumed to be given, while $\varepsilon_{n'}(z)$ and the set of eigenvectors that forms the columns of $\mathfrak{A}_{n'\underline{n}}(z)$ are to be found. A typical self-consistency problem is faced that features a (generalized) eigenvalue problem with a matrix operator that depends on the eigen-solutions. A peculiarity appears as compared to situations familiar from Hartree-Fock or Kohn-Sham theory because $\mathcal{M}(z)$ depends on the eigenvalues, but not on the eigenstates.

5.2.1.1 Exact Diagonalization

The straight forward way to keep the off-diagonal elements in the QP-equation Eq. (5.4) is to aim for exact diagonalization. The remaining z dependence in the self-energy and the with system size cubic growing complexity of this equation makes this a numerically cumbersome task. Therefore an efficient way to find sufficient (approximate) solutions is desirable.

For the exact solution a diagonalization needs to be performed for each single pole $\varepsilon_{n'}(z)$ separately. Each diagonalization gives N_{states} solutions. Hence, in total with each single diagonalization a new full set of poles is generated. The pole which is adiabatically connected to the one from the (non-interacting) KS-system is kept whereas the remaining solutions are ignored. Technically the pole closest to the one used to set up $\Sigma_{\mathrm{c}}(z)$ is kept. In addition it needs to be ensured that one does not cross a pole of the self-energy by the selection of the pole. The solution is plugged back into Eq. (5.4) and a new diagonalization is performed.

This procedure is iterated for each single pole till a self-consistent fixed point is found. The diagonalizing procedure takes into account the off-diagonal elements of the QP-equation and in particular the self-energy, in an exact manner. The drawback is that the iterative diagonalization of the QP-equation for each single pole is computationally highly demanding. Therefore an approach is developed which drastically reduces the dimensionality of the problem, but still takes into account contributions in off-diagonal elements of the QP-equation.

5.2.1.2 Formal Perturbation Theory

The matrix $\mathcal{M}$ has a grading in the sense that its diagonal elements are much larger than the off-diagonal elements. It can be seen in Fig. 5.2 for the sample system Acrolein and in Fig. 5.1 for Benzene. This suggests the following decomposition:

$$\mathcal{M}_{n\underline{n}}(\varepsilon'_n) = \underbrace{\mathfrak{D}_n(\varepsilon'_n)\delta_{n\underline{n}}}_{\text{diagonal}} + \lambda \cdot \underbrace{\mathfrak{M}_{n\underline{n}}(\varepsilon'_n)}_{\text{off-diagonal}} \tag{5.6}$$

With Eq. (5.6) the solutions of the QP-equation Eq. (5.4) depend on λ: $\varepsilon_{n'}(\lambda), \mathfrak{A}_{n'\underline{n}}(\lambda)$. Therefore the grading of $\mathcal{M}$ suggest a perturbative expansion. The expansion up to second order in λ, according to standard perturbation theory reads;

$$\mathfrak{A}_{n'n}(\lambda, \varepsilon_{n'}) = {}_0\mathfrak{A}_{n'n}(\varepsilon_{n'})\delta_{n\underline{n}} + \lambda \cdot {}_1\mathfrak{A}_{n'n}(\varepsilon_{n'}) + \lambda^2 \cdot {}_2\mathfrak{A}_{n'n}(\varepsilon_{n'}) + \mathcal{O}(\lambda^3) \ , \tag{5.7}$$

$$\varepsilon_{n'}(\lambda) = {}_0\varepsilon_{n'} + \lambda \cdot {}_1\varepsilon_{n'} + \lambda^2 \cdot {}_2\varepsilon_{n'} + \mathcal{O}(\lambda^3). \tag{5.8}$$

The aim is self-consistency at every order of λ. In this way the expansion coefficients will effectively pick up their own (weak) $\lambda-$dependency.

5.2.1.3 Self-Consistency Cycle

The iteration cycle is initialized by a first guess for ε'_n. Typically this guess is obtained from a DFT calculation. It is denoted by ${}^{(0)}\varepsilon'_n$ and is called the parent generation. The formalism operates as follows;

(1) For $j = 0, 1, \ldots$ calculate

$$\mathcal{M}_{n\underline{n}}({}^{(j)}\varepsilon_{n'}) \rightarrow {}^{(j)}\mathcal{M}_{n\underline{n};\,n'} \tag{5.9}$$

(2) Decompose into diagonal and off-diagonal parts

$${}^{(j)}\mathcal{M}_{n\underline{n};\,n'} = {}^{(j)}\mathfrak{D}_{n;\,n'}\delta_{n\underline{n}} + \lambda\ {}^{(j)}\mathfrak{M}_{n\underline{n};\,n'} \tag{5.10}$$

(3) Solve in perturbation theory in λ the substitute problem

$$\sum_{\underline{n}} {}^{(j+1)}\mathfrak{A}_{n'\underline{n}}\ {}^{(j)}\mathcal{M}_{n\underline{n};\,n'} = ({}^{(j+1)}\varepsilon_{n'} - \epsilon_n)\ {}^{(j+1)}\mathfrak{A}_{n'\underline{n}} \tag{5.11}$$

The perturbation theory has the structure given with Eq. (5.7) and Eq. (5.8) for the quantities ${}^{(j+1)}\varepsilon_n$ and ${}^{(j+1)}\mathfrak{A}_{n\underline{n}}$.

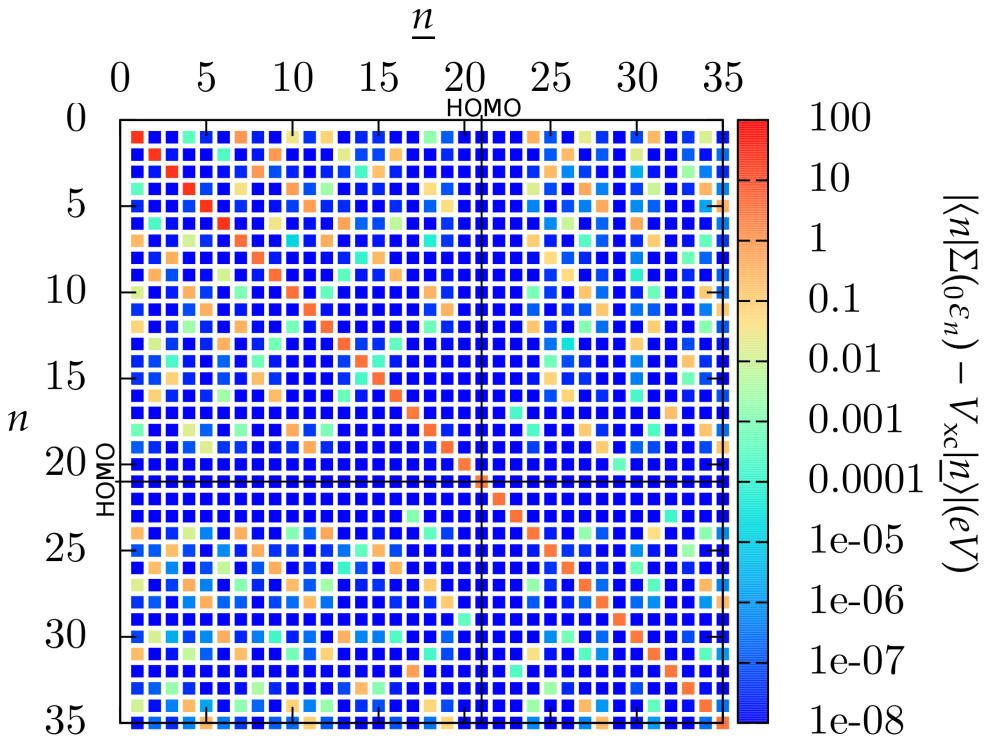

Figure 5.1: Visualization of the matrix which governs the G_0W_0 correction on KS-eigenvalues expressed in KS-reference states for the molecule Benzene. The matrix elements $\langle n|\,\Sigma(_0\varepsilon_n) - V_{\mathrm{xc}}\,|\underline{n}\rangle$ are calculated at fully converged G_0W_0 QP-energies $_0\varepsilon_n$ from the diagonalized QP-equation. The data shows that off-diagonal elements are significantly smaller then the diagonal ones. Thus, a perturbative treatment of off-diagonal elements is motivated. The high number of non-zero off-diagonal elements suggests that they introduce significant corrections on the QP-energies.

(4) Return to step (1) replacing $^{(j)}\varepsilon_{n'}$ with its update $^{(j+1)}\varepsilon_{n'}$

As usual, the perturbation theory is organized via sorting powers of λ after inserting the formal expansions Eq. (5.7), Eq. (5.8) into the expression:

$$\sum_{\underline{n}} \left[{}_0\mathfrak{A}_{n'}\delta_{n'\underline{n}} + \lambda \cdot {}_1\mathfrak{A}_{n'\underline{n}} + \mathcal{O}(\lambda^2)\right] \times \left[\,{}^{(j)}\mathfrak{D}_{n;\,n'}\delta_{n\underline{n}} + \lambda\,{}^{(j)}\mathfrak{M}_{n\underline{n};n'}\right] = \\ \left(\,{}^{(j+1)}\varepsilon_{n'} - \epsilon_n\right)\left[{}_0\mathfrak{A}_{n'}\delta_{n'n} + \lambda \cdot {}_1\mathfrak{A}_{n'n} + \mathcal{O}(\lambda^2)\right] \quad (5.12)$$

where the prefixes of $^{(j+1)}{}_0\mathfrak{A}_{n'}$ and $^{(j+1)}{}_1\mathfrak{A}_{n'n}$ have been dropped in the notation.

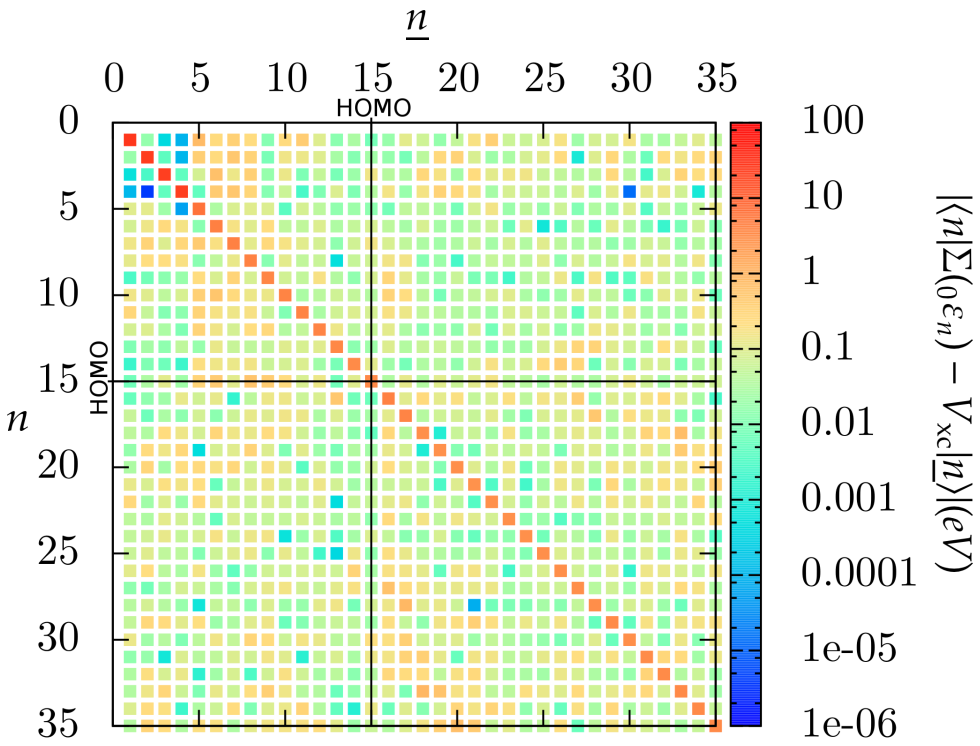

Figure 5.2: Visualization of the matrix which governs the G_0W_0 corrections on KS-eigenvalues expressed in KS-reference states, similar to Fig. 5.1. Here for the molecule Acrolein. Again, we find diagonal matrix elements which at minimum one order of magnitude larger then off-diagonal elements.

5.2.1.4 Zeroth Order Perturbation Theory

In zeroth order the diagonal approximation $\mathfrak{A}_{n'n} \rightarrow \delta_{n'n}$ is obtained,

$$^{(j)}\mathfrak{D}_{n;\,n} = {}^{(j+1)}{}_0\varepsilon_n - \epsilon_n \tag{5.13}$$

$$^{(j)}\mathfrak{A}_{n\underline{n}} = \delta_{n\underline{n}} \ . \tag{5.14}$$

There is no wavefunction update and

$$\langle n|\Sigma(_0\varepsilon_n) - V_{\mathrm{xc}}|n\rangle = {}_0\varepsilon_n - \epsilon_n \tag{5.15}$$

is iterated to self-consistency in ${}_0\varepsilon_n$. This is the standard way to do G_0W_0 and is commonly not further specified in literature. Here, this nomenclature is adopted and the label G_0W_0 refers to the diagonal only solution.

5.2.1.5 First Order Perturbation Theory

The terms of first order in λ are compared,

$$ {}^{(j+1)}{}_0\mathfrak{M}_{n'} \cdot {}^{(j)}\mathcal{M}_{nn';\,n'} + {}^{(j+1)}{}_1\mathfrak{A}_{n'n} \cdot {}^{(j)}\mathfrak{D}_{n;\,n'} = \\ ({}^{(j+1)}{}_0\varepsilon_{n'} - \epsilon_n) \cdot {}_1\mathfrak{A}_{n'n} + {}^{(j+1)}{}_1\varepsilon_n \cdot {}_0\mathfrak{A}_n\delta_{n'n} \ , \quad (5.16) $$

and then two cases are considered. If $n = n'$, then

$$ {}_0\mathfrak{A}_n \cdot {}^{(j)}\mathfrak{M}_{nn;\,n} + {}_1\mathfrak{A}_{nn} \cdot {}^{(j)}\mathfrak{D}_{n;\,n} = ({}^{(j+1)}{}_1\varepsilon_n - \epsilon_n){}_1\mathfrak{A}_{nn} + {}_0\mathfrak{A}_n \, {}^{(j+1)}{}_1\varepsilon_n \ , \quad (5.17) $$

again dropping prefixes of ${}^{(j+1)}{}_0\mathfrak{A}_{n'}$ and ${}^{(j+1)}{}_1\mathfrak{A}_{n'n}$. By construction, the diagonal elements of $\mathfrak{M}, {}_1\mathfrak{A}$ are all zero and therefore the left-hand side of this equation vanishes; hence

$$ {}^{(j+1)}{}_1\varepsilon_n = 0 \ . \quad (5.18) $$

Therefore corrections due to off-diagonal elements in $\mathcal{M}$ appear in the QP-energies ε_n at first to second order in λ.

The linear corrections to the eigenvectors are extracted from the off-diagonal case, $n \neq n'$, leading to

$$ {}_1\mathfrak{A}_{n'n} = {}_0\mathfrak{A}_{n'} \frac{{}^{(j)}\mathfrak{M}_{nn';\,n'}}{{}^{(j)}{}_0\varepsilon_{n'} - \epsilon_n + {}^{(j)}\mathfrak{D}_{n;\,n'}}, \quad n' \neq n \quad (5.19) $$

while ${}_1\mathfrak{A}_{nn} = 0$. Eq. (5.19) gives the leading order mixing of the Kohn-Sham-states into the QP-wave functions. The set of coefficients ${}_0\mathfrak{A}_n$ is found from the normalization condition. It is noteworthy that as long as the interest is only in the leading order corrections to the eigenvectors it is sufficient to first find the self-consistent zero-order solution

$$ \mathfrak{D}_n(z_n^{(0)}) = z_n^{(0)} - \epsilon_n \ , \quad (5.20) $$

where $z_n^{(0)} = {}^{\infty}{}_0\varepsilon_n$ and then obtain the correction in first order;

$$ {}_1\mathfrak{A}_{n'n} = {}_0\mathfrak{A}_{n'} \frac{{}^{(j)}\mathfrak{M}_{nn'}(z_{n'}^{(0)})}{z_{n'}^{(0)} - \epsilon_n + \mathfrak{D}_n(z_{n'}^{(0)})} \ . \quad (5.21) $$

5.2.1.6 Second Order Perturbation Theory

Again all terms of the same order are collected, here order to λ^2

$$ {}_2\mathfrak{A}_{n'n} \Big[{}^{(j)}\mathfrak{D}_{n;\,n'} - ({}^{(j+1)}{}_0\varepsilon_{n'} - \epsilon_n) \Big] + \\ \sum_{\underline{n}} {}_1\mathfrak{A}_{n'\underline{n}} \, {}^{(j)}\mathfrak{M}_{n\underline{n};\,n'} = {}_0\mathfrak{A}_{n'} \, {}^{(j+1)}{}_2\varepsilon_{n'}\delta_{n'n} \ . \quad (5.22) $$

Then, only the diagonal case is considered, $n' = n$:

$$ \sum_{\underline{n}} {}_1\mathfrak{A}_{n\underline{n}} \, {}^{(j)}\mathfrak{M}_{n\underline{n};\,n} = {}_0\mathfrak{A}_n \, {}^{(j+1)}{}_2\varepsilon_n \quad (5.23) $$

where ${}_2\mathfrak{A}_{nn} = 0$ has been employed. Using Eq. (5.19) one finds

$$ {}^{(j+1)}{}_2\varepsilon_n = \sum_{\underline{n}\neq n} \frac{{}^{(j)}\mathfrak{M}_{\underline{n}n;\,n}\ {}^{(j)}\mathfrak{M}_{n\underline{n};\,n}}{{}^{(j+1)}{}_0\varepsilon_n - \epsilon_{\underline{n}} - \ {}^{(j)}\mathfrak{D}_{\underline{n};\,n}} \tag{5.24} $$

This leads to an updated QP-energy,

$$ {}^{(j+1)}\varepsilon_n = \ {}^{(j+1)}{}_0\varepsilon_n + \lambda^2 \cdot \ {}^{(j+1)}{}_2\varepsilon_n + \mathcal{O}(\lambda^3) \ . \tag{5.25} $$

This improved energies (${}^{(j+1)}\varepsilon_n$) are plugged back into **(1)** for updating the matrix elements when iterating the process towards the self-consistent fixed point. The cycle is terminated after a fixed number of iterations. In the presented benchmarks the number of iterations was chosen to be 20. In this way the increment $|\ {}^{(j+1)}\varepsilon_n - \ {}^{(j)}\varepsilon_n|$ is below a threshold of $\delta = 0.1$ meV. For the sake of consistency we stick to the label G_0W_0 for the zeroth order results from Eq. (5.15) and point out the second order treatment by an additional suffix: G_0W_0-2nd.

A comparison of the second order energies from Eq. (5.25) to the qsGW and the G_0W_0 estimates yields a measure of the effect of corrections on the orbitals from qsGW on the energy estimates. Furthermore, using the second order approach allows in principle to access corrections on the spatial shape of the orbitals, see Eq. (5.19). This is not performed primarily due to computational reasons; The transformation matrix is inherently dependend on the pole ε_n. Therefore, the application of the first order update on the orbitals gives neither orthogonal or normalized orbitals. Within the TURBOMOLE framework the orthonormality of the orbitals is essential for low level routines. Hence, the evaluation of properties of non-orthonormal orbitals causes major programming effort. Solving this problem was not done within the project of this thesis. For the presented analysis, the effect on the pole positions due to the orbital corrections is a adequate measure for the modification of the orbitals.

5.2.2 Comparison to Quasiparticle Self-Consistent GW

All presented calculations in this section are done with the same numerical parameters as were in the benchmark of the qsGW method, Sec. 4.1. To point out the chosen nomenclature: the conventional diagonal only G_0W_0 approach is labeled with the common label "G_0W_0". The extension which takes into account off-diagonal contributions from the next higher contribution order in perturbation theory is "G_0W_0-2nd".

Both approaches are based on the screened interaction W_0 calculated from the underlying parent calculation. Therefore it inhabits still a dependence on the choice of the functional in the parent DFT calculation. As it will turn out are the results of G_0W_0-2nd very close to the G_0W_0 results. Therefore, is the dependence on the choice of the amount of exact exchange in the PBE hybrid functional identical to the one reported in the study already performed in Sec. 3.2.3.1.

The calculations performed for the studies in this section employed the PBEλ functional (see Sec. 3.2.3.1) as well. Three different amounts of exact exchange were considered. The

standard PBE functional without any exact exchange contribution, the popular PBE0 functional with 25% exact-exchange and the PBE-hybrid with 75% exact-exachange (PBE75) which was found as the optimum starting point for the G_0W_0 zeroth order calculation, see Sec. 3.2.3.1. This way the optimum starting point can be deduced from the following study.

5.2.2.1 First Ionization Energies

The distance of calculated HOMO energies to the ones obtained from qsGW is the measure whether the approach incorporates the dominant part of the contributions from qsGW.

Fig. 5.3 shows the difference of the calculated HOMO energies of the G_0W_0-2nd and the diagonal only G_0W_0 approach to the qsGW HOMO energies. The starting point varied the amount of exact exchange mixed into PBE hybrid functional of the parent DFT calculation.

The results show that, independent of the chosen starting point, the corrections introduced by the off-diagonal contributions are mostly insignificant. The second order approach introduces in general a correction of only a few meV towards better agreement with the qsGW, typically towards stronger binding. Here one special case is remarkable, the dimer Au_2 with the plain DFT(PBE) parent system. In this case the correction from the second order approach leads to weaker binding, but still to better agreement with qsGW for the PBE starting point.

The statistical measures, Tab. 5.1, supports these findings. It shows that the shift from the second order approach scales with the quality of the starting point. The average improvement from off-diagonals is largest for the PBE starting point of 0.05 eV. Likewise is this the case with the biggest average error at zeroth order level to the qsGW results of 0.75 eV.

Employing an improved starting point, PBE0, gives an overall error of only 0.42 eV at zeroth order level. In comparison is the improvement on top of this result from second order contributions very small. The shift is on average only 0.01 eV towards better agreement.

In contrast leads the application of the second order approach on top of diagonal-only G_0W_0-optimized PBE75 starting points to worsened agreement with the qsGW results. Nevertheless gives, from the three considered starting points, PBE75 the best agreement of the second order approach with qsGW, as well as the zeroth order only approach.

5.2.2.2 Higher Ionization Energies

The consideration of the first IPs, respectively the HOMO energies, over the full test set gives a first impression which correction on the (KS-)Green's Function introduces the major correction towards the qsGW Green's Function. In this section, the test is extended for energetically stronger bound states as well, the higher IPs.

The example molecule Naphthalene is chosen to show the effects on the higher IPs of the second order approach, Fig. 5.4. Additional molecules are considered in the appendix, Fig. C.2. The results show the similar behavior as for the first IPs. The corrections on top of G_0W_0 by the G_0W_0-2nd approach are marginal. The error to the qsGW results is growing with energy on G_0W_0-2nd level as well as it does in G_0W_0 for the calculation with the PBE

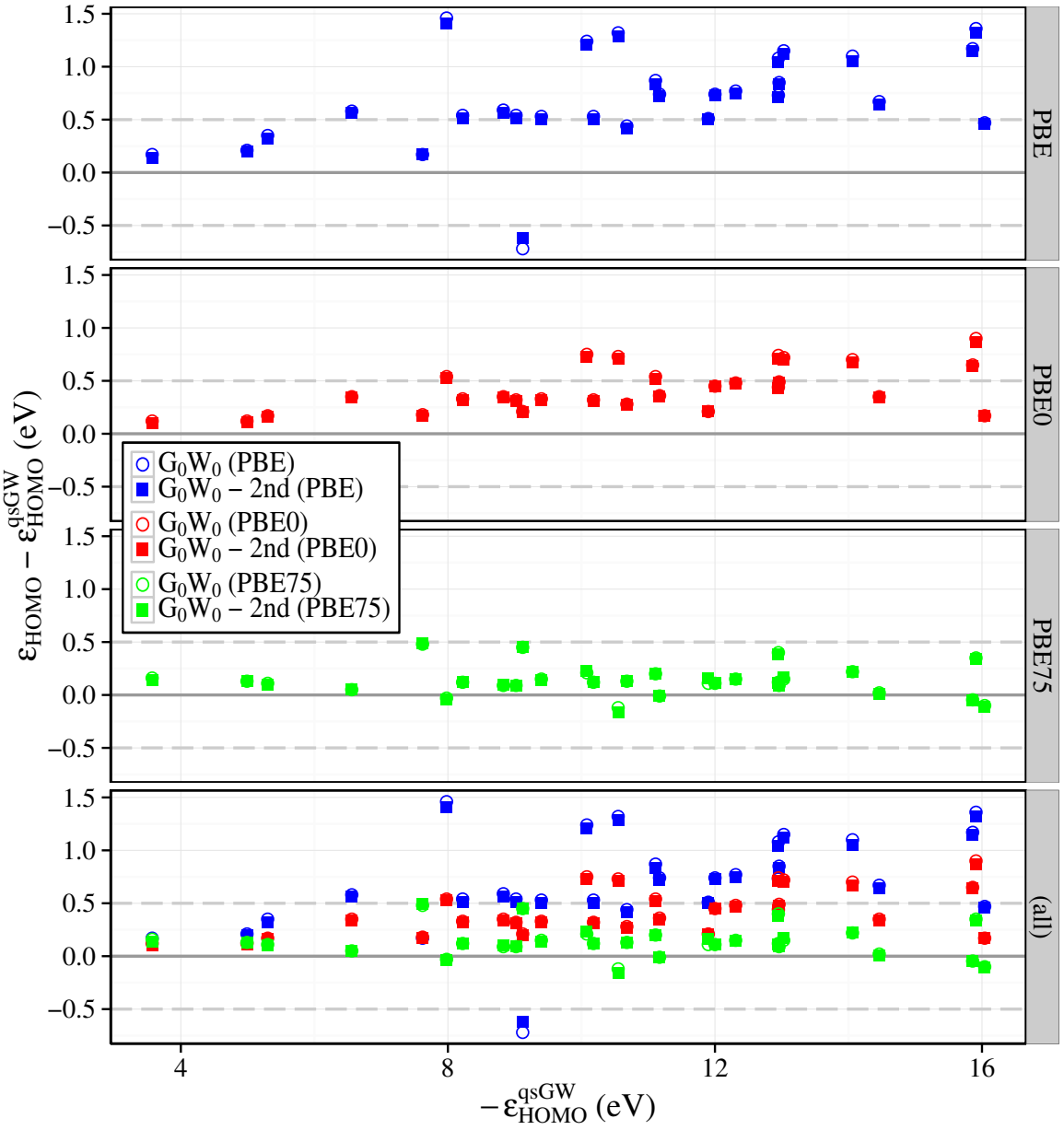

Figure 5.3: The distance of calculated HOMO energies to the qsGW results using G_0W_0 and G_0W_0-2nd. Results are shown for calculations initialized from DFT, employing PBE and PBE hybrid XC-functionals with an exact exchange contribution of 25% (PBE0) and 75% (PBE75). On average the best agreement is achieved by employing the PBE75 starting point, Tab. 5.1.

G_0W_0	@PBE		@PBE0		@PBE75	
	0th	2nd	0th	2nd	0th	2nd
ME	0.70	0.67	0.42	0.41	0.13	0.13
MAE	0.75	0.72	0.42	0.41	0.16	0.16
σ^2	0.20	0.18	0.05	0.04	0.02	0.02
MaxAE	1.46	1.41	0.90	0.87	0.48	0.49
MinAE	0.17	0.14	0.12	0.10	0.01	0.01

Table 5.1: Evaluation over the data from Fig. 5.3. Evaluated is the difference of the calculated G_0W_0 and G_0W_0-2nd HOMO energies to the qsGW HOMO cumulated over the test set. Three different DFT based starting points have been employed. On average, best agreement is achieved with the PBE hybrid XC-functionals with an exact exchange contribution of 75% as the starting point (PBE75). Reported are the mean error (ME), the mean absolute error (MAE), the maximum absolute error (MaxAE) and the minimum absolute error (MinAE) as well as the variance (σ^2).

and PBE0 parent system. Furthermore, the results show again a strong dependence on the starting point. The starting point with an exact exchange of 75% mixed into the PBE functional gives the best agreement, as it is for the diagonal-only G_0W_0 approach as well. Employing the optimized PBE75 starting point removes the energy dependence of the error.

5.3 Quasiparticle Shifts in the Self-Energy

To account for corrections on the pole positions in the Green's Function another approach is suggested in this section. In this approach the orbitals are kept fixed, but updates on the pole positions of the Green's Function G are iterated in the QP-equation, and considered in the construction of the self-energy, till a self-consistent fixed point is found.

5.3.1 Formalism and Implementation

After dropping the running index (i) the QP-equation, Eq. (3.15), from the first qsGW iteration reads;

$$\sum_{\underline{n}} \mathfrak{A}_{n'\underline{n}} \ \langle n| \, \hat{\mathcal{H}}_{\mathrm{H}} + \Sigma(\varepsilon_{n'}) \, |\underline{n}\rangle = \varepsilon_{n'} \mathfrak{A}_{n'n} \ . \tag{5.26}$$

To exclude any effects due to the spatial shape of the orbitals only the diagonal part is considered, $\mathfrak{A}_{n'\underline{n}} \to \delta_{n'\underline{n}}$, as it is done in traditional G_0W_0 respectively in zeroth order perturbation theory, see Eq. (5.15). The remaining diagonal-only G_0W_0 QP-equation reads

$$\langle n| \, \hat{\mathcal{H}}_{\mathrm{H}} + \Sigma(\varepsilon_n) \, |n\rangle = \varepsilon_n \ . \tag{5.27}$$

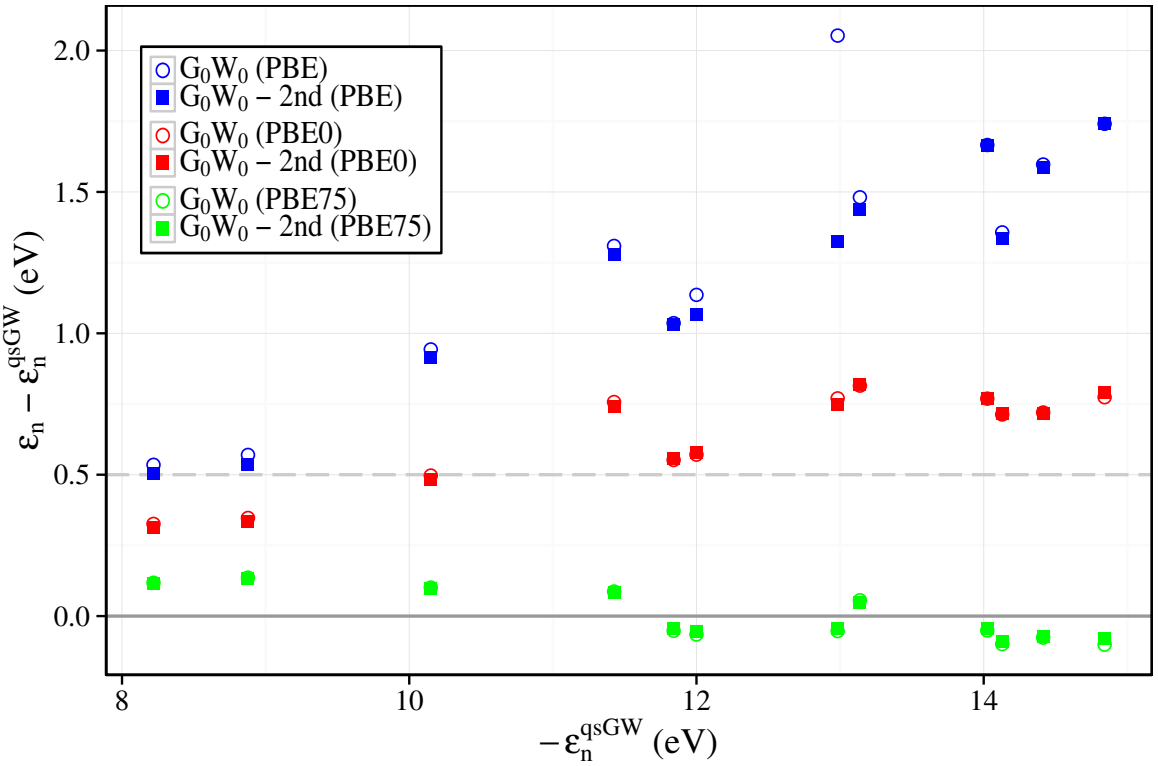

Figure 5.4: The deviation of the QP-energies from diagonal only and second order G_0W_0 from qsGW for Naphthalene. Three different DFT based starting points PBE, and PBE hybrid functional with 25% (PBE0) and with 75% exact exchange (PBE75), were chosen. The best agreement is obtained by the calculation with the PBE75 parent.

5.3.1.1 Self-Consistency in the Quasiparticle Energies

In the $G_{\text{fo}}W_0$ approach the G_0W_0 self-energy is replaced by a self-energy calculated with fixed orbitals (fo) for the updated G. The screening is still based upon the parent system ($\rightarrow W_0$). In practice is the G_0W_0 self-energy $\Sigma(\varepsilon_n)$ replaced by the self-energy with updated poles ε_n at any occurrences of the initial (KS-)energies ϵ_n in the diagonal QP-equation, Eq. (5.27).

Although this approach introduces a self-consistent feature in the Green's Function its computational effort is identical to the effort of traditional G_0W_0. The exchange contribution from the self-energy does not change at all in practice. It still is the sum of the coulomb exchange integrals over the occupied initial (KS-)orbitals, see Eq. (3.35). Thus, it does not need to be reevaluated.

In the calculation of the correlation part of the self-energy does the poles receive a shift by the QP-correction. Hence, still the same sums need to be evaluated, but with exchanged energies at certain contributions. The calculation of the correlation self-energy with shifted

poles and the solution of the QP-equation is performed within a self-consistency cycle till a fixed point is found for each pole ε_n.[1]

During these (intermediate) iterations does the screened interaction W, respectively ρ_m and Ω_m, remains to be based on the parent system. Hence, the computationally expensive calculation of the objects $(\underline{n}n|\rho_m)$ and Ω_n is performed only once. The update is solely performed in the poles of G in a self-consistent manner. The solutions of the QP-equation ε_n are used as the poles of G, i.e. they replace the poles ϵ_n from the KS-system. Taking this update into account the expression for the calculation of the matrix elements of the correlation part of the self-energy $\Sigma_\mathrm{c}(E)$, see Eq. (3.40), reads

$$\begin{aligned}\mathrm{Re}(\langle n|\,\Sigma_\mathrm{c}^{G_\mathrm{fo}W_0}(E)\,|n'\rangle) = \sum_m \Bigg[&\sum_i^{\mathrm{occ}} (in|\rho_m)(\rho_m|n'i) \times \frac{E-\varepsilon_i+\Omega_m}{(E-\varepsilon_i+\Omega_m)^2+\bar{\eta}^2} \\ &+ \sum_a^{\mathrm{unocc}} (an|\rho_m)(\rho_m|n'a) \times \frac{E-\varepsilon_a-\Omega_m}{(E-\varepsilon_a-\Omega_m)^2+\bar{\eta}^2} \Bigg] \ .\end{aligned} \tag{5.28}$$

5.3.1.2 Application in Quasiparticle Self-Consistent *GW*

In the full qsGW formalism it is possible to take advantage of this approach as well. As mentioned before, the computational cost for the calculation of the different contributing objects within each single iteration differs strongly. The dominant part within qsGW is the calculation of the response function χ. In comparison, solving the substitute effective equation Eq. (3.15) is a rather cheap task. Therefore it is computationally favorable to do multiple iterations separately on this equation while the response function is kept fix.

The mapping of the energy dependent self-energy $\Sigma(\mathbf{r},\mathbf{r}',z)$ on the energy independent self-energy $\tilde{\Sigma}(\mathbf{r},\mathbf{r}')$ in Eq. (3.43) shows that the structure of the resulting $\tilde{\Sigma}(\mathbf{r},\mathbf{r}')$ is still dependent on the QP-energies $\varepsilon_n^{(i)}$. Here, it is beneficial to feed back the resulting poles of the diagonalization of the effective equation Eq. (3.15) into the construction of the self-energy. This is identical to the procedure suggested in $G_\mathrm{fo}W_0$. In this way cheaper, intermediate, steps toward a self consistent solution are done without the need to construct the full response function.

Applying this approach in qsGW, the matrix element of the approximate Hermitian contribution, Eq. (3.43) reads ,

$$\left\langle n^{(i)}\right| \tilde{\Sigma}_\mathrm{c}^{G_\mathrm{fo}W_0} \left|\underline{n}^{(i)}\right\rangle = \frac{1}{2}\Big(\left\langle n^{(i)}\right| \hat{\Sigma}^{G_\mathrm{fo}W_0}(\varepsilon_{n'}^{(i+1)}) \left|\underline{n}^{(i)}\right\rangle \delta_{nn'} + \left\langle n^{(i)}\right| \hat{\Sigma}^{G_\mathrm{fo}W_0}(\varepsilon_{n'}^{(i+1)}) \left|\underline{n}^{(i)}\right\rangle \delta_{n\underline{n}}\Big) \ . \tag{5.29}$$

with the $G_\mathrm{fo}W_0$ self-energy from Eq. (5.28). Here, the running index (i) of the qsGW iteration has been restored.

Employing this approximate self-energy and solving the effective problem can be iterated till self-consistency within Eq. (3.15) and the mapping Eq. (3.43) is achieved. Afterwards,

[1] This self-consistency cycle is adopted from the G_0W_0 formalism which aims for a self-consistent solution of the QP-equation for one pole $\varepsilon_{n'}$. Here all occurrences of ε_n are iterated till self-consistency. Typically 20 iterations are sufficient to converge the QP-energies ε_n within 0.1 meV.

the procedure steps back into the full qsGW cycle and proceeds to construct a new response function again.

Taking advantage of this inner cycle saves several iterations within the outer qsGW cycle and still leads to the identical fixed point solution.

5.3.2 Comparison to Quasiparticle Self-Consistent GW

The proceeding for the evaluation of the $G_{\text{fo}}W_0$ method is similar to the one chosen for the G_0W_0-2nd approach, Sec. 5.2.2. All presented calculations in this section are done with the same numerical parameters as were in the benchmark of the qsGW method, Sec. 4.1. To check for the dependence of the results on this initial calculation the PBEλ functional (see Sec. 3.2.3.1) is employed with three different amounts of exact exchange [2] . The standard PBE functional without any exact exchange contribution, the popular PBE0 functional with 25% exact-exchange and the PBE-hybrid with 75% exact-exachange (PBE75) which was found as the optimum starting point for the G_0W_0 zeroth order calculation, see Sec. 3.2.3.1.

5.3.2.1 First Ionization Energies

The distance of calculated HOMO energies to the ones obtained from qsGW is the measure whether the approach incorporates the dominant part of the contributions from qsGW.

The consideration of self-consistency in the pole positions shows strong shift on the HOMO energies, Fig. 5.5. The $G_{\text{fo}}W_0$ HOMOs show strongly improved agreement with the qsGW reference for the PBE and PBE0 starting point in comparison to traditional G_0W_0, Tab. 5.2. In contrast, the initialization from PBE75 gives worse agreement of the $G_{\text{fo}}W_0$ approach, whereas it showed the best agreement with qsGW at diagonal only G_0W_0 level. The MAE of 0.16 eV at G_0W_0 increases to a MEA of 0.18 eV from $G_{\text{fo}}W_0$. Nevertheless, the PBE75 functional as the parent system gives best agreement of the $G_{\text{fo}}W_0$ approach with the qsGW calculation.

5.3.2.2 Higher Ionization Energies

The higher IPs obtained from $G_{\text{fo}}W_0$ for the example Naphthalene are shown in Fig. 5.6. Results for further molecules are reported in the appendix in Fig. C.3. The $G_{\text{fo}}W_0$ improves the agreement with qsGW for the higher IPs in comparison to G_0W_0. The feature that the error increases with the energy, which was present in the diagonal only G_0W_0 and G_0W_0-2nd order results is strongly suppressed in $G_{\text{fo}}W_0$.

Overall the data shows that the correction due to the self-consistency in the pole positions scales with the error from the G_0W_0 calculation. For the rather bad starting point PBE $G_{\text{fo}}W_0$ introduces a strong correction towards better agreement with qsGW. For the

[2] An extended study for this effect is in the appendix in Fig. C.8, employing a PBE hybrid functional with scalable exact exchange, as it was performed already in Sec. 3.2.3.1.

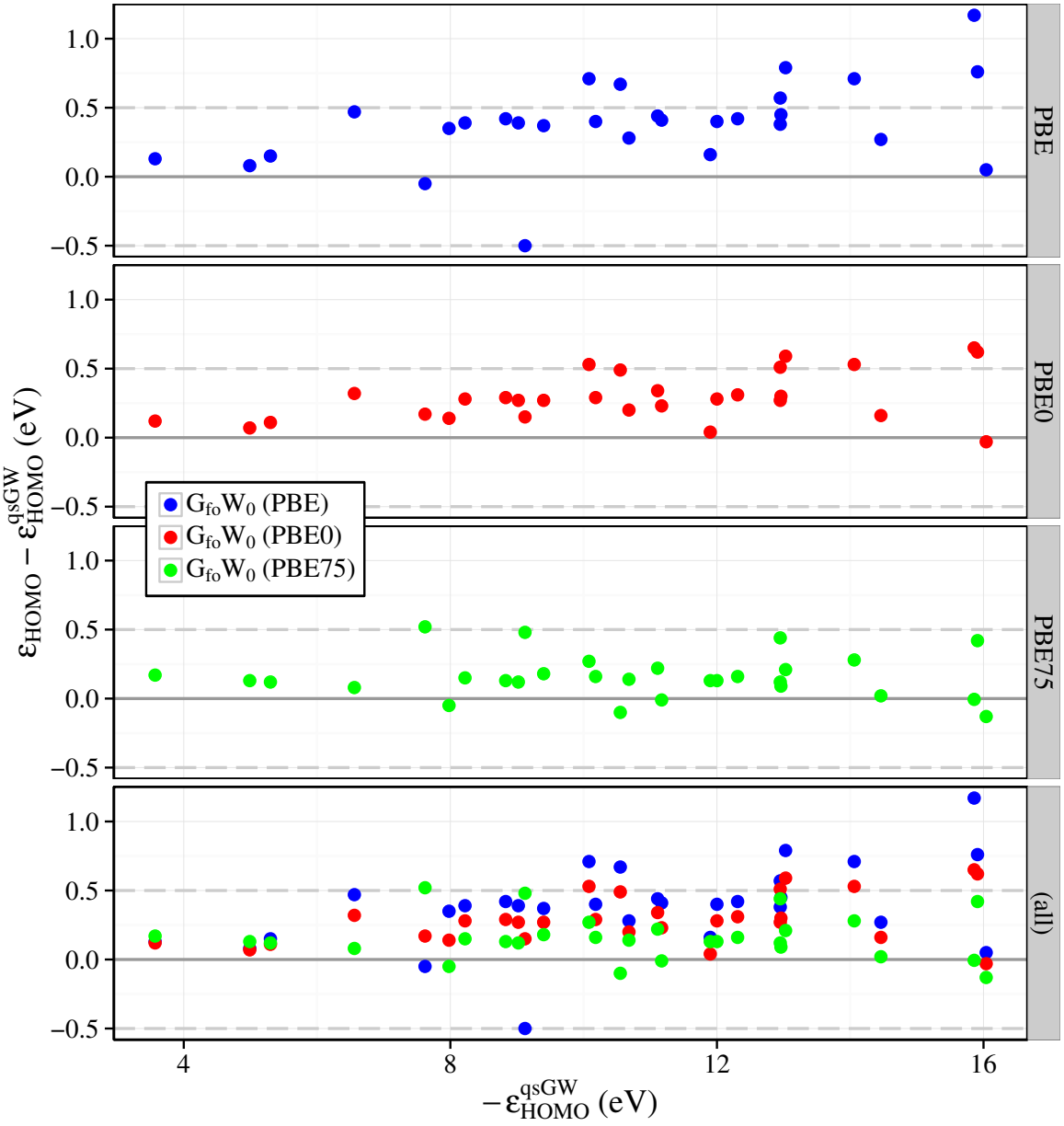

Figure 5.5: The distance of calculated HOMO energies to the qsGW HOMO energie using $G_{fo}W_0$ from DFT(PBEλ) starting points . With increasing exact exchange contribution in the PBEλ parent improves the agreement with qsGW. Nevertheless, we find for all starting points errors which increase with energy. The statistical evalutaiton is reported in Tab. 5.2.

	@PBE			@PBE0			@PBE75		
	G_0W_0		$G_{\text{fo}}W_0$	G_0W_0		$G_{\text{fo}}W_0$	G_0W_0		$G_{\text{fo}}W_0$
	0th	2nd		0th	2nd		0th	2nd	
ME	0.70	0.67	0.39	0.42	0.41	0.29	0.13	0.13	0.16
MAE	0.75	0.72	0.43	0.42	0.41	0.30	0.16	0.16	0.18
σ^2	0.20	0.18	0.09	0.05	0.04	0.03	0.02	0.02	0.02
MaxAE	1.46	1.41	1.18	0.90	0.87	0.66	0.48	0.49	0.53
MinAE	0.17	0.14	0.04	0.12	0.10	0.04	0.01	0.01	0.00

Table 5.2: Evaluation over the data from Fig. 5.3 and Fig. 5.5. Evaluated is the difference of the calculated diagonal only G_0W_0 (0th) and G_0W_0-2nd (2nd) as well as the $G_{\text{fo}}W_0$ HOMO energies to the qsGW HOMO cumulated over the test set. Three different DFT based starting points have been employed. On average, best agreement is achieved with the PBE hybrid XC-functionals with an exact exchange contribution of 75% as the starting point (PBE75).

optimized starting point PBE75, the correction from $G_{\text{fo}}W_0$ is minimal and the agreement with qsGW is nearly identical in comparison with G_0W_0.

5.4 Combining Off-Diagonal Solution and Quasiparticle Shifts in the Self-Energy

The results of the previous section showed that the self-consistency on the pole positions within the Green's Function G introduces already major contributions towards the self-consistent qsGW result. Furthermore it was shown that corrections from the second order approach are rather marginal, but nevertheless introduced corrections towards better agreement with qsGW.

The computational cost of $G_{\text{fo}}W_0$ is identical to G_0W_0. The additional cost from the second order approach is expected to be small. The theoretical scaling for all approaches is dominated from the construction of the response function, which scales with the number of basis functions N with $\sim N^5$ (in theory)[3]. Hence, the combined approach may yield a computationally fast and accurate alternative for the calculation of IPs.

In this section the combination of $G_{\text{fo}}W_0$-2nd, is tested in a benchmark whether it is a reliable tool for the calculation of (higher) IPs. The results show that the combined method improves upon the single separate methods. But, the problem of a strong functional dependence of the results remains.

[3]A benchmark of the computational cost of all approximate approaches is performed in Sec. 5.5.

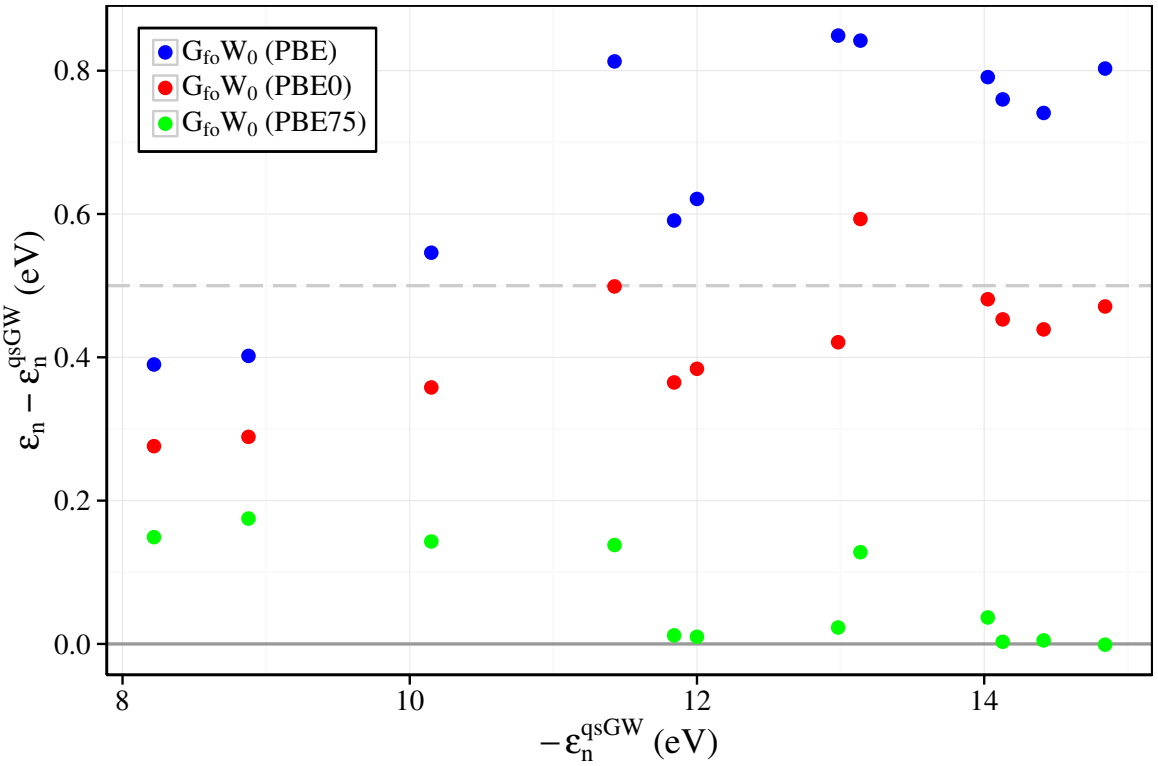

Figure 5.6: The deviation of the QP-energies from $G_{\text{fo}}W_0$ to QP-energies from qsGW for Naphthalene. Three different DFT based starting points employing the PBE, and the PBE hybrid functional with 25% (PBE0) and with 75% exact exchange (PBE75) were chosen. The best agreement yields the calculation with the PBE75 parent. The grey dashed line indicates a deviation of 0.5 eV.

5.4.1 Formalism and Validation

Combining both approaches is done by, on the one hand, solving the QP-equation taking off-diagonal elements into account, as it was described in Sec. 5.2.1.2. On the other hand, the second order solutions, Eq. (5.25), are plugged back into the calculation of the self-energy Σ as it was suggested in the $G_{\text{fo}}W_0$ formalism, Sec. 5.3.

5.4.1.1 Dependence of Ionization Energies on the Initialization

In $G_{\text{fo}}W_0$-2nd the considered screening is based upon the underlying parent calculation. Therefore it inhabits still a dependence on the choice of the functional in the parent DFT calculation. The strength of this effect is studied employing a PBE hybrid function with scalable exact exchange, as it was performed already in Sec. 3.2.3.1.

Fig. 5.7 shows the spread Δ_λ of the HOMO from the $G_{\text{fo}}W_0$-2nd over the spread in the estimates from traditional G_0W_0. The $G_{\text{fo}}W_0$-2nd approach shows a reduced dependence

on the starting point in comparison to traditional G_0W_0 throughout the full test set. Nevertheless, $G_{\text{fo}}W_0$-2nd predicts first IPs which vary up to 1.5 eV (excluding the spacial case H_2) with the choice of the functional.

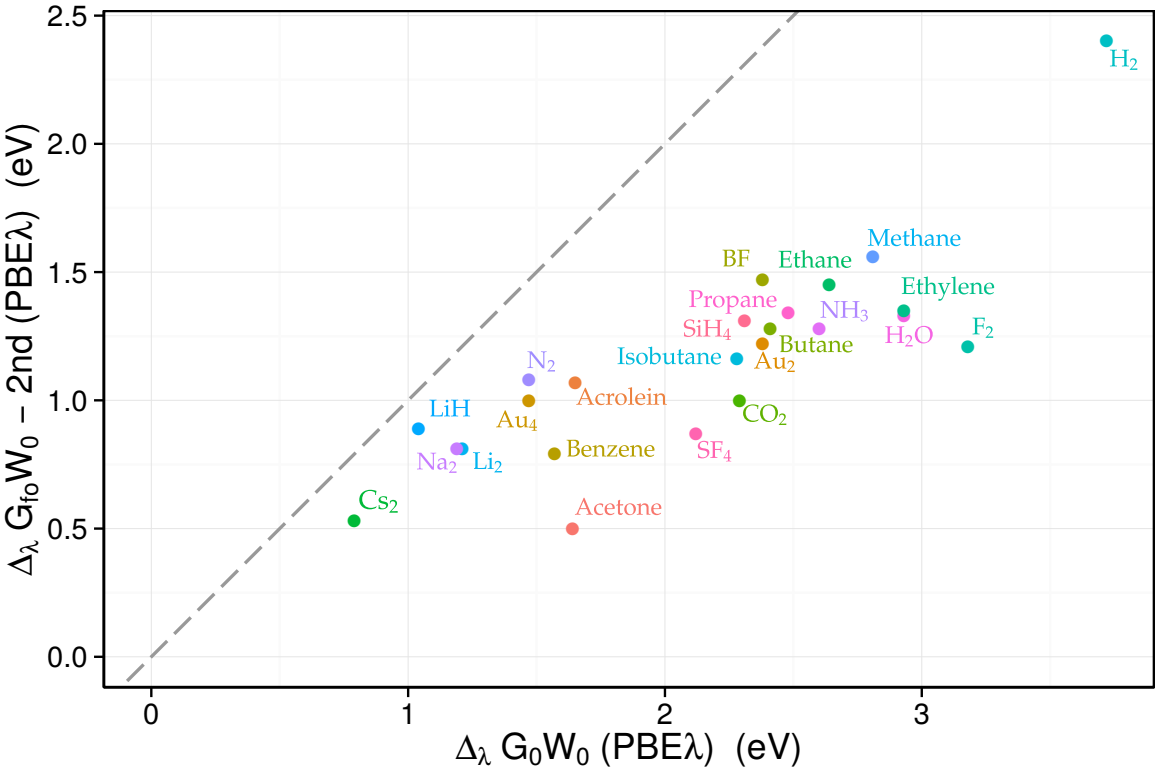

Figure 5.7: Distance from calculated HOMO energy from different intital functionals. Reported is the maximum difference in the $G_{\text{fo}}W_0$-2nd Order calculation (vertical axis) over the maximum in difference in the diagonal only G_0W_0 calculation (horizontal axis). The grey dashed line is the diagonal. Hence, for all data points below the line is the functional dependence in $G_{\text{fo}}W_0$-2nd reduced in comparison to diagonal-only G_0W_0.

5.4.1.2 Validation of Perturbation Theory

$G_{\text{fo}}W_0$-2nd results for the first IP are fetched considered again, to test the validity of the perturbative treatment. As the reference exact diagonalizing results were obtained for a subset of 24 molecules. Fig. 5.8 shows the difference of the calculated HOMO energies obtained from the diagonal $G_{\text{fo}}W_0$ approach and from the $G_{\text{fo}}W_0$-2nd approach to results obtained from a full diagonalization of the QP-equation Eq. (5.4) with the self-consistent treatment of the poles.

The results clearly support the perturbative treatment. The distance from the second order result to the exact diagonalization is negligibly small.

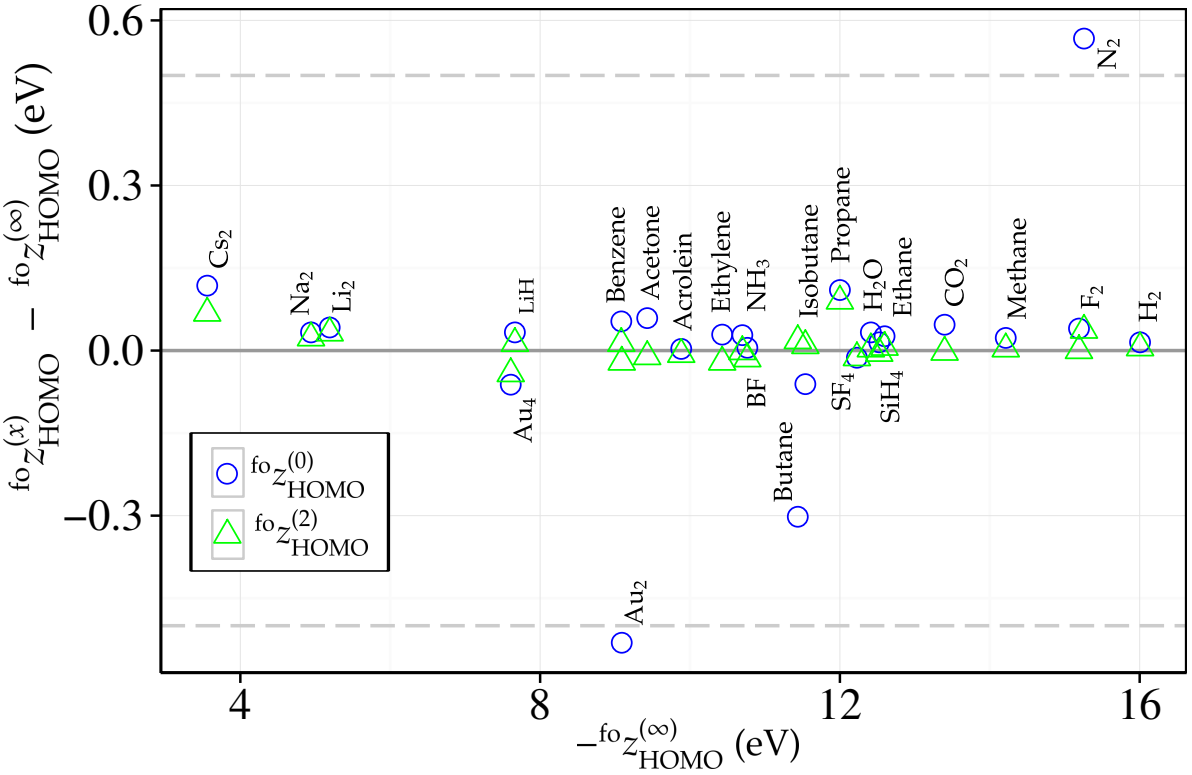

Figure 5.8: HOMO energy obtained from solving the QP-equation with updating the self-energy poles, taking into account only the diagonal contributions ($^{\mathrm{fo}}z^{(0)}_{\mathrm{HOMO}}$) and second order treatment of off-diagonal elements ($^{\mathrm{fo}}z^{(2)}_{\mathrm{HOMO}}$) as deviating from the exact diagonalization results ($^{\mathrm{fo}}z^{(\infty)}_{\mathrm{HOMO}}$). The grey dashed line indicates a deviation of 0.5 eV.

5.4.2 Application in Quantum Chemistry

The combined $G_{\mathrm{fo}}W_0$-2nd will not give further insight into the corrections of qsGW on the Green's Function. It is meant to function as a computationally fast alternative. Therefore, the test is directly performed for the accuracy for the calculation of electronic level-alignment. Updates on the density given by the parent calculation are not accessible with the $G_{\mathrm{fo}}W_0$-2nd approach.

The distance of the calculated HOMO energies to the reference IPs yield as a first measure for the accuracy of the method. This is similar to the analysis in Sec. 4.2.1. The distance to the ΔCCSD(T) reference IPs as well as to the experimental results gives insight whether such an approximate approach may yield a fast and nearly as accurate alternative for the prediction of first IPs.

The considered test set and all numerical parameters were chosen identical to the studies presented before.

5.4.2.1 First Ionization Energies: Comparison to ΔCCSD(T)

The results in Tab. 5.3 show that the $G_{\text{fo}}W_0$-2nd, which accounts for off-diagonal elements and QP-shifts in the self-energy, improves the agreement with ΔCCSD(T). The application of the 2nd order approach does introduce further contributions. The reference result is here the error of the $G_{\text{fo}}W_0$ approach to ΔCCSD(T), which did not take account for off-diagonal elements. For example, the average error reduces from 0.31 eV in diagonal only $G_{\text{fo}}W_0$ down to 0.26 eV in $G_{\text{fo}}W_0$-2nd, employing a DFT(PBE) parent calculation.

	PBE		PBE0		PBE75		qsGW
	$G_{\text{fo}}W_0$	$G_{\text{fo}}W_0$-2nd	$G_{\text{fo}}W_0$	$G_{\text{fo}}W_0$-2nd	$G_{\text{fo}}W_0$	$G_{\text{fo}}W_0$-2nd	
ME	0.27	0.26	0.17	0.15	0.04	0.07	-0.12
MAE	0.31	0.26	0.19	0.17	0.18	0.18	0.22
σ^2	0.10	0.06	0.06	0.06	0.08	0.08	0.07
MaxAE	1.37	1.34	1.25	1.25	1.12	1.12	0.97
MinAE	0.00	0.00	0.00	0.00	0.01	0.00	0.01

Table 5.3: Evaluation of the distance of the calculated diagonal only $G_{\text{fo}}W_0$ and $G_{\text{fo}}W_0$-2nd HOMO energies to the reference ΔCCSD(T) IP, over the full test set. The calculations are initialized from different partent DFT(PBEλ) calculations.

These corrections indicate that the self-consistency in the poles of G give a stronger weight to the off-diagonal elements of the self-energy, which are then taken into account by the second-order approach.

The distance of the IPs calculated from the $G_{\text{fo}}W_0$-2nd approach and from qsGW to the reference ΔCCSD(T) IPs are shown in Fig. 5.9. The statistics, evaluated over the full test set, are reported in Tab. 5.3. The data shows that, independent of the starting point, the $G_{\text{fo}}W_0$-2nd is underestimating the IPs while qsGW tend to overestimate the IPs. Furthermore a dependence on the starting point is still present in the results of the $G_{\text{fo}}W_0$-2nd approach. Surprisingly the best agreement of $G_{\text{fo}}W_0$-2nd with the ΔCCSD(T) result is obtained employing the PBE0 starting point. Using a DFT(PBE0) system as reference gives results which are, with an average error of 0.17 eV in better agreement with ΔCCSD(T) then qsGW. But, on the other hand, the maximum error among the test set is, with 1.25 eV, by more then 0.25 eV larger than the one from qsGW.

In $G_{\text{fo}}W_0$-2nd is the correction systematically towards better agreement with the reference values. For systems with a huge discrepancy on diagonal only level the correction is huge (i.e. Au_2), for systems with already good agreement with the reference the introduced shift is rather small (i.e. Na_2).

5.4.2.2 First Ionization Energies: Comparison to Experiment

The comparison of $G_{\text{fo}}W_0$-2nd IP estimates to experimental (vertical) IPs is reported in Fig. 5.11. ΔCCSD(T) and qsGW estimates are considered as well for reference.

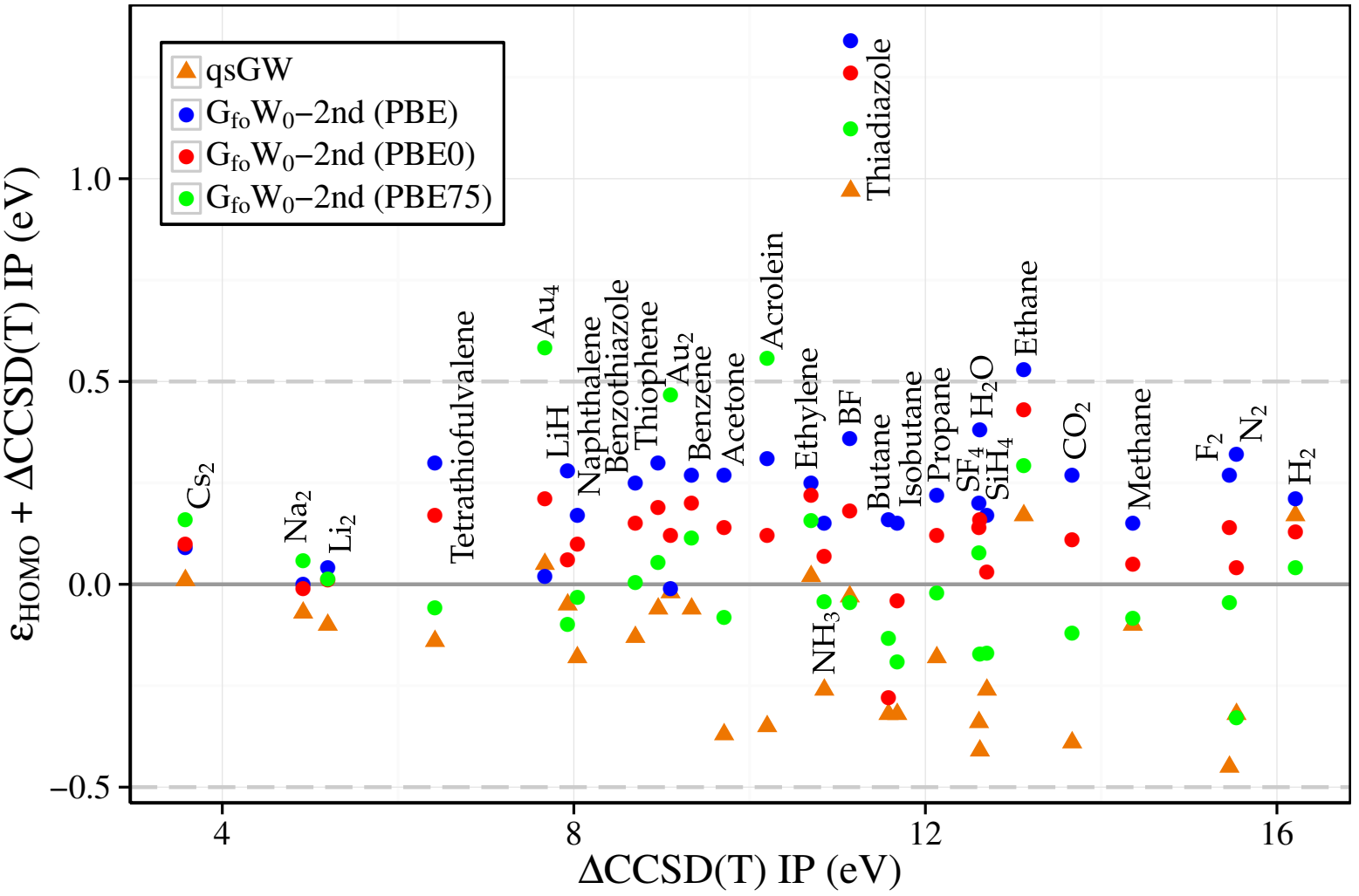

Figure 5.9: The difference of the theoretical ionization energies calculated from the reference CCSD(T) approach to the HOMO energy from the $G_{fo}W_0$-2nd approach and from qsGW (vertical axis) over the ΔCCSD(T) reference. Results were obtained from different DFT (PBEλ) parent calculation. The bare numbers are reportet in the appendix in Tab. C.5.

Overall gives the $G_{\mathrm{fo}}W_0$-2nd approach results which follow the trend of qsGW. For systems for which qsGW showed good agreement with the experiment $G_{\mathrm{fo}}W_0$-2nd does so as well. For systems where qsGW and ΔCCSD(T) were off, i.e. the group of the organic molecules Butane, Isobutane and Propane, $G_{\mathrm{fo}}W_0$-2nd follows their trend. The dependence on the choice of the functional can be best seen for the transition metal molecules Au_2 and Au_4. There the calculated HOMO, using the PBE75 hybrid functional in the parent calculation, is far off the results from calculations with weaker exact exchange mixed into the functional of the parent DFT calculation.

The full statistics, Tab. 5.4, show that the $G_{\mathrm{fo}}W_0$-2nd approach does give better agreement with the experiment than ΔCCSD(T) if the popular PBE0 starting point is employed.

	$G_{\mathrm{fo}}W_0$-2nd			qsGW	ΔCCSD(T)
	PBE	PBE0	PBE75		
ME	0.15	0.04	-0.04	-0.23	-0.11
MAE	0.31	0.28	0.31	0.35	0.27
σ^2	0.11	0.15	0.22	0.15	0.17
MaxAE	0.98	1.14	1.51	0.98	1.12
MinAE	0.03	0.03	0.01	0.00	0.00

Table 5.4: Evaluation of the data from Fig. 5.11. Considered is the deviation of the calculated ΔCCSD(T), $G_{\mathrm{fo}}W_0$-2nd and the qsGW HOMO energies, to the Experimental (vertical) IP of the full test set. $G_{\mathrm{fo}}W_0$-2nd calculations were initialized from different partent DFT(PBEλ) calculations.

5.4.2.3 Higher Ionization Energies: Comparison to Experiment

The benchmark of the $G_{\mathrm{fo}}W_0$-2nd order first IPs against experimental results suggests that this approach is a promising tool for the calculation of IPs. To consolidate this impression the benchmark is again extended for higher IPs.

The difference of the calculated higher IPs from the $G_{\mathrm{fo}}W_0$-2nd calculations and from qsGW to the experimental (vertical) IPs are reported in Fig. 5.10 for the example molecule Naphthalene.

Diagonal only $G_{\mathrm{fo}}W_0$ and G_0W_0-2nd showed an increasing error with increasing energy, Fig. 5.4 and Fig. 5.6. This problem is repaired in the combined approach $G_{\mathrm{fo}}W_0$-2nd. There is no energy dependence in the error anymore. The data shows that the overall error of the $G_{\mathrm{fo}}W_0$-2nd based estimates is comparable to the ones from qsGW, for all starting points.

The results of $G_{\mathrm{fo}}W_0$-2nd typically underestimate the IPs, like qsGW, when the PBE75 functional is employed in the parent DFT calculation. In contrast, the $G_{\mathrm{fo}}W_0$-2nd approach typically overestimate the IPs, when the PBE or the PBE0 functional is employed in the parent system. The calculation with the PBE75 functional gives overall the best agreement with the qsGW results, whereas the calculation with the PBE0 reference gives the best agreement with experiment.

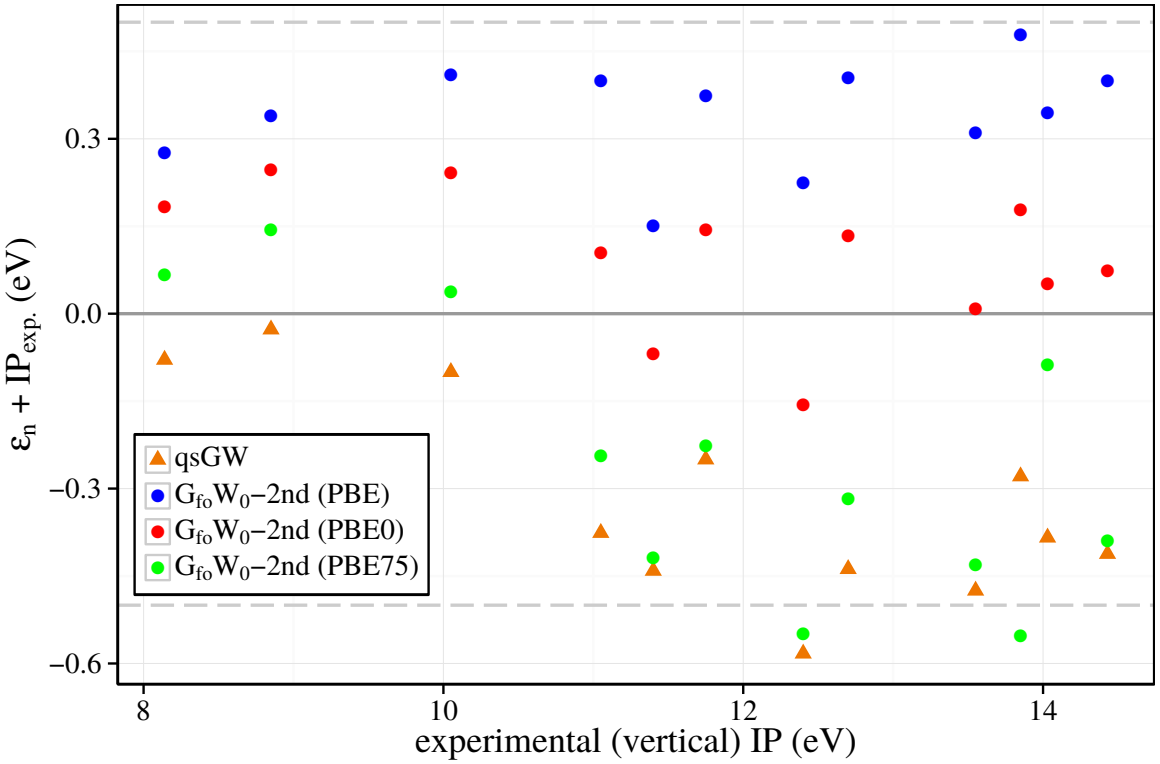

Figure 5.10: The distance of the calculated higher IPs calculated from $G_{\text{fo}}W_0$-2nd with different parent DFT calculations and from qsGW results to the experimental higher (vertical) IPs of the molecule Naphthalene.

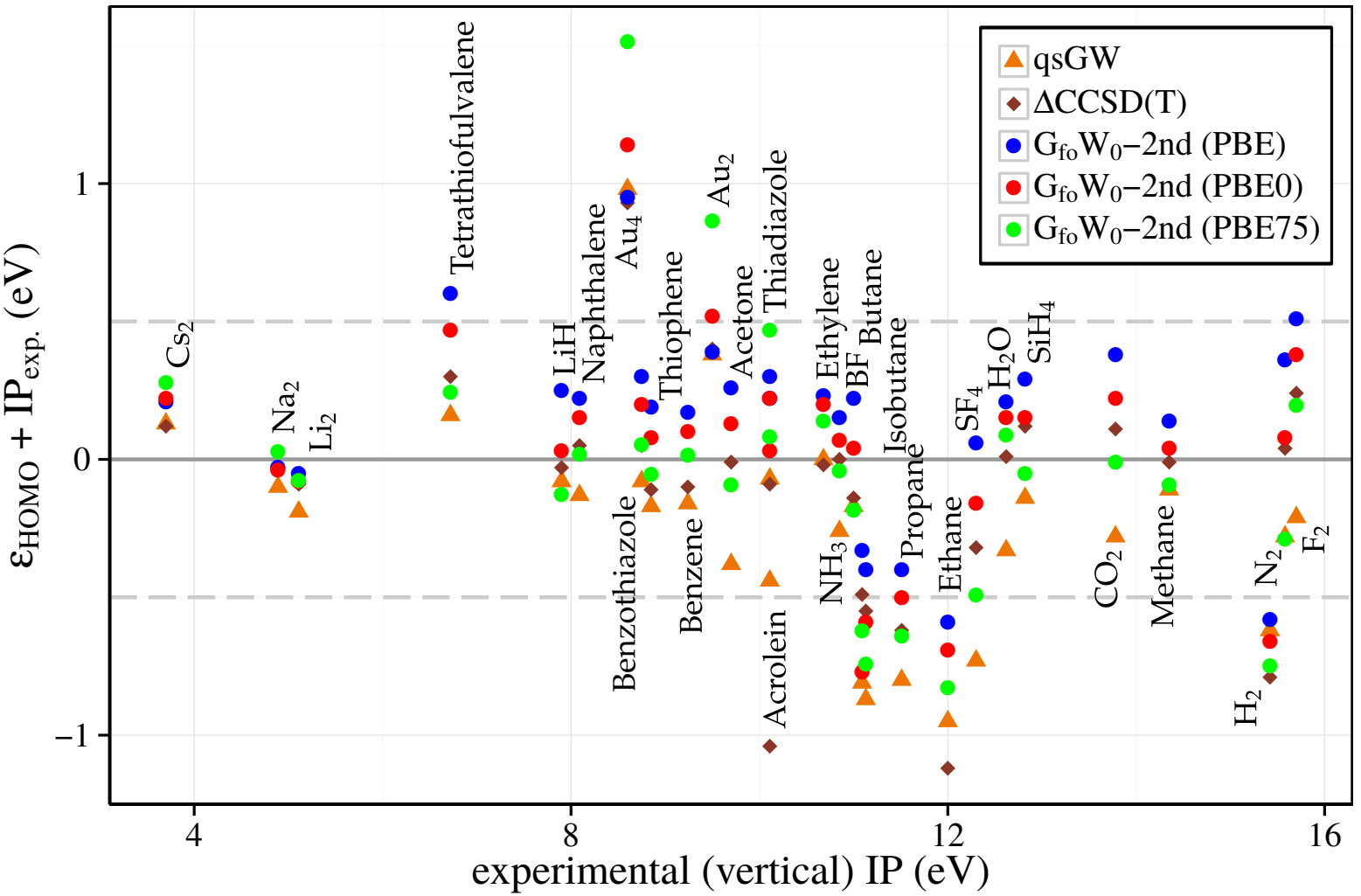

Figure 5.11: The difference of the theoretical ionization energies calculated from the reference CCSD(T) approach, from the $G_{\text{fo}}W_0$-2nd approaches and from qsGW (vertical axis) over the Experimental (vertical) IPs. Results were obtained from different DFT (PBEλ) parent calculation and RPA screening. The bare numbers are reportet in the appendix in Tab. C.5.

5.5 Computational Cost

Fig. 5.12 shows a benchmark of the computational cost for the different considered (approximate) *GW* approaches. The computational time needed for one iteration in *GW* adds up from, first, the calculation of the response function for a given free particle system, and, second, the *GW* part which is dominated by the construction of the self-energy and the solution of the QP-equation. The time needed for the construction of the response function is for all considered approximations identical. The time needed for the second part varies with the approximation for the QP-equation. The computational cost of both of these steps scales with the number of basis function. Depending on the choice for the treatment of the QP-equation does one or the other dominate the overall scaling of the *GW* calculation.

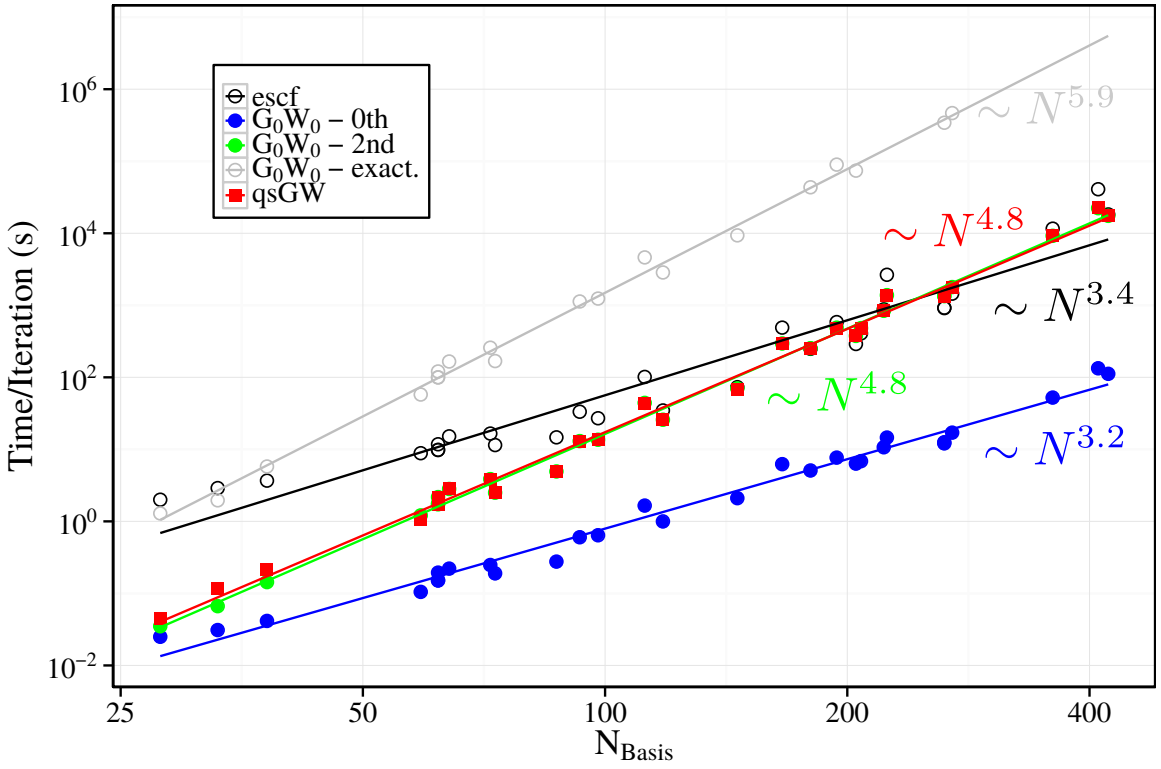

Figure 5.12: The computational time needed for the construction of the response function (escf) and the time needed for a single *GW* iteration over the number of basis functions. Dependent on the approximation in the treatment of the QP-equation the effort increases from the diagonal-only approach (G_0W_0-0th) to a nearly identical effort within the second-order and the diagonalization of the QP-equation from the qs*GW* formalism (qs*GW*). For each *GW* iteration, independent of the chosen approximation, the 'escf' needs to be performed.

In the G_0W_0 related approaches, suggested and tested before in this chapter, the op-

eration of these two parts needs to be performed only once. In contrast, to obtain self-consistency, the iterative execution of these two consecutive steps is necessary. Typically six to eight times till the abort criteria is satisfied. Thus, self-consistency does not have effect on the overall scaling of the procedure. But, it causes a typical factor of six to eight in the computational time.

From the various treatments of the QP-equation is the diagonal only (zeroth order) approach by far the fastest. It shows the best scaling with the number of basis functions of only $\sim N^{3.2}$. Thus, the computational cost for traditional diagonal only G_0W_0 calculations[4] are dominated by the construction of the response function (escf), which has a scaling of $\sim N^{3.4}$.

The iterative diagonalization of the QP-equation which leads to the 'exact' solution scales with $\sim N^{5.9}$, in the implementation on hand. This scaling is more then one power worse then the scaling of the approximate second order approach. Furthermore, the perturbative second order approach captures almost all contributions from off-diagonal elements, which was shown before in Fig. 5.8. Therefore, the second order treatment is considered to be a computationally highly efficient approximation to the full, off-diagonal, solution of the QP-equation.

Both, the second order approach and the qsGW approach which diagonalizes the QP-equation, show a scaling with the number of basis functions N of $\sim N^{4.2}$. In spite of the worse scaling, the computational time needed for the majority of the molecules within the test set is still dominated by the construction of the response function. At first, for the system with more then 340 basis functions starts the GWpart to dominate the computational cost. Therefore, the optimization for best performance within the GW is still an open task within both these implementation. Especially in the qsGW implementation room for improvement can be expected, which would be helpful if one aims for the treatment of larger scale system.

All GW approximations are implemented for parallel computation. For all approaches a nearly perfect scaling with the number of cores is achieved, i.e. the typical setup of 8 core nodes gives a typical speedup of 7.94. Hence, due to very good parallel scaling larger scale systems are tractable.

5.6 Summary

In this chapter three different approximate approaches to GW have been suggested. All of them are closely related to traditional single-shot G_0W_0. The first approach considered corrections on the QP-energies due to off-diagonal elements of the QP-equation, G_0W_0-2nd. The second approach considered the G_0W_0 QP-shift in the construction of the self-energy, $G_{\mathrm{fo}}W_0$. The third approach combined both approaches, $G_{\mathrm{fo}}W_0$-2nd.

[4] The foGW approach, which is suggested in Chap. 6 operates solely on the diagonal part as well. Hence, it has the identical scaling behavior as diagonal only G_0W_0. But, to find a self-consistent solution, typically six iterations are necessary till convergence is achieved. Hence, the total time is the sum of the time needed for the 'escf' part and the G_0W_0 part times six.

G_0W_0-2nd and $G_{\text{fo}}W_0$ were tested to reproduce the results from quasiparticle self-consistent GW (qsGW), for reduced computational demands. The results showed that the corrections from G_0W_0-2nd in comparison to traditional G_0W_0 were insignificant. In contrast, the QP-shift in the self-energy, $G_{\text{fo}}W_0$, introduced relevant corrections towards better agreement with qsGW.

The average deviation of the HOMO to qsGW in $G_{\text{fo}}W_0$ was 0.43 eV. The deviation in G_0W_0-2nd was 0.72 eV. Both for Density Functional Theory (DFT) parents employing the PBE functional. The overall accuracy of both approaches was clearly dependent on the choice of the initializing functional. Best agreement was found for both approaches employing the PBE75 functional. The comparisons for higher IPs showed similar results. The self-consistency in the poles incorporates strong corrections towards the qsGW results. The consideration of off-diagonal elements had rather minimal effects, in comparison to diagonal only G_0W_0.

The combination of both approaches, $G_{\text{fo}}W_0$-2nd, showed that self-consistency in the poles gave larger weight to the off-diagonal elements. The application of the second order approach in combination with the $G_{\text{fo}}W_0$ approach introduced further corrections. The combined method, with a DFT(PBE0) parent calculation, agreed even better with ΔCCSD(T), Tab. 5.9, and also with the experiment, Tab. 5.4, than qsGW.

Although the combined approach is a promising tool, the study shows that the results still have a strong dependence on the chosen functional for the parent DFT caluclation, Fig. 5.7. Calculated HOMO energies vary by up to several eV, depending on the amount of exact exchange in the parent calculation. To overcome this dependence, the following chapter suggests a method with further self-consistency in the pole positions, in the Green's Function G as well as in the calculation of the screened interaction W.

The review on the computational cost favors the diagonal-only treatment of the QP-equation. All considered approaches have improved scaling in comparison to the N^5 scaling of full GW. But, taking only the diagonal elements into account is with a scaling of $N^{3.2}$ clearly favored, for the application for larger systems. This will be taken into account in the development of the approximate, but self-consistent, approach in the next chapter as well.

Chapter 6

6 Approximate Strategies for the GW Self-Consistency Cycle: Fixed Orbitals

The results of the previous chapter showed that the consideration of quasiparticle (QP-)shifts while constructing the self-energy yield a significant correction to the energy-level alignment. In contrast, the energy updates based on corrections on the initial DFT (PBEλ) Kohn-Sham (KS-)Orbitals were negligible small.

In this chapter a method is proposed which takes into account (only) the update on the QP-energies in the calculation of the screened interaction W. This is the so called fixed-orbital GW (foGW). Fixing the orbitals has major computationally benefits in the iterative calculation of W compared to full quasiparticle self-consistent GW (qsGW). The method will be composed in a way that only the zeroth order solution of the QP-equation is needed. In this manner, the computational complexity is reduced by more than one order of magnitude, in comparison to full qsGW and the second order approach. This speedup was verified in a study in Sec. 5.5.

A benchmark shows that foGW improves agreement with qsGW in comparison to $G_{\text{fo}}W_0$. It turns out that foGW results are in better agreement with CCSD(T) than qsGW. Furthermore, the agreement with experiment is improved as well. Although foGW results are dependent on the functional of the parent (DFT) calculation it is shown that foGW results show strongly suppressed functional dependence compared to previously suggested G_0W_0 based approaches.

6.1 Motivation

An approximate approach to qsGW which is capable of reproducing the results of qsGW is developed and tested in this chapter. The major motivation for this is approximation is the reduction computational cost for the calculation of accurate QP-energies.

The previous chapter suggested appropriate G_0W_0 based approaches. Results showed

that the consideration of QP-shifts in the self-energy are crucial. Furthermore, it was shown that corrections from orbital updates did not shift the QP-energies noticeably. This conclusion is adapted for the full qsGW self-consistency cycle in this chapter. The $G_{\mathrm{fo}}W_0$ approach did not consider the update on the pole positions in the calculation of the response function. The screening was still based on the parent KS-system.

The approach presented in this chapter considers the QP-shift in the calculation of the response function as well. Similar to full qsGW this is performed until self-consistency for the QP-energies is achieved. Thus, self-consistency is considered for the poles for the construction of the screened interaction W. The approximation implies keeping the spatial shape of the orbitals fixed at the shape from the initial parent system. Therefore, the excitation densities ρ_m of the response function χ do not change in the iterative flow of foGW. Nevertheless, there is an update in χ. The excitation energies Ω_m are corrected by the shift of the poles ε_n of the Green's Function[1]. Keeping the orbitals fixed yields a further computational benefit. The Coulomb exchange integrals, see Eq. (3.36), do not need to be re-evaluated in each iteration. Therefore, the full exchange part of the self-energy Σ_{x}, Eq. (3.35), needs only one single evaluation.

Orbital corrections are neglected at all steps of this procedure. Hence, the consideration of off-diagonal contributions in the QP-equation is not essential. Taking only the diagonal part of the QP-equation into account is sufficient. This has major computational benefits as well, see Sec. 5.5

6.2 Implementation and Formalism

In the methodology described in Sec. 3.1 turning qsGW into foGW is rather trivial. Simply, the update in the orbitals between the qsGW iterations needs to be suppressed. Hence, the machinery is supposed to operate solely on the initial set of QP-orbitals $\psi^{(0)}(\mathbf{r})$.

In the qsGW formalism the orbital update from Eq. (3.8) is skipped and in all equations the orbitals $\psi^{(i)}(\mathbf{r})$ are replaced with $\psi^{(0)}(\mathbf{r})$. Additionally, in the realization of foGW on hand, the treatment of orbital based corrections, respectively off-diagonal elements, is thoroughly neglected. The application of the quasi-static approximation $\Sigma(\varepsilon_n) \rightarrow \tilde{\Sigma}$ is dropped. Instead the treatment from the traditional G_0W_0 is adopted. Only the diagonal elements of the QP-equation are taken into account. Then, for each pole ε_n the diagonal-only QP-equation, see (5.27), is solved self-consistently.

[1] Keeping the orbitals fixed has the major benefit that the computational expensive task to calculate the excitation densities ρ_m of the response function χ needs to be done only once, for the initial system. In the current implementation this advantage is not considered. Taking this into account would require major programming effort on low-level routines in TOURBOMOLE, which was not doable in the scope of this thesis.

6.2.1 Comparison to Quasiparticle Self-Consistent *GW*

The fo*GW* approach is a direct extension to $G_{\mathrm{fo}}W_0$. Therefore, it is tested whether the further level of self-consistency helps to reproduce qs*GW* results. This is done in three steps. First, the dependence on the starting point is evaluated. Second, the deviation of fo*GW* and $G_{\mathrm{fo}}W_0$ HOMO energies to qs*GW* HOMO energies is considered. This distance serves as a first measure for the overall agreement. Third, a benchmark considers higher IPs respectively lower lying poles as well. This study is performed on five different molecules.

6.2.1.1 Dependence of Ionization Energies on the Initialization

Without any update in the orbitals, the results of the fo*GW* formalism are clearly dependent on the shape of the initial orbitals. Similar to G_0W_0, the initial Green's Function is constructed from a parent DFT calculation. Therefore, dependence on the choice of the functional for the parent calculation is inevitable in fo*GW*. The initializing DFT calculation in combination with the choice for the functional is typically referred to as the starting point.

To test the dependence on the choice of the functional a study has been performed, similar to the one for G_0W_0, see Sec. 3.2.3.1. The formalism is initialized with the hybrid PBEλ functional, varying from $\lambda = 0$ (clean PBE) to 1 in steps of 0.25.

The maximum distance for the calculated HOMO energy (spread Δ_λ) dependent on the choice of λ is strongly reduced in fo*GW*. The spread Δ_λ from fo*GW* is smaller than from traditional diagonal-only G_0W_0, see Fig. 6.1. The majority of the considered molecules show a spread below 0.36 eV. Only the transition metal molecules Au_2, Au_4 and the nitrogen dimer still show stronger dependence on the functional. These results vary by more than 0.8 eV with the amount of exact exchange in the functional. Comparisons of the spread in fo*GW* to the spread from DFT PBEλ is shown in the appendix in Fig. C.5. The comparison to results from $G_{\mathrm{fo}}W_0$ is reported in Fig. C.7.

Overall fo*GW* has the weakest dependence on the amount of exact exchange in the functional of the parent calculation from all considered approximate approaches. Nevertheless, the starting point dependence is prevalent in fo*GW*. In the benchmark for first IPs it is discussed how this dependence effects calculations in practice, in Sec. 6.3.

6.2.1.2 First Ionization Energies

Fig. 6.2 shows the difference of the calculated first IPs from fo*GW* to qs*GW* estimates. The deviation of $G_{\mathrm{fo}}W_0$ results to qs*GW* results are shown as a reference. Results from the $G_{\mathrm{fo}}W_0$ approach deviate from the qs*GW* by up to 1 eV. Furthermore, the error is increasing towards higher energies for the calculations employing the PBE or the PBE0 parent. The self-consistent treatment within the screened interaction W in fo*GW* improves the agreement with qs*GW*. From the statistical quantities in Tab. 6.1 is concluded that the agreement improves from a mean absoltue error over the full test set of 0.43 eV in $G_{\mathrm{fo}}W_0$ to 0.17 eV in fo*GW*. This is based on the results for the standard PBE parent. The improvement from $G_{\mathrm{fo}}W_0$ to fo*GW* is rather insignificant for an initial Green's Function

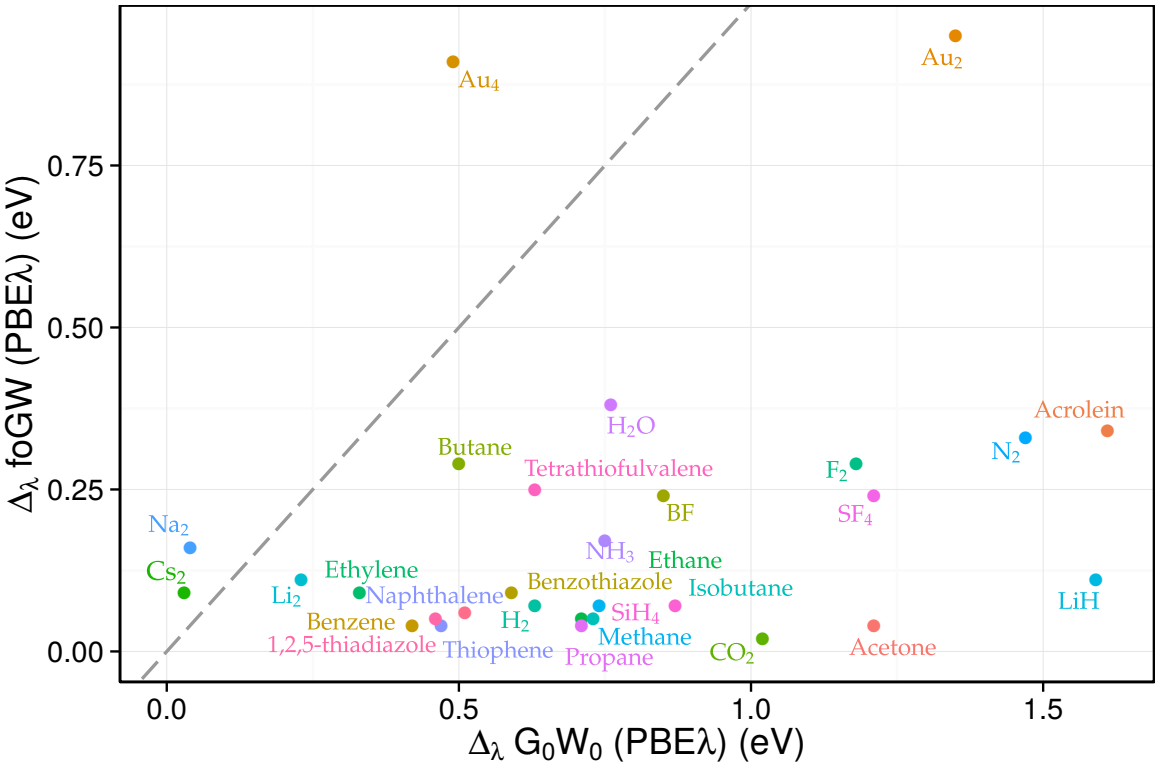

Figure 6.1: Shown is the comparison of the spread Δ_λ using foGW over the spread Δ_λ from G_0W_0. The spread Δ_λ is a measure for the functinal dependence which was introduced before in Sec. 3.2.3.1. Both methods have an inherent dependence on the choice of the functional. The dashed line helps to distinguish cases wheather G_0W_0 or foGW yields the smaller spread. If data points are below this line, foGW has a reduced dependence of the HOMO energy on λ, if points are above G_0W_0 has the smaller dependence on λ.

constructed from a DFT calculation employing the PBE75 functional. For that case, the improvement smaller than 0.01 eV, see Tab. 6.1.

Vice versa, the PBE75 functional is not the optimal choice as a starting point for the foGW method. This is in contrast to previous findings for all G_0W_0 approaches. The traditional G_0W_0 as well as all extensions, showed best agreement with qsGW employing the PBE75 functional, see Sec. 5.3.2, and Sec. 5.2.2. Results reported in Tab. 6.1 show worst (average) agreement of foGW and qsGW for parents employing PBE75. Here, best agreement is achieved with the PBE0 functional. The average distance is only 0.15 eV employing the PBE75 parent. For the PBE75 parent the average distance is larger with 0.18 eV.

The general findings from the starting point study in Sec. 6.2.1.1 can be approved. The dependence of the distance from foGW to qsGW on the DFT functional is strongly sup-

	PBE		PBE0		PBE75	
	$G_{\mathrm{fo}}W_0$	foGW	$G_{\mathrm{fo}}W_0$	foGW	$G_{\mathrm{fo}}W_0$	foGW
ME	0.39	0.09	0.29	0.12	0.16	0.14
MAE	0.43	0.17	0.30	0.15	0.18	0.18
σ^2	0.09	0.03	0.03	0.02	0.02	0.02
MaxAE	1.18	0.39	0.66	0.36	0.53	0.53
MinAE	0.04	0.01	0.04	0.03	0.00	0.00

Table 6.1: Evaluation of the data shown in Fig. 6.2. The mean error (ME), mean absolute error (MAE), the variance (σ^2), the maximum absolute error (MaxAE) and the minimum absolute error (MinAE) of the difference of the calculated foGW and $G_{\mathrm{fo}}W_0$ HOMO energies to the qsGW HOMO is considered. Deviations from results from all 29 molecules of the test were included in the evaluation. The consideration from three different functionals in the parent DFT calculation gives different results in the $G_{\mathrm{fo}}W_0$ as well as in the foGW calculation. Thus, results of both methods are dependent on the choice of the functional.

pressed, in comparison to all G_0W_0 based approaches. The deviation with the starting point is orders of magnitudes smaller then the correction on top of the DFT results. Thus, the dependence will not be crucial in practice. The average deviation to qsGW is for all starting points of comparable size, always below 0.20 eV. This is remarkable improvement in comparison to the dependence in $G_{\mathrm{fo}}W_0$.

6.2.1.3 Higher Ionization Energies

Fig. 6.3 shows the difference of higher IPs from foGW to results from qsGW. For reference results from $G_{\mathrm{fo}}W_0$ are reported as well. This figure considers the example molecule Naphthalene. Results for further molecules are shown in the appendix, see Fig. C.4.

$G_{\mathrm{fo}}W_0$ results show the problematic feature of increasing deviation with increasing energy. This feature was observed for all approaches which relied on a screening exclusively calculated from the parent DFT system, see Sec. 5.3.2.2 and Sec. 5.2.2.2. This unwanted feature is thoroughly repaired in foGW. All calculations do not show any systematic in the error. Overall, the foGW results underestimate (higher) IPs in comparison to qsGW. This is observed for all starting points. Nevertheless, foGW improves the agreement with qsGW in comparison to $G_{\mathrm{fo}}W_0$ remarkably in the calculations employing the PBE or the PBE0 parent. Nevertheless, For the PBE75 starting point results from foGW and qsGW almost do not differ at all.

Best agreement of higher IPs between foGW and qsGW is obtained if the PBE75 functional is employed in the parent DFT calculation, see Fig. 6.3. Finding best agreement of foGW and qsGW for the PBE75 initialization is contrary to the findings from the study for the first IPs. For these calculations the PBE0 parent was favored.

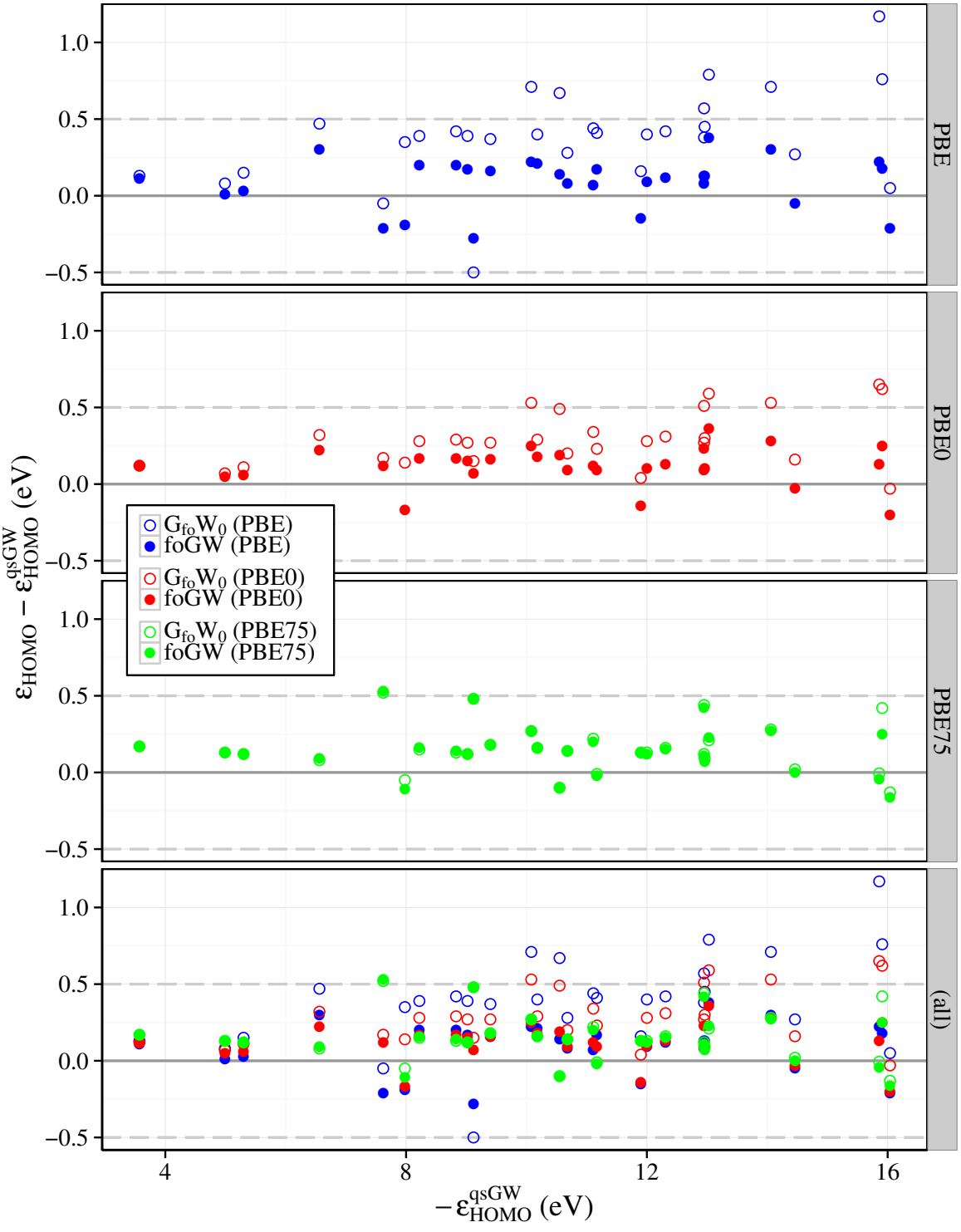

Figure 6.2: The difference of the HOMO energy from foGW and $G_{\mathrm{fo}}W_0$ to the HOMO energy from qsGW (vertical axis) over (minus) the qsGW HOMO energy. The different functionals in the parent calculatons, with consecutive higher amount of exact exchange, are considered to account for the dependence of the results on this choice.

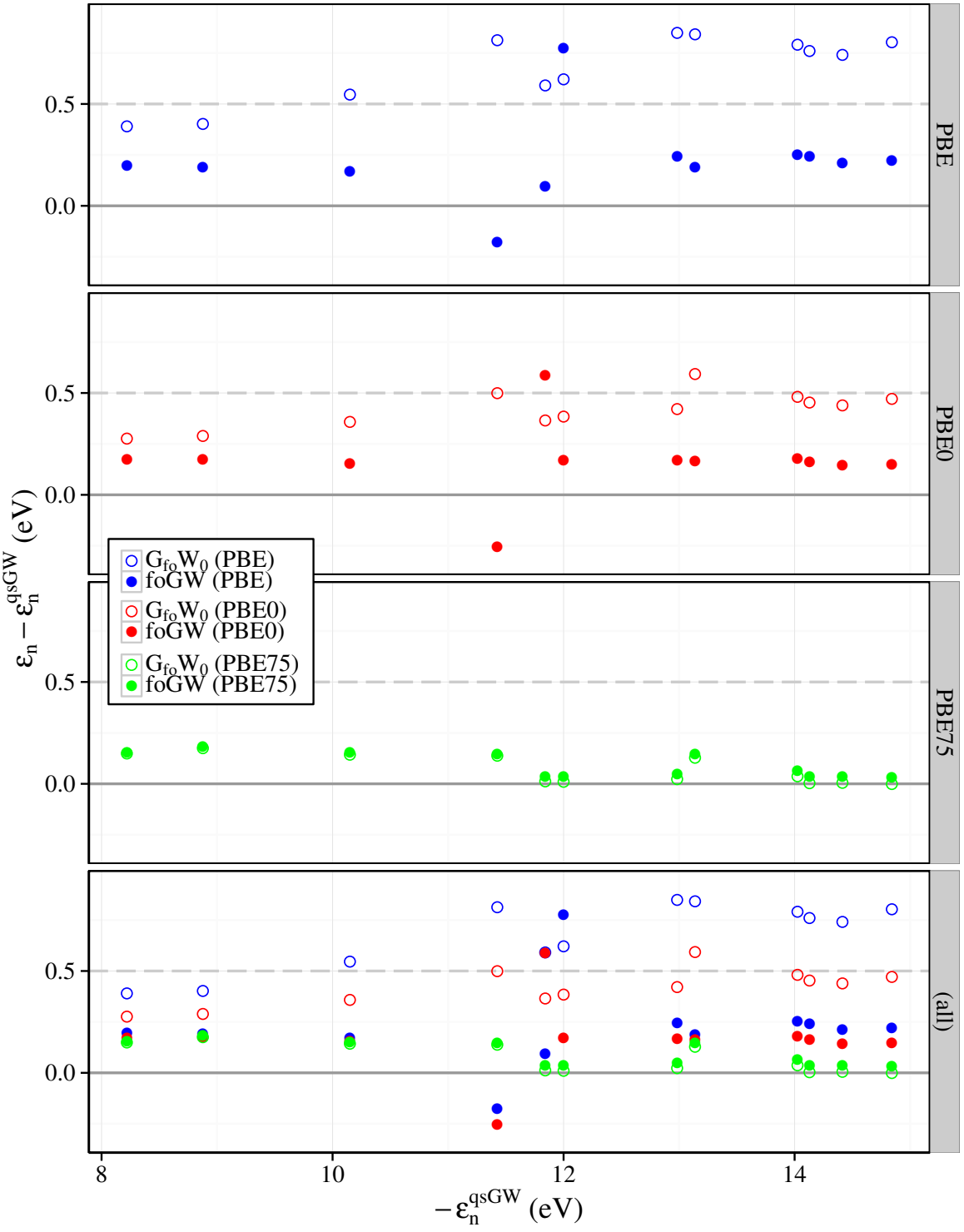

Figure 6.3: The difference of the calculated QP-energies from foGW and $G_{\mathrm{fo}}W_0$ to the qsGW energies over minus the qsGW energies for the example molecule Naphthalene. The different functionals, with consecutive higher amount of exact exchange, are considered in the parent calculation.

6.3 Application of Fixed-Orbital *GW*

The fo*GW* method is tested for practical calculations by performing a benchmark similar to the one in Sec. 4.1. First, the accuracy of calculations of first IPs is tested. The ΔCCSD(T) method will be used as the reference. Additionally, results will be compared to experiment. Second, studies on higher IPs are performed for five molecules. Therefore experiment will function as the reference.

6.3.1 Comparison to Coupled-Cluster

Fig. 6.5 shows the difference of HOMO energies from fo*GW* to ΔCCSD(T) first IPs. For comparison results obtained from G_0W_0 and qs*GW* are shown as well. In the previous section data showed that the dependence on the functional of the parent (DFT) calculation is strongly suppressed in fo*GW*. Therefore, only calculations employing the PBE functional in the parent calculation are shown.

	fo*GW*					G_0W_0	qsGW
	PBE	PBE0	PBE50	PBE75	PBE100		
ME	-0.03	-0.01	0.00	0.02	0.04	0.57	-0.12
MAE	0.19	0.16	0.17	0.19	0.22	0.62	0.22
σ^2	0.08	0.07	0.07	0.09	0.11	0.17	0.07
MaxAE	1.18	1.15	1.13	1.12	1.13	1.49	0.97
MinAE	0.02	0.01	0.01	0.00	0.01	0.14	0.01

Table 6.2: Evaluation of the data shown in Fig. 6.5. The difference of the calculated IP from different *GW* flavors to the ΔCCSD(T) result is considered. In addition to the data shown in Fig. 6.5, fo*GW* results from four further PBE based functionals with consecutive higher exact exchange are shown. The plain PBE functional considers no exact exchange at all, PBE0 has 25% exact exchange, PBE50 refers to 50% exact exchange, and so on. G_0W_0 was initialized from DFT employing the PBE functional.

The suppression of the functional dependence in fo*GW* is verified by the study from Tab. 6.2. The table reports the average deviation from fo*GW* HOMO energies to ΔCCSD(T) IPs, for five starting points. In addition the statistical quantities from qs*GW* and G_0W_0 (initialized from DFT(PBE)), are reported. From the study it is concluded that fo*GW* strongly improves agreement with the reference in comparison to traditional G_0W_0, although both approaches have the identical computational scaling with the number of basis functions, see Sec. 5.5.

The fo*GW* approach shows at worst a mean average error (MAE) of 0.25 eV. In contrast, the worst MAE of G_0W_0 is 0.75 eV. Furthermore, fo*GW* gives comparable good (or even better) agreement with the reference as the qs*GW* approach. These results are dependent on the choice of the functional in the initializing DFT calculation. Nevertheless, for the

considered set of molecules the optimum initialization is $\lambda = 0.25$ respectively the standard PBE0 functional. Using PBE0 as a starting point, the overall mean absolute error (MAE) to the ΔCCSD(T) result is 0.14 eV with a very small variance of $\sigma^2 = 0.02$. The error from qsGW is minimal larger, with 022 eV. Even, for the worst choice, PBE100, gives foGW comparable good agreement as qsGW with the reference with a MAE of 0.24 eV.

6.3.2 Comparison to Experiment

For completeness results will be compared against experimental leading IPs as well. This comparison intends to help to recognize the accuracy in comparison to ΔCCSD(T).

6.3.2.1 First Ionization Energies

The comparison of foGW HOMO energies to experimental vertical first IPs is shown in Fig. 6.6. The agreement with the experiment is overall similar to the results from the qsGW method. Again, to simulate an unbiased application, only results for initializations employing the popular PBE functional are shown.

	foGW					G_0W_0	qsGW	CCSD(T)
	PBE	PBE0	PBE50	PBE75	PBE100			
ME	-0.14	-0.12	-0.11	-0.09	-0.07	0.46	-0.23	-0.11
MAE	0.28	0.29	0.31	0.32	0.35	0.54	0.35	0.27
σ^2	0.15	0.17	0.20	0.22	0.27	0.19	0.15	0.17
MaxAE	0.96	1.10	1.32	1.51	1.69	1.38	0.98	1.12
MinAE	0.00	0.00	0.00	0.01	0.00	0.03	0.00	0.00

Table 6.3: Evaluation of the data shown in Fig. 6.6. The difference of the calculated IP from different GW flavors and from ΔCCSD(T) to the experimental vertical IP is considered. In addition to the data shown in Fig. 6.4, foGW results from four further PBE based functionals with consecutive higher exact exchange are shown. The plain PBE functional considers no exact exchange at all, PBE0 has 25% exact exchange, PBE50 refers to 50% exact exchange, and so on.

On average the optimum choice is $\lambda = 0$ for the PBE functional. Employing the plain PBE starting point yields best agreement of foGW with experiment, see Tab. 6.3. Using PBE as the parent system improves the MAE down to 0.30 eV, which is in better agreement with experiment than the qsGW results ($\text{MEA}_{qsGW} = 0.39$ eV). The variance turns out to be small as well ($\sigma^2 = 0.15$).

6.3.2.2 Higher Ionization Energies

The results obtained for the calculation of higher IPs for the molecule Naphthalene are shown in Fig. 6.4. Again, further molecules are considered in the appendix, see Fig. C.3.

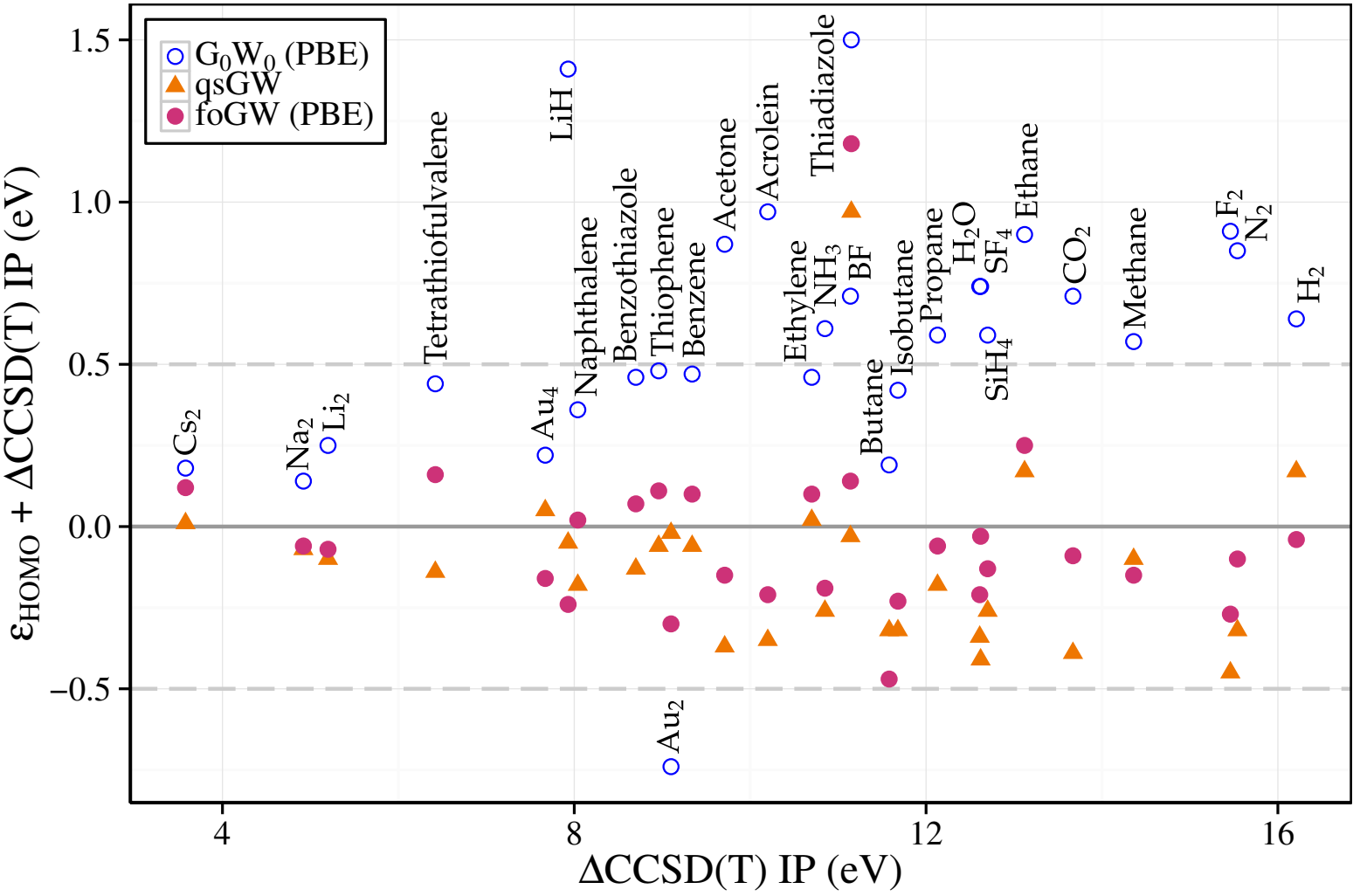

Figure 6.5: The deviation of the theoretical IP calculated from G_0W_0 as well as fo*GW* initialized from DFT employing the PBE functional, and qs*GW* to the reference ΔCCSD(T) results.

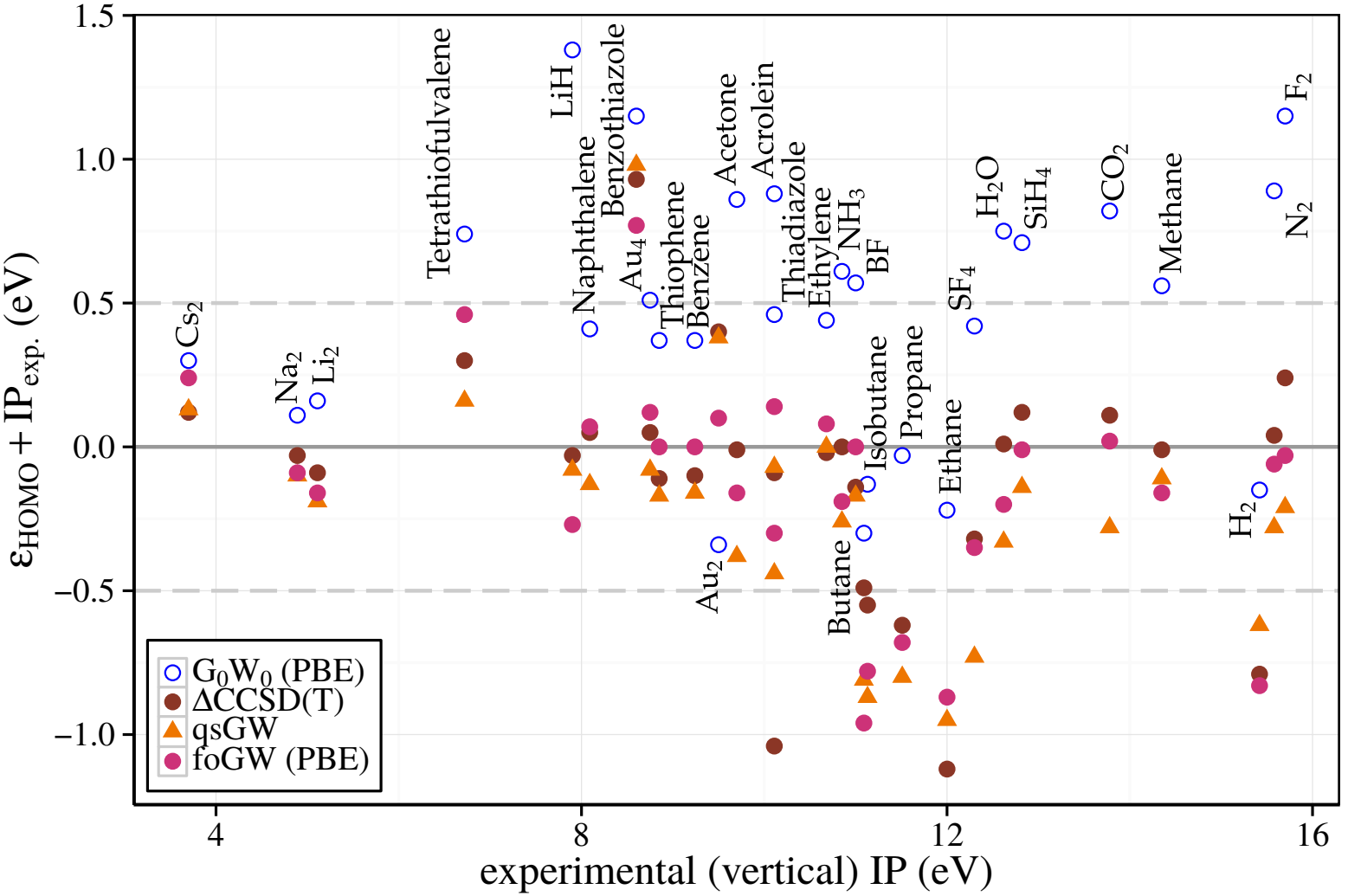

Figure 6.6: The deviation of the theoretical HOMO energy to the experimental vertical Ionization Energy (vertical axis) over the experimental value (horizontal axis). Results were obtained from the approximate approaches G_0W_0 and foGW initialized from DFT calculations emplyoing the PBE functional, as well as results from qsGW and ΔCCSD(T).

The (higher) IP estimates from fo*GW* turns out to be typically in between the sc*GW* and the qs*GW* results. Thus, the fo*GW* method gives the best agreement with experiment on average.

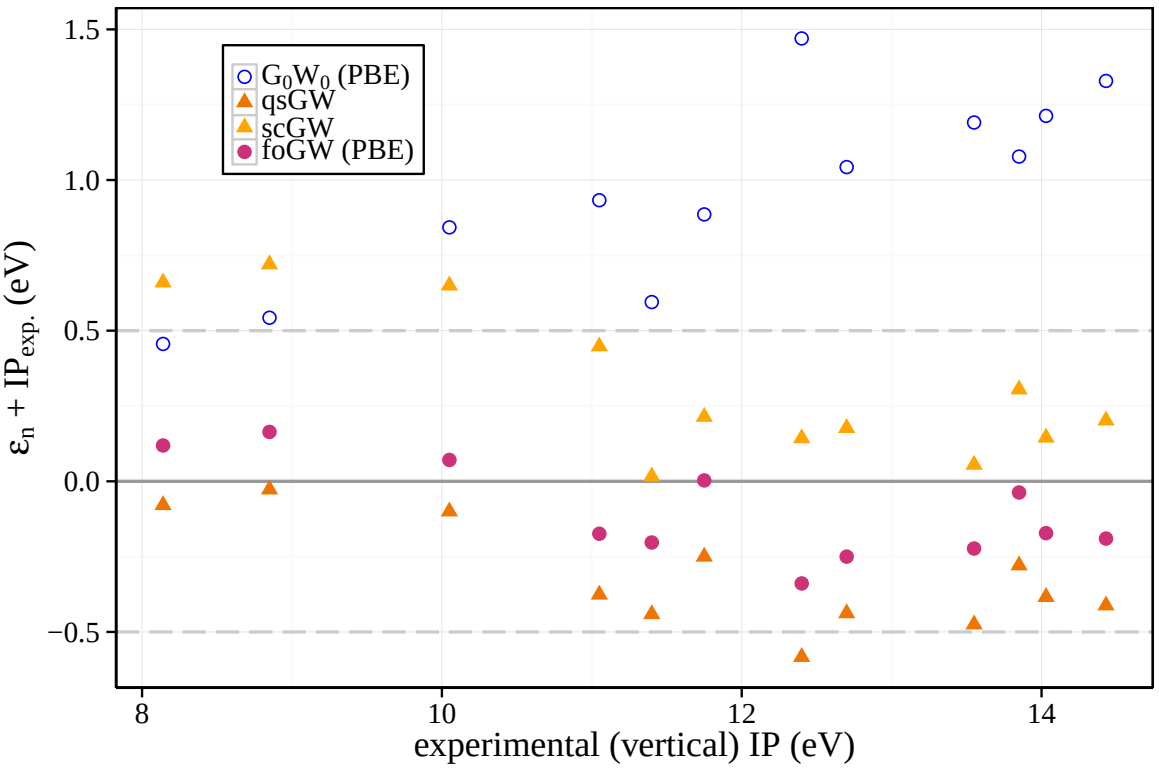

Figure 6.4: The difference of the calculated QP-energies from fo*GW*, $G_{\mathrm{fo}}W_0$ as well as QP-energies from the approximate qs*GW* and full sc*GW* (Caruso et al., 2013) to the experimental vertical IPs over the experimental energies for the molecule Naphthalene.

6.4 Summary

The fixed-orbital *GW* (fo*GW*) was suggested as an approximate to the full quasiparticle *GW* (qs*GW*). Operating solely on the parent Kohn-Sham (KS-)Orbitals and suppressing any changes in the spatial shape has major computational benefits. Sticking to the diagonal-only approximation to the QP-equation reduces the computational complexity by more than one order of complexity, in comparison to full qs*GW*.

The screening in fo*GW* is still based on the spatial shape of the KS-orbitals from the parent calculation. Hence, results are still dependent on the choice of the functional as well. The study presented in this chapter showed that this dependence is strongly reduced

in comparison to the dependence in G_0W_0. Results were in very good agreement with the ΔCCSD(T) reference, independent of the choice of the functional. Furthermore, the agreement with experiment is better than with qsWG.

Concluding, foGW is a computationally fast, very accurate and reliable method for the calculation of ionization energies. Densities and further observables relying on the spatial shape of the orbitals are not accessible on the level of foGW. These would still yield the identical results as the parent Density Functional Theory calculation.

Chapter 7

7 Summary and Outlook

In this thesis a method for the accurate calculation of the electronic structure of molecules and nano-scale systems was developed. Accurate theoretical studies are crucial for the development of new catalytic processes, understanding of still unknown (chemical) reaction pathways and for the development of molecular electronic building blocks. Especially, the understanding of charge transfer processes is a challenging task for which a precise knowledge of the energy level alignment is essential.

Typically, the theoretical calculations are performed employing computational electronic structure methods. Importantly, a method suitable for the treatment of electronic excitations in medium size molecules and nano-scale systems was still missing.

The major part of this work was the development, implementation and extensive testing of a suitable method for the calculation of the electronic structure of molecules which outperforms density functional theory (DFT). In addition, the method is applicable to medium size systems as opposed to high precision methods such as coupled cluster (CC). Three major requirements were formulated in the introduction: (a) The method needs to be able to describe charge excitation processes. (b) The method should not have any adjustable parameters in order to be generally applicable with accurate predictive power. (c) The method has to be computationally efficient and accurate in the calculation of electronic properties of medium size molecules and nano-scale systems. To fulfill these specifications, I adopted the quasiparticle self-consistent GW (qsGW) method for molecules. In order to prove this method, I implemented the qsGW into the quantum chemistry program package TURBOMOLE (Ahlrichs et al., 1989).

Indeed, the qsGW matches all demands and thus is a promising tool for further developments and investigation of the electronic structure of medium size molecules and nano-scale systems, as this work has shown. The requirement (b) to be *independent of adjustable parameters, and hence true 'ab initio'*, is fulfilled by construction. I will comment on the other requirements formulated above. To match the requirement

(a) *Capability of the direct description of charge excitation processes*

I did choose the framework of Green's function technique. More specifically, I adopted the GW-approximation for molecules as the theoretical approach for the calculation of the

Green's function. Benchmarks were performed on a set of 29 molecules ranging from the hydrogen dimer up to complex (organic) molecules which are candidates for solar-cell applications. Furthermore, molecules with pronounced covalent bonding behavior and transition metals were considered. Overall, the tests confirmed that the method accurately describes excitation processes in various kinds of systems. Systems with highly localized as well as homogeneously distributed charge density are equally accurately treated. Furthermore, image charge effects and van der Waals forces are considered in qsGW, in contrast to the lack in practical DFT calculations. Predicted first ionization potentials (IP) from qsGW with average deviations of 22 meV are up to 5 eV closer to the reference CC results in comparison to DFT estimates. This is extraordinary improvement considering that the IPs from the considered molecules range from 3 eV to 16 eV. In fact, the agreement of qsGW first IP estimates with experiment is in the same order of magnitude as the agreement of the aforementioned reference (CC). For higher IPs results from qsGW are as accurate as for the first IP compared to measurements. The higher IPs are are not directly accessible with DFT or CC. Hence, qsGW can be applied in a broader field of applications. Furthermore, the calculated ground state density from qsGW is in very good agreement with experiment as well: The predicted dipole moments from qsGW with an average error below 0.03 Debye are in better agreement with experiment than the DFT estimates by an order of magnitude.

With the aim for computational efficiency to match the requirement

(c) *Suitable for medium size molecules and nano-scale systems*

an approximation to GW is applied, the quasiparticle self-consistent GW (qsGW): The energy dependence of the self-energy is approximated. The advantage is that the quasiparticle (QP) equation needs to be solved only once in each iteration. Otherwise, a separate solution for each pole is necessary. Furthermore, in the presented qsGW formulation, the time consuming task for the numerical solution of energy integrals is omitted since it is already done analytically. In practice, the qsGW method has a computational scaling of $N^{4.2}$ with the number of basis functions N, which is worse than DFT(N^3) but much better than the CC reference (N^7). Because of the low computational demands, it is possible to apply qsGW for medium size molecules and nano-scale systems. The implementation of the method produces converged results for systems containing more than 100 electrons in less than three days on standard workstation computers (4x2.9Ghz, 16GB RAM).

To further reduce the computational demands, I developed and proved approximate approaches to qsGW. Most promising from this study is the so called fixed-orbital GW (foGW) approach. It operates similar to qsGW, but with the limitation that the orbitals are kept fixed at their initial choice (typically DFT). Employing this approximation reduces the computational complexity down to $N^{3.2}$. A benchmark showed that the estimates from foGW are in excellent agreement with the qsGW results.

A property of foGW is that the electron density is identical to the one from the initializing (DFT) calculation. This can be an advantage or disadvantage; depending on how close the DFT (reference) density is to the exact one. Furthermore, foGW is not self-consistent, its results inherently depend on the choice of the functional in the parent DFT system.

But, it was shown that the dependence is strongly reduced in comparison to other approximation methods, e.g. traditional G_0W_0.

A comprehensive description of processes relevant in scientific and industrial applications of molecules requires further extensions of the qsGW machinery. Fundamental molecular device concepts for photovoltaic applications rely on optical excitations, i.e. excitons: the charge neutral state with one excited electron and a hole. Fundamental experimental methods rely on excitonic effects as well. For example, in catalysis, experiments observe reaction mechanisms employing single molecule fluorescence spectroscopy (e.g. Janssen et al., 2014). For a better quantitative description of optical excited states numerical methods need to take into account the interaction of holes and excited-electron states. This interaction is not considered in GW. Instead, GW regards two single-particle excitations, electron and hole, which do not interact.

The *de-facto* standard for excitation-state simulations in quantum chemistry is the *time-dependent* DFT (TDDFT). As a direct extension of DFT, it also relies on a description of correlation physics by approximate functionals and has further inherent shortcomings. A direct extension to the GW framework overcomes these problems and accurately describes excited states. This extension is based on an approximate solution of the famous Bethe-Salpether equation (BSE). The application of the BSE-framework on top of G_0W_0, as well as on other approximate GW schemes, proofed to be promising (Boulanger et al., 2013, Faber et al., 2014). Nevertheless, the accuracy and the computational demand of the BSE approach are strongly connected to the underlying (approximate) GW calculation. Therefore, the extension of the qsGW implementation in the TURBOMOLE package for the BSE approach promises to be a reasonably fast and accurate tool for the description of optical excitations.

Concluding, a method for the theoretical calculation of the electronic structure of molecular matter and nano-scale systems has been developed, implemented and extensively tested. Overall, this numerical tool produces highly accurate results and is computationally fast. The approach comes with major benefits especially for the description of charged excitation processes. Furthermore, the method is suitable for challenging problems like Coulomb blockade systems and interfaces where image charge effects are crucial. The treatment of these system is next to go about.

Based on the existing method, extensions to describe optical excitations are within reach. Thus, in a close future, accurate comprehensive evaluations of models for molecular devices, catalytic processes, and a comprehensive theoretical support of experiments is achievable.

Appendix

Appendix A

A Coupled Cluster Approach

In this work the accuracy of different flavors of GW are tested for the calculation of ionization energies. Typically, the reference for the first ionization potential (IP) is obtained from Coupled Cluster (CC) calculations in the ΔCCSD(T) approximation. The CC method is know to be highly accurate for such kind of calculations. Hence, CC is a fairly popular within the Quantum Chemistry community and a well known approach. However, a physicist likely has never come into contact with the CC method. Therefore, this chapter gives a short introduction into the numerical calculation of the electronic structure of molecules employing the CC approximation.

The structure of the following introduction is adapted from (Szabo and Ostlund, 1996). CC can be understood as a direct extension of the Hartree-Fock (HF) approximation. Therefore, although HF is a well know approach, the full route to the final HF-equations is drafted. Firstly, the problem is stated and the separation of the Hartree-Contribution of the full many-body problem is suggested. Secondly, a remainder of the Hartree-Fock approximation is given. Then, based on the Slater-Determinant wavefunction from HF the Coufiguration-Interaction (CI) extension is presented. Finally, the derivation of the CC approach is given.

All methods for the calculation of the electronic structure of molecules aim for an approximate solution of the full many-body Hamiltonian,

$$\hat{\mathcal{H}} = \sum_i \left[-\frac{\hbar^2}{2m}\nabla_i^2 + \hat{V}_{\text{ext}}(\mathbf{r}_i) \right] + \frac{1}{2}\sum_{ij} v(\mathbf{r}_i, \mathbf{r}_j) \ . \tag{A.1}$$

Here, the first term in the sum over all electrons on the right hand site is the kinetic contribution $\hat{T}_i = -\frac{\hbar^2}{2m}\nabla_i^2$. The second term in the sum is the interaction of the individual electrons with $\hat{V}_{\text{ext}}(\mathbf{r}_i)$, the external potential created by the ions. Furthermore, the Born-Oppenheimer Approximation is applied already. Thus, the ions are assumed to be static in comparison to the motion of the electrons. The following double sum on the right hand side takes account for the full electron-electron interaction, employing the Coulomb interaction

$$v(\mathbf{r}_i, \mathbf{r}_j) = \frac{e^2}{4\pi\epsilon_0 |\mathbf{r}_i - \mathbf{r}_j|} \ . \tag{A.2}$$

In the following all single-particle contributions are separated from the remaining contributions. This way the easily solved single-particle problem is separated from the complicated full electron-electron interaction. The bare one-particle operator

$$\hat{h}(\mathbf{r}) = -\frac{\hbar^2}{2m}\nabla_i^2 + \hat{V}_{\text{ext}}(\mathbf{r}) \ . \tag{A.3}$$

is considered. Further single-particle contributions in Eq. (2.23) are collected into the Hartree-contribution

$$\hat{\mathcal{H}}_{\text{H}} = \hat{h}(\mathbf{r}) + \underbrace{\frac{e^2}{4\pi\epsilon_0}\int \frac{n(\mathbf{r}')}{|\mathbf{r}-\mathbf{r}'|}\,\mathrm{d}^3r'}_{V_{\text{H}}(\mathbf{r})} \ . \tag{A.4}$$

The Hartree potential $V_{\text{H}}(\mathbf{r})$ describes the interaction of one test charge with the full electron density $n(\mathbf{r})$, even with itself. A solution of the Hartree problem $\hat{\mathcal{H}}_{\text{H}}$ is found employing a free article picture. In shorthand notation the Hartree-Hamiltonian is written as follows,

$$\hat{\mathcal{H}}_{\text{H}}(n) = \hat{T} + \hat{V}_{\text{ext.}} + \hat{V}_{\text{H}}(n) \ . \tag{A.5}$$

A.1 Hartree-Fock Theory

The Hartree-Fock (HF) approximation plays an important role in quantum-chemistry. Not only for it's own sake but as a starting point for further more advanced techniques, which do include correlation effects. Therefore, a brief reminder about the HF will be given at this point although it is a well established and a well know approach.

The fundamental aim of HF-Theory is to find the best set of single particle orbitals ψ_n which form a single determinant of the form

$$|\Phi_0\rangle = |\psi_1, \psi_2, \psi_3, ...\psi_{n-1}, \psi_n\rangle \, . \tag{A.6}$$

Best in the sense that $|\Phi_0\rangle$ is the optimum approximate to the real ground state of the full many-body problem Eq. (A.1). According to the variational principle the optimum orbitals are the ones which minimize the HF-energy E_{HF} from

$$E_{\text{HF}} = \langle\Phi_0|\,\hat{\mathcal{H}}\,|\Phi_0\rangle \tag{A.7}$$

$$\begin{aligned} &= \sum_i \int \mathrm{d}\mathbf{r}\ \psi_i^+(\mathbf{r})\hat{h}(\mathbf{r})\psi_i(\mathbf{r}) \\ &+ \frac{1}{2}\sum_{i,j}\int\int \mathrm{d}\mathbf{r}_1\ \mathrm{d}\mathbf{r}_2\ \psi_i^+(\mathbf{r}_1)\psi_i(\mathbf{r}_1)v(\mathbf{r}_1,\mathbf{r}_2)\psi_j^+(\mathbf{r}_2)\psi_j(\mathbf{r}_2) \\ &+ -\frac{1}{2}\sum_{i,j}\int\int \mathrm{d}\mathbf{r}_1\ \mathrm{d}\mathbf{r}_2\ \psi_i^+(\mathbf{r}_1)\psi_j(\mathbf{r}_1)v(\mathbf{r}_1,\mathbf{r}_2)\psi_j^+(\mathbf{r}_2)\psi_i(\mathbf{r}_2) \end{aligned} \tag{A.8}$$

To improve readability the, common short hand notation for the so called *Coulomb (Exchange) integrals* is introduced;

$$(ij|kl) = \int\int \mathrm{d}\mathbf{r}_1\ \mathrm{d}\mathbf{r}_1\ \psi_i^+(\mathbf{r}_1)\psi_j(\mathbf{r}_1)v(\mathbf{r}_1,\mathbf{r}_2)\psi_k^+(\mathbf{r}_2)\psi_l(\mathbf{r}_2) \ . \tag{A.9}$$

The rotated notation of the spacial and wavefunction indices needs to be noticed. In quantum chemistry a different notation then the standard bracket notation physicist are used to, is established . Using the shorthand notation of a matrix element of the many-body Hamiltonian, see Eq. (A.8), reads

$$\langle \Phi_0 | \, \hat{\mathcal{H}} \, | \Phi_0 \rangle = \sum_i \langle i | \, \hat{h} \, | i \rangle + \frac{1}{2} \sum_{i,j} (ii|jj) - (ij|ji) \quad . \tag{A.10}$$

The minimum is found by systematic variation of the orbitals ψ_i under the orthonormal constraint

$$\langle \psi_i | \psi_j \rangle = \delta_{i,j} \quad . \tag{A.11}$$

The first of the two Coulomb Exchange integral contributions in the matrix element Eq. (A.10) is the so called *coulomb* term which is already accounted for in the Mean-field Hartree Theory. The last term in Eq. (A.10), the *exchange* contribution, arise solely due to the antisymmetric nature of the determinantal wavefunction.

The minimum energy E_{HF} is found using a Slater-Determinant $|\Phi_0\rangle$ as an approximate ground state wavefunction. E_{HF} is in turn an approximate to the true ground state energy of the full many-body Hamiltonian Eq. (A.1). Nevertheless, there exist an Hamiltonian $\hat{\mathcal{H}}_{\mathrm{HF}}$ for which $|\Phi_0\rangle$ is an exact Eigenfunction with

$$\hat{\mathcal{H}}_{\mathrm{HF}} \, | \psi_i \rangle = \epsilon_i \, | \psi_i \rangle \quad . \tag{A.12}$$

Collecting all contributions not considered in $\hat{\mathcal{H}}_{\mathrm{HF}}$ into a perturbing term $\mathcal{V}$ via

$$\mathcal{V} = \hat{\mathcal{H}} - \hat{\mathcal{H}}_{\mathrm{HF}} \tag{A.13}$$

allows to separate all energy contributions which are not considered in $\hat{\mathcal{H}}_{\mathrm{HF}}$. A perturbative expansion of the energy via

$$E = E_0^{(0)} + E_0^{(1)} + E_0^{(2)} + E_0^{(3)} + ... \tag{A.14}$$

with the zeroth-order contribution $E_0^{(0)} = \langle \Phi_0 | \, \hat{\mathcal{H}}_{\mathrm{HF}} \, | \Phi_0 \rangle$ and the first order contribution $E_0^{(1)} = \langle \Phi_0 | \, \mathcal{V} \, | \Phi_0 \rangle$ gives to the HF-energy

$$E_{\mathrm{HF}} = \langle \Phi_0 | \, \hat{\mathcal{H}} \, | \Phi_0 \rangle \tag{A.15}$$

$$= E_0^{(0)} + E_0^{(1)} \quad . \tag{A.16}$$

The error of HF towards the exact energy of the many-body system $\mathcal{E}_0$ is

$$E_{\mathrm{c}} = \mathcal{E}_0 - E_{\mathrm{HF}} \quad , \tag{A.17}$$

which is known as the *Correlation Energy* E_{c}.

Within this work the interest is especially in ionization energies. Koopmans (1934) formulated a theorem which provides the theoretical justification for the interpretation of single HF orbital-energies as ionization energies.

A.2 Configuration Interaction

The HF procedure generates from a set of $2K$ orbitals ψ_i the optimum ground state Slater-Determinant $|\Psi_0\rangle$. In total one can construct from the set of orbitals a total of

$$\binom{2K}{N} = \frac{(2K)!}{N!(2K-N)!} \tag{A.18}$$

different determinants for N electrons. The HF-ground state is just one of them. A convenient way to describe the other determinants is to take the HF ground-state as a reference and classify the other ones in relation to it. The other ones can be interpreted as approximate excited states of the system. Furthermore, theses determinants can be used in linear combination with $|\Psi_0\rangle$ for a more accurate description of the ground-state or an excited state.

A singly excited determinant has one electron promoted from orbital ψ_a in the HF ground state to an unoccupied orbital ψ_r which generates a determinant

$$|\Phi_a^r\rangle = |\psi_1, \psi_2, ...\psi_r, \psi_b, ..., \psi_{n-1}, \psi_n\rangle \quad . \tag{A.19}$$

The same logic is applied for doubly excited determinants with two electrons excited from orbitals ψ_a and ψ_b to the orbitals ψ_r and ψ_s. Thus, a double excited state reads

$$|\Phi_{ab}^{rs}\rangle = |\psi_1, \psi_2, ...\psi_r, \psi_s, \psi_c, ..., \psi_{n-1}, \psi_n\rangle \quad . \tag{A.20}$$

Consequently all possible determinants can be classified either as the HF ground state or singly, doubly, triple, quadruply, ..., N-tuply excited states. It can be shown that any arbitrary antisymmetric wavefunction of N-variables can be exactly expanded in terms of all unique determinants formed from a complete set of one-variable states $\{\psi_i\}$ (Szabo and Ostlund, 1996). Taking this into account and recalling the possibility to express all possible determinants in reference to the HF ground state leads to the conclusion that the exact wavefunction $|\Phi\rangle$ for any state of the system can be written as

$$|\Phi\rangle = c_0 \underbrace{|\Phi_0\rangle}_{\text{HF}} + \sum_{r,a} c_a^r \underbrace{|\Phi_a^r\rangle}_{\text{Singles}} + \sum_{\substack{a<b \\ r<s}} c_{ab}^{rs} \underbrace{|\Phi_{ab}^{rs}\rangle}_{\text{Doubles}} + \sum_{\substack{a<b<c \\ r<s<t}} c_{abc}^{rst} \underbrace{|\Phi_{abc}^{rst}\rangle}_{\text{Triples}} + ... \quad . \tag{A.21}$$

The summation over $a < b$ considers the summation of all a and over all b greater than a (i.e. over all unique pairs of occupied spin orbitals). The logic applies analogously for the higher excitations, such that all unique doubly, triply and higher excited determinants are considered. Thus, the infinite set of N-electron determinants $\{|\Phi_i\rangle\} = \{|\Phi_0\rangle, |\Phi_a^r\rangle, |\Phi_{ab}^{rs}\rangle, ...\}$ is a complete set for the expansion of any N-electron wave function.

The complete set $\{|\Phi_i\rangle\}$ allows access to the exact energy of the ground-state and all excited states of the system. They are the eigenvalues of the Hamiltonian matrix with the elements $\langle\Phi_i|\,\hat{\mathcal{H}}\,|\Phi_j\rangle$. Every $|\Phi_i\rangle$ is defined by a specific configuration of spin orbitals. The name of the procedure is *Configuration Interaction* (CI).

The CI procedure allows, in theory, for access to the exact solution of the many-body problem. But, for the construction of such a solution an infinite set of basis function would be necessary. This is in practice not available, for obvious reasons. Nevertheless, the diagonalization of the finite Hamiltonian matrix formed from the full set of determinants within the limited set of basis functions leads to solutions which are exact within the one-electron subspace spanned by the orbitals. Such a solution is called *full CI*. For practical calculations on all but the smallest molecules full CI is computationally too demanding, even with the smallest basis sets. Using a one electron basis of moderate size, there are so many possible configurations that the full CI matrix becomes tremendously large (e.g. the dimensionality exceeds $10^9 \times 10^9$).

To overcome the problem of the computational demands of the full CI, there exists schemes which truncate the full CI amtrix, respectively the CI expansion. A systemic way would be to consider only a specific subset of excited determinants in the construction The simplest of these schemes would be to consider only Singles and Doubles in addition to the HF ground state (SDCI). There exist variational principles to take advantage of these truncated approaches for a numerical calculation of e.g. the correlation energy of molecules. Unfortunately all truncated CI approaches have a major drawback in common, they deteriorate as the number of electrons increase. That means that the correlation energy of N non-interacting minimal basis H_2 molecules is proportional to $N^{1/2}$ as N becomes large. But, the energy of a macroscopic system is an extensive thermodynamic property, therefore it must be proportional to the number of particles. Hence, truncated CI is not a satisfactory approach as well as the full CI. Nevertheless, there is still great effort in the development in CI based methods, especially to overcome the drawbacks, hence the approach is a valid competitor in the broad field of approaches in Quantum Chemistry.

A.3 Coupled Cluster Approximation

The Coupled Cluster (CC) approach aims, like the (truncated) CI approaches, for an approximate expression for the many-body wavefunction using excited determinants based on a HF ground state. The first derivation of the CC equations and the derivation of the method goes back to the work by Cizek and Paldus (1980).

The previously introduced (truncated) CI methods have, besides the high computational demands, the major drawback to describe the scaling of the correlation energy with the number of particles wrong. This is, for obvious reasons, crucial especially in the analysis of infinite extended systems. But even for finite systems it is desirable to have a method which gives results that can be meaningfully compared for molecules of different size. A typical application would be the dissociation of a molecule. For the analysis of this process a method which gives meaningful results for the intact full molecules and the resulting fragments as well is needed. Appropriate methods give energies which scale linearly with the number of particles as the size of the system increases. They are said to be *size consistent*. In contrast to CI the CC-approach is size consistent.

While the CC approach, which will be derived in the following, comes with the beneficial

feature of being size consistent, it does not have one desirable property. The CI approaches are so called *variational*. In contrast, CC is not variational. In praxis this condition affects such that the total energy obtained from CC must not be higher then the true energy. The energy obtained from CI is always an upper bound.

To begin the introduction to the Coupled Cluster approach the ansatz from the full CI approach is considered again. For the sake of simplicity the presenece of single, triple etc. excitations is ignored in the introductionary example. Hence, the intermediate normalized wave function is

$$|\Phi\rangle = |\Phi_0\rangle + \sum_{\substack{a<b \\ r<s}} c_{ad}^{rs} |\Phi_{ab}^{rs}\rangle + \sum_{\substack{a<b<c<d \\ r<s<t<u}} c_{abcd}^{rstu} \left|\Phi_{abcd}^{rstu}\right\rangle + ... \tag{A.22}$$

where the dots represent hextuple and higher excitations. To determine the variational energy of this wave function one starts from the defining equation for the correlation energy

$$(\hat{\mathcal{H}} - E_{\mathrm{HF}}) |\Phi\rangle = E_{\mathrm{corr}} |\Phi\rangle \tag{A.23}$$

and subsequently multiply by $\langle\Phi_0|, \langle\Phi_{ab}^{rs}|, \langle\Phi_{abcd}^{rstu}|$, etc. to obtain the following set of equations.

$$\sum_{\substack{a<b \\ r<s}} \langle\Phi_0| \hat{\mathcal{H}} |\Phi_{ab}^{rs}\rangle c_{rs}^{ab} = E_{\mathrm{corr}} \tag{A.24}$$

$$\langle\Phi_{ab}^{rs}| \hat{\mathcal{H}} |\Phi_0\rangle + \sum_{\substack{c<d \\ t<u}} \langle\Phi_{ab}^{rs}| \hat{\mathcal{H}} - E_{\mathrm{HF}} \left|\Phi_{cd}^{tu}\right\rangle c_{cd}^{tu} + \sum_{\substack{c<d \\ t<u}} \langle\Phi_{ab}^{rs}| \hat{\mathcal{H}} - E_{\mathrm{HF}} \left|\Phi_{abcd}^{rstu}\right\rangle c_{abcd}^{rstu} = E_{\mathrm{corr}} c_{ab}^{rs} \tag{A.25}$$

and so on. These equations form a hierarchy in which the correlation energy depends on the coefficients of the doubles c_{rs}^{ab}, but the equations for these coefficients involve a dependence on the coefficients of the quadruples c_{abcd}^{rstu} and hence again implicitly on higher terms. To formulate a practical approach it is necessary to terminate this coupled dependence of increasing orders. The obvious approach would be to terminate by setting e.g. all c_{abcd}^{rstu} to zero, which is identical to the truncated CI approach DCI.

The approximation in CC is to express the coefficients of the quadruples in terms of the doubles coefficients and hence generate a closed set of equations. Thus, it reads symbolically

$$c_{abcd}^{rstu} \approx c_{ab}^{rs} \star c_{cd}^{tu} \ . \tag{A.26}$$

This notation implicates that c_{abcd}^{rstu} is not just the plain product of c_{ab}^{rs} and c_{cd}^{tu}. A quadruple excitation of the electrons in the orbitals *abcd* to the orbitals *rstu* can not only be obtained by exciting $\substack{a\to r \\ b\to s}$ and $\substack{d\to u \\ c\to t}$ but e.g. via the process $\substack{a\to r \\ b\to t}$ and $\substack{d\to u \\ c\to s}$ as well. In total there are 18 distinct ways to construct such a quadruple excitation from independent double excitations. The star in Eq. (A.3) indicates that all possible combinations are considered implicitly within this approximation.

Inserting the approximation Eq. (A.3) into Eq. (A.25) and taking advantage of Eq. (A.24) gives

$$\langle\Phi_{ab}^{rs}|\,\hat{\mathcal{H}}\,|\Phi_0\rangle + \sum_{\substack{c<d\\t<u}} \langle\Phi_{ab}^{rs}|\,\hat{\mathcal{H}} - E_0\left|\Phi_{cd}^{tu}\right\rangle c_{cd}^{tu} + \sum_{\substack{c<d\\t<u}} \langle\Phi_{ab}^{rs}|\,\hat{\mathcal{H}} - E_0\left|\Phi_{abcd}^{rstu}\right\rangle (c_{ab}^{rs} \star c_{cd}^{tu} - c_{ab}^{rs}c_{cd}^{tu}) = 0 \quad \text{(A.27)}$$

which gives in combination with Eq. (A.23) the defining equation for the correlation energy.

Starting from the presented straight forward approach for the approximate expression for the wave function the Cluster Expansion is introduced. Therefore the double excited determinant $|\Phi_{ab}^{rs}\rangle$ is written in second quantization

$$|\Phi_{ab}^{rs}\rangle = a_r^+ a_s^+ a_b a_a\,|\Phi_0\rangle \quad . \tag{A.28}$$

For example the double excited CI wave function $|\Phi_{\mathrm{DCI}}\rangle$ reads in this notation

$$|\Phi_{\mathrm{DCI}}\rangle = \Big(1 + \sum_{\substack{a<b\\r<s}} c_{ad}^{rs} a_r^+ a_s^+ a_b a_a\Big)\,|\Phi_0\rangle \quad . \tag{A.29}$$

The Cluster expansion aims for an expression of the wave function in a way as described above such that the coefficients of the $2n$th-tuple excitations are approximated by products of n doubly excited coefficients. The related wave function $|\Phi_{\mathrm{CCA}}\rangle$, can be written as

$$|\Phi_{CCD}\rangle = \exp(\mathcal{T}_2)\,|\Phi_0\rangle \tag{A.30}$$

with

$$\mathcal{T}_2 = \frac{1}{4}\sum_{abrs} c_{ad}^{rs} a_r^+ a_s^+ a_b a_a \quad . \tag{A.31}$$

Together with the expansion of the exponential $\exp(x) = 1 + x + \frac{1}{2}x^2 + ...$ it can be shown after some lengthy calculations, which will be omitted here, that the expression in Eq. (A.30) leads to a wave function that reads

$$|\Phi_{CCD}\rangle = |\Phi_0\rangle + \sum_{\substack{a<b\\r<s}} c_{ad}^{rs}\,|\Phi_{ab}^{rs}\rangle + \sum_{\substack{a<b<c<d\\r<s<t<u}} c_{ab}^{rs} \star c_{cd}^{tu}\left|\Phi_{abcd}^{rstu}\right\rangle + ... \quad . \tag{A.32}$$

This approach can be generalised for example by employing in addition the single excitations

$$\mathcal{T}_1 = \sum_{ra} c_a^r a_r^+ a_a \tag{A.33}$$

in an extended exponential for the wavefunction expansion

$$|\Phi_{CCSD}\rangle = \exp(\mathcal{T}_1 + \mathcal{T}_2)\,|\Phi_0\rangle \tag{A.34}$$

$$\approx \Big(1 + \mathcal{T}_1 + \frac{1}{2}\mathcal{T}_1^2 + \mathcal{T}_2 + \mathcal{T}_1\mathcal{T}_2 + \frac{1}{3!}\mathcal{T}_1^3 + \mathcal{T}_2^2 + \frac{1}{2}\mathcal{T}_1^2\mathcal{T}_2 + \frac{1}{4!}\mathcal{T}_1^4\Big)\,|\Phi_0\rangle \quad . \tag{A.35}$$

This approach can be extended to consider even higher excitations in the exponential. In this way the different approaches within the CC method are distinguished by the order of the excitation coefficients that are considered in the construction of the wave function. The label of the separate approaches is directly linked to the included coefficients, hence the approach with the bare consideration of doubles (as in Eq. (A.30) is called CCD, taking additionally single excitation coefficients into account (as done in Eq. (A.34) is labelled with CCSD. This can be extended to triples (CCSDT) and even further.

The CCSDT can be speed up by a perturbative treatment of the Triple excitations, this approach is known as CCSD(T). The CCSD(T) has shown to be one of the most accurate methods to investigate ground state properties of molecules. Furthermore, the ΔCCSD(T) method, which calculates the difference of the ground state energy of the neutral and the ionized system using CCSD(T) gives highly accurate estimates for the first Ionization Potential (IP) (McKechnie et al., 2015). In spite of this success, the CCSD(T) approach is computationally very demanding which makes in not practical for the investigation of medium size and larger molecules. Due to this demand it is as well not practical for the application on a screening of whole sets of molecules. The next drawback, which the CC has in common with the other wave function based methods is that it does not allow for a direct description of charged excitations, besides the first IP.

B Appendix B
Implementation

To perform a *GW* calculation the successive execution of three different modules is needed. Fig. B.1 shows the flow of the different modules within the TURBOMOLE package. In practice a script controls the flow through the iterative cycle. The user specifies only few parameters for the calculation. The control parameters for the qs*GW* cycle are described in Sec. B.4. First, some choices for the technical realization are explained and commented in Sec. B.1.

B.1 Embedding in the TURBOMOLE Framework

The technical flow of the Green's function is performed on the *mos* file. On the one hand, the file contains the full transformation matrices which define the spatial shape of the QP-orbitals in terms of the basis functions. On the other hand, the file contains, in addition, the QP-energies from all QP-orbitals. Hence, the *mos* file defines the full (free-particle) Green's function in each *GW* iteration. The qs*GW* cycle uses the output of a standard density functional theory (DFT) or Hartree Fock (HF) output, which actually is the *mos* file with the named structure, as the first guess for the Green's function. From then on, the *ridft* and *escf* module are used to calculate objects relevant for the construction of the self-energy and the mean-field contribution based on the system given in the *mos* file. The *escf* and *ridft* modules have been modified to pass the required output to the *gw* module via file out- and input, respectively. After the initialization, only the *gw* module changes the entries in the *mos* file. Hence, it calculates all updates on the QP-orbitals and the QP-energies via solving the QP-equation and passes the solution to the mos file.

The communication of the *gw* module with the *escf* and *ridft* via file I/O is from the point of view on computational speed critical, especially for small systems, compared to an operation solely on the (shared) memory. But, there are strong arguments for the present I/O solution. Passing information via files was chosen for the following reasons: First, the method is scalable to larger systems where the information can not be kept simultaneously in the memory.[1] The solution is to operate only on separate chunks of the information

[1]This is the case already for the system anthracene. Solely all integrals over excitation densities require

and keep the remaining objects on the hard disk. The size of the chunks can be controlled via input parameters, or is adjusted automatically from the program to fit the available memory. Second, the communication via file I/O allows for easier realization of job-queues. Typically, on supercomputers the granted time for the execution of one program is limited. Hence, especially for large systems with many electrons, the time granted is insufficient to achieve a full converged solution. Taking advantage of the I/O structure allows for an straight forward passing of data from one job to a subsequent one.

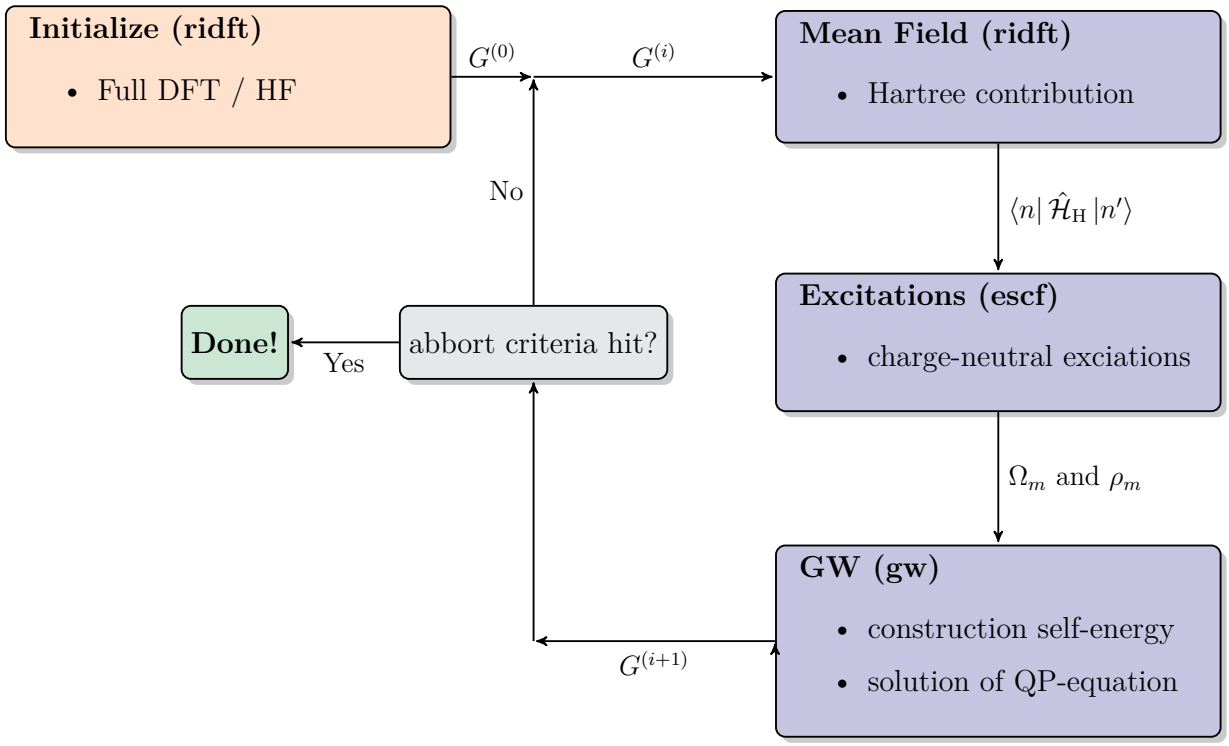

Figure B.1: Schematic representation of the technical realization of the *GW*-cycle.

B.2 Role of the Executables

Initialization (ridft) A full qs*GW* calculation starts with the (full) initializing density function theory (DFT) or Hartree Fock (HF) run. A standard setup as described in the TURBOMOLE manual is required. Effect on the final result of the qs*GW* will have only the choice for the *basis set*. The impact of the choice on the final result and a benchmark for the optimum choice is performed in Sec. 3.2.1. The choice for an optimized functional can reduce the required number of iterations in the full qs*GW* cycle drastically, as discussed in Sec. 3.2.1.3. From the full converged

more then 200Gb. The recent standard workstation computers offer at maximum 64Gb. Hence, a separation in smaller chunks is essential.

DFT / HF calculation a first guess for the Green's function ($G^{(0)}$) will be constructed. Technically, there are all transformation matrix entries which define the (QP-)orbitals and all (QP-)energies written to the *mos* file.

Mean Field (ridft) Given there is the related switch set, the call of the *ridft* calculates the mean-field contribution of the system given by the Green's function defined in the *mos* file. The full matrix of the Hartree-Contributions (in the basis of QP-orbtials) is written to a file.

Excitations (escf) The *escf* module calculates all excitation energies Ω_m and all integrals over the excitations densities $(pq|\rho_m)$. The results are then passed to a file as well. This step strongly accelerates with the RI-approximation. But, results slightly change with the approximation. Hence, it is up to the user whether the option is used or not. The default is to take advantage of it as it reduce the computational complexity by roughly one order, in practice.

GW (gw) The *gw* module operates on an inner loop which iterates a self-consistency cycle over the QP-equation. The self-energy is constructed in a first step: The exchange part is directly calculated from coulomb-exchange integrals. The correlation contribution is constructed in the chosen approximation, employing the data written to the file from the preceding *escf* run. Then, in a second step is the QP-equation solved in the chosen approximation. The resulting energies are then used to construct a updated self-energy. Then, in turn, is the QP-equation solved with the updated self-energy. This is iterated till all energies are converged within a chosen cutoff. Typically the energies are converged in 20 iterations up to 1 meV. Last, based on the solution of the QP-equation new QP-orbitals and QP-energies are written to the *mos* file. A comparison to the entries in the file from the previous iteration allows to check for the convergence in the outer qs*GW* cycle, applying the criteria from Sec. 3.2.2. If the criteria is not hit yet, the cycle passes back to the *ridft* module to calculate the mean-field contributions.

B.3 Structure of the GW Program

The structure of the *gw* program is visualized in Fig. B.2. The code is organized in a flat structure which directly relates to the operation of the program. In a first step the program loads a module for the chosen approximation for the gw program. It allocates the related variables (the requirements are strongly different fromt he diagon-only treatment of the QP-equation to the full energy dependent solution). Then the code passes to a loop over the number of iterations over the QP-equation. In the loop, in principle only to calls are iteratively performed. First, the matrix elements of the correlation part of the self-energy are calculated. Second, the QP-equation is solved. The calculation of the correlation part of the self-energy is, in turn, again a loop over all excitations m, see Eq. (3.40). This loop has been fully parallelized. For the solution of QP-equation the code takes advantage of

existing routines from the Lapack package to diagonalize the equation(s). Hence, it runs in parallel as well.

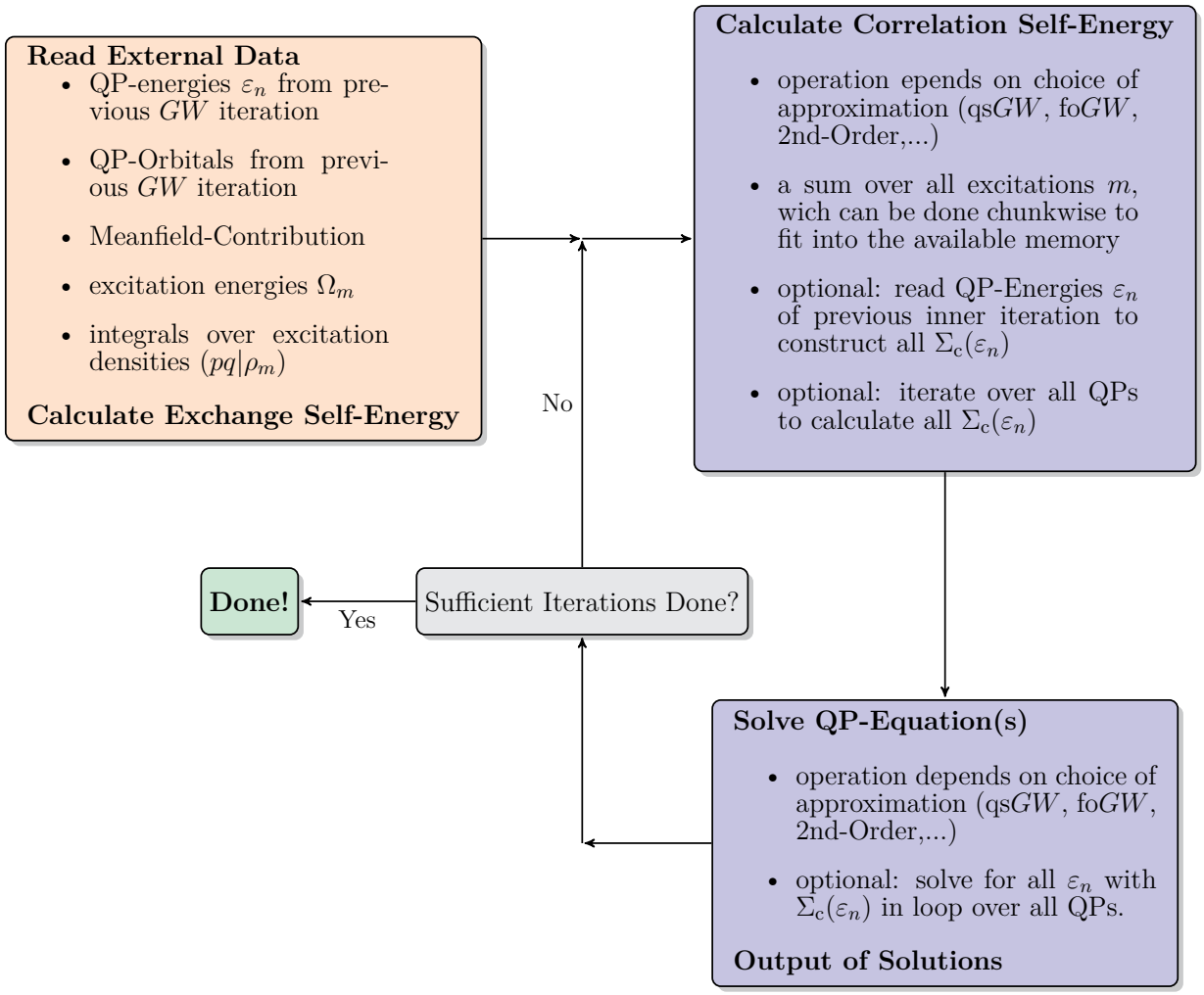

Figure B.2: Schematic representation of the technical realization of the solution of the QP-Equation in the gw program. First, the programm allocates the required amount of memory and organized, if needed, the chunkwise treatment of the sum over the excitations m. Dependent on the choice for the approximation, the related module is loaded. It follows an loop which iteratively calculates the self-energy and then solves the QP-equation.

B.4 Controls

During the time of this thesis several skripts were created to control the flow of the qsGW cycle. One has proven to be the central one and is for all further modifications a very good starting point. The script automatically performs a full qsGW calculation till convergence

employing the def2-TZVPP basis. It operates such that the required structural data file *coord* is placed in a folder with the name *Backup*. Furthermore, a file with name *lambda* which contains only the amount of exact-exchange in the PBEλ functional for the initial run (i.e. 0.25 if one would like to start from PBE0) needs to be placed in the folder. In addition the *GW*-control file with the name *gwinp* needs to be placed in the Backup folder as well. Details on the *gwinp* file will follow. First details on the script, which is called via:

conv_lambda.sh $1 $2 $3 $4

with four parameters. The first parameter $1 controls, via integer numbers, which *GW* approach is chosen, i.e. qs*GW*, fo*GW*, $G_{\mathrm{fo}W_0}$,... . Choosing $1 = 1 gives the qs*GW* cycle. The second parameter $2 controls the maximum number of *GW* iterations, a typical choice would be $2 = 20. The third parameter $3 is the value of the cutoff parameter, a typical choice would be $3 = $1e-8$. The last parameter $3 lets the user switch between abort criteria, i.e. $3 = 1 lets the convergence be tested for the criteria introduced in Eq. (3.51).

The specific parameters for the gw programm are specified in the related control file, *gwinp*. Following flags are most importent and need to be set:

$qpsc boolean Via a boolean is controlled whether there should be done a G_0W_0 like one shot calculation or it is aimed for a qs*GW* like self-consistent solution. Choose *.true.* for the self-consistent treatment.

$gworder x This flag chooses the approximation for the treatment of the QP-equation:

- $x = -2$ approximation of the self-energy as suggested in (3.43)
- $x = -1$ self-consistent solution of the QP-equation with energy-dependent self-energy
- $x = 0$ diagonal only treatment of the QP-equation
- $x = 2$ second-order treatment of off-diagonals of the QP-equation

$gam x The value of x specifies the final value of η in eV (i.e. $gam 0.001) in the calculation of the correlation part of the self-energy (3.43).

$qpeiter x This parameters controls the number of times the QP-equation is solved iteratively in each single qs*GW* iteration. A typical choice is $x = 20$.

$wpqmem x This parameter sets the amount of memory that is available for the excitation integrals (in MB). Based on this this number is the size of the separate chunks constructed.

$linmix x This parameter controls the mixing between two *GW* iterations, as discussed in Sec. 3.2.3.2. The choice $x = 0.3$ has proven to grand fast and stable convergence.

Appendix C

C Additional Data

In this chapter additional data is reported, which was not presented in the main part of the thesis . It does not add new fundamental findings on top of the results of the thesis. Nevertheless, it completes the general message and supports several shown results.

C.1 Ionization Energies

In Tab. C.3 to Tab. C.4, statistical error of the calculated first ionization potential (IP) of the approximate approaches to the experimental (vertical) IP as well as the calculated IPs from ΔCCSD(T) is reported. The data supplements the findings from the specific chapters, which are named in the captions of the tables.

Tab. C.5 to Tab. C.8 reports the bare calculated HOMO energies for all methods. These yield as reference data if one is interested in the results for one specific system. Furthermore, these tables report the data which was the basis for the statistical evaluations.

Fig. C.2 to Fig. C.3 report the calculated higher IPs for four addition molecules.

G_0W_0	@PBE		@PBE0		@PBE75		qsGW	CCSDT(T)
	0th	2nd	0th	2nd	0th	2nd		
ME	0.46	0.44	0.19	0.18	-0.10	-0.10	-0.23	-0.11
MAE	0.54	0.52	0.35	0.34	0.32	0.32	0.35	0.27
σ^2	0.19	0.18	0.14	0.14	0.22	0.22	0.15	0.17
MaxAE	1.38	1.33	1.16	1.15	1.46	1.47	0.98	1.12
MinAE	0.03	0.05	0.01	0.01	0.01	0.01	0.00	0.00

Table C.1: Evaluation over the data from Tab. C.5. These results complement the findings from Sec. 3.2.3.1. The results from the G_0W_0 method are strongly dependent on the chosen starting point. For an improved starting point, the average agreement with experiment is in the same order of magnitude as from qsGW and even CCSD(T).

G_0W_0	@PBE		@PBE0		@PBE75		qsGW
	0th	2nd	0th	2nd	0th	2nd	
ME	0.57	0.55	0.29	0.30	0.01	0.01	-0.12
MAE	0.62	0.60	0.30	0.31	0.19	0.19	0.22
σ^2	0.17	0.15	0.05	0.05	0.08	0.08	0.07
MaxAE	1.49	1.47	1.28	1.29	1.08	1.08	0.97
MinAE	0.14	0.12	0.04	0.05	0.00	0.00	0.01

Table C.2: Evaluation over the data from Tab. C.5. These results complement the findings from Sec. 3.2.3.1. Similar to the results shown in Tab. C.3, for an improved starting point (PBE75) is the G_0W_0 in very good agreement with the CCSD(T) estimates (on average)

.

	@PBE		@PBE0		@PBE75		qsGW	CCSDT(T)
	G_0W_0	$G_{\text{fo}}W_0$	G_0W_0	$G_{\text{fo}}W_0$	G_0W_0	$G_{\text{fo}}W_0$		
ME	0.46	0.16	0.19	0.06	-0.10	-0.07	-0.23	-0.11
MAE	0.54	0.35	0.35	0.30	0.32	0.32	0.35	0.27
σ^2	0.19	0.15	0.14	0.16	0.22	0.22	0.15	0.17
MaxAE	1.38	0.93	1.16	1.15	1.46	1.50	0.98	1.12
MinAE	0.03	0.02	0.01	0.03	0.01	0.00	0.00	0.00

Table C.3: Evaluation of the deviation to experimental vertical ionization energies of HOMO energies calculated from traditional diagonal-only G_0W_0 (0th) and from G_0W_0 taking into account QP-shift in the construction of the self-energy ($G_{\text{fo}}W_0$). Data from Tab. C.6.

	@PBE		@PBE0		@PBE75		qsGW
	G_0W_0	$G_{\text{fo}}W_0$	G_0W_0	$G_{\text{fo}}W_0$	G_0W_0	$G_{\text{fo}}W_0$	
ME	0.57	0.27	0.30	0.17	0.01	0.04	-0.12
MAE	0.62	0.31	0.31	0.19	0.19	0.18	0.22
σ^2	0.17	0.10	0.05	0.06	0.08	0.08	0.07
MaxAE	1.49	1.37	1.29	1.25	1.08	1.12	0.97
MinAE	0.14	0.00	0.05	0.00	0.00	0.01	0.01

Table C.4: Evaluation of the deviation to CCSD(T) results of results of HOMO energies calculated from traditional diagonal-only G_0W_0 (0th) and from G_0W_0 taking into account QP-shift in the construction of the self-energy ($G_{\text{fo}}W_0$). Data from Tab. C.6.

G_0W_0	@PBE		@PBE0		@PBE75		qsGW	CC	Exp.
	0th	2nd	0th	2nd	0th	2nd			
H_2	15.57	15.58	15.87	15.87	16.14	16.15	16.04	16.21	15.42
Li_2	4.95	4.98	5.13	5.14	5.19	5.20	5.30	5.20	5.11
Na_2	4.78	4.79	4.87	4.88	4.86	4.86	4.99	4.92	4.89
Cs_2	3.40	3.43	3.45	3.47	3.41	3.43	3.57	3.58	3.70
F_2	14.55	14.59	15.01	15.04	15.56	15.57	15.91	15.46	15.70
N_2	14.69	14.71	15.21	15.22	16.71	16.71	15.86	15.54	15.58
BF	10.43	10.45	10.81	10.82	11.18	11.18	11.17	11.14	11.00
LiH	6.52	6.57	7.44	7.45	8.01	8.02	7.98	7.93	7.90
CO_2	12.96	13.01	13.36	13.39	13.84	13.84	14.06	13.67	13.78
H_2O	11.87	11.91	12.21	12.24	12.55	12.57	12.95	12.61	12.62
NH_3	10.24	10.28	10.57	10.59	10.91	10.91	11.11	10.85	10.85
SiH_4	12.11	12.13	12.47	12.48	12.87	12.87	12.96	12.70	12.82
SF_4	11.88	11.91	12.31	12.33	12.88	12.86	13.03	12.62	12.30
Au_2	9.84	9.74	8.91	8.92	8.67	8.67	9.12	9.10	9.50
Au_4	7.45	7.45	7.44	7.45	7.14	7.13	7.62	7.67	8.60
Methane	13.79	13.82	14.11	14.12	14.44	14.45	14.46	14.36	14.35
Ethane	12.22	12.24	12.51	12.52	12.83	12.84	12.95	13.12	12.00
Propane	11.54	11.56	11.83	11.84	12.16	12.16	12.31	12.13	11.51
Butane	11.39	11.40	11.69	11.69	11.79	11.74	11.90	11.58	11.09
Isobutane	11.26	11.27	11.55	11.55	11.89	11.89	12.00	11.68	11.13
Ethylene	10.24	10.26	10.40	10.41	10.55	10.55	10.68	10.70	10.68
Acetone	8.84	8.87	9.33	9.35	9.87	9.85	10.08	9.71	9.70
Acrolein	9.23	9.26	9.82	9.84	10.67	8.14	10.55	10.20	10.11
Benzene	8.87	8.90	9.07	9.08	9.25	9.26	9.40	9.34	9.24
Naphthalene	7.68	7.71	7.89	7.90	8.10	8.10	8.22	8.04	8.09
Thiophene	8.48	8.51	8.70	8.71	8.93	8.93	9.02	8.96	8.85
Benzothiazole	8.24	8.27	8.48	8.49	8.74	8.73	8.83	8.70	8.75
1,2,5-thiadiazole	9.65	9.68	9.86	9.87	10.06	10.06	10.18	11.15	10.11
Tetrathiofulvalene	5.98	6.00	6.21	6.22	6.51	6.51	6.56	6.42	6.72

Table C.5: HOMO energies calculated from traditional diagonal-only G_0W_0 (0th) and from G_0W_0 taking into account off-diagonal elements of the QP-equation (2nd). All G_0W_0 calculations were initialized from DFT employing the PBE functional,and a PBE hybrid with 25% exact exachange (PBE0) and 75% (PBE75). HOMO energies from qsGW, experimental (vertical) Ionization Potentials (Exp.) and estimates from ΔCCSD(T) (labeled with CC, data from Krause et al. (2015)). All numbers are in units of eV. The G_0W_0 method is introduced in Sec. 2.5.2.

	$G_{\mathrm{fo}}W_0$					
	@PBE	@PBE0	@PBE75	qsGW	CC	Exp.
H_2	15.99	16.07	16.17	16.04	16.21	15.42
Li_2	5.15	5.19	5.18	5.30	5.20	5.11
Na_2	4.91	4.92	4.86	4.99	4.92	4.89
Cs_2	3.44	3.45	3.40	3.57	3.58	3.70
F_2	15.15	15.29	15.49	15.91	15.46	15.70
N_2	14.69	15.21	16.70	15.86	15.54	15.58
BF	10.76	10.94	11.18	11.17	11.14	11.00
LiH	7.63	7.84	8.03	7.98	7.93	7.90
CO_2	13.35	13.53	13.78	14.06	13.67	13.78
H_2O	12.38	12.44	12.51	12.95	12.61	12.62
NH_3	10.67	10.77	10.89	11.11	10.85	10.85
SiH_4	12.51	12.66	12.87	12.96	12.70	12.82
SF_4	12.24	12.44	12.82	13.03	12.62	12.30
Au_2	9.62	8.97	8.64	9.12	9.10	9.50
Au_4	7.67	7.45	7.10	7.62	7.67	8.60
Methane	14.19	14.30	14.44	14.46	14.36	14.35
Ethane	12.57	12.68	12.83	12.95	13.12	12.00
Propane	11.89	12.00	12.15	12.31	12.13	11.51
Butane	11.74	11.86	11.77	11.90	11.58	11.09
Isobutane	11.60	11.72	11.87	12.00	11.68	11.13
Ethylene	10.40	10.48	10.54	10.68	10.70	10.68
Acetone	9.37	9.55	9.81	10.08	9.71	9.70
Acrolein	9.88	10.06	10.65	10.55	10.20	10.11
Benzene	9.03	9.13	9.22	9.40	9.34	9.24
Naphthalene	7.83	7.94	8.07	8.22	8.04	8.09
Thiophene	8.63	8.75	8.90	9.02	8.96	8.85
Benzothiazole	8.41	8.54	8.70	8.83	8.70	8.75
1,2,5-thiadiazole	9.78	9.89	10.02	10.18	11.15	10.11
Tetrathiofulvalene	6.09	6.24	6.48	6.56	6.42	6.72

Table C.6: HOMO energies calculated from $G_{\mathrm{fo}}W_0$ taking into account QP-shifts of the poles in the self-energy. All $G_{\mathrm{fo}}W_0$ calculations were initialized from DFT employing the PBE functional,and a PBE hybrid with 25% exact exachange (PBE0) and 75% (PBE75). HOMO energies from qsGW, experimental (vertical) Ionization Potentials (Exp.) and estimates from ΔCCSD(T) (labeled with CC, data from Krause et al. (2015)). All numbers are in units of eV. The data is discussed in Sec. 5.3.2.1.

	$G_{\mathrm{fo}}W_0$-2nd					
	@PBE	@PBE0	@PBE75	qsGW	CC	Exp.
H_2	16.00	16.08	16.17	15.42	16.07	15.99
Li_2	5.16	5.19	5.19	5.11	5.19	5.15
Na_2	4.92	4.93	4.86	4.89	4.92	4.91
Cs_2	3.49	3.48	3.42	3.70	3.45	3.44
F_2	15.19	15.32	15.50	15.70	15.29	15.15
N_2	15.22	15.50	15.87	15.58	15.21	14.69
BF	10.78	10.96	11.18	11.00	10.94	10.76
LiH	7.65	7.87	8.03	7.90	7.84	7.63
CO_2	13.40	13.56	13.79	13.78	13.53	13.35
H_2O	12.41	12.47	12.53	12.62	12.44	12.38
NH_3	10.70	10.78	10.89	10.85	10.77	10.67
SiH_4	12.53	12.67	12.87	12.82	12.66	12.51
SF_4	12.24	12.46	12.79	12.30	12.44	12.24
Au_2	9.11	8.98	8.63	9.50	8.97	9.62
Au_4	7.65	7.46	7.09	8.60	7.45	7.67
Methane	14.21	14.31	14.44	14.35	14.30	14.19
Ethane	12.59	12.69	12.83	12.00	12.68	12.57
Propane	11.91	12.01	12.15	11.51	12.00	11.89
Butane	11.42	11.86	11.71	11.09	11.86	11.74
Isobutane	11.53	11.72	11.87	11.13	11.72	11.60
Ethylene	10.45	10.48	10.54	10.68	10.48	10.40
Acetone	9.44	9.57	9.79	9.70	9.55	9.37
Acrolein	9.89	10.08	9.64	10.11	10.06	9.88
Benzene	9.07	9.14	9.23	9.24	9.13	9.03
Naphthalene	7.87	7.94	8.07	8.09	7.94	7.83
Thiophene	8.66	8.77	8.91	8.85	8.75	8.63
Benzothiazole	8.45	8.55	8.70	8.75	8.54	8.41
1,2,5-thiadiazole	9.81	9.89	10.03	10.11	9.89	9.78
Tetrathiofulvalene	6.12	6.25	6.48	6.72	6.24	6.09

Table C.7: HOMO energies calculated from $G_{\mathrm{fo}}W_0$-2 taking into account QP-shifts of the poles in the self-energy and off-diagonal elements of the QP-equation. All $G_{\mathrm{fo}}W_0$-2nd calculations were initialized from DFT employing the PBE functional,and a PBE hybrid with 25% exact exachange (PBE0) and 75% (PBE75). HOMO energies from qsGW, experimental (vertical) Ionization Potentials (Exp.) and estimates from ΔCCSD(T) (labeled with CC, data from Krause et al. (2015)). All numbers are in units of eV. The data is presented and discussed in Sec. 5.4.2.

	foGW							
	@PBE	@PBE0	@PBE50	@PBE75	@PBE100	qsGW	CC	Exp.
H_2	16.25	16.24	16.22	16.20	16.18	15.42	16.21	16.04
Li_2	5.27	5.24	5.21	5.18	5.16	5.11	5.20	5.30
Na_2	4.98	4.94	4.90	4.86	4.82	4.89	4.92	4.99
Cs_2	3.46	3.45	3.43	3.40	3.37	3.70	3.58	3.57
F_2	15.73	15.66	15.59	15.66	15.44	15.70	15.46	15.91
N_2	15.64	15.73	15.82	15.90	15.98	15.58	15.54	15.86
BF	11.00	11.08	11.14	11.19	11.24	11.00	11.14	11.17
LiH	8.17	8.15	8.12	8.09	8.06	7.90	7.93	7.98
CO_2	13.76	13.78	13.79	13.79	13.78	13.78	13.67	14.06
H_2O	12.82	12.72	12.63	12.53	12.44	12.62	12.61	12.95
NH_3	11.04	10.99	10.95	10.91	10.87	10.85	10.85	11.11
SiH_4	12.83	12.86	12.88	12.89	12.90	12.82	12.70	12.96
SF_4	12.65	12.67	12.73	12.80	12.88	12.30	12.62	13.03
Au_2	9.40	9.05	8.83	8.64	8.46	9.50	9.10	9.12
Au_4	7.83	7.50	7.28	7.09	6.91	8.60	7.67	7.62
Methane	14.51	14.49	14.48	14.46	14.44	14.35	14.36	14.46
Ethane	12.87	12.86	12.85	12.84	12.82	12.00	13.12	12.95
Propane	12.19	12.18	12.17	12.16	12.14	11.51	12.13	12.31
Butane	12.05	12.04	12.03	11.77	11.76	11.09	11.58	11.90
Isobutane	11.91	11.90	11.89	11.88	11.86	11.13	11.68	12.00
Ethylene	10.60	10.59	10.57	10.54	10.51	10.68	10.70	10.68
Acetone	9.86	9.83	9.81	9.81	9.82	9.70	9.71	10.08
Acrolein	10.41	10.36	10.36	10.65	10.75	10.11	10.20	10.55
Benzene	9.24	9.24	9.24	9.22	9.20	9.24	9.34	9.40
Naphthalene	8.02	8.05	8.06	8.06	8.06	8.09	8.04	8.22
Thiophene	8.85	8.87	8.89	8.90	8.90	8.85	8.96	9.02
Benzothiazole	8.63	8.66	8.89	8.69	8.72	8.75	8.70	8.83
1,2,5-thiadiazole	9.97	10.00	10.02	10.02	10.02	10.11	11.15	10.18
Tetrathiofulvalene	6.26	6.34	6.41	6.47	6.52	6.72	6.42	6.56

Table C.8: HOMO energies calculated from foGW. All foGW calculations were initialized from DFT employing the PBE functional, and a PBE hybrid with 25% exact exachange (PBE0), 50% (PBE50), 75% (PBE75) and 100% (PBE100). HOMO energies from qsGW, experimental (vertical) Ionization Potentials (Exp.) and estimates from ΔCCSD(T) (labeled with CC, data from Krause et al. (2015)). All numbers are in units of eV. The data is presented and discussed in Sec. 6.3.

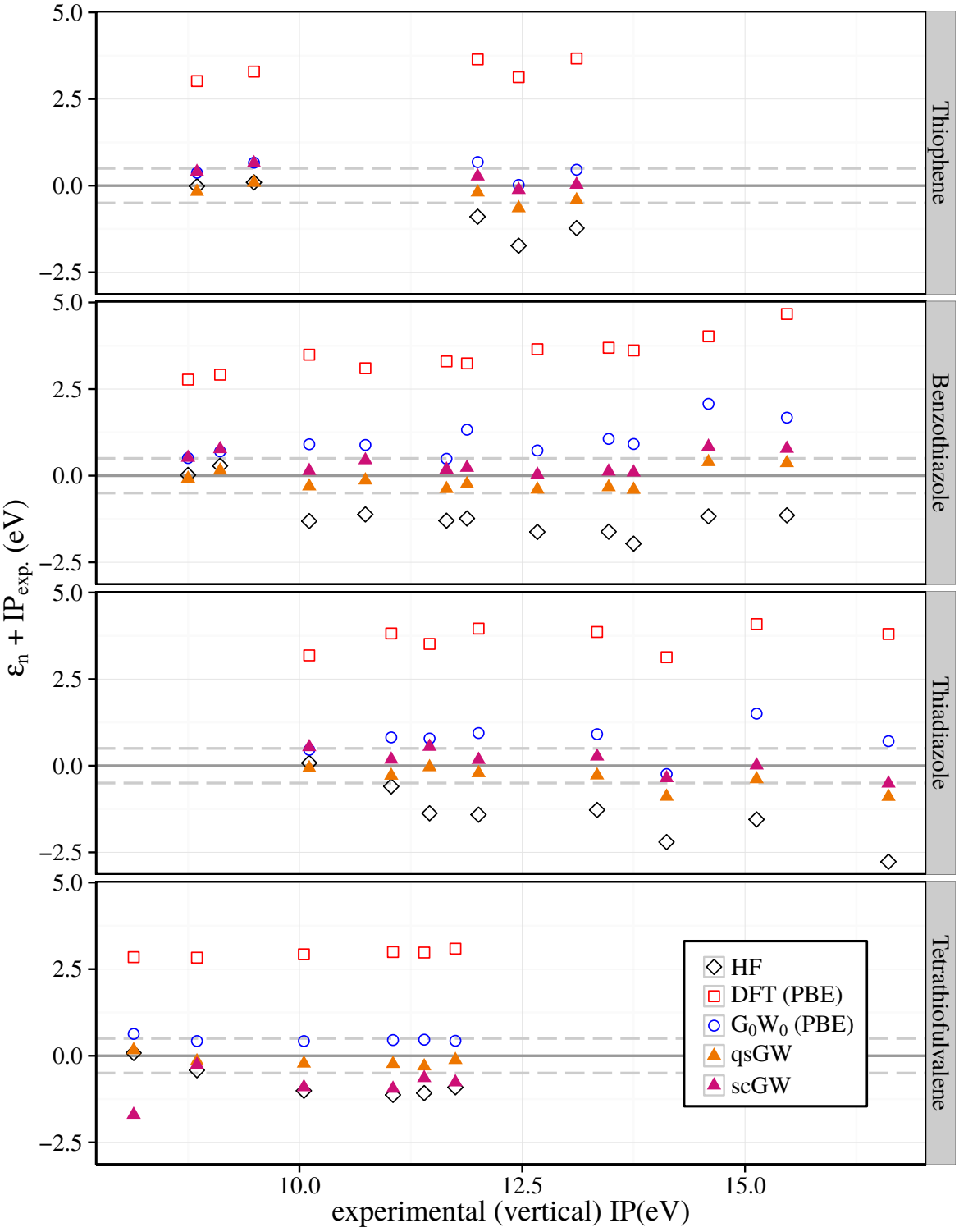

Figure C.1: Higher ionization energies (IP) of further molecules, which are candidate system for photovoltaic applications, obained from qs*GW* and further (approximate) appraoches. This results support the findings from Sec. 4.3.

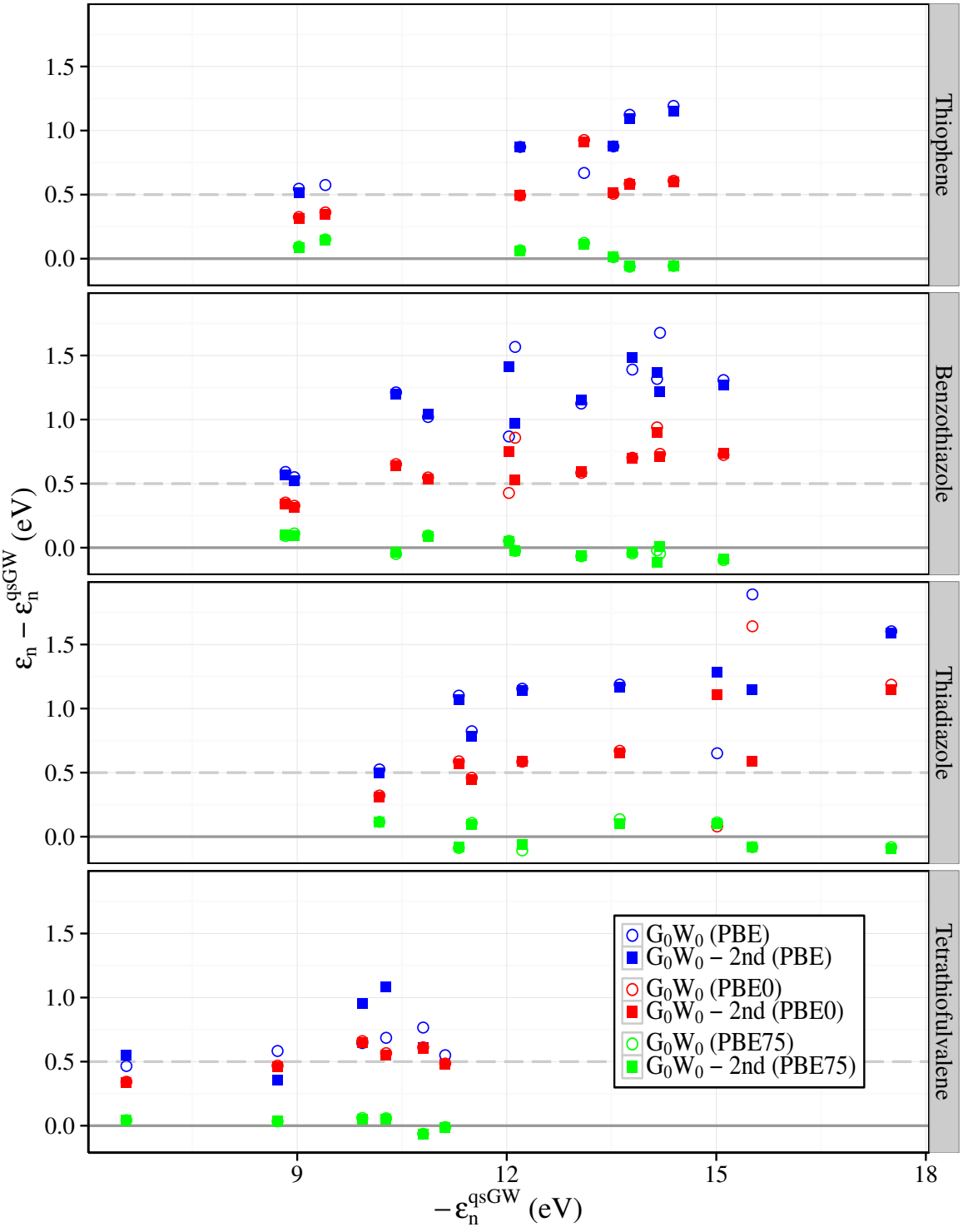

Figure C.2: Deviation of the QP-energies from diagonal only and second order G_0W_0 from qsGW of canditade mulecules for photovoltaic applications. Three different DFT based starting points, were chosen. The best agreement is obtained by the calculation with the PBE75 parent. The data comlement the findings from Sec. 5.2.2.2.

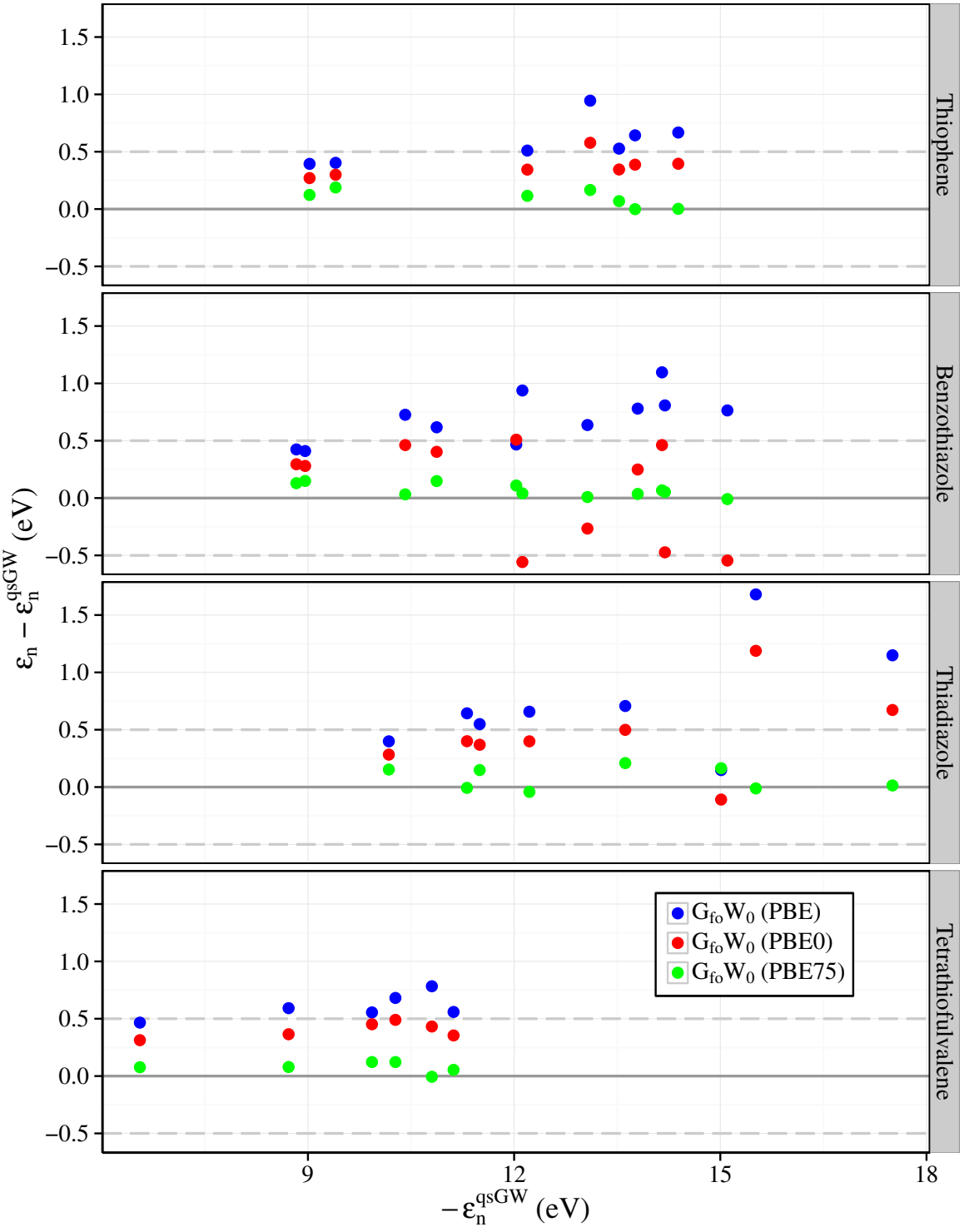

Figure C.3: The deviation of the QP-energies from $G_{fo}W_0$ to results from qsGW for molecules which are candidates for photovoltaic applications. Three different DFT based starting points were chosen. The best agreement is obtained by the calculation with the PBE75 parent. The data complements the findings from Sec. 5.3.2.2.

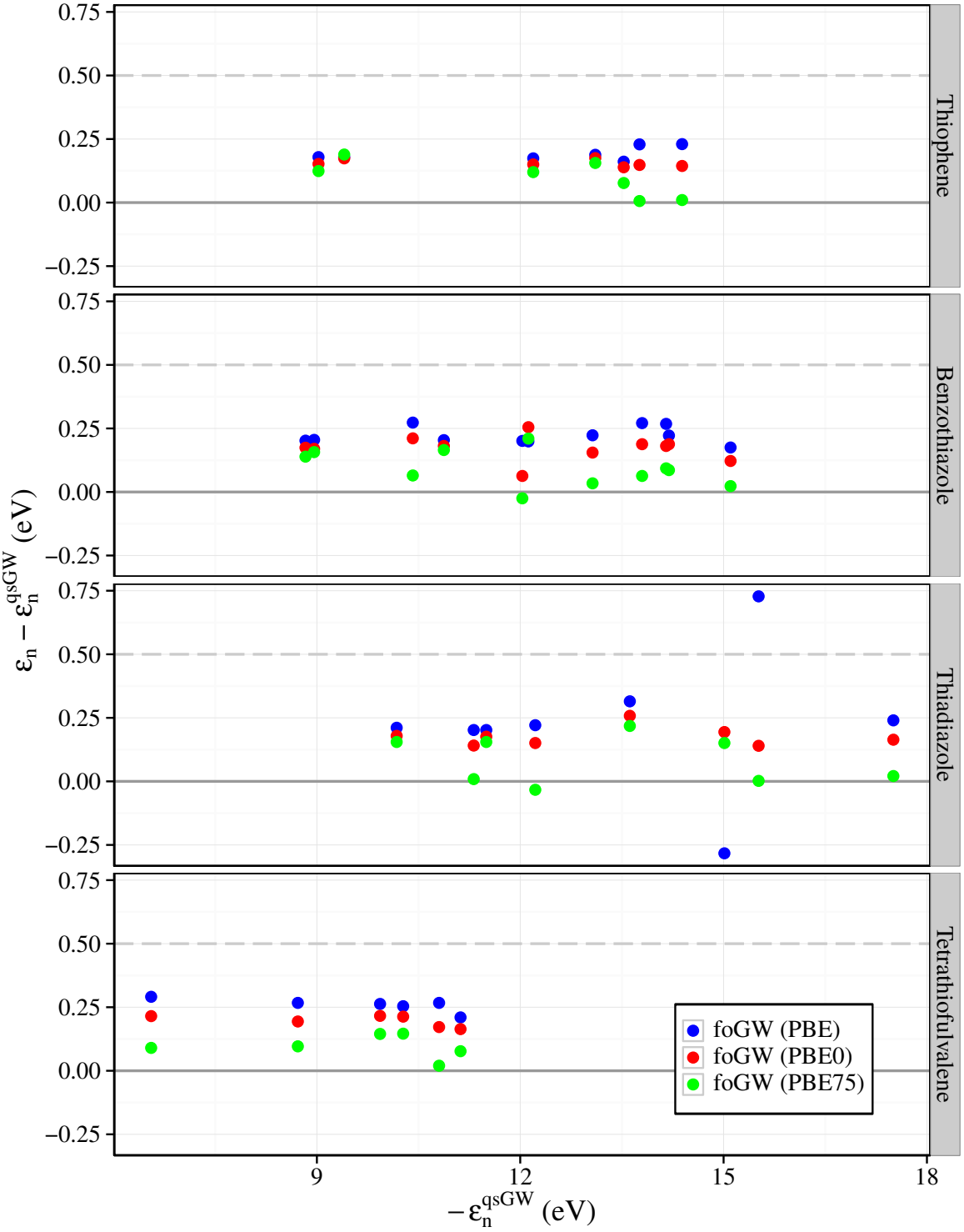

Figure C.4: Figure similar to Fig. C.3 here for the fo*GW* method. The data complements the findings from Sec. 6.2.1.3.

C.2 Starting Point Dependence of $G_{\mathrm{fo}}W_0$ and foGW

The approximate foGW which was developed in the thesis still exhibit a dependence on the starting points. But, it has proven to be strongly reduced. In addition to the study presented Sec. 6.2.1.2 the study is complemented by the comparisons in Fig. C.5 and Fig. C.6. In comparison to DFT method and G_0W_0 vary calculated HOMO by an order of magnitude less with the choice of the amount of exact exchange in the functional.

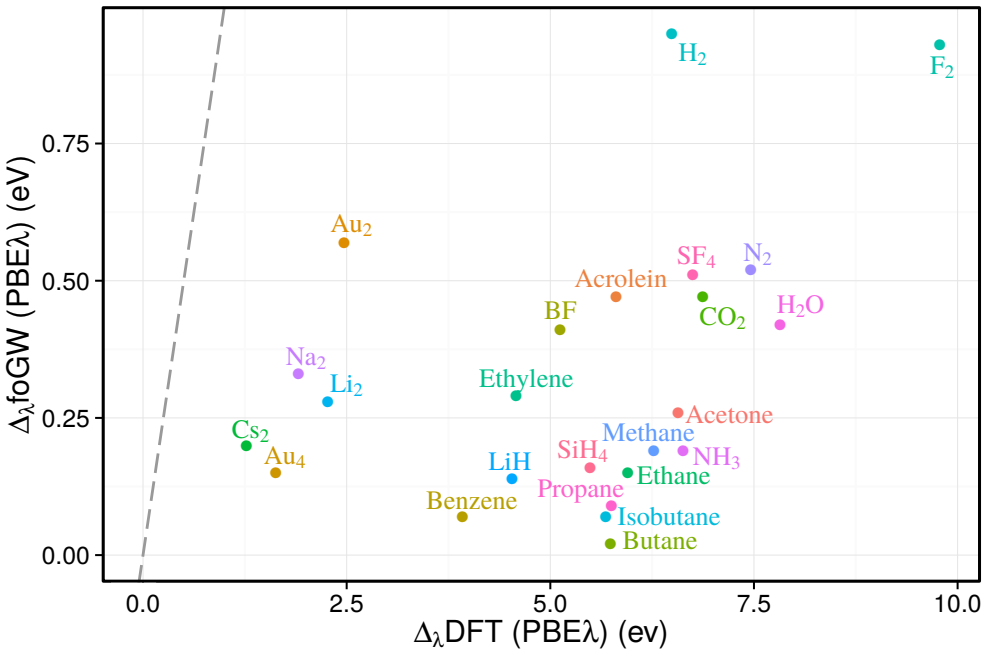

Figure C.5: Shown is Δ_λ from foGW plotted over Δ_λ from DFT (PBEλ) for the full test set of molecules. Δ_λ is the maximum distance of the calculated HOMO energy based on the choice of λ. The foGW calculation is initialized from a parent DFT (PBEλ) calculation and hence has a ramaining inherent, although strongly reduced, dependence of the results on the choice of the functional in DFT. The dashed line is the diagonal. If data points are below this line, foGW has a reduced dependence in the HOMO on λ. The data complements the findings from Sec. 6.2.1.2.

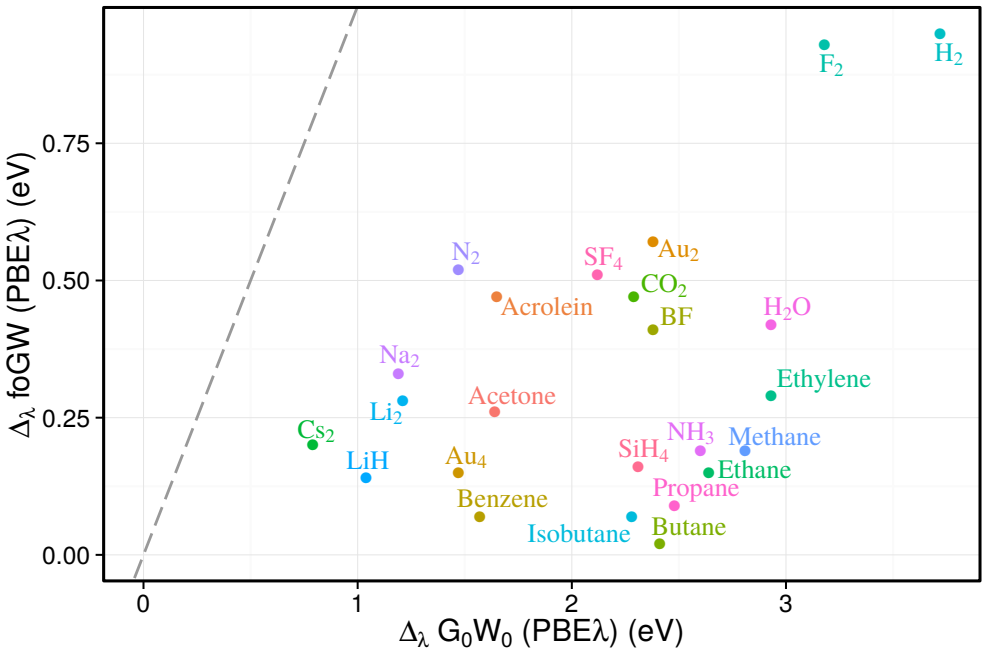

Figure C.6: Plot similar to the one in Fig. C.5, here with the spread Δ_λ from foGW over Δ_λ from G_0W_0 0th. The data complements the findings from Sec. 6.2.1.1.

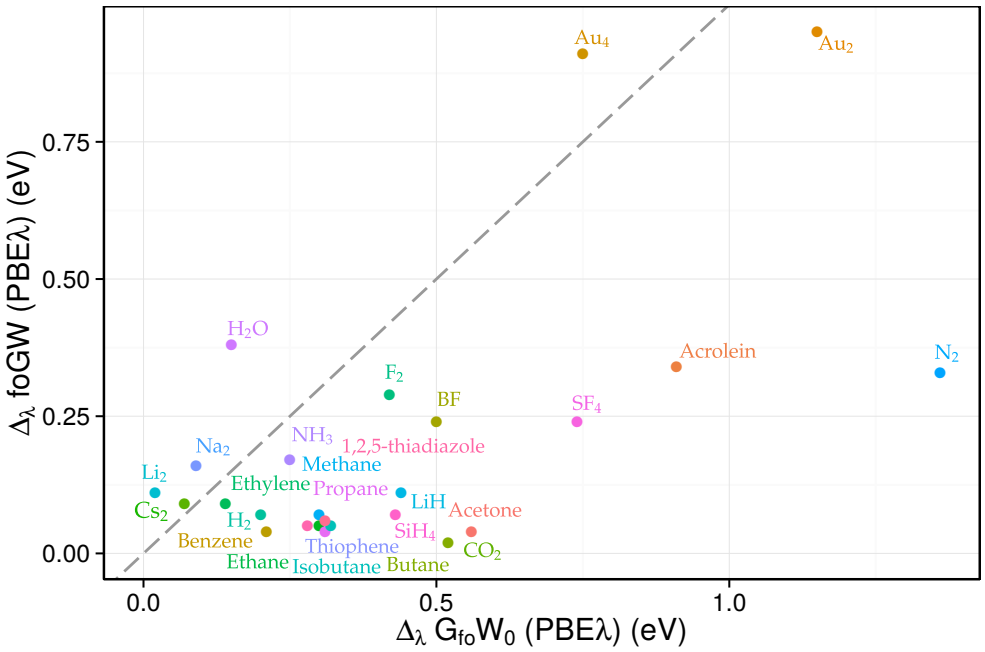

Figure C.7: Plot similar to the one in Fig. C.5, here with the spread Δ_λ foGW plotted over Δ_λ from $G_{\text{fo}}W_0$. The data complements the findings from Sec. 6.2.1.1.

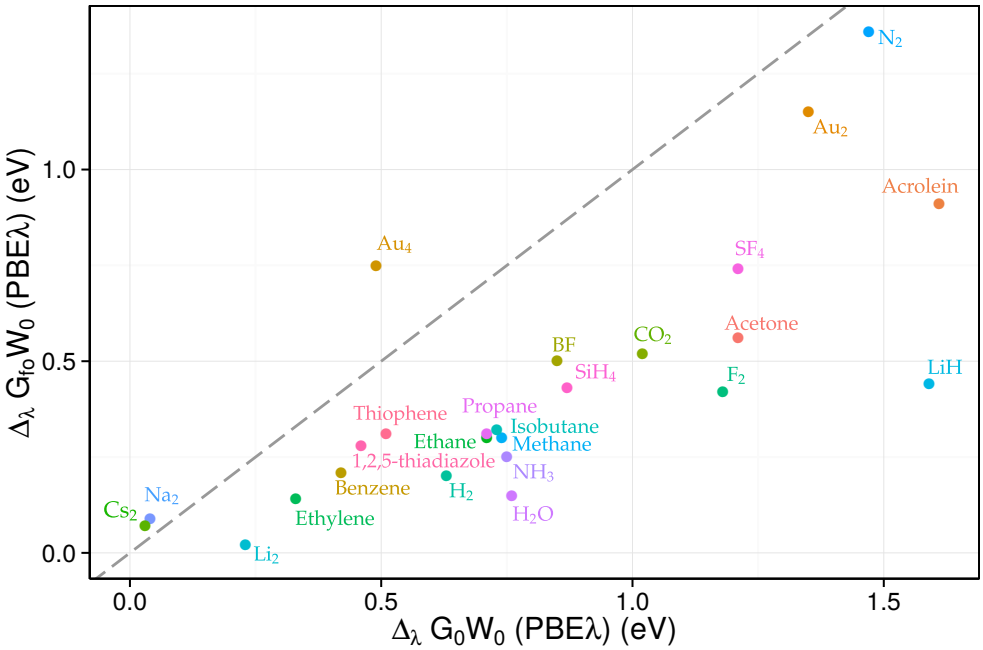

Figure C.8: Plot similar to the one in Fig. C.5, here with the spread Δ_λ *GW* from $G_{\mathrm{fo}}W_0$ plotted over Δ_λ from G_0W_0. The data complements the findings from Sec. 5.3.2.

List of Figures

List of Tables

Bibliography

A. A. Abrikosov, L. P. Gorkov and I. E. Džalošinskij. *Methods of quantum field theory in statistical physics*. Dover Publ. (1975)

R. Ahlrichs, M. Bär, M. Häser, H. Horn and C. Kölmel. Electronic structure calculations on workstation computers: The program system turbomole. *Chemical Physics Letters*, vol. 162 (3): pp. 165–169 (1989)

F. Aryasetiawan and O. Gunnarsson. The GW method. *Rep. Prog. Phys.*, vol. 61 (5): pp. 237–312 (1998)

S. Baroni, G. Pastori Parravicini and G. Pezzica. Quasiparticle band structure of lithium hydride. *Physical Review B*, vol. 32 (6): pp. 4077–4087 (1985)

B. Baumeier, D. Andrienko, Y. Ma and M. Rohlfing. Excited States of Dicyanovinyl-Substituted Oligothiophenes from Many-Body Green ' s Functions Theory (2012)

G. Baym and L. Kadanoff. Conservation Laws and Correlation Functions. *Physical Review*, vol. 124 (2): pp. 287–299 (1961)

F. Bechstedt, K. Tenelsen, B. Adolph and R. Del Sole. Compensation of Dynamical Quasiparticle and Vertex Corrections in Optical Spectra. *Physical Review Letters*, vol. 78 (8): pp. 1528–1531 (1997)

A. D. Becke. Density-functional exchange-energy approximation with correct asymptotic behavior. *Physical Review A*, vol. 38 (6): pp. 3098–3100 (1988)

X. Blase and C. Attaccalite. Charge-transfer excitations in molecular donor-acceptor complexes within the many-body Bethe-Salpeter approach. *Applied Physics Letters*, vol. 99 (17): pp. 10–13 (2011)

X. Blase, C. Attaccalite and V. Olevano. First-principles \mathit{GW} calculations for fullerenes, porphyrins, phtalocyanine, and other molecules of interest for organic photovoltaic applications. *Phys. Rev. B*, vol. 83 (11): p. 115103 (2011)

P. Boulanger, D. Jacquemin, I. Duchemin and X. Blase. Fast and Accurate Electronic Excitations in Cyanines with the Many- Body Bethe − Salpeter Approach (2013)

F. Bruneval. Ionization energy of atoms obtained from GW self-energy or from random phase approximation total energies. *Journal of Chemical Physics*, vol. 136 (194107): pp. 1–10 (2012)

F. Caruso, P. Rinke, X. Ren, A. Rubio and M. Scheffler. Self-consistent GW: All-electron implementation with localized basis functions. *Physical Review B*, vol. 88: pp. 1–15 (2013)

B. Champagne, E. a. Perpete, S. J. a. van Gisbergen, E.-J. Baerends, J. G. Snijders, C. Soubra-Ghaoui, K. a. Robins and B. Kirtman. Assessment of conventional density functional schemes for computing the polarizabilities and hyperpolarizabilities of conjugated oligomers: An ab initio investigation of polyacetylene chains. *The Journal of Chemical Physics*, vol. 109 (23): p. 10489 (1998)

J. Cizek and J. Paldus. Coupled Cluster Approach. *Physica Scripta*, vol. 21: pp. 251–254 (1980)

C. J. Cramer. *Essentials of Computational Chemistry*. Wiley (2004)

C. C. C. DataBase and Benchmark. http://cccbdb.nist.gov/ (2015)

M. L. Del Puerto, M. L. Tiago and J. R. Chelikowsky. Excitonic effects and optical properties of passivated CdSe clusters. *Physical Review Letters*, vol. 97 (9): pp. 1–4 (2006)

K. Eichkorn, M. Htiser, R. Ahlrichs, K. Eichkorn, O. Treutler, H. Marco and R. Ahlrichs. Auxiliary basis sets to approximate Coulomb potentials (Chem . Phys . Letters 240 (1995) 283) * Auxiliary basis sets to approximate Coulomb potentials. *Chemical Physics Letters*, vol. 240 (September): pp. 283–290 (1995)

M. Elbing, R. Ochs, M. Koentopp, M. Fischer, C. von Hänisch, F. Weigend, F. Evers, H. B. Weber and M. Mayor. A single-molecule diode. *Proceedings of the National Academy of Sciences of the United States of America*, vol. 102 (25): pp. 8815–8820 (2005)

C. Faber, P. Boulanger, C. Attaccalite, I. Duchemin and X. Blase. Excited states properties of organic molecules: from density functional theory to the GW and Bethe-Salpeter Green's function formalisms. *Philosophical transactions. Series A, Mathematical, physical, and engineering sciences*, vol. 372 (2011): p. 20130271 (2014)

S. Faleev, M. Van Schilfgaarde and T. Kotani. All-electron self-consistent GW approximation: Application to Si, MnO, and NiO. *Physical Review Letters*, vol. 93 (September): pp. 12–15 (2004)

A. L. Fetter and J. D. Walecka. *Quantum theory of many-particle systems*. Dover Publ. (2003)

C. Fonseca Guerra, J. G. Snijders, G. Te Velde and E. J. Baerends. Towards an order-N DFT method. *Theoretical Chemistry Accounts: Theory, Computation, and Modeling (Theoretica Chimica Acta)*, vol. 99 (6): pp. 391–403 (1998)

F. Fuchs, J. Furthmüller, F. Bechstedt, M. Shishkin and G. Kresse. Quasiparticle band structure based on a generalized Kohn-Sham scheme. *Physical Review B - Condensed Matter and Materials Physics*, vol. 76 (115109): pp. 1–8 (2007)

R. Godby, M. Schlüter and L. Sham. Quasiparticle energies in GaAs and AlAs. *Physical review. B, Condensed matter*, vol. 35 (8): pp. 4170–4171 (1987)

L. Hedin. Method for Calculating the One-Particle Green's Function with Application to the Electron-Gas Problem. *Phys.Rev. B*, vol. 139: pp. 796–823 (1965)

L. Hedin. Electron Correlation : Keeping Close to an Orbital Description. *International Journal of Quantum Chemistry*, vol. 56 (1 995): pp. 445–452 (1995)

L. Hedin. On correlation effects in electron spectroscopies and the GW approximation. *Journal of Physics: Condensed Matter*, vol. 11 (42): pp. R489–R528 (1999)

L. Hedin and B. Lundqvist. Explicit local exchange-correlation potentials. *Solid State Phys.*, vol. 2064 (1971)

K. Held, C. Taranto, G. Rohringer and A. Toschi. Hedin Equations, GW, GW+DMFT, and All That (2011)

B. Holm and U. von Barth. Fully self-consistent GW self-energy of the electron gas. *Physical Review B*, vol. 57 (4): pp. 2108–2117 (1998)

J. Hubbard. The Description of Collective Motions in Terms of Many-Body Perturbation Theory. *Proceedings of the Royal Society A: Mathematical, Physical and Engineering Sciences*, vol. 240 (1223): pp. 199–211 (1957)

J. Hubbard. The Description of Collective Motions in Terms of Many-Body Perturbation Theory. II. The Correlation Energy of a Free-Electron Gas. *Proceedings of the Royal Society A: Mathematical, Physical and Engineering Sciences*, vol. 243 (1234): pp. 336–352 (1958a)

J. Hubbard. The Description of Collective Motions in Terms of Many-Body Perturbation Theory. III. The Extension of the Theory to the Non-Uniform Gas. *Proceedings of the Royal Society A: Mathematical, Physical and Engineering Sciences*, vol. 244 (1237): pp. 199–211 (1958b)

M. Hybertsen and S. Louie. Electron correlation in semiconductors and insulators: Band gaps and quasiparticle energies. *Physical Review B*, vol. 34 (8): pp. 5390–5413 (1986)

K. P. F. Janssen, G. De Cremer, R. K. Neely, A. V. Kubarev, J. Van Loon, J. a. Martens, D. E. De Vos, M. B. J. Roeffaers and J. Hofkens. Single molecule methods for the study of catalysis: from enzymes to heterogeneous catalysts. *Chemical Society reviews*, vol. 43 (4): pp. 990–1006 (2014)

S. Ke. All-electron GW methods implemented in molecular orbital space: Ionization energy and electron affinity of conjugated molecules. *Physical Review B*, vol. 84 (20): pp. 1–6 (2011)

W. Kohn and L. Sham. Self-Consistent Equations Including Exchange and Correlation Effects. *Physical Review*, vol. 140 (4A): pp. A1133–A1138 (1965)

T. Koopmans. Über die Zuordnung von Wellenfunktionen und Eigenwerten zu den Einzelnen Elektronen Eines Atoms. *Physica*, vol. 1 (1-6): pp. 104–113 (1934)

T. Kotani, M. Van Schilfgaarde and S. Faleev. Quasiparticle self-consistent GW method: A basis for the independent-particle approximation. *Physical Review B - Condensed Matter and Materials Physics*, vol. 76: pp. 1–24 (2007)

K. Krause, M. Harding and W. Klopper. Coupled-cluster reference values for the GW27 and GW100 test sets for the assessment of GW methods. *Molecular Physics*, (April 2015): pp. 1–9 (2015)

G. Kresse and J. Furthmüller. Efficiency of ab-initio total energy calculations for metals and semiconductors using a plane-wave basis set. *Computational Materials Science*, vol. 6 (1): pp. 15–50 (1996)

S. Kubatkin, A. Danilov, M. Hjort, J. Cornil, J. Brédas, N. Stuhr-Hansen, P. Hedegård and T. Bjørnholm. Single-electron transistor of a single organic molecule with access to several redox states. *Nature*, vol. 425 (6959): pp. 698–701 (2003)

D. C. Langreth and M. J. Mehl. Beyond the local-density approximation in calculations of ground-state electronic properties. *Physical Review B*, vol. 28 (4): pp. 1809–1834 (1983)

H. L. H. Lee, L.-E. Y. L.-E. Yu, S.-W. R. S.-W. Ryu, J.-W. H. J.-W. Han, K. J. K. Jeon, D.-Y. J. D.-Y. Jang, K.-H. K. K.-H. Kim, J. L. J. Lee, J.-H. K. J.-H. Kim, S. C. J. S. C. Jeon, G. S. L. G. S. Lee, J. S. O. J. S. Oh, Y. C. P. Y. C. Park, W. H. B. W. H. Bae, H. M. L. H. M. Lee, J. M. Y. J. M. Yang, J. J. Y. J. J. Yoo, S. I. K. S. I. Kim and Y.-K. C. Y.-K. Choi. Sub-5nm All-Around Gate FinFET for Ultimate Scaling. *2006 Symposium on VLSI Technology, 2006. Digest of Technical Papers.*, vol. 25 (9): pp. 2005–2006 (2006)

M. Lopez Del Puerto, M. L. Tiago and J. R. Chelikowsky. Ab initio methods for the optical properties of CdSe clusters. *Physical Review B - Condensed Matter and Materials Physics*, vol. 77 (4): pp. 1–10 (2008)

N. Marom, F. Caruso, X. Ren, O. Hofmann, T. Körzdörfer, J. Chelikowsky, A. Rubio, M. Scheffler and P. Rinke. Benchmark of GW methods for azabenzenes. *Physical Review B - Condensed Matter and Materials Physics*, vol. 86 (24): p. 245127 (2012)

R. M. Martin. *Electronic structure : basic theory and practical methods*. Cambridge Univ. Press (2005)

J. Matthiesen, S. Wendt, J. Hansen, G. K. H. Madsen, E. Lira, E. Lira, P. Galliker, E. K. Vestergaard, R. Schaub, E. Laegsgaard, B. Hammer and F. Besenbacher. Observation of all the intermediate steps of a chemical reaction on an oxide surface by scanning tunneling microscopy. *ACS nano*, vol. 3 (3): pp. 517–26 (2009)

S. McKechnie, G. H. Booth, A. J. Cohen and J. M. Cole. On the accuracy of density functional theory and wave function methods for calculating vertical ionization energies. *The Journal of Chemical Physics*, vol. 142 (19): p. 194114 (2015)

J. Perdew, J. Chevary, S. Vosko, K. Jackson, M. Pederson, D. Singh and C. Fiolhais. Erratum: Atoms, molecules, solids, and surfaces: Applications of the generalized gradient approximation for exchange and correlation. *Physical Review B*, vol. 48 (7): pp. 4978–4978 (1993)

J. Perdew and M. Levy. Reply to "Comment on 'Significance of the highest occupied Kohn-Sham eigenvalue' ". *Physical Review B*, vol. 56 (24): pp. 16029–16030 (1997)

J. P. Perdew and M. Levy. Physical content of the exact kohn-sham orbital energies: Band gaps and derivative discontinuities. *Physical Review Letters*, vol. 51 (20): pp. 1884–1887 (1983)

J. P. Perdew, R. G. Parr, M. Levy and J. L. Balduz. Density-functional theory for fractional particle number: Derivative discontinuities of the energy. *Physical Review Letters*, vol. 49 (23): pp. 1691–1694 (1982)

J. C. Phillips. Generalized Koopmans' theorem. *Physical Review*, vol. 123 (2): pp. 420–424 (1961)

K. Raghavachari, G. Trucks, J. Pople and M. Head-Gordon. A fifth-order perturbation comparison of electron correlation theories. *Chemical Physics Letters*, vol. 157 (6) (1989)

X. Ren, P. Rinke, C. Joas and M. Scheffler. Random-phase approximation and its applications in computational chemistry and materials science. *Journal of Materials Science*, vol. 47 (21): pp. 7447–7471 (2012)

P. Rinke, A. Qteish, J. Neugebauer, C. Freysoldt and M. Scheffler. Combining GW calculations with exact-exchange density-functional theory: An analysis of valence-band photoemission for compound semiconductors. *New Journal of Physics*, vol. 7 (2005)

P. Rinke, A. Qteish, J. Neugebauer and M. Scheffler. Exciting prospects for solids: Exact-exchange based functionals meet quasiparticle energy calculations. *Physica Status Solidi (B)*, vol. 245 (5): pp. 929–945 (2008)

C. Rodenbeck. *Bachelor Thesis* (2014)

C. Rostgaard, K. Jacobsen and K. Thygesen. Fully self-consistent GW calculations for molecules. *Physical Review B - Condensed Matter and Materials Physics*, vol. 81 (8): pp. 1–10 (2010)

E. Runge and E. K. U. Gross. Density-functional theory for time-dependent systems. *Physical Review Letters*, vol. 52 (12): pp. 997–1000 (1984)

R. Sakuma, T. Miyake and F. Aryasetiawan. Effective quasiparticle Hamiltonian based on Löwdin's orthogonalization. *Physical Review B - Condensed Matter and Materials Physics*, vol. 80 (23): pp. 1–8 (2009)

A. Schindlmayr and C. Friedrich. *Publication Series of the John von Neumann Institute for Computing (NIC) NIC Series*, vol. 31 (2006)

L. Sham and M. Schlueter. Density-functional theory of the band gap. *Physical Review B*, vol. 32 (6): p. 3883 (1985)

S. Sharifzadeh, I. Tamblyn, P. Doak, P. T. Darancet and J. B. Neaton. Quantitative molecular orbital energies within a G0W0 approximation. *The European Physical Journal B*, vol. 85 (9): pp. 1–5 (2012)

T. Stein, L. Kronik and R. Baer. Prediction of charge-transfer excitations in coumarin-based dyes using a range-separated functional tuned from first principles. *The Journal of Chemical Physics*, vol. 131 (24): p. 244119 (2009)

A. Szabo and N. S. Ostlund. *Modern quantum chemistry : introduction to advanced electronic structure theory*. Dover Publ. (1996)

R. van Leeuwen and E. J. Baerends. Exchange-correlation potential with correct asymptotic behaviour. *Physical Review A*, vol. 49 (4) (1994)

M. Van Schilfgaarde, T. Kotani and S. Faleev. Quasiparticle self-consistent GW theory. *Physical Review Letters*, vol. 96 (June): pp. 1–4 (2006)

M. Van Setten, F. Weigend and F. Evers. The GW -Method for Quantum Chemistry Applications: Theory and Implementation. *Journal of Chemical Theory and Computation*, vol. 9 (1): pp. 232–246 (2013)

F. Weigend. Accurate Coulomb-fitting basis sets for H to Rn. *Physical chemistry chemical physics : PCCP*, vol. 8 (9): pp. 1057–1065 (2006)

B. M. Wong, M. Piacenza and F. Della Sala. Time-dependent density-functional theory. *Physical Chemistry Chemical Physics*, vol. 11 (22): p. 4436 (2009)